University of Southampton

Faculty of Engineering and Applied Science
Department of Civil and Environmental Engineering

Analysis and Design of Semi-Continuous Sway and Non-Sway Frames

By

Christopher Fisher, BEng

For the degree of Doctor of Philosophy

Supervisors: Dr. R. Y. Xiao & Dr. S. S. J. Moy

May 2001

University of Southampton

Faculty of Engineering and Applied Science
Department of Civil and Environmental Engineering

Analysis and Design of Semi-Continuous Sway and Non-Sway Frames

By

Christopher Fisher, BEng

ABSTRACT

Frames are traditionally designed as being perfectly pinned or perfectly rigid. These connections do not actually exist in real structures, with connection behaviour being between these extremes. Assuming that the connection is pinned leads to an overly conservative design as no moment transfer can occur at the connection, meaning bigger steel sections being used for the beams than are necessary.

Site monitoring of the first building to make use of the semi-continuous design approach was conducted. The monitoring covered a primary and secondary beam during the construction and later loading of the structure. After the site monitoring the structure was modelled, using the ANSYS software package for finite element analysis. The results for this were compared to those from the site monitoring, and the results were found to be very close, so the model was used in further analyses.

In the next set of analyses the connection stiffnesses and column base stiffnesses were changed, by making changes to the M-ϕ curve. It could then be seen how the joint stiffnesses affect the flexibility and strength of the frame. The model was then expanded to model multi-storey construction. Analysis techniques were used to show the trends that exist in the finite element results. The results were compared by means of a strength ratio, which was defined as the strength of any frame divided by that of a fully-fixed frame.

Analyses were conducted on the results of frames with different section properties, different connection stiffnesses, and numbers of storeys. Curve fitting techniques were used to show trends for each of these variables. By changing the connection stiffness it was found that the strength ratio changed with a third-order logarithmic relationship. The relationship between the number of storeys of the frame and the strength ratio was demonstrated to be almost linear.

The work detailed in this thesis has shown that semi-rigid connections can be used to improve the efficiency of frameworks. The frameworks can be designed using connections that are currently in use, but taking into account their inherent stiffness makes frame design more efficient. This efficiency is in the form of savings on steel costs, and a reduction in the beam depth required, which allows either an increase in the ceiling height within buildings, a shortening of buildings, or more space for services in the service space between the floors of buildings.

Acknowledgements

I would like to thank Dr. R. Y. Xiao and Dr. S. S. J. Moy for their help, guidance and encouragement through the duration of the research. I would also like to thank Gifford and Partners, and Amey Construction for their generous assistance with the experiment.

Thanks are also due to my colleagues Simon, Tom, Jirka and Simon for the riveting discussions that have taken part in the office.

I would also like to thank my wife, Margaret, and my friends and family for the encouragement and understanding that they have showed me.

The work in this PhD thesis is dedicated to David Fisher.

Contents

Chapter Four: Finite Element Analysis Modelling

Chapter Five: Single-Storey Frame Analysis

Chapter Six: Multi-Storey Frame Analysis

Chapter Seven: Analysis of FEM Results

Chapter Eight: Conclusions and Further Work

Chapter 1

Introduction

1.1 Background

Beam-to-column connections are usually classified as being perfectly pinned or perfectly rigid. These ideals do not actually exist in real structures, with connection behaviour being between these extremes. Connections are usually designed as pinned, because the fabrication costs are lower, and the design is simpler, than for rigid connections. This leads to an overly conservative design, as no moment transfer is accounted for at the connection, meaning that bigger steel sections are used for the beams than are necessary. Design using semi-rigid connections could provide a way of saving steel costs, as it takes into account the real behaviour of structures. It has been suggested **[1]** that introducing semi-rigid connections into the design process could make a saving of 15% of the steel in a structure over that used for a structure designed with simple connections.

The Eurocodes **[2]** give a classification for connections as pinned, rigid, or semi-rigid. There has been some research in recent years to classify connection types by strength, stiffness and ductility. The moment-rotation behaviour of a connection can then be shown using an M-ϕ curve. Other research has shown the behaviour of column bases to

be semi-rigid. There has been some experimental study using semi-rigid connections, involving the study of full-scale, semi-rigidly connected frames. This is discussed in the literature review.

Currently, the Steel Designer's Manual **[3]** states that design using semi-rigid connections is complex, and their wider application depends on the development of simple design procedures based upon experimental evidence. Due to this, many connections which exhibit semi-rigid behaviour are presently used as simple connections.

1.2 Research

For the research in this project, an experiment was conducted on a building that made use of the semi-rigid design approach, the first of its kind in Europe. Two of the supporting beams were monitored: a pre-cambered secondary beam, and a primary beam that was propped during construction. The deflections of the beams were monitored during the construction stages and later loading of the structure. The deflections of the beams were measured using displacement transducers on each beam. The concrete pour was observed with a video camera throughout so that it would be possible to match up any jumps in deflection with stages of the concrete pour. The fourth floor was chosen for the site monitoring as this floor supports the greatest loads, particularly the plant room, and hence the floor slab is thicker than those of other floors. The plant room floor is in three stepped levels of thickness, 130mm, 175mm and 250mm, the latter two of these being constructed from normal weight concrete and the 130mm thickness from lightweight concrete. The layout of the fourth floor is shown in Figure 3.4, with the monitored beams at grid reference just beyond E5-H5 and H5-H1. The layout for the experiment is shown in Figure 1.1.

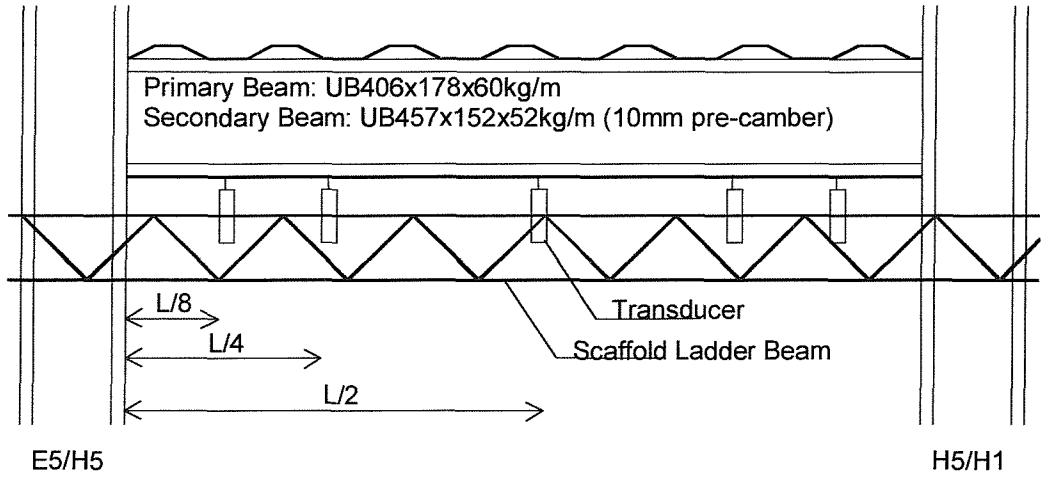

Figure 1.1 Experimental layout

Once the experimental data had been collected, the structure was modelled using two different software packages: QSE, which solves using the stiffness method, and ANSYS, which solves using finite elements. QSE is unable to solve problems with semi-rigid connections, or to perform non-linear analyses, so it was only used for analysing the beams as if they were pinned or fully fixed. The ANSYS package is more flexible, with over 100 elements available in its element library, which can be further customised to perform specific tasks. The computer analyses were compared to the experimental data and shown to give very similar results, so it was then possible to develop further models with different section properties to those in the experiment.

The ANSYS models were constructed using beam elements, either BEAM3, a two dimensional elastic beam, or BEAM23, a two dimensional plastic beam. The connections were modelled using either COMBIN14, a linear elastic spring, or COMBIN39, a non-linear spring. The element types used depend on whether a model is being constructed for elastic, or plastic behaviour.

Using ANSYS, it was possible to model many frames, with different section sizes for the beams and columns, and different beam-to-column and column base stiffnesses. This was done for both single storey and multi-storey frames, for sway and non-sway modes. Using the batch file system, ANSYS is able to solve many frames in succession, using a few common geometry files that are called from a main file to set up the final model.

The models have shown that the beam-to-column connections have a dramatic influence on the beam deflections of both sway and non-sway frames, and also on the sway deflection of sway frames. The connection stiffness can also change the mode of failure of a frame, with the failure either occurring in the connection, or with a plastic hinge forming in the beam or column section. For this research, the frames were generally analysed until a deflection limit was reached. This deflection limit was set to L/200 for the beam deflections and L/300 for the sway deflections (L/150 for the single storey portal frames). For showing the collapse mechanisms, the deflection limit was greatly increased to ensure that the frame had failed.

The results in this research have been shown using the frame rigidity factor K_a. This is the factor that describes the ratio of strength between a fully-fixed frame, and a frame with semi-rigid connections. This simplifies comparing results of frames with different beam and column sections with one another, as then the rigidity factors can be compared, instead of the load that the frame was able to carry. Also, as the frame rigidity factor is found by dividing the load carried by the semi-rigid frame by the load carried by the fully-fixed frame, it means that the loading applied to the frame for the analysis is not critical, as long as it is the same value for both the semi-rigid and the fully-fixed frame, and greater than the value required to reach the deflection limits.

1.3 Structure of this Report

Chapter 2 presents a literature review of completed research into semi-rigid connections that is relevant to this project. Experimental work and numerical modelling of semi-rigid connections and column bases, which has been conducted by other researchers, is discussed.

The onsite experiment is described in detail in Chapter 3. The experimental layout is described, along with the monitoring procedure. The results of the experiment are shown throughout the construction and later loading of the building. The measured deflections are plotted for both primary and secondary beams. Structural analysis software, QSE, is used to show a comparison between the experimental results and those predicted.

Chapter 4 introduces the Finite Element Method, along with the ANSYS package that was used for the analysis in this research. The elements used in the elastic and plastic modelling are described, and the suitability of the elements for use in the model is discussed. The method of non-linear analysis is also described. Results from the model are shown with the results from the experiment, and compared.

Chapter 5 introduces the single storey models that are used in the research. Both elastic and plastic non-linear models are presented for sway and non-sway frame analysis. The elastic frames were analysed with a constant loading, and the plastic frames were loaded until a set deflection limit had been reached, with the frame either yielding at any point or remaining elastic. Several different frames were analysed with different sections used for the beams and columns. The batch file method was then used to analyse the models with a span of beam-to-column connection and column base stiffnesses from pinned to fully rigid. Similarities and differences between the results for the various models are shown and discussed.

Chapter 6 continues with the research in the previous chapter, with the models being altered to allow for multi-storey modelling. Frames of two, five and ten storeys are covered in this chapter. The essence of the model remains the same as that described earlier. With the increase in floor numbers, the PΔ effect becomes more obvious and its effects are shown here. The collapse mechanisms are shown for some of the frames that have been analysed, to demonstrate how the connection stiffness affects this.

The results from the models are summarised in Chapter 7. Curve fitting and dimensional analysis is then used on the results to form relationships for the semi-rigid connections and the section properties of the beams and columns with the strength of the frames. Comparisons are shown between the single and multi-storey frames.

Chapter 8 summarises all the research and presents the conclusions. The effectiveness of semi-rigid connections is further discussed. Some suggestions are also made for future work to further the knowledge and use of semi-rigid connections.

Chapter 2

Literature Review

2.1 Introduction

The following sections document the relevant work that has already been conducted by other researchers into the area of semi-rigid connections. The reviews have been split into several sections, depending on the area of work covered in the papers. The areas covered are frame design and experiments, analysis of semi-rigid connections, column bases, and finite element analysis.

2.2 Frame Design and Experiments: Two-Dimensional Frames, Three-Dimensional Frames, and Composite Structures

Lloyd and Wright conducted an experiment on an in situ composite floor system **[4]**. The experiment was set up close to the completion of the structure to assess the impact of the real boundary conditions on the structural characteristics of the floor system. The building consisted of pad foundations and a braced steel frame with composite beams and floor deck. Extensive instrumentation was built into the structure to monitor it during the construction stage and into its service life.

The permanent monitoring apparatus consisted of:
Vibrating wire strain gauges, installed both on the inner beam flange surfaces at their mid- and quarter-spans and within the composite floorslab over the beam midspans and to the midslab spans.
Slip gauges, installed along one half-span of the test beam, its adjacent main beam and their adjoining beams.
Uniaxial inclinometers, installed around the structural joints of the test beam and adjacent main beam.

In addition to these, a number of displacement transducers were positioned under the midspans of the beams and floorslabs. A framework of scaffolding supported these.

The floor was loaded to the required dead load by using a 'water pillow'. This is a large self-supporting water reservoir. The water pillow was used to apply load in 100mm (0.987 kN/m^2) increments. At each increment readings were taken from all the instrumentation and displayed graphically to ensure that the structure remained within its working load range.

The test results were compared to those from analysis, and it was found that the test results gave far lower deflections. This was due to the additional end restraint provided by the connection details. A finite difference model was then used to model the beam with built-in end conditions, which allowed for no rotation, but allowed slip to occur. The model gave results lower than those from the experiment, showing that the real end connections lay between simply supported and fixed assumptions.

Using the end conditions measured during the experiment in the finite difference model gave a midspan deflection 77% greater than that measured in the experiment. This demonstrated that the transverse slab actions between the loaded test beam and the unloaded neighbouring beams were substantial.

The authors concluded that the tensile strength of the composite floorslab over the beam supports contributed to the rotational capacity of the structural joint. The composite floorslab represented a transverse element of significant stiffness. The end connection details appeared to affect the observed stiffness of the beams to an

appreciable extent. The test beam with partial endplate connections and a continuous composite floorslab over one of the supports was found to have an effective stiffness of 2 to 3 times that of a simple, roller supported beam.

Kim and Chen's 1996 paper **[5]** presents three practical advanced analysis procedures for a two-dimensional semi-rigid steel frame design. The proposed methods for modelling can predict the combined non-linear effects of connection geometry, and material, on the behaviour and strength of semi-rigid frames. The results from the models have been compared to available experimental results.

The semi-rigid connections influence the moment distribution in beams and columns as well as the drift and P-Δ effect of the frame. These effects can be accounted for by using a direct second-order inelastic frame analysis, "Advanced Analysis". The Advanced Analysis can capture the limit state strength and stability of a structure and its members so that separate member capacity checks are not required.

The research is limited to two-dimensional steel frames. Lateral torsional buckling is assumed to be prevented by adequate lateral braces. The study covers both braced and unbraced semi-rigid frames. A plastic section is assumed so that the section can develop full plastic moment capacity without buckling.

The three factors that influence the behaviour of semi-rigid frames are listed as connection, geometric and material nonlinearities.

- **Non-linear behaviour of connections**

The forces transmitted through the beam-to-column connection are listed as: axial force, shear force, bending moment, and torsion. It is noted that the effects from axial force and shearing force are negligible since their deformations are small compared with the rotational deformation of connections. Torsion is also neglected in this study.

The connections are assumed to unload with the initial slope of the moment-rotation curve. The loading and unloading behaviours of the connections are accounted for by using the tangent stiffness and initial stiffness.

- **Geometric nonlinearity**

The bending moments in a beam-to-column connection consist of primary and secondary bending moment. Applied end moments and/or transverse loads on members cause primary moments. Secondary moments are caused by axial compressive force acting though the displacements of the member. The paper also considers the effects from geometric imperfections due to building tolerances.

- **Material nonlinearity**

The principle that the yield stresses start from the outermost fibres and the stresses of the interior fibres will be less. The gradual yielding effect leads to the concept of a hardening plastic hinge.

The model proposed by Kishi and Chen **[6]** is used to find the moment-rotation relationship. The Kishi-Chen power model uses initial connection stiffness, ultimate connection moment capacity, and a shape parameter to define the moment-rotation curve of semi-rigid connections.

The researchers went on to do a verification study of a two-storey, single bay structure. The frame's connections were bolted top and seat angle connections. The column bases were pinned supports. Gravity loading of 10.7kN was applied to third points of the first floor beam. A lateral load was applied as the second loading sequence. The lateral load displacement relationship was provided by the experimental work. The results from the experiment are shown to fit those from the Kishi-Chen power model satisfactorily. So the proposed method is adequate in predicting the behaviour and strength of semi-rigid connections. The authors go on to suggest an analysis/design procedure, as follows:

- **Step 1:** Preliminary analysis/design assuming rigid frame.
- **Step 2:** Preliminary selection of connection type and dimension. These are selected by considering the overall flexibility of a structural system. So flexible connections such as single/double web angles may be used for a braced system, or relatively rigid connections such as extended header plates may be used for an unbraced system.

- **Step 3:** Determination of connection parameters. The power model contains three parameters, shown earlier, that can be found using equations in the paper.
- **Step 4:** Analysis of semi-rigid structure. The plastic hinge analysis is carried out to consider the effect of semi-rigid connections and geometric imperfections.
- **Step 5:** Check for strength, serviceability and ductility.
- **Step 6:** Local strength checks of members and connections. The proposed analysis only accounts for the global behaviour effects. Independent local strength checks of members and connections must still be carried out based on LRFD specifications (Load and Resistance Factor Design).
- **Step 7:** Adjustment of member and connection sizes. For example, if there is too much lateral drift, the drift can be reduced by increasing member size, or by using stiffer connections. Iteration of steps 2-7 leads to an optimised design.

The researchers carry out an example using a further two-storey single-bay structure with semi-rigid connections. The member sizes found by the proposed methods are compared to those determined using the modified LRFD method. The frame is shown in Figure 2.1 below.

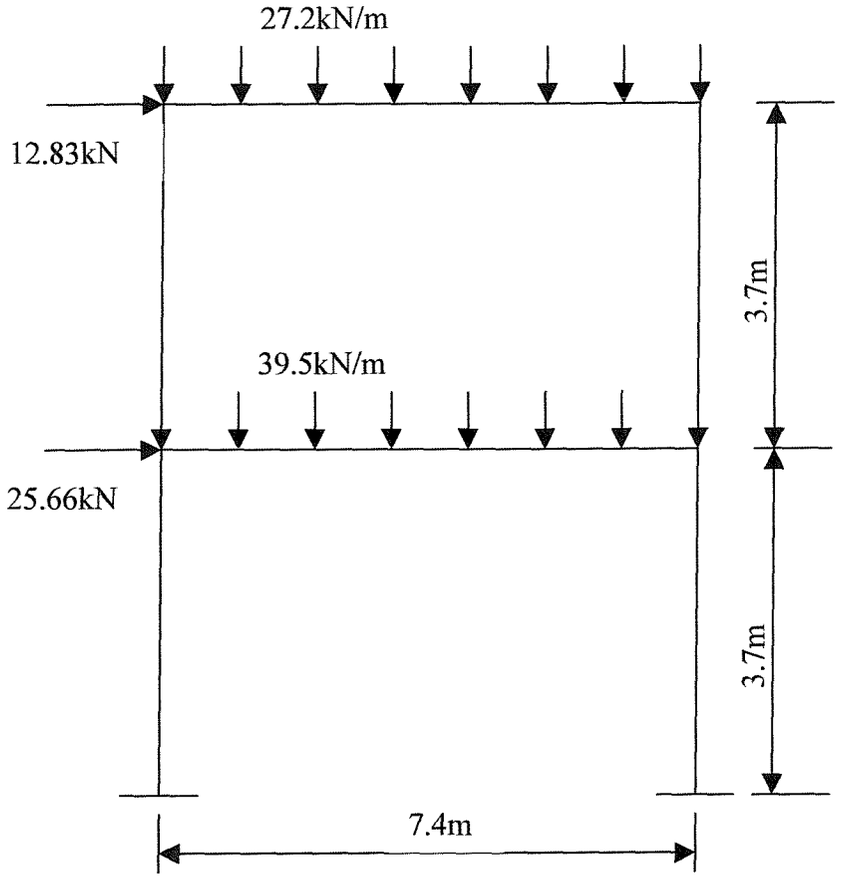

Figure 2.1 Example Frame Used by Kim and Chen

The methods proposed in the paper generally found a member size one smaller than those found by the LRFD method.

Moore, Nethercot and Kirby [7] carried out a series of tests on five full-scale, multi-storey steel frames. The frames were 11m, three storeys, in height, and were 10m, two bays, wide. The frames were tested under gravity loading in a non-sway mode. Measurements were taken to derive the member deflections, joint rotations, bending moment distribution, and column loading.

The five frames were designed to incorporate semi-rigid connections. The details of these connections are shown in Table 2.1 below.

Table 2.1 Connections Used in Testing

Frame	Joint type	Column orientation	Beam size	Column size
1 and 2	Flush and extended endplates of between 12 and 25 mm thickness	Major	254x146UB43	203x203UC71
3	Flange cleats, lower cleat is 125x75x8RSA	Major	254x102xUB22	152x152UC23
4	Flange cleats, lower cleat is 125x75x8RSA	Minor	254x102xUB22	152x152UC23
5	Flush and extended endplates of between 12 and 15 mm thickness	Major	254x102UB28 254x146UB37	152x152UC37

Therefore frames 1 and 2 have relatively stiff connections with moment capacity approaching M_p for the beams. These connections increase the load the beam can carry, and reduce deflections, compared to ideally pinned connections. Frames 3 and 4 used grade 8.8 bolts sufficiently tightened to approximate normal site conditions. Frame 5 used light endplates that are commonly regarded as only capable of transmitting shear. Separate joint tests were also conducted for each joint type.

Frames 1 and 2 were designed to investigate the influence of very stiff moment resisting connections on the performance of beams in a non-sway frame. Loading

patterns were selected to achieve the most critical state for the beams and their connections. The sway supports were also removed to allow the frame to sway as a consequence of unequal bay widths and gravity loading; no extra horizontal loading was applied. Frames 1 and 2 were loaded under working (dead + live loading), and design (dead x 1.4 + live x 1.6) for the sway and non-sway conditions. The final test was for non-sway where the beams were loaded to the safe working load capacity of the loading system. The beams still had a reserve of strength and collapse was induced by moving the loading points.

Frames 3, 4 and 5 were designed to study the influence of flexible and semi-rigid connections on the performance of the columns in a non-sway frame. Each beam was loaded in increments up to the dead load. Frames 3 and 4 were then loaded up to design load, except one beam that remained at dead load. For frame 5 all beams were loaded up to design load. The next stage of loading consisted of column loading. The column loading was used due to earlier studies by Nethercot that showed that different column behaviour could be obtained by changing with sequence of loading. The loading cases were (I) axial column load only and (II) beam loads applied, followed by column axial load. For case (I) the connections would be acting in the initial, stiffer, section of the M-ϕ curve. For case (II) the beam loading would have taken up this initial stiff section, so change in connection type is more pronounced.

The authors found that generally the peak moments occurred at the loading points or the connections for the beams, and the connections for the columns. This is as expected for any frame.

For frames 1 and 2 the internal connections attracted the higher proportion of the load. The frame response remained linear for design load, and none of the beams had attained a 3-hinge plastic mechanism. After the moving of the load points to attain failure, failure occurred in a sudden manner and was caused by a fracture of the endplate welds, which were found to have an insufficient penetration. The weld size was therefore increased for frame 2.

Frame 2 formed plastic hinges at the connections; the redistribution of the moments then caused plasticity in the beam flanges at the loading points.

For frames 3 and 4, the initial loading was applied so that the columns restrained the beams, followed by a second phase up to column collapse during which the beams restrained the columns. The deflected shape of the frames showed that there was significant interaction between all members of the frames, so the relatively flexible flange cleat connections were able to transmit interaction between the beams and columns. Bending moment diagrams showed that with the connections in the initial linear section of the M-ϕ characteristic the points of inflection remain constant.

Direct column loading in frame 3 caused failure in the top storey of the internal column, and the bottom storey of the external column. For frame 4 the failure occurred in the top storey of the external column and the two lower storeys of the internal columns.

The results showed that the design methods in BS 5950 give inconsistent predictions of column load carrying capacity. Results were over-predicted where the beams fitted onto the major axis of the column, and under-predicted for beams that fitted onto the minor axis of the column.

For frame 5 the moments were attracted from the mid-span due to the effect of the semi-rigid connections. The moments are then transferred to the columns, showing significant interaction between all frame members. A greater proportion of the free bending moment was attracted by the extended endplate than by the flush endplate connection.

Failure occurred in the frame when the column was unable to sustain a steady axial load at an applied deformation. With the application of direct axial load there was a decrease of column moment. This was attributed to the development of plasticity within the column because of the increased direct axial load and the consequent increase in column end rotation.

In their subsequent detailed appraisal **[8]**, Moore and Nethercot proposed modifications to current design principles that take into account the contributions from the semi-rigid connections. The methods more accurately predict actual behaviour that can result in savings in construction.

The usual practice for multi-storey design is to use either simple or continuous construction. Simple construction assumes that all resistance is provided by a system of braced bays, cores, shear walls or rigid frames, with the main steel work designed to withstand gravity loading only. Continuous construction utilises the main framing to resist both lateral and gravity loading. This produces a greater degree of interaction between the members.

Simple construction is easy to design, as each member can be treated separately. The rigid connections used in continuous design are expensive to construct and the savings in steel over simple construction are not considered sufficient.

The authors introduced a design method using their earlier experimental results. The method is based on the traditional design approach for simple frames.

- **Design of major-axis beams**

The beams are designed for strength using a plastic approach. In the case of a beam with constant cross section and subject to a uniformly distributed load the plastic section modulus is given as:

$$Z_p = \frac{wL^2}{2(1+k)P_y}$$

Where:

w is the intensity of the uniformly distributed load.

L is the length of the beam.

k is Mj/Mp (Mj is the moment capacity of the joint, Mp is the plastic moment capacity of the beam.

p_y is the yield strength.

The above assumes that adequate bracing is supplied for the beam and that the connections have sufficient rotational capacity.

The problem with the method is finding a suitable value for k. The authors suggest a value between 0 and 0.25 for weak connections (top and bottom cleats, flexible endplates, flush endplates and finplates) and between 0.5 and 1.0 for heavier connections (extended endplates).

- **Serviceability**

If the rigidity factor is known then the following can be used to calculate the deflections at serviceability.

$$\delta = \delta_s - R[\delta_s - \delta_r]$$

Where:

δ_S is the calculated beam deflection assuming simple supported ends.

δ_r is the calculated beam deflection assuming fixed ends.

R is the rigidity factor for the joints.

- **Column design**

Semi-rigid connections influence the load-carrying capacity of a column in two ways. The moment capacity of the connections is greater than that assumed by the traditional approach, so these moments need to be incorporated into the design; and the restraint from the connections has a beneficial effect, reducing the effective length of the column and therefore increasing its resistance.

The major-axis column moments should be calculated as:

- **For an external column**

$$M_c = M_J + \frac{wL}{2}\frac{d}{2}$$

- **For an internal column with an unbalanced arrangement of beams and loads**

$$Mc = (M_{JL} + M_{JR}) + \left(\frac{w_1 L_1}{2} \frac{d}{2} - \frac{w_2 L_2}{2} \frac{d}{2} \right)$$

These proposed calculation methods predict actual behaviour more accurately to the method currently given in BS5950.

Composite construction offers the benefits of having the concrete floor slab in compression, with the steel section in tension; this substantially increases the moment capacity over when the materials are used separately. The problem with the system is then how to detail the beam/column/slab area. Present practice is to provide only light anti-crack reinforcement, and to detail the beam-to-column connection as a simple connection.

Li, Moore, Nethercot and Choo **[9]** believe that elastic theory is inappropriate due to the incompatibility of the high support moments and the lesser resistance of a composite beam in hogging. Plastic hinge theory requires substantial degrees of plastic rotation from the beam in the support region if the full sagging moment capacity is to be developed in the span. The authors' 1996 paper therefore looked towards 'semi-continuous framing' using semi-rigid connections.

Analytical work has sought to establish the rotational requirements of the connections so that degrees of moment distribution may be achieved in non-sway composite frames. This has resulted in a quasi-plastic approach that has much in common with the plastic hinge method for steel frames. The difference is that the rotations for moment distribution now take place in the connections.

The paper contains the first major experimental study of semi-rigid joint action in a complete frame. The test frame is shown in Figure 2.2 below.

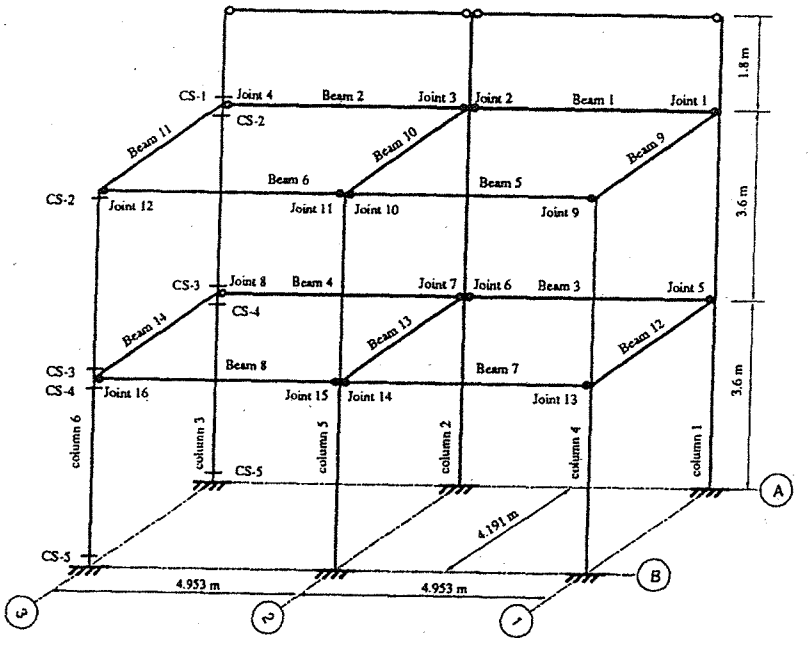

Fig. 1. General layout of the frame specimen.

Figure 2.2 Semi-Rigid Frame Used in Testing

The frame can be divided into two, two-span, plane frames. One frame has the beams connected to the major axes of the columns; the other frame has the beams connected to the minor axes of the columns. As the study was mainly to investigate the semi-rigid connection effects on the frame, a finite width of concrete slab was used instead of a full slab layout. This made the load path clearer.

Flush endplate connections were used for all the beam-to-column connections. The frame is non-sway, so horizontal constraints were used at each floor level.

The frame moment distribution was based on strain measurements taken in the columns, as the steel stress-strain relationship is well defined, and the columns were designed to remain elastic for the beam loading stage. From the measured strains the column moment and axial force distributions can be determined. By incorporating the applied beam loads and free bending moments of the beams it is possible to calculate the moment distribution for the beams. Beam strains were also measured at one of the point load sections to obtain the strain distribution of the composite beam section.

Inclinometers were used to measure rotations of the connections. Displacement transducers were used at quarter points to measure beam deflection. Vertical displacements were also measured at the connections so that the absolute deflections could be obtained. Shear slip was measured using small range displacement transducers.

In the first frame, with the beams connected to the major axes of the columns, one of the top storey beams failed first. This failure was from large vertical deflections and local buckling of the lower flange. It was also seen that failure had started to take place on the other beams at the lower flange through local buckling. Column web horizontal deformations were also visible at all the connections.

In the second frame, with the beams connected to the minor axes of the columns, one of the lower storey beams was the first to fail; this was triggered by local crushing failure of the concrete slab. This occurred at one of the connections, suddenly reducing the moment capacity, and redistributing the moment to the beam span. This resulted in the beam failing suddenly and the test had to be stopped.

The crushing failure did not occur in the previous frame, which may have been due to lack of vibration and tamping owing to the concrete being inside the column flange.

The paper concludes that failures were generated in a variety of components: local buckling of the beam compression flanges adjacent to columns; crushing of the slab adjacent to columns for the joints subject to highly non-symmetrical moments; and local failure of columns.

Li, Moore, Nethercot and Choo published a more detailed appraisal of their experimental results in 1996 **[10]**, including conclusions for design principles.

It was found that the moment distributions from the experiments with composite frames differed greatly from those from analysis of rigid or pinned connection frames. So neither approach is appropriate for semi-rigid frame analysis. The research found that appropriate analyses are moment distribution and quasi-plastic analysis.

The moment capacities for the connections in the frame were lower than those found in the isolated joint tests. This could have been due to the unbalanced loads in the frame tests.

The linear strain distribution assumption is true for composite beam sections subject to low moments. It is not true for higher moments when the beam approaches the ultimate load and yielding starts to occur.

The serviceability calculations from BS5950 are smaller than those found in the experiments. This was because of the yielding that started to occur in the test when deflections reached L/340.

Yield and ultimate moment capacities of the beams were accurately predicted by BS5950, with the predicted values being more conservative.

Quasi-plastic analysis gave the closest predictions to the experimental results, and the authors recommend that this be used for the design of semi-rigid non-sway composite frames. The quasi-plastic method also does not require the time-consuming integrated structure analysis to be carried out.

The design steps for the quasi-plastic method are as follows:

- **Step 1:** Select beam size and connection from previous experience.
- **Step 2:** Calculate the load carry capacity of the beam.
- **Step 3:** Check if capacity is greater than factored imposed load. Repeat steps 1 and 2 until it is satisfactory.
- **Step 4:** Calculate column internal forces from moments and shear forces at connections. Determine section size using codes.
- **Step 5:** If pattern loading is required then the effect can be conservatively considered by reducing the moments of the connections with dead load to half their design moments.

Further guidelines for using semi-rigid connections in braced frames were discussed by Jaspart and Maquoi **[11]**. The authors comment on the second order effects on the

behaviour of braced frames, saying that the axial forces on the columns decrease the flexural stiffness, and have an influence on the bending-moment diagram which could cause a premature collapse of beams or beam-to-column connections. Snijder and Bijlaard **[12]** state that the second order effects can be neglected when the beam-span to column-height ratio is larger than 1.0, or when the moment capacity of the beam is larger than that of the column.

Jaspart and Maquoi say that the frame should be designed using a first-order linear elastic analysis, and then the designer should check that the second-order effects in the frame at collapse do not exceed the plastic moment capacity of the beam, or the connections. For the analyses presented in the paper, a straightforward bi-linear curve is used for the representation of the beam-to-column connection. The column base is assumed to be fully fixed. A 5m x 5m frame, restrained against sway loading with a uniformly distributed load on the beam section, shows that the collapse using a first-order analysis is from buckling in the column, followed by yielding of the beams and connections. A second-order analysis shows that there is an influence from the axial loads in the columns on the bending moment in the beam and connections, which could cause plastic hinge to occur in the beam section.

Liew et al produced two papers **[13, 14]** on the limit state design of semi-rigid frames using advanced analysis. The works presented in reference 13 are the models that are suggested for representing different forms of connection. The models are an adaptation of the three-parameter models proposed by Kishi (presented below) **[15]** for connections made using angles. The authors' second paper **[14]** uses the model of the connection for commenting on frame design. The connections are introduced into a plastic hinge design method, and a design method is proposed. The design method is as follows:

- Design the frame as if it had rigid connections.
- Select the connection that is to be used and find its initial stiffness and moment capacity.
- Check the ductility of the connections.

- Perform a second-order inelastic analysis of the frame using the semi-rigid connection properties.
- Check limit states.
- Repeat the analysis to find the most cost-effective sections for the frame.

This design method does create more work for the designer, increasing the design time for the building. In a design example given in the paper, connection stiffnesses between 9.8 and 88kNm/mRad are used. The authors use the example to show that the design method can be used for ultimate and serviceability load states, but they do not compare the cost of the final structure against that of a conventionally designed simple or fixed frame. The example in the paper was a simple frame, and a more complex structure would be much more expensive to design, both for the designer and in terms of computer time. The three-parameter power model is also used by Christopher and Bjorhovde in their research **[16]**.

A further paper by Liew et al **[17]** covers the testing of semi-rigid unbraced frames. The researchers carried out tests on both frames and individual connections, to see if individual connections behave in the same way when they are a part of a frame. The frame tests are compared to the results from second-order inelastic analysis. Ten unbraced, single-storey, single-bay, portal frames, eleven connections, and two column bases were tested in the program. The types of connection tested were top-seat-double-web angle, and extended end-plate connections.

It was found that most of the frames failed due to significant deformation in the connections, leading to frame instability. One of the frames failed due to distortion of the beam-to-column connection, and a plastic hinge forming at the top of one of the columns. This frame had full-strength connections, and the column moment capacity was smaller than that of the beam. The researchers comment that the extended end-plate connections behave differently under hogging and sagging. It is believed that these are the same tests as those described in the paper in the next section by Yu et al **[18]**.

For the tests of the connections, six end-plate connections, and five bolted angle connections were tested. For the test the column was pin connected at each end, and a cantilever test arrangement was used for the beam section. Each test for the end-plate connections was conducted twice, with the end-plate being extended either at the top or the bottom of the connection. The initial stiffnesses for the connections were found to be from 5.308kNm/mRad to 51.387kNm/mRad, with rotation capacities from 71.85mRad, for a specimen with no lateral torsional buckling bracing, to 190.37mRad. The tests for the end-plate connections found that those with the plate extended at the top of the connection could be classified as full-strength, whereas those with the plate extended at the bottom of the connection could be classified as semi-rigid. Moment capacities for those extended at the top were 27-70% higher than those extended at the bottom, and the initial stiffnesses were 225-288% higher. The tests for the angle connections showed that the initial stiffness remained constant for about 15%-18% of the ultimate moment. The stiffness decreased rapidly after this point, but was still almost linear in behaviour. The column base tests gave initial stiffnesses of around 25kNm/mRad. The initial stiffness was tested by applying a point load of 500kN to the top of the columns, and then applying a horizontal load until failure. It was found that the analysis used for the theoretical results generally underestimated the collapse load of the frame.

2.3 Analysis of Semi-Rigid Connections

Johnson and Hope-Gill were among the first to design a method of using a semi-rigid connection in composite frames **[19]**. They believed that neither simple nor rigid beam-to-column connections were ideal. Simple design assumes discontinuity between two beams supported at the same column. It also assumes that moment transferred to the column is small. However, this can be incorrect if reinforcing crosses the column, as for two-way floor systems, or from crack-control reinforcement. If both beams are loaded to flexural failure, then cracking ensures that little of the force is transferred to the column by compression of the column flange. The worst case for the column is if one beam is unloaded: then the other beam will have a large compressive force in the bottom flange, and the column will largely resist this. This leads to an inefficient

column design. To solve the problem the rigidity of simple connections could be reduced and the crack-control reinforcement limited.

Rigid connections are made by welding or friction-grip bolting. The beams are then designed as continuous, using plastic theory. This only works well for the collapse limit state for beams of compact cross-section. Negative moment regions have inadequate rotation capacity, and each yield at a load which is too low a proportion of the plastic collapse load for the beam as a whole. Rigid connections are also expensive for materials and labour.

It is for these reasons that the authors developed a design for a semi-rigid connection with a large rotation capacity and a predictable flexural strength.

Experiments carried out on the semi-rigid connection showed that they provide a well-defined stiffness and moment of resistance at the support. This can result in smaller beam sections, and is cheaper than a fully rigid connection. The semi-rigidly connected members have greater resistance to buckling and much greater rotation capacity than rigidly connected members.

Johnson and Hope-Gill also commented that strain hardening can occur in the negative moment regions before the design collapse load of a continuous beam is reached.

Wong and Mak **[20]** modelled connections as rotational springs in order to be able to classify them. A 2m x 2m steel frame was set up, and tested under dynamic and static loading. Three types of connection were used in the experiments, T-stub, web-seat angle, and web-T. The authors comment that a rotational spring gives a good representation for the connection. Their final results show connection stiffnesses of around 2.5 – 5.5kN/mRad, but the section sizes used in the frames are very small. The research by these authors seems very brief, with only one section size being tested in the frame, UB203x133x25kg, and UC152x152x23kg.

Ioannides and Tarpy **[21]** have conducted research into semi-rigid beam-to-column end-plate connections. The authors comment that frame analysis can be conducted using the stiffness method, using springs for the connections, but there is a lack of data

for the M-ϕ curves for the connections. The researchers used a finite element model for the production of M-ϕ curves. The construction of the model is explained in detail in the paper, but is not relevant to this thesis. The authors state that it is possible to represent the connection as a linear spring for most analyses, with the spring stiffness being the gradient of the M-ϕ curve. Unfortunately the authors do not give a table of stiffness values found from the numerical models. In an example calculation, they give a value of 734,690 kip-inch/Rad (83kNm/mRad). The researchers use this value for the analysis of a five-storey, three-bay frame. They find that the end-moments of the beams are reduced by 6% to 12% from those for a fixed connection, and the column moments range from 12% lower to 14% higher than those in the frame with fixed connections. Deflections were shown to be greatly affected, with the sway deflections increasing by 20%, and beam deflections increasing by 30% for exterior and 50% for interior beams.

Cunningham **[22]** demonstrates the use of semi-rigid connections in steel frameworks, and a 'fixity factor' that can be used in the design of the frames. The author comments that the M/ϕ curve for the connections can suitably be simplified as a linear stiffness model for the use of design, instead of the non-linear characteristics that are found during experimentation.

The fixity factor defines the stiffness of the connection relative to the beam section. The fixity factor is the ratio of the rotation of the end of the beam with a unit end moment, to the rotation of the beam plus the connection for the same moment. This gives a fixity factor of 0 for a pinned beam, and 1 for a fixed beam.

The author comments on the use of semi-rigid connections for several frame types, by using moment distribution and the fixity value for the connections. For single-storey portal frames, it was found that the sway deflection was greatly reduced as the fixity of the column base was increased. For braced multi-storey frames, the author finds that the weight of the structure could be reduced, at the cost of design time, by utilising the semi-rigid relationship of the existing connections. However, careful checking of the columns would have to be carried out, due to the transfer of the bending moments. (In fact, as the connections are semi-rigid anyway, perhaps this checking should already be

done.) For unbraced, low-rise multi-storey frames, the author comments that if the connection is over-designed, there is a danger that the connection will attract more moment to the column and the columns could be overstressed. However, if the connections are not assumed to be stiff enough, the frame will tend to sway more, causing problems for serviceability.

To simplify the connections it is suggested that a linear spring is used, as this gives adequate accuracies for the design of frames using semi-rigid connections.

Kishi et al **[23, 24]** discuss of the behaviour of tall frames combining rigid and semi-rigid connections. A frame of 4 bays and 8 storeys is numerically analysed by the researchers. The frame was analysed four times, with different combinations of semi-rigid and rigid connections. The authors found that all combinations tried gave a sway deflection of $\Delta/H < 1/400$, allowing semi-rigid connections to be rationally used in tall frames. The four combinations of connections that the researchers used are shown in Figure 2.3 below.

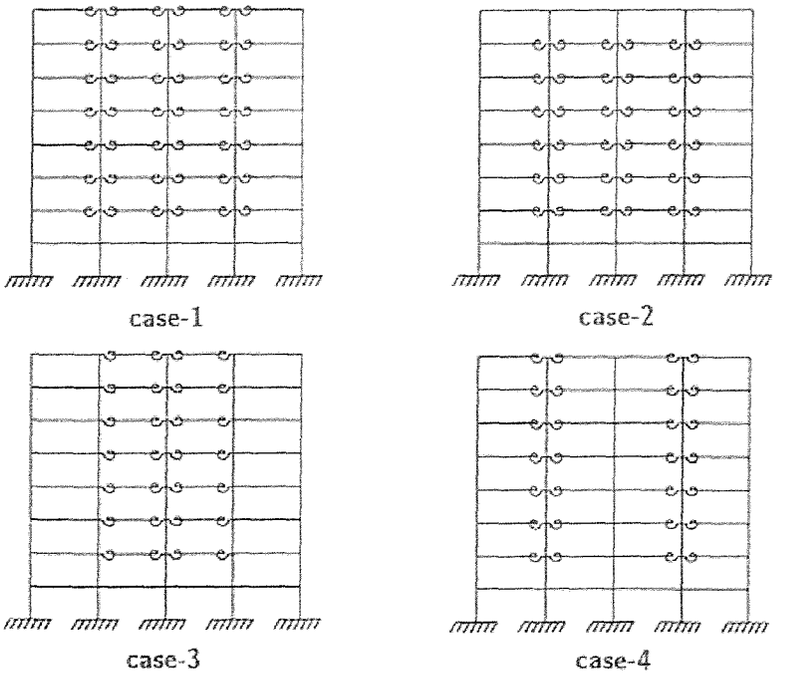

Figure 2.3 Connection Combinations Used by Kishi et al

It was found that cases 1 and 2 gave very similar results, showing that the connections on the roof beams may not add to the overall sway stiffness. Although cases 3 and 4 contain the same number of semi-rigid connections, it was found that case 4 gave a stiffer structure against sway loading. The final results from the analysis gave:

Rigid Frame: $\Delta/H = 1/880$

Case 3 and 4: $\Delta/H < 1/400$

Case 1 and 2: $\Delta/H < 1/500$

So although the authors state that it is possible to use semi-rigid connections in tall buildings, their results do show that the sway deflection is greatly increased when these connections are used. This could add complications to the design of the buildings. The authors do not state why the positioning of the semi-rigid connections affects the sway deflection of the frame, and they do not comment on the effects of the connections on beam deflections.

Guo-Qiang and Mativo **[25]** presented work on the approximate estimation of the maximum load of semi-rigid steel frames. Their simplified method, for use in the design office, is in the form of a multiple linear regression relationship between the maximum load and frame and section properties. Numerical analysis is used to obtain the results. Again the authors have used a rotational spring element in the modelling to represent the beam-to-column connections. The loading on the frames is added in small increments, as the frame behaviour is non-linear, due to the rotational spring relationship. For the plastic analysis the steel sections are assumed to yield with ideal plastic hinges, between these hinges the steel is assumed to behave elastically. An existing computer program was adjusted to allow for the semi-rigid analysis. There are several assumptions made in this unknown program. It does not allow for any out of plane loading or stability; plastic hinges are assumed to have a zero length, it does not allow for local buckling, or shear stresses; all members are considered to be ideally straight, it does not allow for lateral bracing; and it does not deal with serviceability. Plastic hinges are checked for at the mid-span, and at the nodes only. The authors do not comment on the numbers of nodes used, but they could only be at the connections.

An initial stiffness of 684,600 in-kip/Rad (77.35kNm/mRad) was used in the analyses. A three-storey, one-bay frame was analysed in order to verify the model. To find the parameters that had most effect on the behaviour of the frames, the authors modelled a number of different frames with fixed column base connections. They find that by increasing the number of bays of the frame, the overall load carried by the structure increases. An increase in storey number decreases the overall load carried by the structure. Increasing the length of the beams decreases the load, as did increasing the length of the columns. Increasing the second moment of area of the beams and columns increased the load carried by the structure. Many of these observations are surely what the researchers expected, and are true for pinned and fixed frames.

Linear regression was carried out on the results from the analysed frames, for frames with varying section length and second moment of area, varying number of bays and number of storeys, with the load carried by the frame to failure. Failure is classified as the point at which either the column buckles, or the frame forms a mechanism. The research in this thesis shows that not all these relationships are linear. The examples given in the paper show errors of up to 22%; they list an accuracy of +20% to –20% from comparing their simplified approach to the results from the computer program. The R^2 values for the linear regression were between 0.75 and 0.86, showing that there could be problems extrapolating the data beyond that used for the regression analysis. The authors do comment that the errors became larger when the frames went beyond 9 storeys.

The calculation of serviceability deflections for non-sway frames with semi-rigid connections was researched by Gibbons et al **[26]**. The technique to calculate the connections assumed that the frame followed elastic behaviour, and that the connections had a linear stiffness. The paper presents equations for the support rotations, for beams with a uniform load. The rotation at the beam ends was given as being:

$$\phi_b = \frac{wL_b^3}{24EI_b} - \frac{M_{sr}L_b}{2EI_b}$$

The column rotation is given as:

$$\phi_c = \frac{M_{sr} L_c}{6EI_c}$$

$\phi b - \phi c$ then gives the total rotation of the connection. The researchers go on to show an equation that gives the total deflection at any point along the beam. The equation is validated by an experiment on a three-storey, two-bay frame, the results of which are compared to the results from analysing the frame as if it were simply connected, and rigidly connected. The deflections from the experiment were slightly higher than those from the theory presented, but the results were closer to those for semi-rigid connections than either for pinned or rigid connections. The beam-to-column stiffnesses found during the experiment were between 1.3 and 90.9kNm/mRad. Beams were UC254x102x22kg, and columns were UC 152x152x23kg, with spans of 4953mm, and heights of 3600mm.

A design aid for semi-rigid connections for frame analysis was developed by Kishi et al **[15]**. The design aid aims to give values for the initial stiffness of connections, the ultimate moment capacity, and a shape parameter. The researchers looked at four connection types; single web-angle connections, double web-angle connections, top- and seat-angle with double web-angle connections and top- and seat-angle without double web-angle connections. The theory they used to produce the formulae is not relevant to this research, and so is not listed here. The researchers present a numerical analysis of a frame using semi-rigid connections, using the presented model for the connections. However, the values used for the connections are not stated in the paper. Reading from their graphs suggests a beam-to-column stiffness of up to around 12kN/mRad, though end-plate connections are stiffer. The frame analysis carried out by the researchers does not add anything to the other papers discussed in this chapter - it is really only used to demonstrate the model used for the connection, which is made up of the initial stiffness and ultimate moment for the connection.

Yu et al **[18]** tested ten sway frames with end plate connections up to collapse load. The experimental results were compared to those from theory. The test frames are single-storey, single-bay frames. Different column-to-beam stiffness ratios, and

different end plate thicknesses were used in the frames. A refined plastic hinge analysis was conducted for the test frames. The power model proposed by Kishi and Chen was used to represent the beam-to-column connections **[5]**, and this was applied to a rotational spring. For the experiments the vertical load and horizontal loads were applied proportionally until a chosen vertical loading was reached. Then the horizontal load was increased until failure was reached. In the first test, where the column-to-beam stiffness ratio was 0.5 and the end plate thickness was 30mm, this caused a hinge to form in one of the columns, and then partial yielding of the connections. The connection in this case had an initial stiffness of approximately 55kNm/mRad. A further test, with column-to-beam ratio of 1.0, and end plate thickness of 25mm caused a hinge to form in the beam, near to the connection. A third frame with column-to-beam stiffness ratio of 2.0, and a 20mm end plate thickness failed due to instability with no plastic hinges forming. It was also found that end plate connections behaved differently in hogging and sagging. In contradiction of some of the other papers reviewed here, the researchers state that the theoretical results can compare well with those from experiments if the connection is carefully modelled. It was also found that the stiffness of the column base greatly affected the sway behaviour of the frames. This would become more critical as the height of the structure was increased as the second order effects would be greater. Although the researchers have studied ten frames, only three of them are described in the paper.

Anderson and Benterkia **[27]** analysed semi-rigid steel frames to find some criteria for their design. A program using the stiffness method is altered for the design, so that the connections can be added. The connections are represented by multi-linear rotational springs. Stability functions are used to take second-order effects into account. In the analysis the second-order effects are ignored if the elastic critical load is greater or equal to ten times the design load, as these were found to affect the sway deflection and bending moment by less than 12%, except for the more flexible frames. The researchers found that under normal combined loading it would be the sway deflection that controlled the design, and not the ultimate strength of the frame.

Ahmed and Kirby **[28]** researched into semi-rigid non-sway frames to find the maximum connection rotations. Finite element analysis was used by the researchers to model the semi-rigid frames. The models were solved until they no longer converged -

the load step before that was taken as being the ultimate load for the frame. The results were shown to fit well with a test frame. The finite element model was of a three-storey, two-bay, non-sway frame. A parametric study was then carried out covering connection behaviour, geometric dimensions, and loading. The steel properties were taken as being perfectly elastic-plastic, with the yield stress as 285N/mm^2 and the modulus of elasticity as 210kN/mm^2. It was found that the behaviour of the flange cleat, flush end plate and extended end plate connections were similar, although the stiffer connections had a smaller rotation. It was found that rotations at the point of frame failure were less than 18mRad. The level of imperfection in the frames did not significantly affect the final rotation of the columns. The larger rotations were for the flexible flange cleat connections, and longer beam sections. The M-ϕ curve up to this point for most connections is linear, so this shows that a linear approach to approximating the semi-rigid connections is justifiable.

Li, Choo and Nethercot developed a general procedure for incorporating the effects of joint flexibility into standard methods for the analysis of frames **[29]**. Their paper applied the method to several examples using moment distribution technique, slope deflection equations, and matrix stiffness method.

Several techniques had been used previously to incorporate the effects of joint flexibility. These include the graphical method, for which the M-ϕ curve must be known, and methods for slope deflection and moment distribution. By the 1960s the matrix stiffness method of structural analysis had been established, utilising the increase of computer power. The effects of semi-rigid connections could be incorporated into the matrix stiffness method by modifying the beam stiffness matrix. To establish the dynamic behaviour of semi-rigid frames, equivalent springs have been used.

All these methods incorporate the semi-rigid connection characteristics into modified beam elements. This means that the resulting beam slope-deflection equations, beam stiffness and carry-over coefficients, and the beam stiffness matrix would all differ from those in the conventional approach. Li, Choo and Nethercot wanted to analyse

semi-rigid frames using conventional analyses, but to treat the connection as an independent element.

In their research the semi-rigid connection is modelled by a multi-degree spring element. The advantages of using a connection element are as follows:

- As the connections are considered separately from the other members in the slope deflection and moment distribution analyses, there is no longer the need for complex coefficients and equations.
- The use of connection elements in matrix stiffness analysis does not require any modifications to the stiffness matrices of the beams and columns to establish connection effects.
- It is easier to consider the shear and axial deformations of the connections.
- Neglecting the connection length has very little influence on the column buckling capacities, especially for non-sway frames.
- Due to the increase of computer storage it is not a problem that this method increases the number of nodes and elements used.

Yau and Chan's 1994 paper **[30]** presents a beam-to-column element with springs connected in series for efficient and effective geometric and material nonlinear analysis of steel frames with semi-rigid connections. The models have been used to find the effects of semi-rigid connections and material yielding. Proposed mathematical models for different joint types and assumed patterns for material yielding have been simulated independently. The paper proposes a simple method to trace the equilibrium path of steel frames, allowing for geometrical, material, and joint stiffness nonlinearities up to the ultimate load.

An efficient and user-friendly computer method is essential for the promotion of analysis of steel frames that accounts for semi-rigid connections for engineers in practice. The paper presents a technique for developing an element with ends having a pair of springs connected in series, for incorporation into linear and nonlinear analysis. Experimental data on the stiffness of various types of joint can be fed into the analysis program. The degrading curve for the various sections, due to the spread of plasticity

across the section, can also be incorporated into the program independently of the connection details. Figure 2.4 below shows the element.

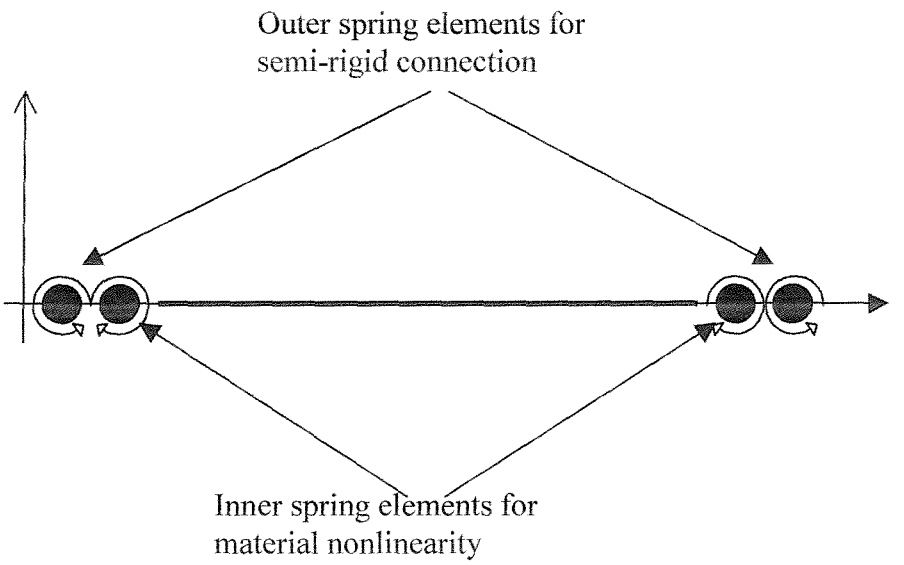

Figure 2.4 Beam-to-Column Element with Springs in Series

The paper presents some numerical examples where the element has been used, as follows:

- **Inelastic analysis of a portal frame.** It was found that the material yielding affects the ultimate load, and the postbuckling behaviour of the structure. For rigid connections the elastic buckling load for the frame was $1.80EI/L^2$. With the nonlinear material properties included this fell to $1.49EI/L^2$. For the semi-rigid example the load fell from $1.49EI/L^2$ to $1.39EI/L^2$.

- **Two-storey frame with fixed supports.** An exponential model describes the nonlinear moment-rotation behaviour of the beam-to-column connection. For this analysis the elastic stability loads fell from 11,260kN for connections and 7,230kN for semi-rigid connections, to 2,060kN for rigid and 2,040kN for semi-rigid connections, when material yielding was taken into account. This shows that the frame's ultimate load capacity is controlled by material yielding, due to the

similarity of the results after material yielding is considered. The consideration of material yielding is indispensable to the accurate analysis of a typical steel frame.

- **Six-storey two-bay frame with semi-rigid connections.** The six-storey frame has proportionally increasing distributed gravity loads and concentrated lateral loads. The frame has been analysed previously by Vogel **[31]**; his analysis assumed all the connections to be rigid, with a frame imperfection of 1/450 of the storey height. Yau and Chan's paper presents the results for four different types of connection - extended end plate, flush end plate, top and seated angle with double web cleats, and a single web angle - to study the influences of semi-rigid connections on the inelastic structural response of the six-storey frame. In this example the frame is more sensitive to the joint type than in the last examples. This is because the loading is applied uniformly as opposed to point loading, which results in larger moments at the connections. The load-deflection results for all but the very stiff extended end plate example do not follow those for the rigid connection assumption, so this assumption cannot be used for the other connection types.

The authors then investigate the assumption of linear joint stiffness to see if it can be adopted in the design of semi-rigid jointed frames. Again, for all but the stiffest connection, this assumption is shown to be insufficient. However, it is suggested that the secant stiffness may be used for practical design allowing for semi-rigid connections and based on the linear assumption; this would allow for the reduction in joint stiffness at large joint rotations.

Li, Choo and Nethercot **[32]** have developed a method for the calculation of the necessary joint rotations to permit the use of moment redistribution for the design of semi-continuous steel and composite frames. A quasi-plastic approach to design is used. This design approach regards the joint rotations as being composed of an elastic and a plastic part and determines each contribution separately. The plastic calculations were calibrated against test results.

The required rotation θ_r is divided into the elastic rotation θ_{er} and the plastic rotation θ_{pr}. The elastic rotation is expressed by:

$$\theta_{er} = \frac{M_d L}{EI} f_u(\alpha, \beta, \gamma)$$

Where:

$\alpha = M'_1/M_d$

$\beta = M'_2/M_d$

$\gamma = EI'/EI$

M_d = mid-span design moment

M'_1 and M'_2 are the support moments

EI' and EI are the stiffnesses of the hogging and sagging cross-sections.

The plastic part of the required rotations is caused by the mid-span plastic deformation. If M_d is less than the yield moment then no plastic deformation will occur and therefore the section is slender or semi-compact. The plastic rotation requirement at the support is given as:

$$\theta_{pr} = \frac{L - L_m}{L} \theta_{pq}$$

Where:

L = Beam length

L_m = position of hinge

θ_{pq} = plastic part of the mid-span rotation that occurs at M_d

θ_{pq} is dependent on the magnitude of curvatures at the mid-span design moment, the beam span and the load arrangement. There are empirical formulae for the beam curvatures.

An example of a uniformly loaded beam is used to show how the value of θ_{pq} is found. Figure 2.5 below shows the example beam.

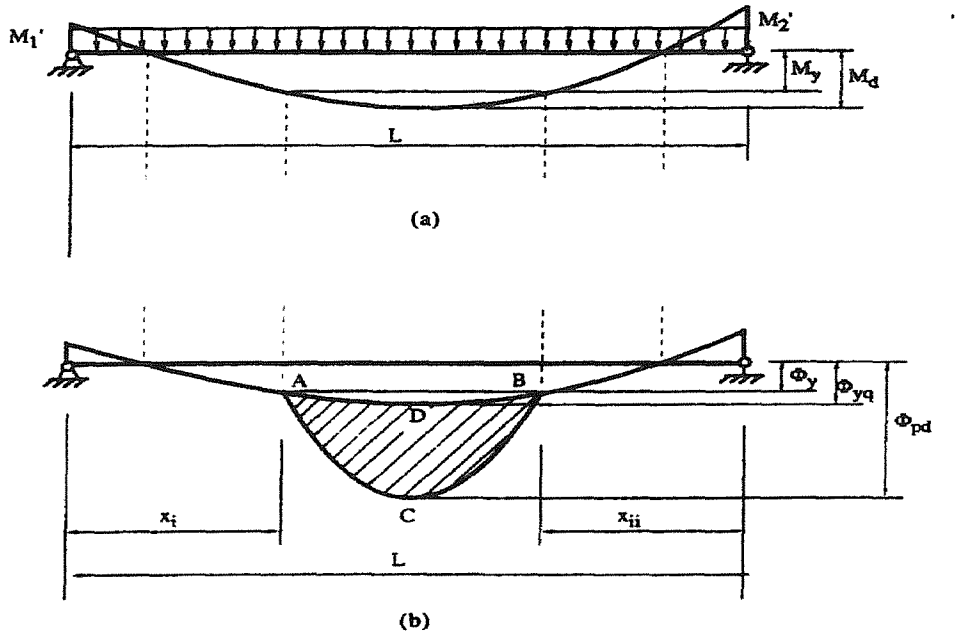

Figure 2.5 Beam Example to Show θ_{pq}

Diagram (a) shows the load and moment diagram and diagram (b) shows the curvature distribution.

From (b) the quasi-plastic rotation at mid-span is equal to the area of the semi-circle ABC. ABD has already been considered in the elastic analysis. So the effective area is found by the shaded area ABCD and θ_{pq} is given by:

$$\theta_{pq} = 0.533(L - x_i - x_{ii})(\phi_{pd} - \phi_{yq})$$

Where $\phi_{yp} = M_d/EI$ is the quasi-yield curvature.

The paper presents similar analyses for a single point loaded beam, and a beam with two point loads.

The characteristics of a frame and its connections are non-linear, and the current studies of analysis and design aim to incorporate such semi-rigid concepts into the models. There are a large variety of connections in use in practice, and it is not feasible to utilise the properties of individual connections. Bjorhovde, Colson and Brozzetti **[33]**

developed a scheme in 1990 to enable the classification of connections in term of strength, stiffness, and ductility. Testing and theoretical data were used to achieve this. The authors also considered some special cases, such as connections with softening-stiffening characteristics, connections with low ductility, and connections with properties that vary as a function of the applied load. The classification system that this research has produced can be used to add new connection types to the current database.

The classification system incorporates the three basic joint types: (1) flexible connections (pinned); (2) rigid connections (fixed); and (3) semi-rigid connections. For the research the M-Φ diagrams are simplified into linearised regions. These simplified M-Φ diagrams are also useful as then the results can be used for ultimate and serviceability limit state designs. The classification system that is developed is meant for use with semi-rigid beam-to-column connections in steel structures.

For the experiments the authors used beams with a length equal to five times the depth of the beam, as this was found to place the connection in the middle of the semi-rigid range. A value of $0.2M_p$ is taken as being the boundary between flexible and semi-rigid, and $0.7M_p$ as being the boundary between semi-rigid and rigid connections. Figure 2.6 below shows the final classification system.

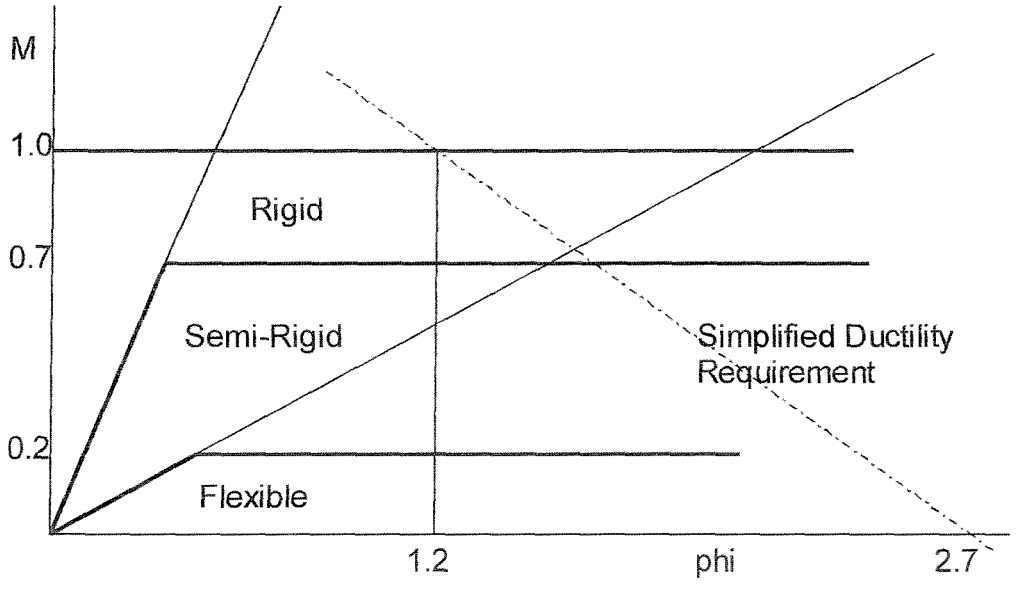

Figure 2.6 Connection Classification System

The simplified ductility requirement is based on the magnitude of the rotation capacity. This diagram can be used with any beam-to-column connection for steel structures to determine its stiffness, strength and overall ductility characteristics.

2.4 Column Bases

Aristizabal-Ochoa's 1994 paper **[34]** presented two formulas to evaluate the stability K-factor (slenderness factor) of columns with semi-rigid connections. The design formulas account for the rigidity of the connections as well as intermediate axial loads along the height and concentrated end loads. The formulas can be applied to cases of unbraced and partially braced columns. The formulas have been tested against analytical results.

The design examples used to demonstrate the formulas were a symmetrical frame with side sway and a partially braced frame (diagonal truss bracing).

The formula for K is as follows:

$$K^2 = \frac{\{40+8(\rho_a^2+\rho_b^2)+\rho_a\rho_b(\rho_a+\rho_b+3\rho_a\rho_b-34)+\gamma[20+10(\rho_a-\rho_b)+3\rho_a^2+5\rho_b^2-\rho_a\rho_b(3\rho_a-4\rho_b-1.5\rho_a\rho_b+17]\}}{\left[3(4-\rho_a\rho_b)(\rho_a+\rho_b+\rho_a\rho_b)+\frac{5(4-\rho_a\rho_b)^2}{2\pi^2}\frac{S_\delta}{\frac{EI}{h^3}}\right]}$$

For the case of a column under a heavy uniformly distributed axial loading q, and light end load P the following equation is proposed:

$$K^{*2} = \frac{[20+10(\rho_a-\rho_b)+3\rho_a^2+5\rho_b^2)-\rho_a\rho_b(3\rho_a-4\rho_b-1.5\rho_a\rho_b+17)]}{\left[3(4-\rho_a\rho_b)(\rho_a+\rho_b+\rho_a\rho_b)+\left\{\begin{matrix}\frac{5}{2}(4-\rho_a\rho_b)^2S_\delta h-P[40+8(\rho_a^2+\rho_b^2)+\\ \rho_a\rho_b(\rho_a+\rho_b+3\rho_a\rho_b-34)]\end{matrix}\right\}\frac{h^2}{\pi^2EI}\right]}$$

Where:

K = Slenderness factor

ρ_a, ρ_b = fixity factor at column top and base respectively

h = column height

E = Young's modulus for the column material

I = second moment of area for column

These are long formulas but they could be input into a computer. It is also necessary to know the column connection rigidity.

Column bases are usually modelled in a very simple way. Displacement constraints are applied to the bottom nodes of the first storey columns. This means that the column bases are either completely fixed, with the nodes restrained from rotating, or ideally pinned with the nodes allowed to rotate freely. In reality the column bases act as being semi-rigid. The strength, stiffness and deformation capacity of the column base depends on the design procedure and the adopted detailing of the base.

Stojadinovic, Spacone, Goel and Kwon's paper **[35]** presents a parametric study evaluating the consequences of using semi-rigid models for moment-resisting column bases. Two three-storey MRF steel frame buildings designed according to U.S codes were modelled using the finite element software packages SNAP-2D and FEAP. The column bases were modelled as rotational springs. The stiffness of these springs could then be varied to represent a range of semi-rigid behaviour from virtually rigid to virtually pinned.

The data used to model the column bases comes from a finite element analysis using the ABAQUS software package. These models showed that with an unrealistically thin base plate the connection could be classified as pinned. However, even with an unrealistically thick base plate the connection never reaches the stiffness required to classify the base as rigid.

The final frame models analyse the effects of bases from pinned to fully fixed, with six intermediate stiffnesses. These stiffnesses are associated with column bases with plate thickness of 25, 50, 75, and 100mm.

Pushover analyses are used to compare the strength and stiffness of different frame models, and the plastic hinge formation sequence and deformation mechanisms are also found. A seismic study is also carried out using a time-history analysis. The seismic analysis gives information on inter-storey drift and roof displacement.

The paper concludes that the rotation demands on the first-storey beams and connections increase as the stiffness and strength of the column bases is reduced. The fixed-base frame has a uniform rotation demand distribution along its height. As the column base becomes less rigid the rotation demand distribution shifts towards the first floor beam.

There may be an unintended reduction in column base stiffness, which may be due to poor workmanship, long-term deformation and deterioration of the foundation concrete, or the effects of previous earthquakes.

The behaviour of the fixed-base frame is representative of the behaviour of the models with realistic semi-rigid column bases. Therefore the use of fixed-supports to model the bases in moment resisting steel frames may be justified.

2.5 Finite Element Analysis of Frames

Mei-xin, Nethercot and Li **[36]** used the finite element software package ABAQUS to analyse the full-range behaviour of composite frames with semi-rigid and partial-strength connections. The results are compared with full scale frame test results.

The columns were modelled using three-node I shaped beam elements and the material properties found from steel coupon tests. There was no standard element that could be used to model the composite beam, due to the difference in behaviour in hogging and sagging of composite beams. A three-noded general beam section was used, which

used the moment-curvature relationship of a composite beam. The relationship assumed no contribution from the concrete in the hogging region once cracked. The beam-to-column connections were modelled by a two-node non-linear spring element. One node was attached to the column centreline, the other to the end of the beam. The two nodes were given the same co-ordinates, and allowed to rotate. The test moment-rotation curves of the connections were used for the spring elements.

The data from the frame experiments by Li et al **[9, 10]** was modelled. This frame used 203x203UC60 columns and 254x102UB25 beams. For the model the columns were divided into ten elements and the beams into six. It is shown that the results of the model are fairly close to those for the experiment, except where the small moments developed.

The model was then used with some of the parameters changed, to find how they affected the frame. The authors concluded that:

- Modelling the frame with rigid connections led to results far from the experimental results.
- Using the sagging region second moment of area throughout had little effect on the moment distribution of the frame. However, this may have been because of the short hogging moment region.
- Assuming that the beams were elastic throughout loading leads to higher beam span moments and lower connection moments.
- Increasing column size has little effect on the moment distribution of the frame. However, it has a large effect on rigid frames.
- Connection rotations are reduced if the beams are assumed to remain elastic.
- Changing the column size does affect the connection rotation.

The authors also concluded that the ABAQUS package was an appropriate tool for the analysis of semi-rigid composite frames.

Rodrigues et al **[37]** used finite element analysis to model steel plane frames with semi-rigid connections. The element they used to model the connections was a spring

element consisting of two nodes, each with three degrees of freedom. The actual element is made from a combination of three springs: a rotational spring simulating the connections' rotational behaviour, an axial spring in the x-direction simulating the connections' axial behaviour, and an axial spring in the y-direction simulating the connections' shear behaviour. An incremental loading is used so that the connections' behaviour can be represented accurately at each stage. The authors state that the stiffness of the axial springs was taken as being infinitely high, so really they could have been omitted from the model. The rotational spring is set to zero for pinned connections, or made infinitely high for the fixed connections. The authors found that this spring model gave good results when used in their analyses. Unfortunately no comparisons are shown in the paper.

Pertold and Xiao **[38]** have examined the influence of rigidity of beam-to-column connections and column base connections on non-sway frame behaviour. The plastic load capacity of a frame was calculated using finite element analysis for four different frame profiles. A rigidity factor, K, is defined as a ratio between the plastic load capacity of the semi-rigid and rigid frame for serviceability and ultimate limit state. The capacity of the frame is then found by multiplying the factor K by the capacity of the frame with rigid connections.

The method was developed via four stages:

- **Stage 1:** Using finite element analysis to find the capacity of the frame with differing beam-to-column connection plastic rotations, and column base plastic rotations $\phi\alpha$, $\phi\beta$ and different member sections.
- **Stage 2:** Defining the plastic rotations Φ_α, Φ_β as a function of frame geometry, member section and material characteristics.
- **Stage 3:** Defining the connection rigidity coefficients α_α and α_β for the beam-to-column and base connections as a function of Φ_α and Φ_β.
- **Stage 4:** Defining the frame rigidity factor K_α as a function of α_α and β_α.

The single-bay, single-storey frames were modelled in ANSYS using non-linear spring elements for the connections and plastic beam elements for the beams and columns. Six elements were used to model each beam and column. Local buckling and shear

deflection were not taken into account. Bilinear curves were used to model the connection rigidity. A serviceability state of L/200 was considered.

The values of the modified plastic rotations Φ_α and Φ_β can be found from the following equations:

$$\Phi_\alpha = \frac{\phi_\alpha . E . I_{y,b}}{L_b . M_{pl,b} . r_{z,b}}$$

$$\Phi_\beta = \frac{\phi_\beta . E . I_{y,c}}{L_c . M_{pl,c} . r_{z,c}}$$

Where:

Φ_α and Φ_β = the modified plastic rotations for the beam-to-column connection and the column base

ϕ_α and ϕ_β = the plastic rotation of the beam-to-column connection and the column base

E = Young's modulus

L = length of beam (b), length of column (c)

r_z = radius of gyration of beam (b), and column (c)

M_{pl} = plastic moment of element

I = second moment of area

The connection rigidity coefficients α_a and β_a are then given, found from:

$$\alpha_a = 0.803 - 0.182 \ln(\Phi_\alpha) - 0.057 \ln^2(\Phi_\alpha) + 0.014 \ln^3(\Phi_\alpha)$$

$$\beta_a = 0.764 - 0.167 \ln(\Phi_\beta) - 0.048 \ln^2(\Phi_\beta) - 0.007 \ln^3(\Phi_\beta)$$

And finally the calculation of K_a is given by:

$$K_a = K_{a,pp} + (1 - K_{a,pp}).[k.\alpha_a + (1-k).\beta_a]$$

where k is 0.963

And K_{pp} from:

$$K_{a,pp} = \frac{M_{pl,b}}{M_{pl,b} + \min(M_{pl,b}, M_{pl,c})}$$

This method gives an error of less than 7% from the finite element models.

Pertold and Xiao **[39]** then used the same models and theory to analyse frames acting in the non-sway mode. The calculations for the values required to find K differed from the non-sway frame due to the increased influence on ultimate load from the column base rigidity. For the non-sway frame, it was found that the influence from the column base on load capacity was only 5%, but for the sway frame the influence is increased to 45%.

The equations for α_{sa} and β_{sa} are found from:

$$\alpha_{sa} = 0.888 - 0.177\ln(\Phi_\alpha) - 0.051\ln^2(\Phi_\alpha) + 0.012\ln^3(\Phi_\alpha)$$

$$\beta_{sa} = 1.065 - 0.066\ln(\Phi_\beta) - 0.104\ln^2(\Phi_\beta) - 0.015\ln^3(\Phi_\beta)$$

The frame rigidity factor K_{sa} can then be calculated from:

$$K_{sa} = k.\alpha_{sa} + (1 - k_{sa}).\beta_a]$$

Where $k_{sa} = 0.549$

The method gives an error of less than 11% compared to the finite element models.

Chapter 3

Onsite Experiment

3.1 Introduction

The following sections describe the procedure used to monitor and measure the deflections of the primary and secondary beams at Southampton Institute's East-Park Terrace building. The structure was designed by Gifford and Partners consulting engineers, and is the first in Europe to make use of the semi-continuous design approach. Figure 3.1 shows a location map of the building in Southampton, and Figure 3.2 shows a photo of the finished structure, the Michael Andrews building. The building is used for a new information technology suite for the business school, and for administration offices.

The building was monitored during construction and subsequent loading of the plant room floor after the concrete hardened. The results from this experiment will be used for the calibration of a finite element model so that the effects of semi-rigid connections can be analysed.

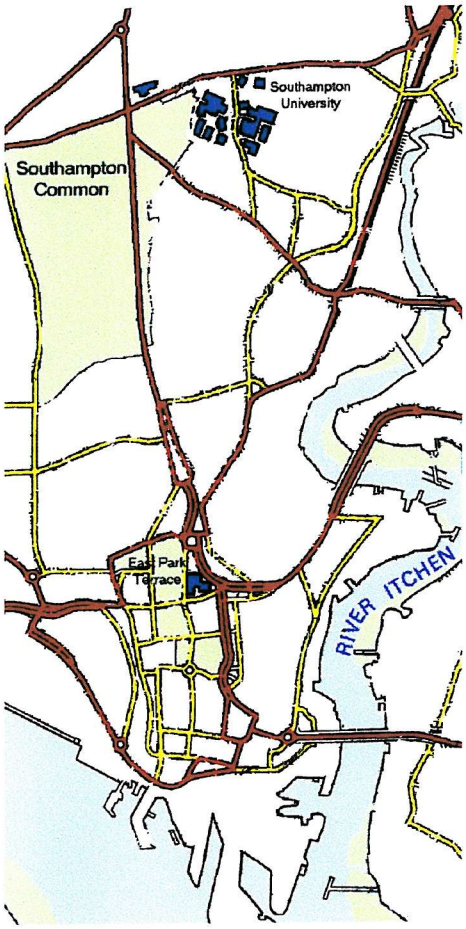

Figure 3.1 Location map of East-Park Terrace, Southampton

Figure 3.2 The Michael Andrews Building, East-Park Terrace, Southampton

3.2 Structural Layout

The fourth floor was chosen for monitoring as this floor supports the greatest loads. The fourth floor supports the plant room, and hence the floor slab is thicker than those of other floors. The plant room floor is in three stepped levels of thickness, 130mm, 175mm and 250mm, the latter two of these being constructed from normal weight concrete and the 130mm thickness from lightweight concrete.

Two of the supporting beams were monitored: a pre-cambered secondary beam, and a propped primary beam. The beam-to-column connections for these two beams are shown in Figure 3.3 below. These beams were chosen so that they were under the thickest of the floor areas and therefore subject to the highest loading cases. Both these beams were equipped with transducers so that the deflections could be found during the concrete pour, and then during later loading of the floor due to the placing of the plant. The layout of the fourth floor is shown in Figure 3.4.

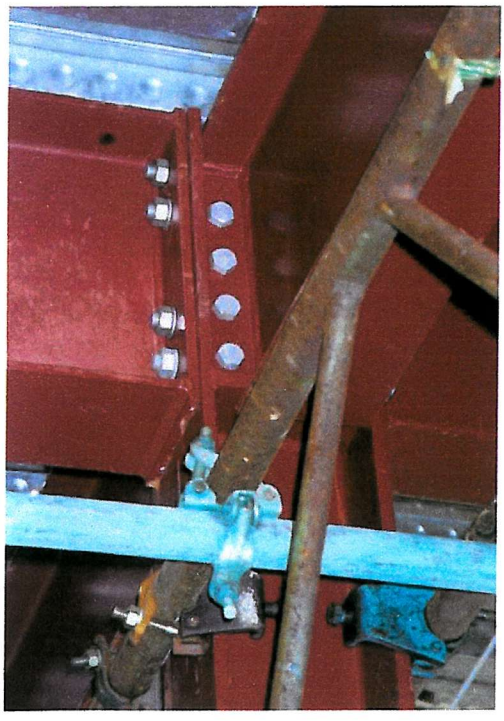

Figure 3.3 Beam-to-Column Connection

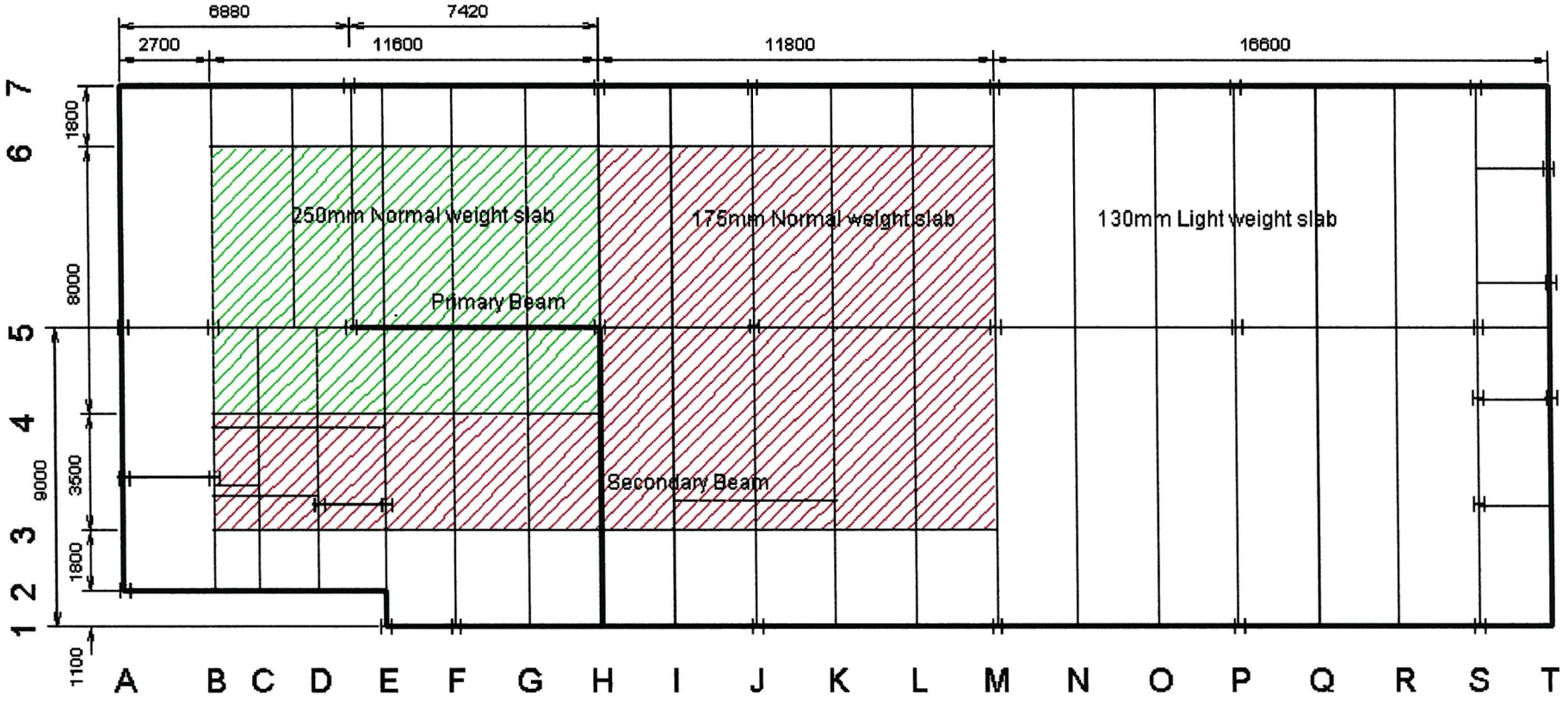

Figure 3.4 Diagram of Level 4, showing the steel layout, and the position of the monitored beams

3.3 Monitoring Apparatus

The following sections describe the apparatus that was used in the onsite experiment. The apparatus had to be durable due to the harsh conditions onsite, and the fact that it would be in situ for several weeks. Failing this, it had to be possible to remove the apparatus from the site in between the separate stages of the experiment.

3.3.1 Transducers

The deflections of the universal beams were measured using transducers. These were attached to the underside of both the universal beams. The transducers were supported using scaffold ladder beams, which were attached to the columns at each end of the beams being monitored. Six 50mm transducers were used on each of the beams being studied. The spacing used for the transducers is shown in Figure 3.5. This spacing was chosen so that the transducers would be sited at the points of most interest, and would give a good indication of the deflected shape. Two transducers were placed at the mid-point of the span, as this is where the maximum deflection along the beam would occur. This point was of greatest interest, and therefore a reliable result was required. Having two transducers at mid-span allowed for any problems that might have occurred with one of them, and it would also show if any gross torsional deformation occurred in the beam. Figure 3.6 shows this set-up photographically.

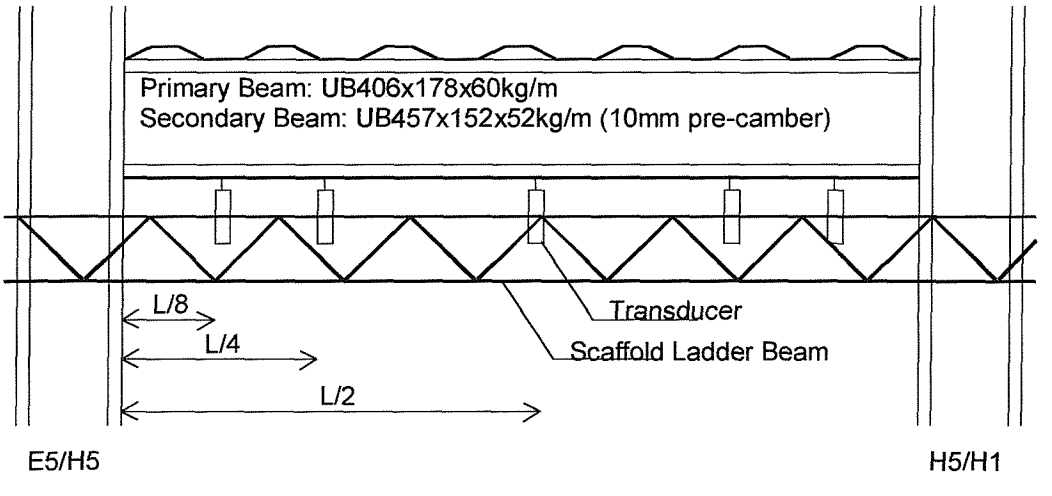

Figure 3.5 Positioning of the Transducers

Figure 3.6 The Experimental Set-Up

3.3.2 Strain Gauges

In the original experimental set-up proposal, strain gauges were to be attached to the beams used for the experiment. These were to be placed at mid-span and at the beam-ends, on the lower flange, to find the maximum compressive strains at the beam ends and tensile strains at the mid-spans. Due to the construction method it would not be possible to attach strain gauges to the top flange.

Gauges were also to be attached to the web of the column near the semi-rigid joint so that the strains and deformations could be found. It was hoped that these gauges could then stay in place during the life of the structure so that regular readings could be taken during normal loading.

However, due to the speed of construction of the structure, and the fact that there was very limited storage space on the building site, it was not possible to attach the strain gauges before the beams were bolted into place. Also, it was not possible to fix these gauges when the beams were in place due to safety reasons.

The information on the strains in the beams was not vital, as the primary aim of the experiment was to gather data for the calibration of a finite element model, which could be achieved using only the deflections found by the transducers.

3.3.3 Data-Logger

A data-logger was used to record the data from all the transducers. The transducers were connected to the data-logger so that resistance across the potentiometer was measured. The transducers were calibrated in the laboratory using a basic test rig and metric slip gauges. The relationship between electrical resistance and transducer displacement was found to be linear, as expected. Each transducer was calibrated to find its linear calibration factor. These factors were input into the data-logger so that the displacements could be read directly from the data-logger. The transducers were re-calibrated after the experiment to check that they had remained constant throughout the duration of the experiment. It was found that there was very little difference between the two sets of calibration data, and therefore no modifications were made to the test results.

The data-logger was programmed so that the displacements would be measured for all the transducers, and both saved onto analogue tape and printed out onto paper roll as a back up. The program was run manually throughout the experiment so that it was possible to control when the readings were taken. It was important to have as much data as possible at the times when the concrete was being poured directly over the beams being monitored (i.e. the times of greatest change in deflection). Fewer results were required when the concrete pour was taking place further away, as this would have a negligible effect on the deflections of the monitored beams. This arrangement proved to work well through the course of the experiment.

3.3.4 Video Camera

The floor was filmed during the pouring of the concrete, as it was important that the times of the concrete pour and the pour pattern could be accurately noted. The filming

took place from an adjacent building that overlooks the site, giving a good, and safe, vantage point to set up the video camera. It was then possible to concentrate on the data logger during the experiment itself, and to use the video after the experiment was completed to note the concrete pour pattern, comparing the video to the deflection measurements that were taken. The clocks on the video and the data-logger were activated, and the time was noted on any notes made through the day so that the measured results could be compared accurately with the concrete pour pattern. A drawing has been made from the video recording to show the pour pattern, and the times for each area of the pour have been noted on this drawing (Figure 3.9).

3.4 Monitoring Procedure

The following describes how the apparatus was used to obtain the deflection values of the beams during the concrete pour, and plant placing stages of the experiment.

3.4.1 The Concrete Pour Experiment

Initial readings were taken before the start of the concrete pour. These readings were used as the offset readings for the transducers, and these values were input into the data-logger as part of the calibration stage, along with the calibration factors. However, these values were taken before the props were placed under the primary beam. Further offsets have been used when analysing the results by taking the initial deflection after the props were placed.

The first area of concrete to be poured was the area furthest from the monitored beams, so only a few readings were taken at this stage. Once the concrete pour was over the monitored beams, readings were taken at one or two minute intervals. The filming of the site also concentrated mainly on the area above the concrete pour. The experiment ran satisfactorily with no problems from any of the equipment used.

3.4.2 Extraction and Plots of Results

The primary beam was propped during the concrete pour, and these props were left in place until the concrete had cured sufficiently. The secondary beam was pre-cambered and was therefore not propped. Both ends of the primary beam were connected to a column with a semi-rigid connection, and this beam was propped at the third points along the beam. The secondary beam was connected with simple connections to a column at one end and a primary beam at the other. It was assumed that there was no vertical deflection at the beam-to-column connections, but this assumption could not be made for the beam-to-beam connection. Unfortunately it was not possible to place a transducer under the beam-to-beam connection due to falsework constraints on the site. However, the deflections from the other transducers positioned under the secondary beam have been used to estimate the deflection under the beam-to-beam connection, using the approaches described in this section.

Offsets were implemented in the spreadsheet so that all initial readings at the point where the props were positioned under the primary beam were zero. These same offsets were also used in the analysis of the results for the later experiments carried out on the composite slab.

Where two transducers were placed at the mid-span of each beam, the values for displacement were averaged between them with no bias. This would have been done differently if it had been shown that the reliability of one of the transducers was poor when compared to the other. However, the results from the experiment show that both transducers gave very similar deflection values, and no problems were detected when the calibrations of the transducers were checked in the laboratory after the experiments had finished. The transducers proved to be very reliable, and the initial calibrations had remained unchanged.

The problem with not knowing the deflection at the primary beam to secondary beam connection was solved in two different ways. Firstly, extrapolation was used to find the deflection. The displacements from the two transducers closest to the beam-to-beam connection were used for this. The values were extrapolated as if the deflected shape was linear after these two transducers. The deflection values were found for the

deflection at the beam-to-beam connection for each stage in the loading. Secondly, a function was found that defined the deflected shape: for this the least squares method was used. This function could then be used to determine the deflections at any points along the beam. The problem with this method is that there are few points that can be used, and therefore the accuracy of the function suffers. However, a quadratic function was found that fitted the deflected shape approximately, and the results given by this method were better than those from the extrapolation method. It was then possible to apply these deflections along the length of the beam as a linear transformation, and thereby to find the deflected shape of the secondary beam as if both ends of the beam were restrained against vertical movement.

In the following, the values found for the deflections will be discussed and plotted with reference to the reading number, as opposed to the time. This gives a clearer plot to work from, due to the frequency with which the readings were taken when the concrete pour was directly overhead.

The results are shown below in two ways. The displacement for each transducer has been plotted against the reading number: this shows where the results have changed the most, and these points can be compared to the notes and the concrete pour pattern drawing (Figure 3.9) to discover what caused the large increase in displacement. The displacement of each transducer has also been plotted against the length along the beam: this gives the deflected shapes of the beams.

3.4.3 Change in Deflection

The following graphs, Figures 3.7 and 3.8, plot the increase in displacement for each transducer with the reading number. These reading numbers can be compared against those on the drawing of the floor, showing the concrete pour pattern (Figure 3.9).

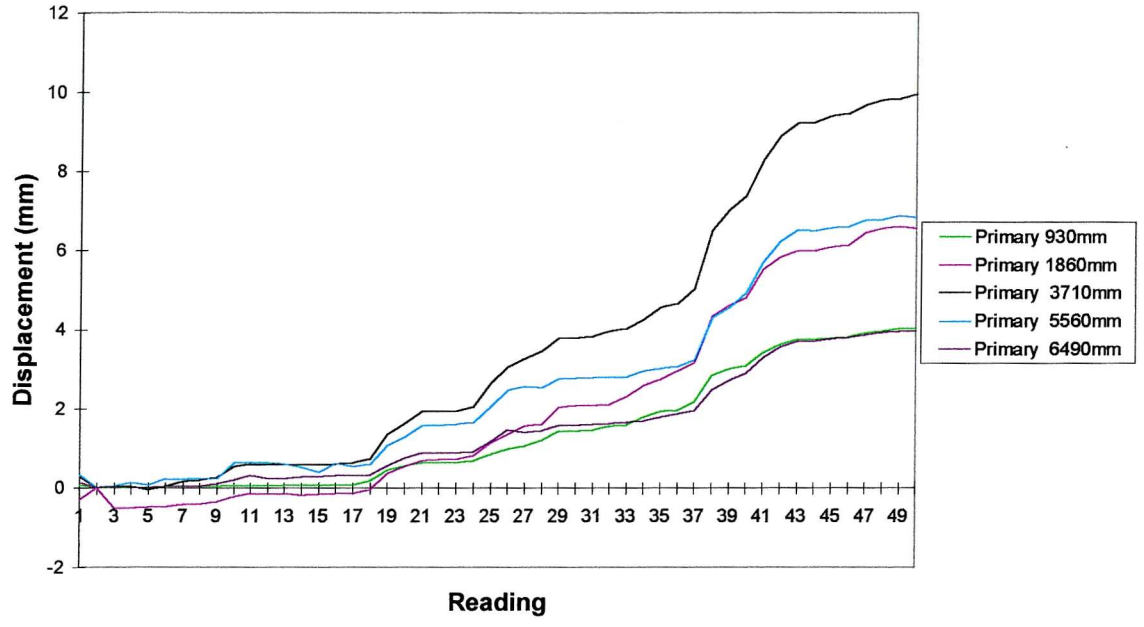

Figure 3.7 Primary Beam Transducer Displacements

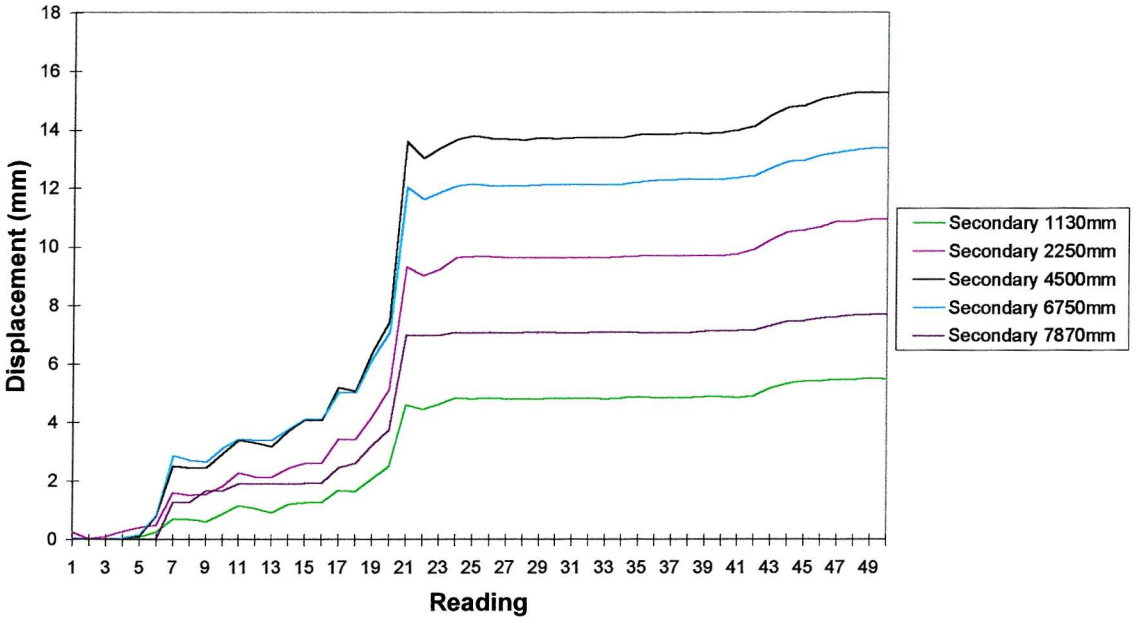

Figure 3.8 Secondary Beam Transducer Displacements

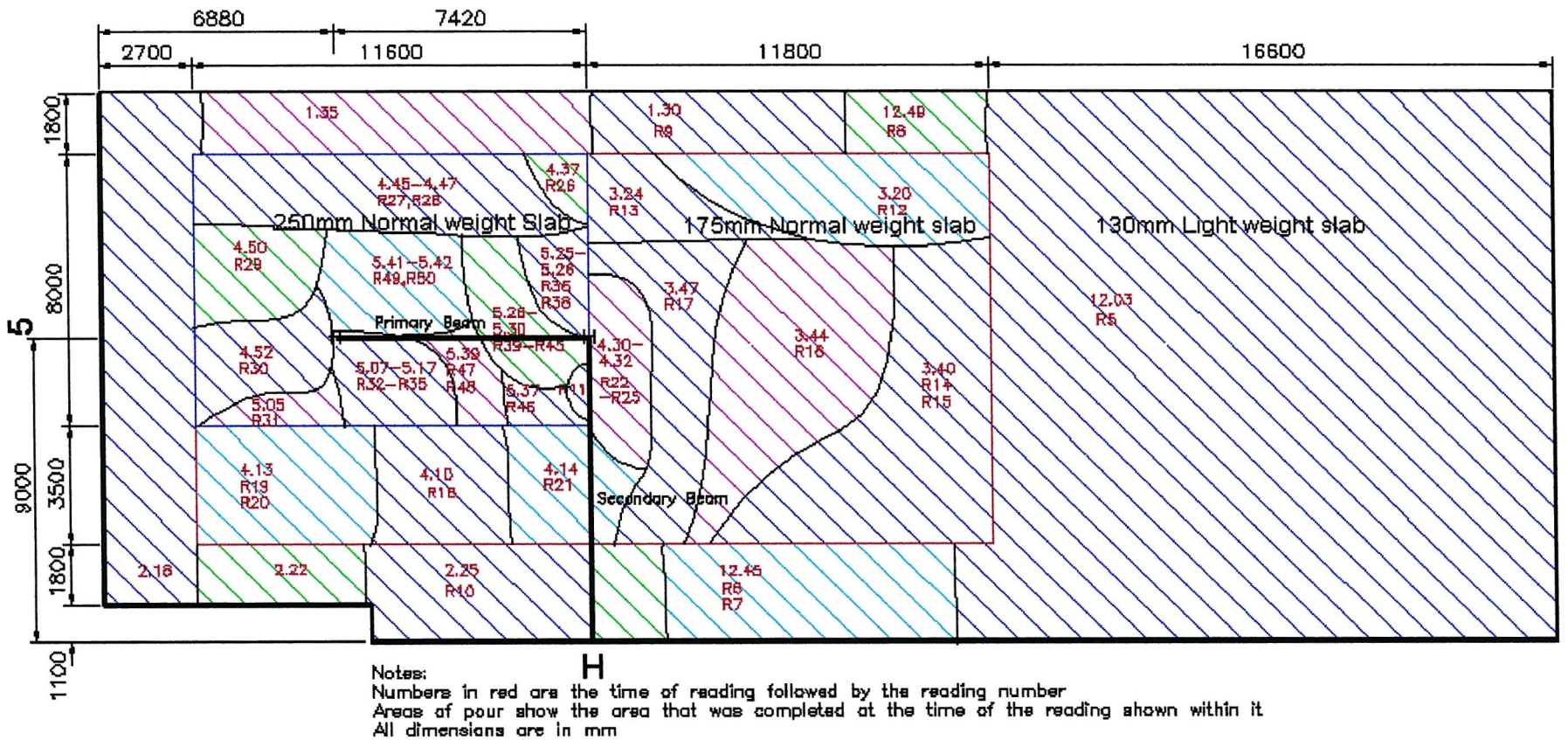

Figure 3.9 Diagram of Level 4, showing the concrete pour pattern in relation to the monitored beams

Figures 3.7 and 3.8 show that the two monitored beams behaved rather differently. Both graphs go through zero on reading 2, as this is when the props were placed under the primary beam, and this was taken as being the initial, zero, reading. Figure 3.8, showing the secondary transducer displacements, shows that the deflection appears to go up in two main steps, between readings 6 and 7, and then between readings 20 and 21. Figure 3.9 shows that at reading 6 the area towards the end of the secondary beam was being poured: at this end of the secondary beam there is a beam-to-beam connection, and therefore the concrete being poured in this area would cause a greater deflection than would have been the case for a beam-to-column connection. The biggest jump in transducer displacement occurred as the concrete was being poured directly over the centre of the span of the secondary beam, as expected. The concrete pour then moved away from the secondary beam and there is no further large increase in displacement.

The transducer displacements for the primary beam go up more steadily. The concrete pour is also steadier around this area, taking place over a larger number of transducer readings. Once again, however, the majority of the displacement occurs when the concrete pour is directly over the primary beam. The deflections for this beam are more symmetrical than those for the secondary beam. This is probably due to the fact that each end of the primary beam ended in beam-to-column connections, and also to the fact that the loading was more consistent along the length of the primary beam.

Further plots of deflection are shown in Figures 3.10 and 3.11. These graphs show the deflections of the beams for some of the readings taken. To plot these graphs, it was assumed that there was no deflection at the beam-to-column connections, and so the graphs go through zero at these points. The secondary beam ended with a beam-to-beam connection, and therefore there would have been a deflection at this point, so it is not possible to make the same assumption.

The graph for the primary beam (Figure 3.10) shows that the last reading for the primary beam produced a symmetrical curve. This did not occur for the earlier readings, due to the concrete pouring pattern, the equipment used for the concrete pour, and the presence of site personnel working on the concrete pour. The graph for the secondary beam (Figure 3.11) shows how the deflections for the earlier readings were

greatest towards the end of the beam, as this was where the concrete was being poured at that stage. Later, they became greater towards the mid-span, as the concrete was poured over those areas at that stage.

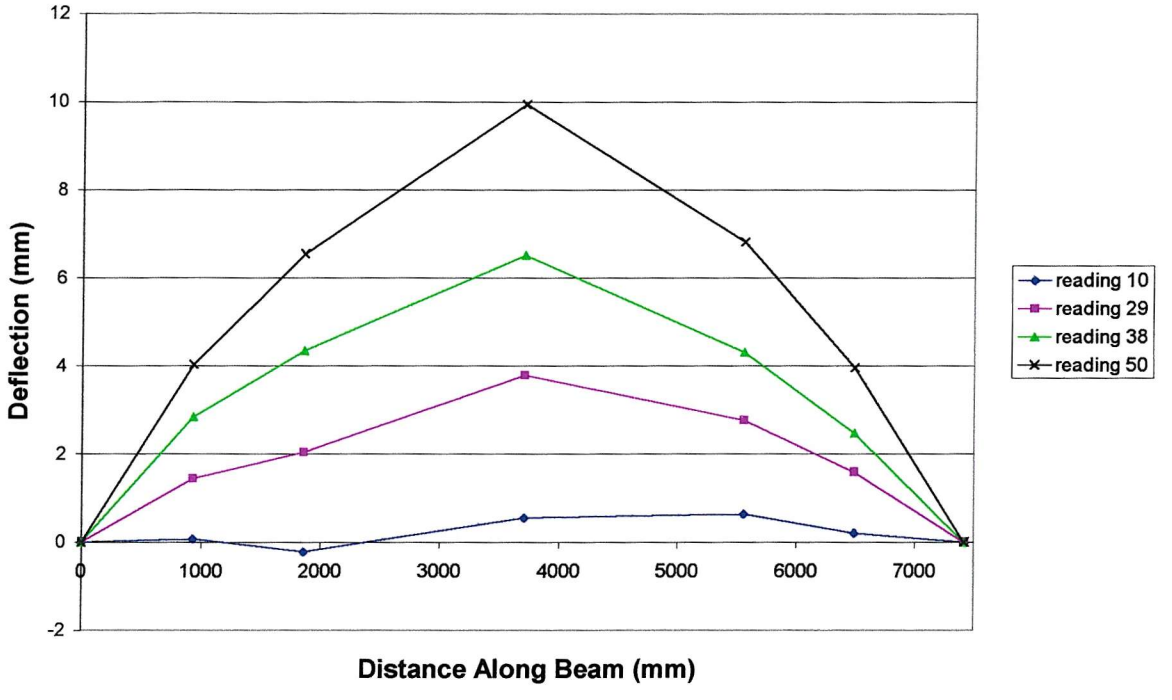

Figure 3.10 Primary Beam Deflections

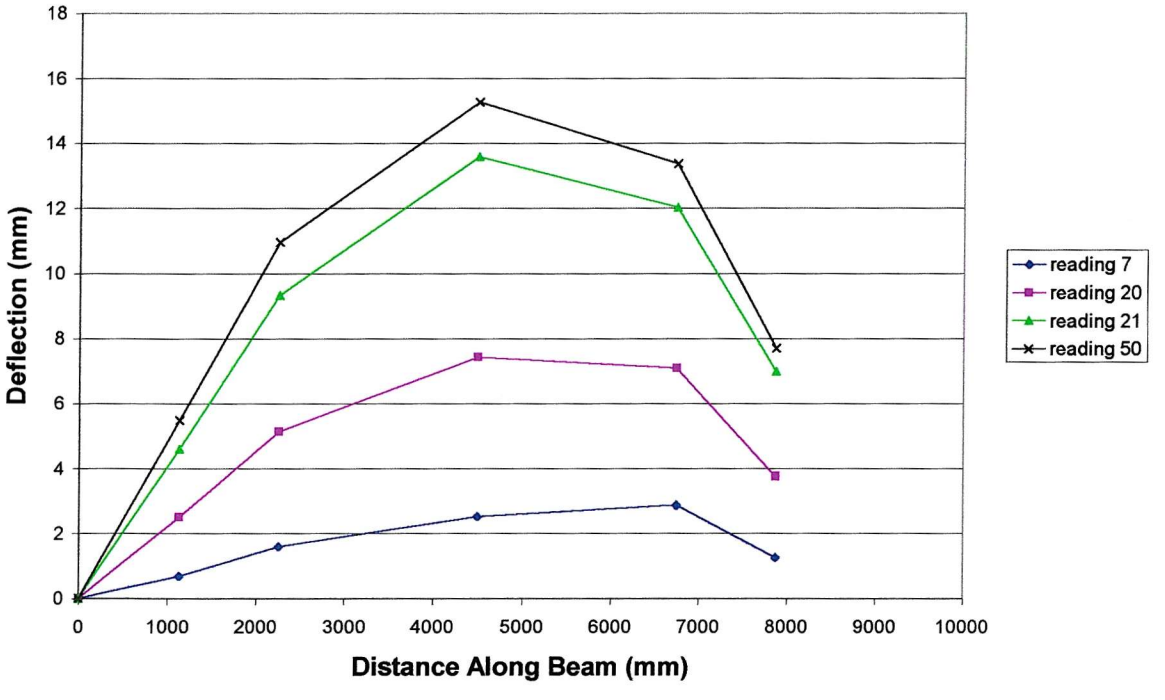

Figure 3.11 Secondary Beam Deflections

3.5 Modelling of the Monitored Beams

3.5.1 The Secondary Beam

The secondary beam was modelled using the 'QSE Plane' structural analysis program, which uses the stiffness method. The beam was modelled as a beam with pinned connections, as it was designed with simple connections on the building. The wet concrete loads were used for the analysis, and these loads were distributed as rectangular loads. Figure 3.12 shows how these loads were distributed.

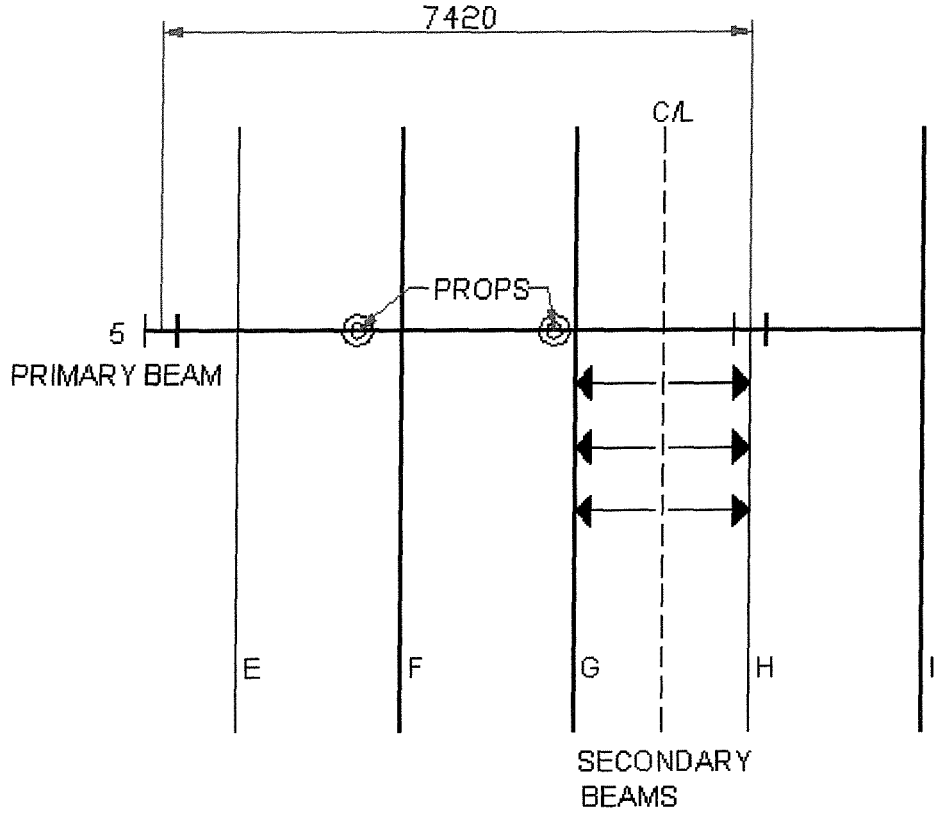

Figure 3.12 Load Distribution

Other methods for distributing the loads were also tried, but the results from these were very similar to those found from this simple method. The loads for the primary beam were found in the same way. The built-in database that QSE contains was used for the assignment of beam properties, and the loads were applied as a uniformly distributed load.

The chart below (Figure 3.13) plots the results from the QSE analysis and those measured from the onsite experiment.

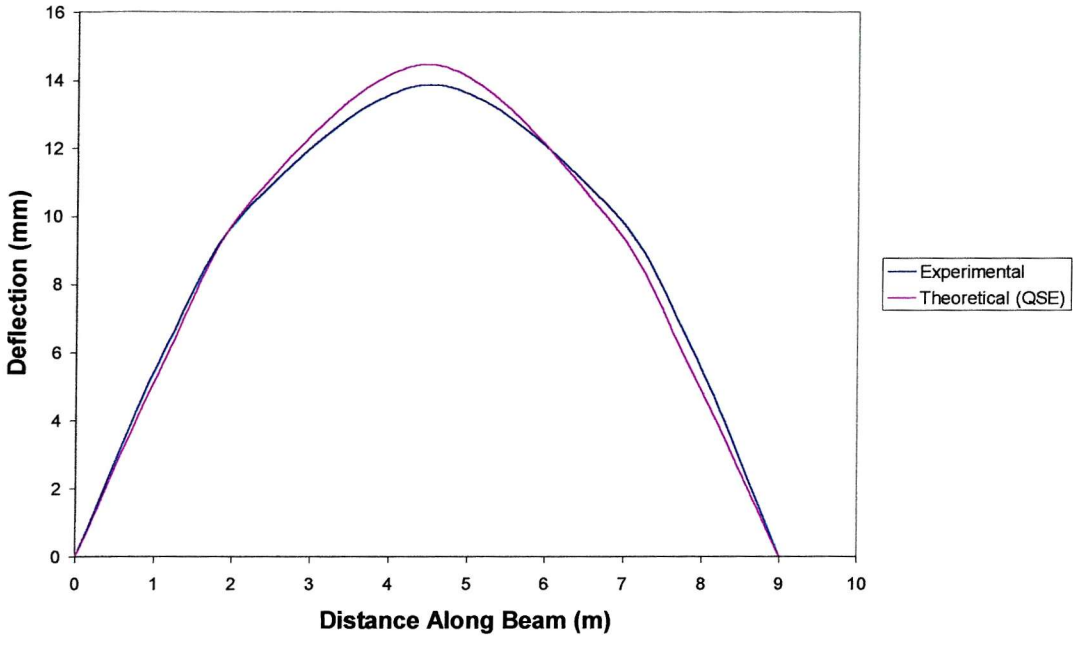

Figure 3.13 Comparison of Experimental and Theoretical Results for the Secondary Beam with the Deflections Altered with a Linear Transformation

This graph shows that the experimental results are very similar to those that would be expected from a theoretical analysis. The data used here as the experimental data is that which has been analysed using the least squares method (see Section 3.4.2), so that the data is found as if both ends of the secondary beam ended in a beam-to-column connection. This made the analysis of the beam more straightforward, and made it easier to compare the results.

Although these results compare well, it is also important to consider errors that may have occurred. As the experiment was carried out on site, it is not possible to be certain that the thickness of the floor slab was exactly that which was stated in the design. During the construction of the building there were site personnel on the monitored floor, which would add to the deflections, although not greatly. There was also the equipment used to pour the concrete, notably the heavy pipe used to carry the concrete to the portion of floor being poured. The least squares technique could also introduce errors if it does not give an accurate value for the deflection at the beam-to-beam

connection. This error would then be transferred along the length of the beam, with the greatest errors being in the area of the beam-to-beam connection. This could explain why the graphs for the experimental and theoretical deflections fit more closely to each other for the first part of the beam.

3.5.2 The Primary Beam

The primary beam was also modelled using QSE. Due to the fact that the primary beam was designed with semi-rigid connections, it would not be correct to model this as a pin connected beam, as was done for the secondary beam. It would also be inaccurate to model the beam as if it had rigid connections. The props are a further complication, as they do not provide full support against beam deflection. However, owing to the limitations of this software, the only option was to model the beam as if it was pin connected, and then to remodel it as if it was fully fixed at each end, giving the extreme connection conditions for the beam.

The maximum deflection at mid-span, measured after the concrete pour, was 9.95mm. A simple support analysis gave 35.13mm, and a fixed support analysis gave 7.016mm, as the deflections in the mid-span. As would be expected, the experimental results fell between those given by the model for a simple connection and those for a rigid connection. These results did not take the props into consideration.

These analyses demonstrated that to produce an accurate model of the primary beam, a finite element model would have to be developed, so that a value of stiffness could be applied to the connections; this could be done using a spring element.

3.6 The Plant Placing Experiment

The second stage of the experiment was to measure the deflections of the two monitored beams once the concrete had cured and the structure was acting as a composite structure. This was carried out in two stages. The first stage consisted of measuring the deflections whilst pallets of building blocks were situated directly over

the mid-span of the monitored beams. The second stage was to measure the deflections once the plant, consisting of cooling units for the air-conditioning, was placed. At the stage of the plant being placed, the props had also been removed from beneath the primary beam.

Initial readings were taken before anything was moved, so that the results could be compared with those from the concrete pour experiment. It was shown that there was very little movement of the monitored beams over the time between the two stages of the experiment.

It was not necessary to use the video camera for these stages of the experiment, as the loading conditions were either controlled or constant. The following sections of this report describe the results from the experiment.

It was necessary to remove the experimental set-up after these experiments were completed, in order not to interfere with or interrupt the building work that was taking place in close proximity to the set-up.

3.6.1 Results of the Plant Placing Experiment

The first experiment after the concrete had cured was to use pallets of building blocks as weights over the monitored beams so that the deflections of the beams could be monitored. The props were still in position under the primary beam at this stage. Initial readings were taken, and it was found that these did not vary much from the final results taken at the end of the concrete pour experiment.

It was found that the mass of the pallets was not sufficient to cause much deflection of the beams. The primary beam's deflections were negligible, which would be due to: the props still being in position under the beam; the semi-rigid connections; and the fact that the floor was very stiff and designed to support a far greater load, i.e. the plant. The deflection of the secondary beam was also only slight, with a maximum deflection of 0.2mm. It is not felt that the accuracy of the experimental set-up is good enough for these results to be significant.

The next results were taken once the plant had been placed onto the fourth floor. At this time the props had also been removed from under the primary beam. These were the last readings to be taken before the apparatus was removed. The results are plotted in Figure 3.14 below.

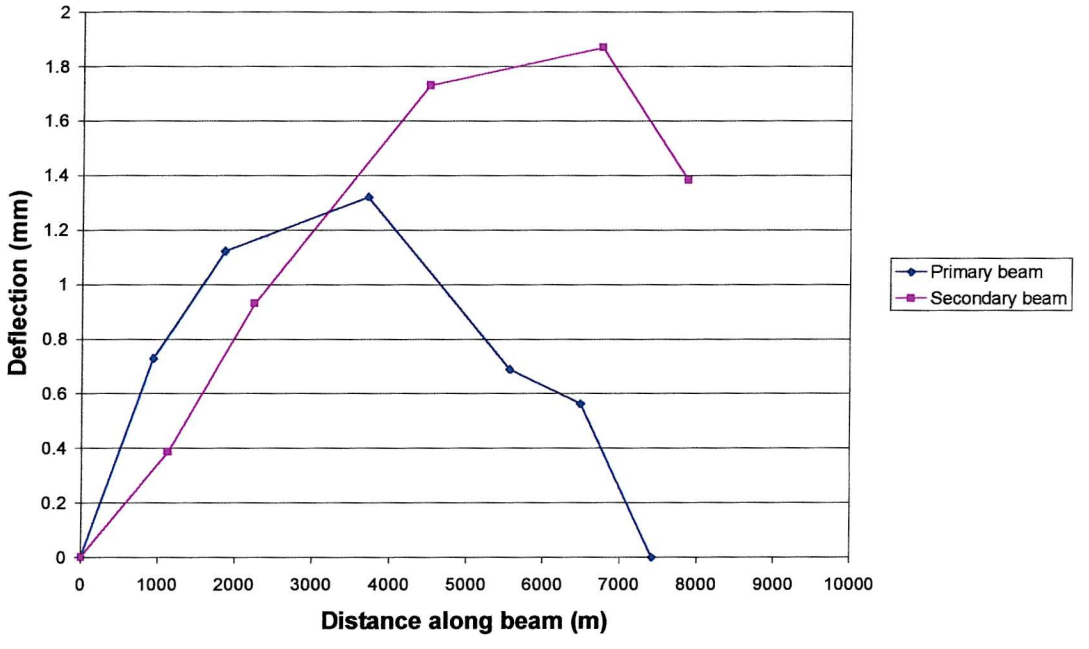

Figure 3.14 Final On-Site Readings

The chart shows the changes in deflection between the last two visits to site, that is, the changes in deflection after the plant had been placed. The props under the primary beam had also been removed. The deflections for the secondary beam have been shown as the experimental results, and not in the compensated form shown earlier (as if the end of the beam was fixed to a column). Some of the increase in deflection of the primary beam will also be due to the removal of the props.

Least squares analysis was used to show what the deflections for the secondary beam would have been if the beam were connected to a column at both ends. The deflection results were fitted to a quadratic and a cubic curve. The deflection result for the beam at 9m was then used to linearly transform the deflection results. This is the same method as that described in Section 3.4.2. Figure 3.15 shows the attempts at fitting

curves to the results, and Figure 3.16 shows how the deflections look after the linear transformations have been applied.

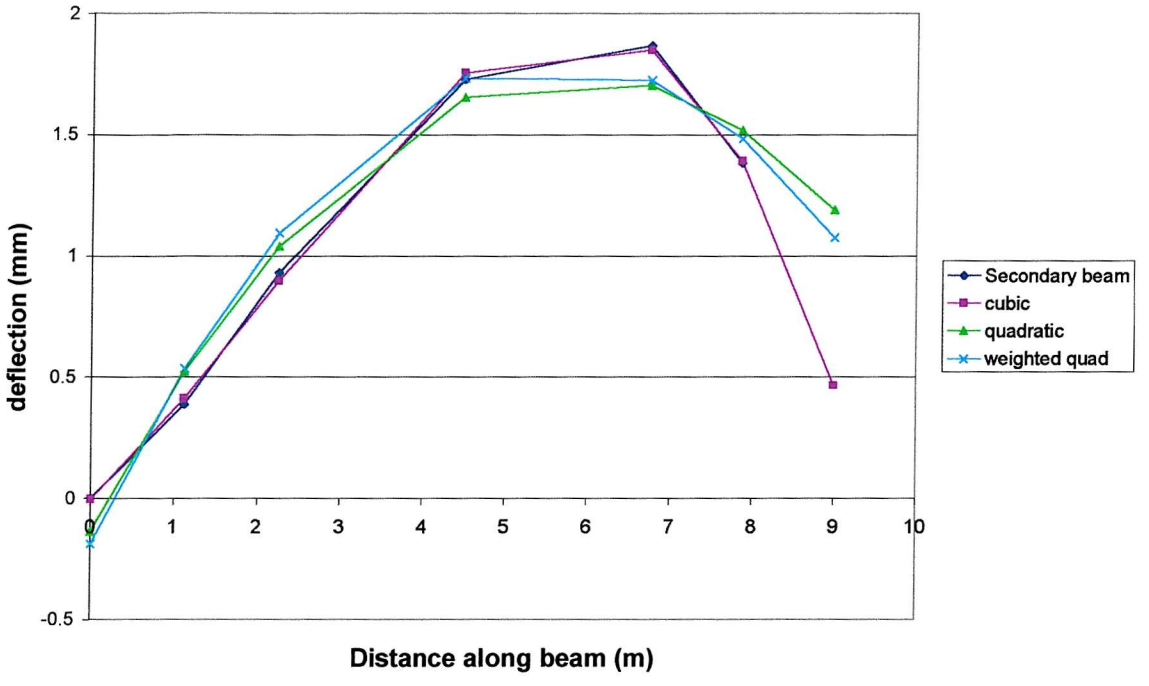

Figure 3.15 Fitting Curves to the Secondary Beam Deflections

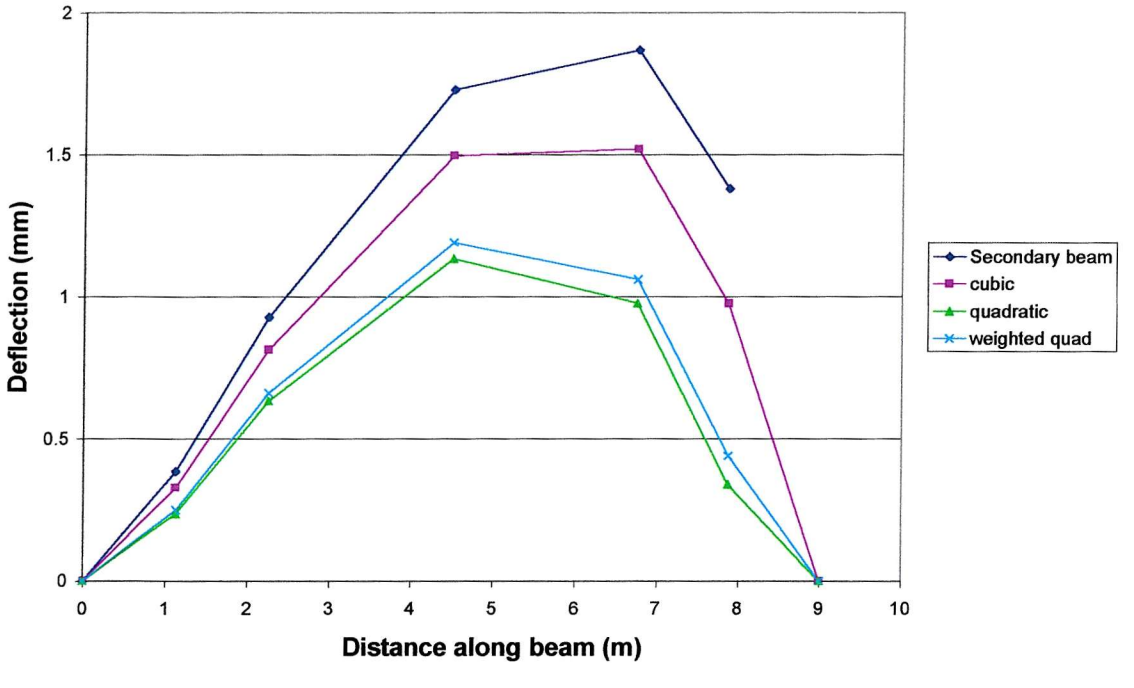

Figure 3.16 Secondary Beam Deflections After Linear Transformation

Two attempts were made to fit a quadratic curve to the secondary beam deflection results. It was found that the quadratic curve did not fit well to the deflections for the end of the beam nearest the beam-to-beam connection. For this reason a weighting was added to these deflections to try and make the curve fit better to these results. However, this did not make much impact on the final curve, and it was found that a cubic curve fitted far better to the secondary beam deflections. Figure 3.16 shows how much difference choosing different curves makes to the transformed deflections of the secondary beam.

3.7 Summary

Considering the experiment was taking place on a busy building site during the construction of a floor slab, the experiment ran very smoothly. A great deal of deflection data was collected. The initial analysis of the secondary beam showed that the first computer models agreed very well with the actual data collected. However, the software package used for this initial analysis was not flexible enough to deal with the analysis of the primary beam, or with the more complex analysis needed for the later stages of this research. It was therefore necessary to use a finite element approach to continue. With this method, it is possible to model the semi-rigid behaviour of the connections. It will also be possible to go further with the analysis and introduce material non-linearalities, and the non-linear behaviour of the connections. The results from the secondary beam can be used for the calibration of a finite element model. The finite element method, and the models constructed using it, are described in the following chapter.

Chapter 4

Finite Element Analysis Modelling

4.1 Introduction

An alternative to the experimental approach to researching structures is that of using the finite element method. Finite element analysis has many advantages over the experimental approach. After the initial investment in the necessary computing equipment and software, it is possible to analyse many different structures with no additional cost, except the user's time. Once a model is constructed, it is easy to change the properties of the materials used and the dimensions of any part of the model. Increases in computing power make it possible to solve ever more complex models, more quickly. Parametric studies can be carried out to produce far more results than would be financially feasible using experimental methods. However, it is essential to be able to check the results from a finite element model against those from an experiment, to show that the model is behaving as expected with no errors. This chapter aims to validate the finite element model against the results obtained from the on-site experiment.

The finite element package used in this research is the ANSYS package that was introduced in 1970 by Swanson Analysis Systems Inc. It is a general purpose package

that can be used for solving structural, mechanical, electromagnetic, electrical, electronic, thermal, fluid and biomedical analyses.

To build, solve and view the results of an analysis three separate processor stages are used. These are the pre-processor (/Prep7), the solution (/Solu) and the post-processor (/Post1, /Post26). These are described in more detail below.

4.1.1 The Pre-Processor

The first processor entered by the user is the pre-processor. Here the geometry of the model is built up. The model is made up of nodes, elements, material properties, real constants and boundary conditions. ANSYS has a library of over 100 elements that can be chosen to construct the model; these elements can be further customised by use of the real constant sets. For this research, elastic and plastic beam elements, and linear and non-linear spring elements have been used. These are described in more detail in the later sections of this chapter. For the beam elements, the real constants are used to specify a general cross section (as opposed to a rectangular or circular section). Later releases of the ANSYS software also included an I section, but this was not present in the versions available at the time this research was carried out. The real constant sets also gave the dimensions of the beam. For the spring element, the real constants were set to allow it only to rotate, and to have no lateral movement. The real constant sets also specify the stiffness of the spring.

The material properties can be defined in two ways, depending on whether the material will remain in its linear stage during the analysis, or whether the loading is going to be such that the non-linear behaviour of the material will be reached. The linear material properties are defined with information such as Young's modulus, Poisson's ratio and the shear modulus. The non-linear material properties can be given in several ways by specifying bi-linear or multi-linear curves. In this research bi-linear curves were used to specify the material properties of steel.

Once the elements have been chosen and the material properties set, the geometry of the model can be built up. This can be done in two ways, using either direct generation

or solid modelling. Both are useful depending on the complexity and size of the model. For smaller models, direct modelling is useful, as it allows the user to place each node. Nodes can be located in the sites of greatest interest, and the spaces between nodes can be filled with more nodes, then the nodes can finally be joined up using the elements. However, this is a slow way of generating a model. For solid modelling, on the other hand, the user only needs to specify the boundaries of the model, the size constraint required for the element mesh, and the element type. ANSYS then meshes the model, placing the nodes and elements.

In this research, as the frames modelled are relatively basic, direct generation has been used, which has allowed the accurate positioning of the nodes in the points of most interest. As this is a slow method of generating a model, the batch file system has been utilised, so that the model can be altered using a text file instead of having to access the user interface each time.

4.1.2 The Solution Processor

After the geometry has been set in the pre-processor the user enters the solution stage. Here the loading pattern is set, along with the solution parameters for the problem. The loading applied to the model can be in the form of point loading, pressures, displacements or temperatures. For a model constructed by direct modelling, these forces are applied directly to the nodes and elements. In the case of solid modelling, the forces are applied to the geometric model, which then transfers the forces to the mesh. For this study, point loads were either applied directly to the nodes, or, for a uniformly distributed load, the loading was applied as a pressure to the elements.

The boundary conditions can be applied to the model either in the pre-processor or in the solution stage. For this research, to set the boundary conditions for the column bases, two nodes were positioned at the same point. One of these nodes was fully constrained, and the other was joined to this by a rotational spring element. For the beam to column connections, two nodes joined by a rotational spring were placed at the same point, and a constraint was applied to ensure that both nodes kept a common x and y position.

Next, the solving criteria are set. The solving criteria depend on whether a linear or non-linear analysis is to be solved. For a non-linear analysis, it is important to give a gradual increase in loading so that an accurate solution is obtained. The convergence criteria are also defined by the user - they can be set to converge a variety of values including stress and deflection. Once all the loading and solution criteria are chosen, the user can set ANSYS to run the analysis. Results are then written to the output and results files.

4.1.3 The Post-Processor

Now the model has been solved, the post-processors are used to view the results. The results can either be viewed at a chosen load and sub-step, or a particular result can be displayed over the whole load history. These results can either be viewed and saved as tables, for later analysis of the results, or viewed as a contour plot to give a more visual description of the results.

The post-processing stage is also important so that the results can be compared against those from experience and experiments. It is at the post-processing stage that most errors in the model will be found.

4.1.4 Batch method

The description of ANSYS above deals with the interactive method, where the user is interacting with the graphical user interface to construct a model. Another method of creating a model is to use batch files. In the batch file method, the model is constructed in text files that describe the geometry of the model, the boundary conditions, loading, and solving criteria. This method is very useful for the more advanced user, as the model can be constructed and then altered far more quickly. The batch files can also be submitted to solve in the 'background', to make better use of computing facilities. The files can be set to call other files, making it possible to solve a great many analyses in succession and save the results that are required. Batch files were used for this research, as frames were being solved with many different beam-to-column connection

properties. All the geometry files could be created and saved, and then the connection properties were saved separately in individual files. This greatly cut down on the number of models that needed to be produced.

4.2 Elastic Modelling

Linear modelling is the simplest form of analysis in ANSYS. The material properties are set so that each element behaves elastically, then the load is applied. No sub-steps are required for this form of analysis as the full load can be applied directly. For the elastic analyses in this research two elements were used: the 2D elastic beam element, BEAM3, and the spring-damper element COMBIN14. These elements are described in more detail in the following sections.

4.2.1 Elastic Beam Element – BEAM3

BEAM3 is a uniaxial element with tension-compression and bending capabilities. It has three degrees of freedom at each of its two nodes. These are translations in the nodal x and y directions, and rotation at the nodes about the z-axis.

Its two nodes, the cross-sectional area, second moment of area, the height and the material properties define the element.

Distributed loads can be applied as surface loads on the element faces. Point loads are applied at the nodes.

BEAM3 allows many options for the final output data. Those that are most relevant to this analysis are the nodal displacement, stresses, and member moment about the z direction.

Important assumptions that this element uses are that the beam element can have any cross-sectional shape for which the second moment of area can be calculated, but the stresses are determined as if the distance from the neutral axis to the extreme fibre is

half the height. This is not a concern for this analysis, as the beams being modelled are symmetrical and this assumption is correct. The element must lie in the x-y plane and cannot have zero length or area. There are further assumptions that concern thermal calculations, but these are not relevant to this analysis.

4.2.2 Spring-Damper Element – COMBIN14

COMBIN14 has longitudinal or rotational capability in one-, two-, or three-dimensional applications. The longitudinal spring-damper option is a uniaxial tension-compression element with up to three degrees of freedom at each node, which are the translations in the x, y, and z directions. In the longitudinal option no bending or torsion is considered. The rotational spring-damper option is a purely rotational element. It also has three degrees of freedom and these are the rotations about the nodal x, y, and z axes. In this case no bending or axial loads are considered.

COMBIN14 has no mass, and if this is needed it has to be added using an appropriate mass element. The spring or damping capability may be removed from the element.

The input data for the element is the position of the two nodes, a spring constant (k) and damping coefficients (CV)1 and (CV)2. As the concern here is only with static analysis the damping coefficients are not used, and the key-options are set so that the spring works in one dimension as a torsional spring-damper.

Assumptions and restrictions of this element are that:

- If KEYOPT(2) is zero then the length cannot be zero, i.e. if the spring is in more than one dimension then its nodes cannot have the same co-ordinates, as the node locations determine the spring orientation.
- The longitudinal spring element stiffness acts only along its length.
- The torsion spring element stiffness acts only about its length.
- The element allows only a uniform stress in the spring.
- If KEYOPT(2) is greater than zero then the element has only one degree of freedom; this is the same for both nodes.

4.3 Plastic Modelling

Non-linear and plastic modelling are more complex forms of analysis. Non-linear modelling needs to be used when the material has passed its elastic limit, when the material does not deform linearly, or when there are geometric non-linearalities in the model. Plastic modelling is required when a material is deforming plastically. Sub-steps are required for non-linear and plastic analysis.

In the non-linear and plastic analysis the two previous elements were replaced with two more versatile elements; these were a 2D plastic beam element, BEAM23, and a non-linear spring element, COMBIN39. The beam element allowed for the input of a general beam section, which was used as there was no allowance for an 'I' beam section. The non-linear spring element allowed for the rotational stiffness to change as the moment increased. This was not possible with the spring element used for the elastic analysis.

4.3.1 Plastic Beam Element – BEAM23

BEAM23 is a uniaxial element with tension-compression and bending capabilities. It has three degrees of freedom at each of its two nodes. These are translations in the nodal x and y directions, and rotation at the nodes about the z-axis. The element has plastic, creep and swelling capabilities, which are the differences between this element and the elastic beam BEAM3.

The element is defined by two nodes, the cross-sectional area, moment of inertia, the height for rectangular beams, the outer diameter and the wall thickness for thin-walled pipes, the outer diameter for solid circular bars, and the isotropic material properties.

There is an option to input a general cross-section (KEYOPT(6)). This will be required in the analyses as ANSYS does not have input options for I-beams. The input data required by ANSYS then comes from functions of area and length at integration points over the height of the cross-section; these are shown in Figure 4.1 below.

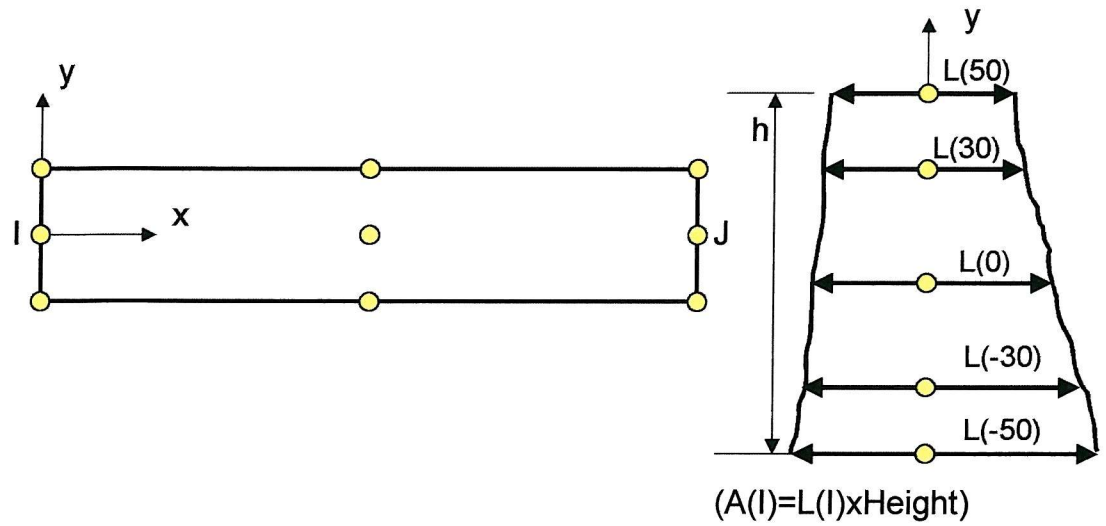

Figure 4.1 Input Data for the BEAM23 element

The output data for this beam element differs from that for BEAM3 in that the data can be obtained at different locations in the element. The solution printout contains the stresses and strains at nine locations in the beam. The locations are at three points through the height of the element (bottom, middle, and top) at each of the three axial stations (end I, mid-length, and end J). For more detailed results the ETABLE command can be used to show the postdata items - these contain the stresses and strains at the five weighted-area locations at each of the three axial stations.

Assumptions and restrictions of this beam are that it must lie in the x-y plane and must not have zero length or area. The height is used in calculating the bending stresses and for locating the integration points used for calculation of the section properties. For a rectangular section the height, area and moment of inertia must be constant with one another.

4.3.2 Non-Linear Spring Element – COMBIN39

COMBIN39 is a unidirectional element with non-linear generalised force-deflection capability. The element has longitudinal or torsional capability in one-, two-, or three-dimensional applications. The longitudinal spring-damper option is a uniaxial tension-compression element with up to three degrees of freedom at each node, which are the translations in the x, y, and z directions. In the longitudinal option no bending or torsion is considered. The torsional spring-damper option is a purely rotational element. It also has three degrees of freedom and these are the rotations about the nodal x, y, and z-axes. In this case no bending or axial loads are considered.

Figure 4.2 below shows how COMBIN39 can be better used to model the properties of a connection.

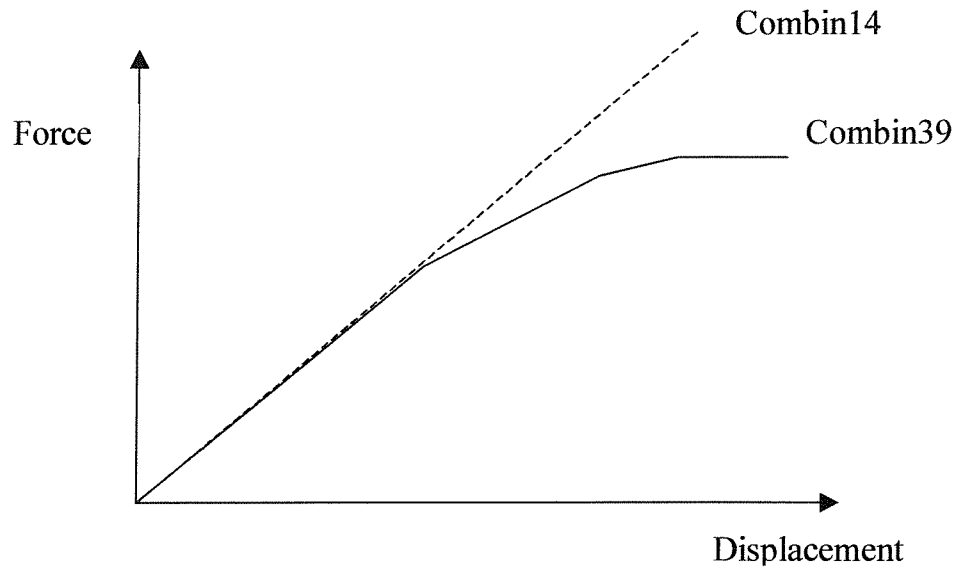

Figure 4.2 Force-Displacement Chart for Combin14 and Combin39

The element is defined by two points and a generalised force-deflection curve. The assumptions and restrictions for this element are the same as those for COMBIN14 for the length restrictions.

The element is non-linear and requires an iterative solution. Loading and unloading should occur gradually. The real constants may not change from their initial values. If the force deflection curve is exceeded then the last defined gradient is maintained.

4.4 Modelling of East-Park Terrace using the Finite Element Method

The QSE package used in the initial analysis did not allow for modelling the stiffness of beam-to-column connections, or of the column bases. The next stage of this research was therefore to model the steel frame using the ANSYS release 5.3 finite element analysis package. The results from the experiment described in Chapter 3 were used to check the results from the model. A further frame was also analysed to discover the effects of beam-to-column connections and of the column base connections on deflections.

As with the QSE stiffness method analysis, the secondary and primary beams were modelled separately. As described above, the beams and columns of the frame were modelled with the 2-D elastic beam element (element type 3), and the beam-to-column connections were modelled with the linear elastic spring element (element type 14). As the experiment was carried out on the fourth floor, and the columns continued down through the building, the column bases were modelled as being fixed at the base of the fourth storey.

The same loading was applied to the frames as that used for the QSE stiffness method analysis. This loading is shown in Figure 4.3.

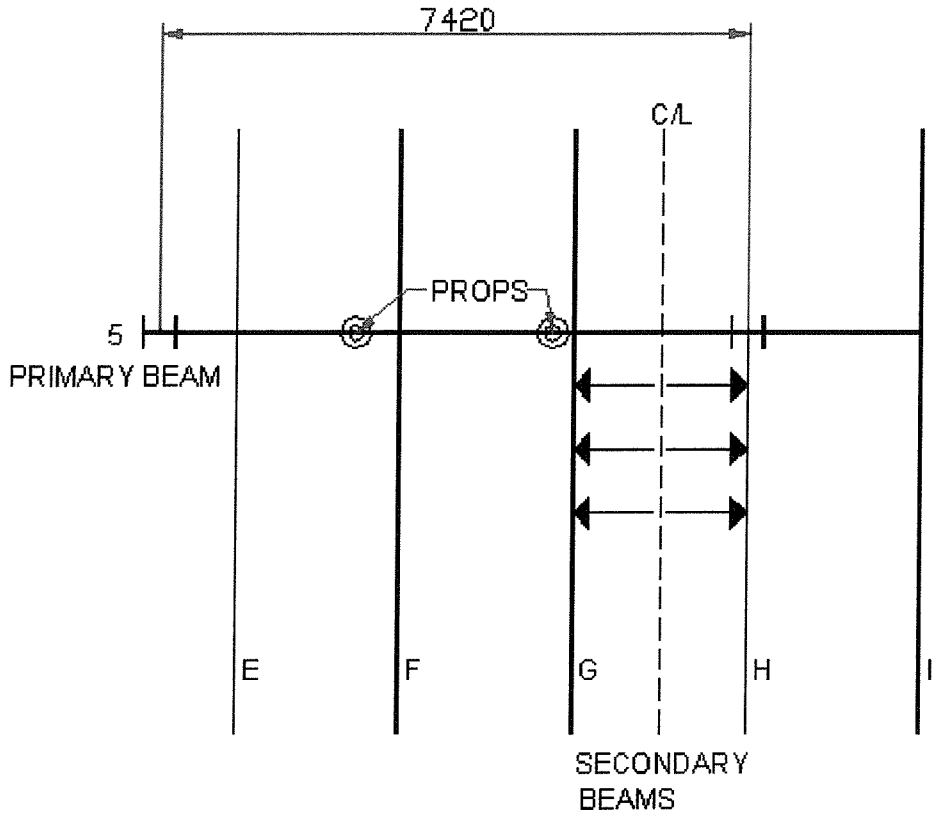

Figure 4.3 Load Distribution

The models were generated directly using nodes and elements. Meshing was not necessary for these models, and by modelling directly with nodes it was possible to place them as required. The elements used for these beam and frame models are described in the previous sections. Further frame modelling using plastic beam elements and a non-linear spring element is described later in this report.

4.4.1 The Secondary Beam

The secondary beam is connected to the column with pinned connections. It was therefore modelled with pinned connections in ANSYS to test whether the results agreed with those from using the stiffness method, and with those from the experiment. Figure 4.4 shows the geometry used for this analysis.

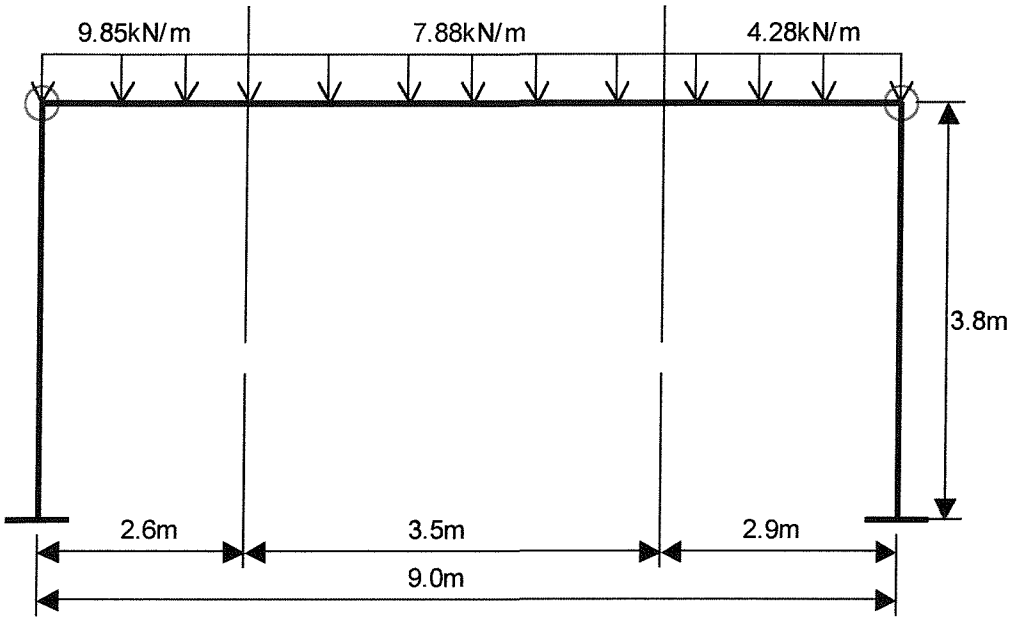

Figure 4.4 Secondary Frame Analysis

The data that was used for the secondary beam frame analysis was taken from steel tables, and is shown in Table 4.1 below.

Table 4.1 Steel Data for Secondary Frame

	Size	**Depth (mm)**	**Width (mm)**	**Area (mm^2)**	**I_{xx} (mm^4)**	**I_{yy} (mm^4)**
Beam	457x152x52	449.8	152.4	6650	$21.3x10^7$	$0.645x10^7$
Column	203x203x71	215.9	206.2	9110	$7.65x10^7$	$2.54x10^7$

The secondary beam had already been modelled using the QSE stiffness method with success. The results from the stiffness method were very close to those measured on site. The finite element method approach, with no joint stiffness at the beam-to-column connections, again gave very similar results; the results are plotted in Figure 4.5 below.

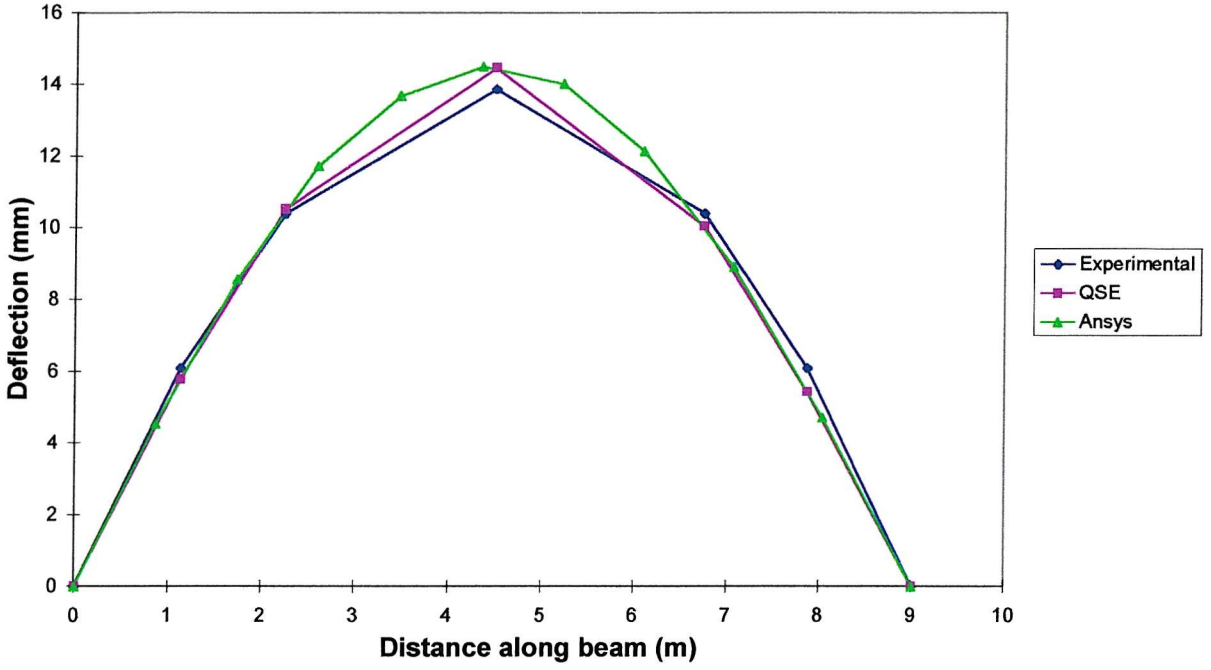

Figure 4.5 Comparison of Results

As this chart shows, all the results for the secondary beam compare very well. For the stiffness method analysis, the nodes were positioned where the transducers were attached in the experiment. However, for the finite element method, more nodes were used, so that the deflected shape could be shown in more detail. These results show that the beam-to-column connection for the secondary beam is acting like a simple connection with low rigidity. The chart also shows that the model has been constructed correctly to give the close correlation of results to the experimental and previous theoretical results.

4.4.2 The Primary Beam

As discussed in Chapter 3, the QSE stiffness method analysis gave no meaningful results for the primary beam, as it was not possible to model the semi-rigid properties of the beam-to-column connection. Comparisons have therefore not been drawn with that analysis in the following material.

The primary frame analysis is more complex than that of the secondary frame. The primary beam has semi-rigid connections, and it was also propped during the construction of the floor above. This causes complications, as the joint stiffness is unknown, and the influence from the propping on the deflection of the primary beam is also unknown. For the analysis of the primary beam, the stiffness of the beam-to-column connection was varied to show how it affects the deflection of the primary beam. During the analysis the properties of the prop were also varied, and it was found that the use of propping has a large influence over the beam deflection.

The unknowns in this analysis are mainly due to the props. The floor below supports the props. This floor was not completely rigid. The props are also placed on wooden blocks, which would deform as the loads were applied to the floor above. The props are adjustable, via a screw thread and locking pin; this would cause a small amount of 'slack' that would be taken up as the load was applied. The exact properties of the props used at East-Park Terrace are also unknown. As explained below, changes to the area of the prop were used to simulate the role of all these factors, to examine how the stiffness of the whole propping arrangement affects the deflections of the beam.

The results will be shown in the form of charts, some of which will show the deflected shape of the beam, whilst others will concentrate just on the mid-span deflection where the deflection was the greatest.

The primary beam has semi-rigid connections. The frame was modelled with different spring rigidities at the connection, ranging from pinned to fully fixed ($K=0$ to $K=\infty$). The effects of the propping were also modelled, using 2-D elastic beam elements. Two props were used, as in the experiment, and they were placed one-third and two-thirds of

the way along the length of the beam. The effects that the propping had on the stiffness of the structure were investigated by altering the cross sectional area of the props (from A=0 to A=706mm^2). Figure 4.6 shows the geometry of the primary beam frame.

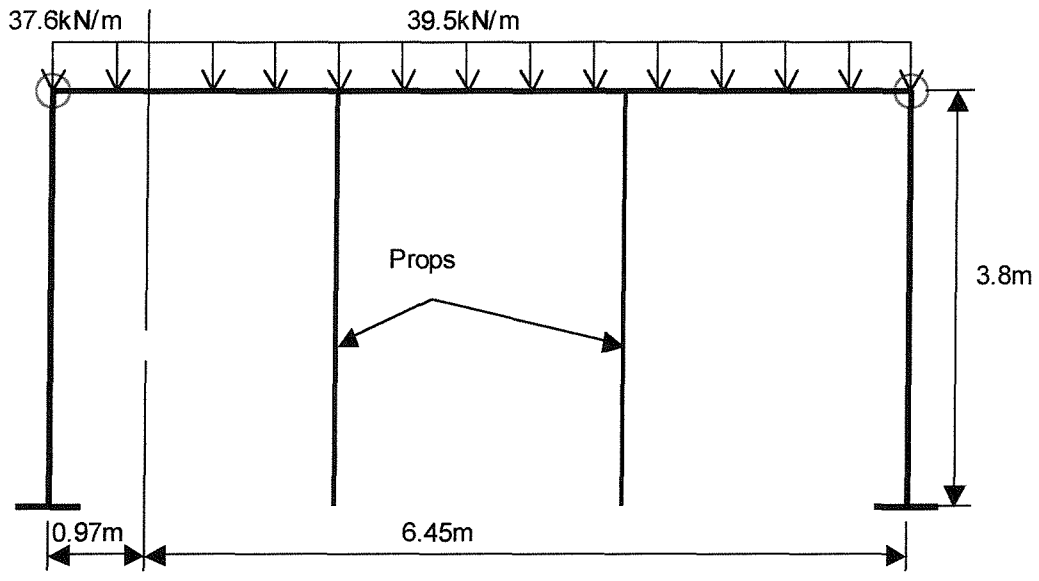

Figure 4.6 Primary Frame Geometry

The steel data used for the analysis was taken from steel tables, and is shown in Table 4.2 below.

Table 4.2 Steel Data for Primary Frame

	Size	**Depth (mm)**	**Width (mm)**	**Area (mm^2)**	**I_{xx} (mm^4)**	**I_{yy} (mm^4)**
Beam	406x178x60	406.4	177.8	7600	21.5×10^7	1.2×10^7
Column	203x203x71	215.9	206.2	9110	7.65×10^7	2.54×10^7

4.4.3 Modelling With No Props

To start with the primary frame was modelled with no props; the results of this analysis are shown in Figure 4.7, along with the experimental results.

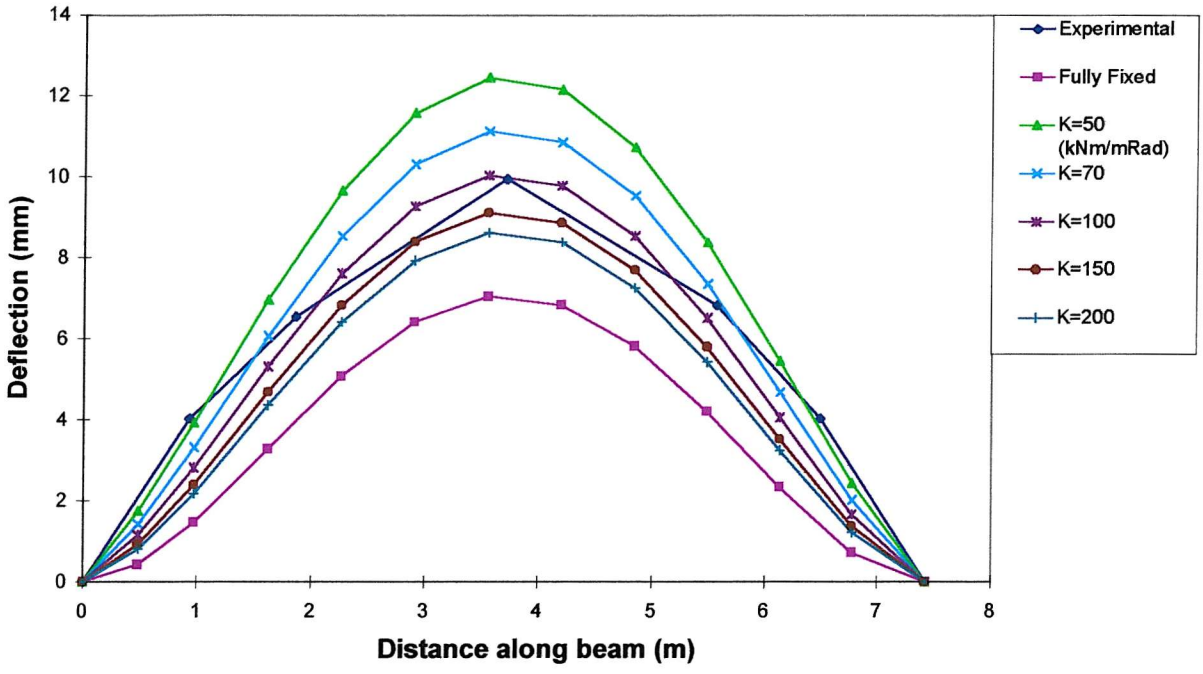

Figure 4.7 Primary Beam Deflections with Change in Joint Stiffness

This chart shows that joint stiffness of the model needs to be very stiff to get the results close to the monitored deflections from the experiment. At the stage of the experiment (the concrete pour) the connection was only a bare steel connection, so stiffness of this order would not be expected. The chart shows that a stiffness of about 100kNm/mRad would be needed to produce the deflections for the experimental load. The deflected shape also did not follow that of the experiment. These results would be due to the fact that the props were not modelled. These would both reduce the deflection on the beam, and change the deformed shape of the beam.

These results do show that, as would be expected, using stiff connections as opposed to simple ones drastically reduces the beam's deflection.

4.4.4 Modelling With Props

As noted earlier, the precise properties of the propping arrangement were unknown. Several factors in this arrangement affect the deflection of the primary beam. The beam is propped, and the props (which are adjustable) are supported on wooden blocks, which in turn are supported on the completed floor slab beneath. As the complete properties of all these are unknown, the area of the prop was varied to create a pseudo-stiffness that would act as a proxy for the role of all the elements in the propping arrangement. The primary frame was analysed for prop areas ranging from zero to infinite (fully fixed props acting as supports). The props were modelled using the 2-D elastic beam element (element type 3).

4.4.4.1 Beam Deflections

It was found that the prop area has a large influence over the beam deflection; the relationship of prop area and deflection is plotted in Figure 4.8.

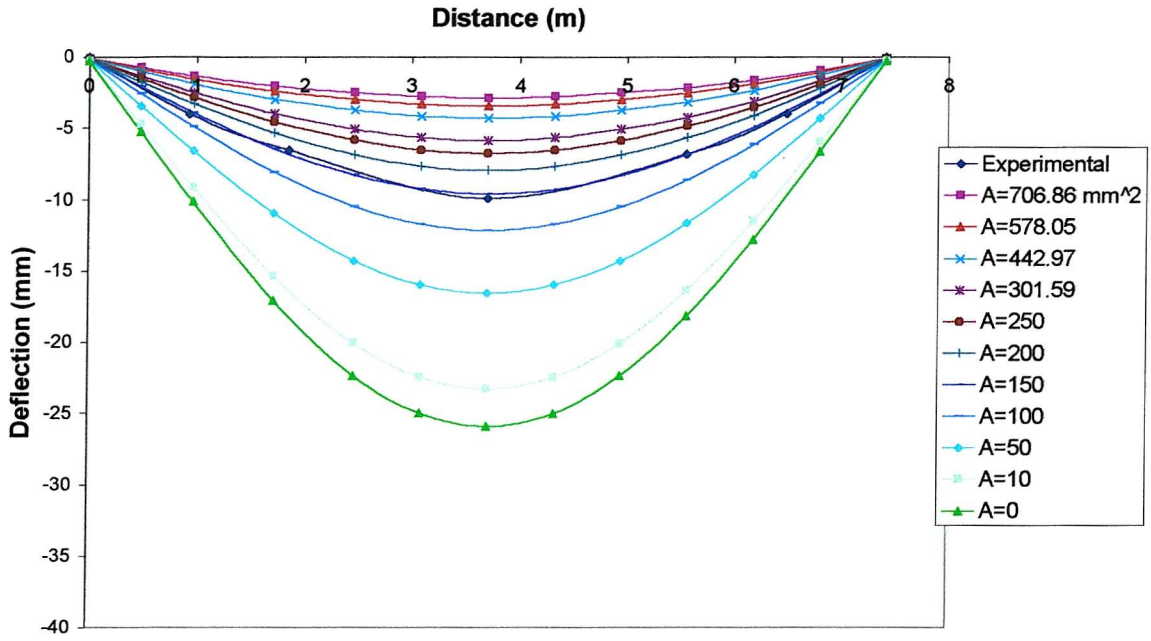

Figure 4.8 Deflections of Primary Beam with Change in Prop Area: Joint Stiffness k=10kNm/mRad

Figure 4.8 shows the deflections with a joint stiffness of 10kNm/mRad, and with differing prop areas as shown in the chart legend. Mid-span deflections for this example range from 25.9mm for an unpropped beam, to 2.9mm for a prop area of 707mm^2 (prop with external diameter of 50mm and a 5mm wall thickness). An area of around 150mm^2 seems to give the closest agreement with the experimental results for this joint stiffness.

150mm^2 is very low for a prop area. The regulations for a prop are given in BS4074 **[40]**: the external diameter of the outer tube must be at least 60.3mm, with a wall thickness of 4.5mm; the inner tube must have an external diameter of at least 48.3mm, with a wall thickness of 4.0mm. This gives cross sectional areas of 560.5mm^2 and 788.9mm^2. As the prop area found from this analysis was so low compared to the minimum required prop area given in BS4074, this would seem to indicate that the role of the other elements in the propping arrangement has a considerable influence on the

deflection of the primary beam. Blocks of wood are placed between the prop and the structure, and they would deform under loading. Slack would be taken up within the prop as the screw thread and locking pin bedded in. The props were also supported by the completed floor below, which would deflect under loading.

The following charts show how both the prop area and the joint stiffness affect the deflections.

Figure 4.9 shows how the mid-span deflection changes when the joint stiffness is altered. Each of the lines of the chart represents a different prop section area in mm^2. These prop areas are given in the chart legend.

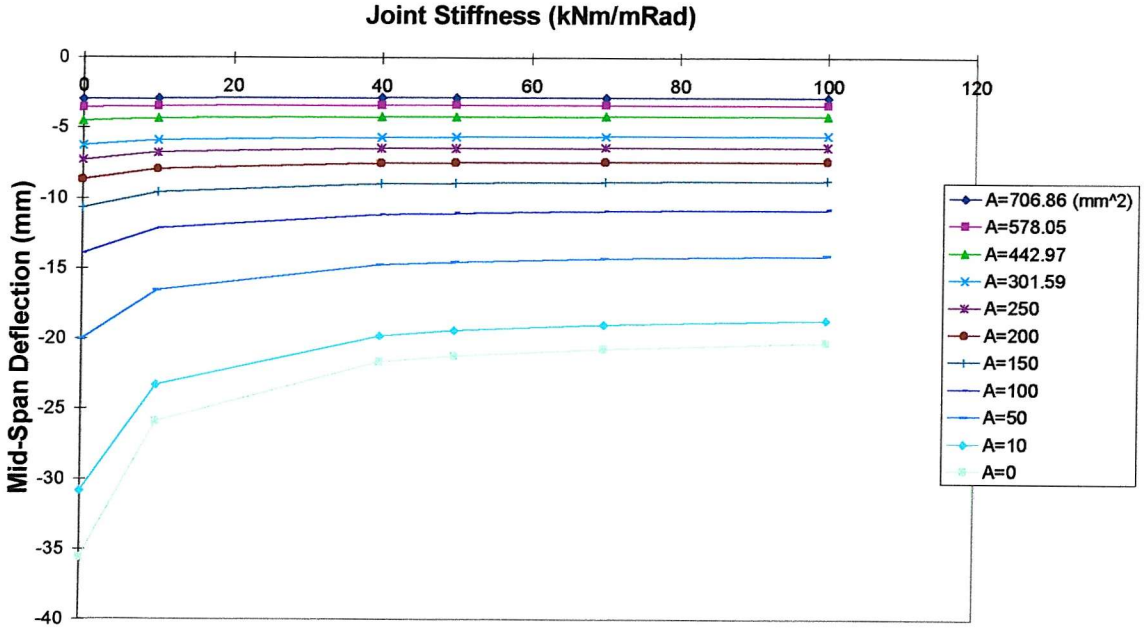

Figure 4.9 Influence of Joint Stiffness on Deflection

Figure 4.9 shows that initially the connection stiffness has an effect on the beam deflection, but its influence rapidly decreases as the connection becomes stiffer. However, the prop area seems to have a very large influence over the mid-span deflection of the beam. Figure 4.10 shows this trend better. Here the x-axis represents the prop area, and each line on the chart represents a different connection stiffness, as shown in the legend.

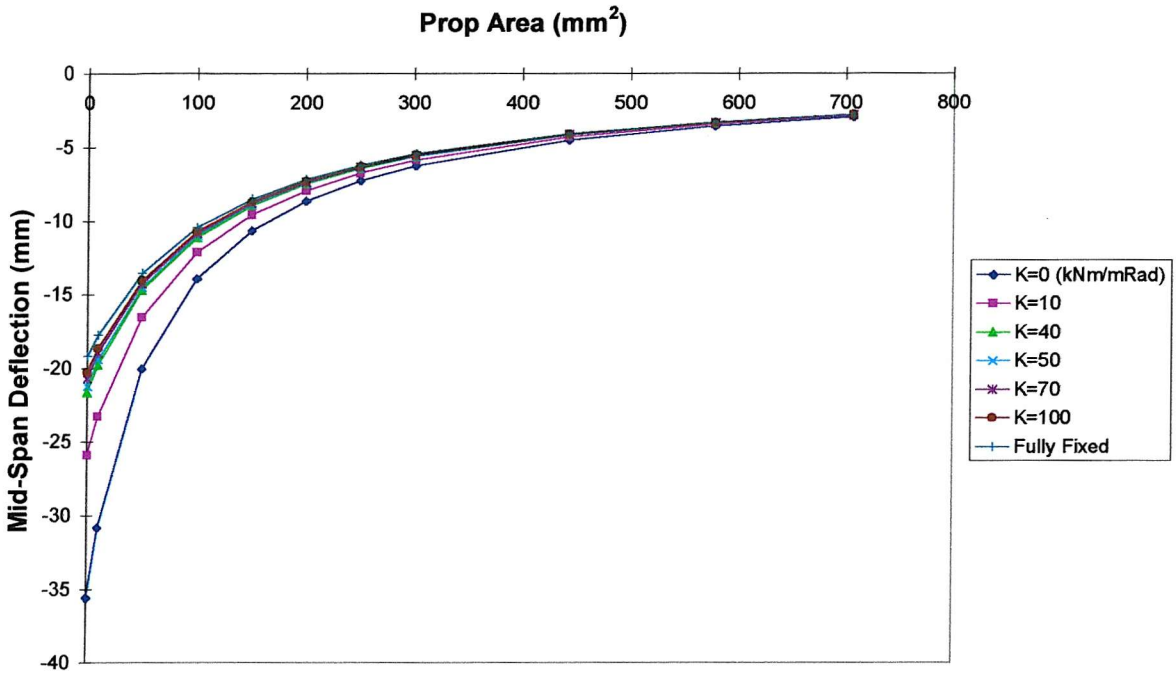

Figure 4.10 Influence of Prop Area on Deflection

Figure 4.10 demonstrates the influence of prop area on the mid-span deflection of the beam.

The two charts above show that although connection stiffness is important, the importance of propping should not be overlooked during the construction phase. Good propping can drastically reduce the deflection of the beam, and therefore reduce the final sag in the beam after construction. The connection stiffness will be considerably more important once the construction is complete and the building is in use. The connections will then be composite connections, which will be far stiffer than those of the bare steel connections. The extra stiffness is due to the reinforcing bars, and the long lever arm from the base of the connection.

So far, only changing the properties of the prop have been discussed. Of course, the deflection is also going to be greatly affected by the number of props supporting the loaded beam.

4.4.4.2 Bending Moments

The effects that the props would have on the bending moments along the beam were then investigated. It was found that, similarly to the deflections, props greatly reduced the bending moments in the modelled beam.

Figure 4.11 below illustrates how the bending moments along the primary beam decrease with an increased prop section area.

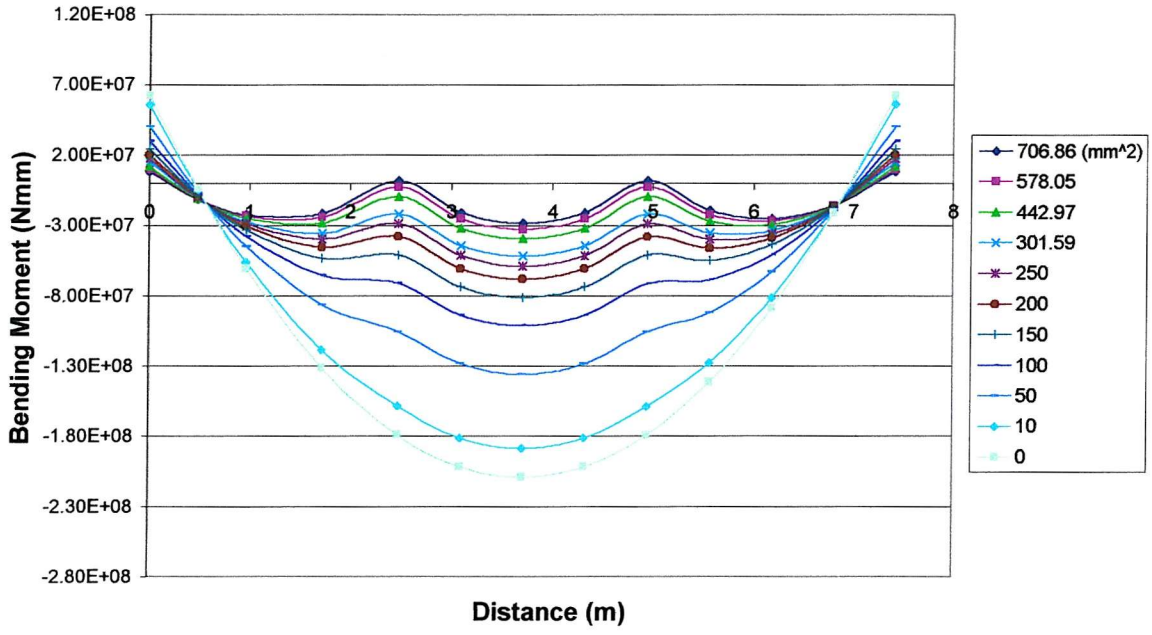

Figure 4.11 Influence on Bending Moments of Prop Section Area (k=10kNm/mRad)

The results shown in this chart are for a beam with a low beam-to-column stiffness, and the connection stiffness is kept constant for each analysis. The decrease in bending moment is from the propping only. The prop area is shown in the legend (mm^2). The largest bending moment at the beam mid-span that would be experienced with no props is $2.09x10^5$kNmm, for this example. This value drops to $5.20x10^4$kNmm if two props of area of $300mm^2$ are used to prop the beam. This is a reduction in bending moment

to around one quarter of the original value. The moment will drop still lower with larger prop areas. Obviously the moment would drop still more with the introduction of more props. The bending moment shown here is the bending moment in the steel beam during the construction loading. The bending moment will increase once the props are removed, but by this time the composite action of the steel beams and concrete floors will produce a very strong and stiff section. Also the connections between the beams and columns will be composite, and far stiffer than they are during construction.

The influence on bending moment from the propping does decrease with the increase in connection stiffness, but it still has a large influence even with very stiff connections. Figure 4.12 illustrates an example of this.

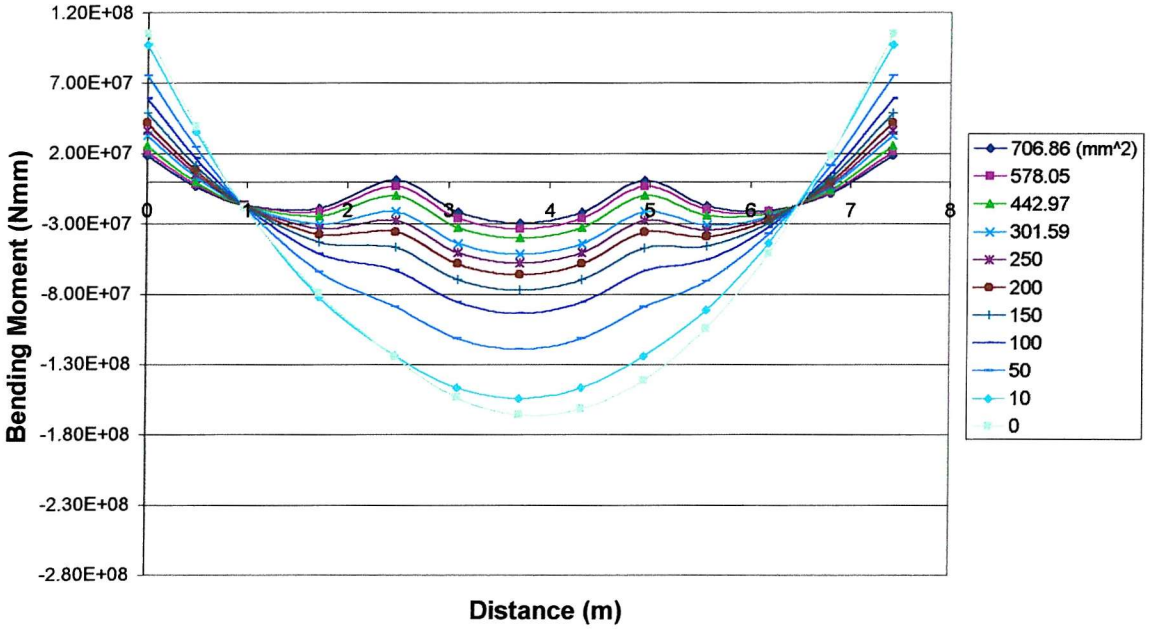

Figure 4.12 Influence on Bending Moment from Prop Area (k=Fully Fixed)

This chart shows the opposite extreme of connection stiffness to that shown in the previous chart: this time the beam-to-column connection is taken as being fully fixed. As the chart shows, the props still play a large part in the bending moments. They not

only decrease the bending moments in the sagging area in the mid-span, but also decrease the bending moments at the connections in the hogging area. In this example the largest bending moment with no propping is $1.66x10^5$kNmm; this drops to $5.17x10^4$kNmm when 300mm^2 section area of props is used. This gives a reduction in bending moment to around one third of the original value. So these analyses have shown that through a careful propping arrangement it is possible to greatly reduce the bending moments during the construction stages. The analyses have shown that the bending moments are reduced in both the hogging and sagging sections of the beam when props are used, and that the propping has a greater effect when the rigidity of the beam-to-column connections is low.

4.5 Applying Sway Loading

The next stage in the analysis was to see how the beam-to-column connection affected deflections from any sway loading that may be applied to the steel frame. For this analysis the East-Park Terrace frame was still used, with the addition of a sway load as shown in Figure 4.13 below. The building was a braced frame, so this analysis is not relevant to the building, but the analysis has been conducted to find out how the semi-rigid connections can affect the sway deflection of frames. The applied sway load was chosen to give sensible sway deflections, around the deflection limit set in British Standards.

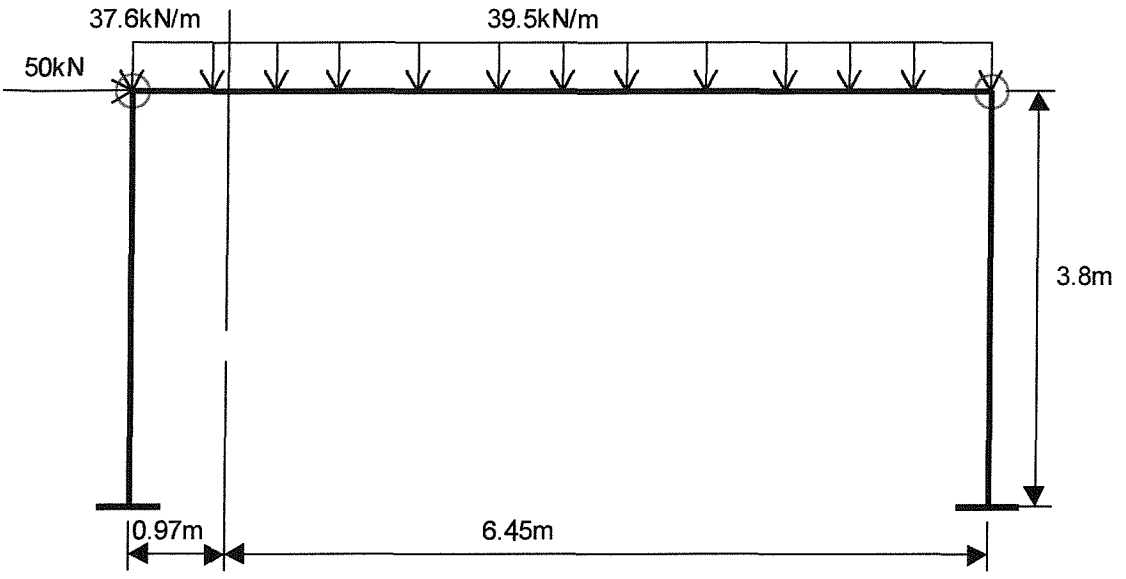

Figure 4.13 Sway Loading on Primary Frame

As the props gave no horizontal resistance against sway they were removed from the analysis. In initial analyses it was found that the props reduced the sway deflection. The lower deflections occurred because when the props were in place, the deflection in the beam was lower, which meant that the tops of the columns experienced reduced lateral movement.

It was found that by increasing the beam-to-column stiffness the sway deflection is decreased, as would be expected.

Figure 4.14 plots the deformation of the column for different beam-to-column stiffnesses.

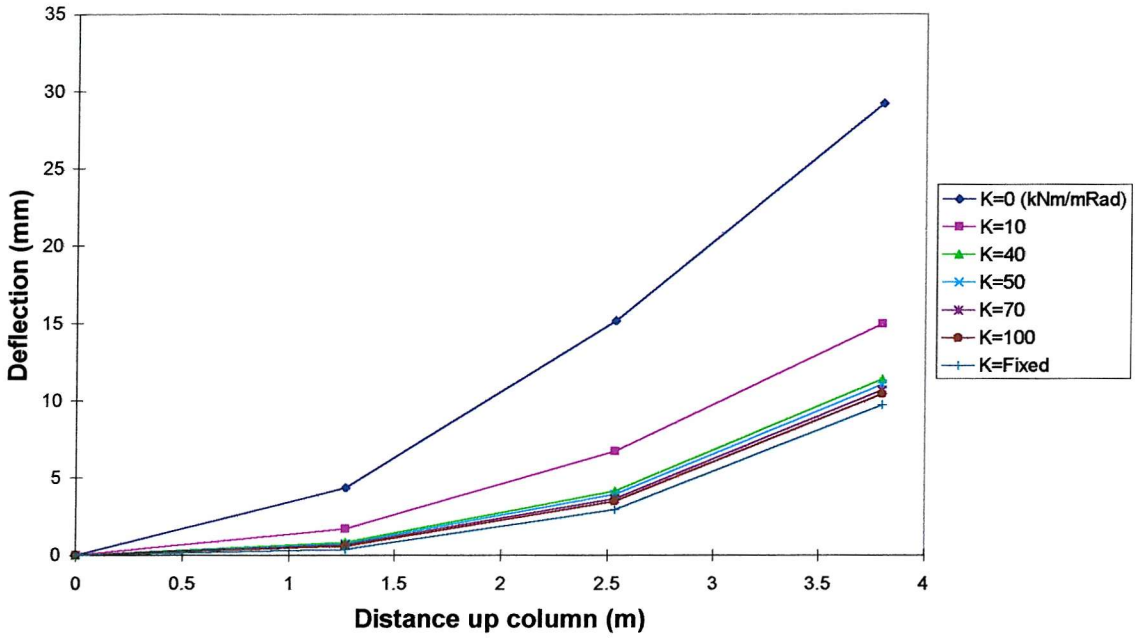

Figure 4.14 Horizontal Deflection for Changes in Joint Stiffness

As this chart shows, the beam-to-column stiffness affects the sway deflection. For this analysis the base connection rotational stiffness of the frame was constant and fully fixed, so the only change is from the beam-to-column stiffness. The chart shows that increasing the joint stiffness at lower stiffnesses has a greater effect than increasing them at a higher stiffness. This is demonstrated by Figure 4.15, which plots the sway deflection at the top of the column, where the load is applied, against the connection stiffness.

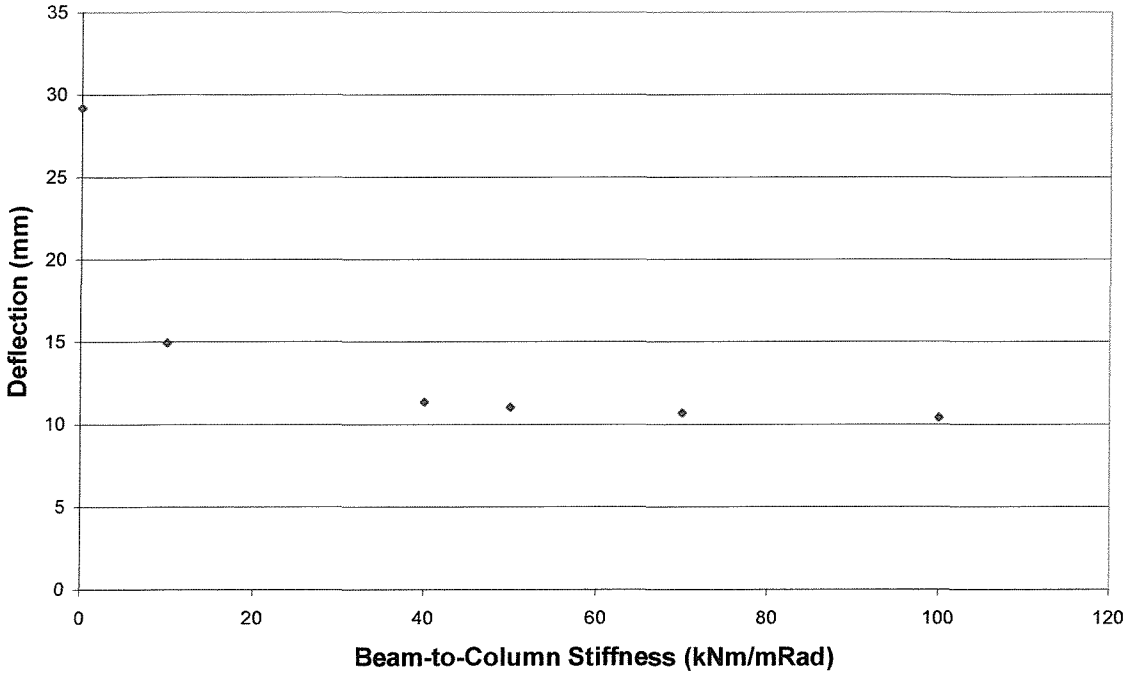

Figure 4.15 Maximum Sway Deflection

As discussed previously, the above chart shows that initially the sway deflection decreases greatly with an increase in connection stiffness.

4.6 Summary

This chapter has shown that the finite element method can be used to great effect in the analysis of semi-rigid frames. The elements chosen for the modelling performed well in the analysis.

The validation work in this chapter has shown that the finite element model has agreed closely with the results from the on-site experiment, with a discrepancy of less than 5% for the secondary beam deflection at mid-span.

The finite element model based on the primary beam has been used to examine the effects of joint stiffness on bending moment, mid-span deflection and sway deflection.

It was found that an increase in joint stiffness greatly reduces the sway and mid-span deflections, and also the bending moments at mid-span.

The next chapter considers the analysis of single-storey structures in more depth, using elastic and plastic models of sway and non-sway frames.

Chapter 5

Single-Storey Frame Analysis

5.1 Introduction

In this chapter finite element analysis is used to model a single-storey frame. This work is a direct development from the beam analysis in the previous chapter. The frame has been analysed using both elastic and plastic models with a range of connection stiffnesses from pinned to fully-fixed. The research in this chapter is an introduction to the techniques that will be used for the multi-storey modelling of the later chapters.

5.2 Elastic Analysis

The elastic models were constructed using the elastic beam and spring damper element that were presented in Chapter 4. The batch file system was used to make it possible to solve many frames in succession with different beam-to-column stiffnesses, but keeping the same geometry file.

5.2.1 Non-Sway Analysis

For this stage of the research both the beam-to-column and the base rotational stiffness were changed to see how the sway deflection and the beam deflection were affected. The model that was used for these analyses is shown in Figure 5.1 below. These frame dimensions were chosen to be the same as those used by Pertold **[38, 39]** in his analyses.

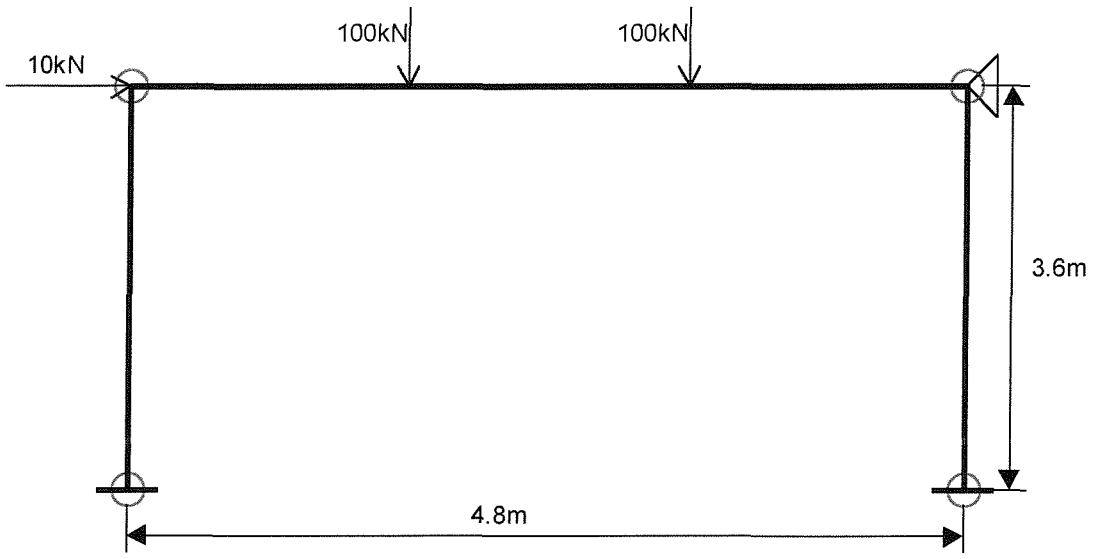

Figure 5.1 Frame Loading for Non-Sway Analysis

The frame is made from just one cross section to keep it simple. This cross section of the beam and column can easily be changed independently of each other in the ANSYS file to model a different frame. The properties of the beam and column are shown in Table 5.1 below.

Table 5.1 Steel Data for Non-Sway Frame

	Size	Depth (mm)	Width (mm)	Area (mm^2)	I_{xx} (mm^4)	I_{yy} (mm^4)
Beam	254x254x89	260.4	255.9	11400	$14.3x10^7$	$4.85x10^7$
Column	254x254x89	260.4	255.9	11400	$14.3x10^7$	$4.85x10^7$

ANSYS batch files were set up so that one analysis would run directly after another, and the real constants for the column bases and beam-to-column connections would be changed in each analysis. The deflection results were then written to an output file, giving a set of results for input into a spreadsheet, and the input data could be easily altered if needed in later analyses.

For the initial analysis the same beam-to-column connection stiffnesses were used as in the East-Park Terrace analyses, presented in Chapter 4. The results from these analyses showed that most of the effect on deflection was from increasing the joint stiffnesses at the most flexible end of the range. Because of this, the connection stiffnesses were altered so that they started much lower, at 1kNm/mRad. The connection stiffnesses for this analysis were then doubled in each of the subsequent analyses until a value of 64kNm/mRad was reached, and finally the fully fixed case was analysed. Changing the beam-to-column and the base rotational stiffness independently of each other produced a table of 81 values for the beam deflection at mid-span. The results are given in the table below.

Table 5.2 Non-Sway Deflection Results

	K Beam kNm/mRad								
K Column	0	1	2	4	8	16	32	64	Fixed
0	-13.621	-12.858	-12.245	-11.323	-10.164	-8.9979	-8.0605	-7.4332	-6.6464
1	-13.621	-12.858	-12.244	-11.32	-10.158	-8.988	-8.0462	-7.4155	-6.6238
2	-13.621	-12.857	-12.244	-11.318	-10.153	-8.9788	-8.0329	-7.3989	-6.6028
4	-13.621	-12.857	-12.242	-11.314	-10.144	-8.9623	-8.0089	-7.3692	-6.5649
8	-13.621	-12.856	-12.24	-11.307	-10.129	-8.9352	-7.9694	-7.3201	-6.5022
16	-13.621	-12.855	-12.237	-11.298	-10.107	-8.8964	-7.9129	-7.2497	-6.4121
32	-13.621	-12.854	-12.233	-11.287	-10.082	-8.8512	-7.8465	-7.1669	-6.3059
64	-13.621	-12.853	-12.229	-11.277	-10.059	-8.809	-7.7846	-7.0893	-6.2059
Fixed	-13.621	-12.851	-12.223	-11.26	-10.018	-8.7329	-7.672	-6.9479	-6.023

These results are plotted in Figure 5.2 below.

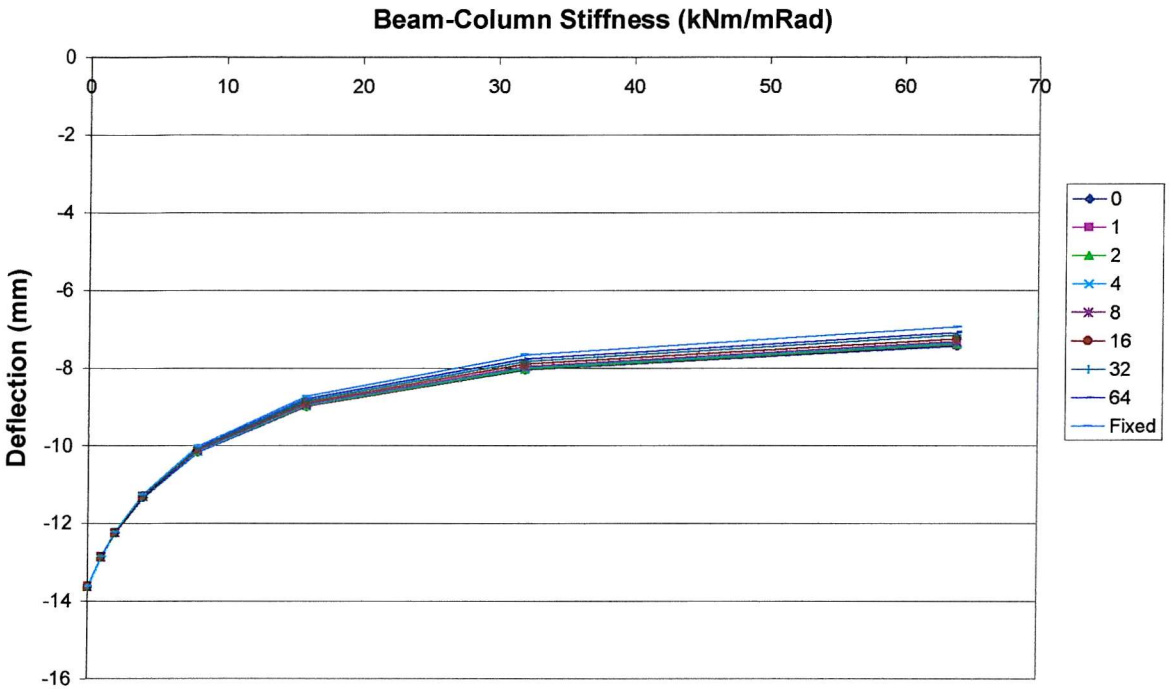

Figure 5.2 Non-Sway Vertical Deflections

The x-axis of the chart shows increasing beam-to-column stiffnesses. The chart demonstrates that the beam-to-column connections have a large influence over the mid-span deflection of the beam, especially with increases at the lower end of the scale of stiffness. The influence becomes less with larger stiffnesses. Each of the lines represents a different column base stiffness. As the lines are very close to each other, it is shown that, in this case, the column base stiffness has very little influence over the mid-span deflection of a non-sway frame.

The bending moments were also calculated from ANSYS; the charts below show the results from those analyses.

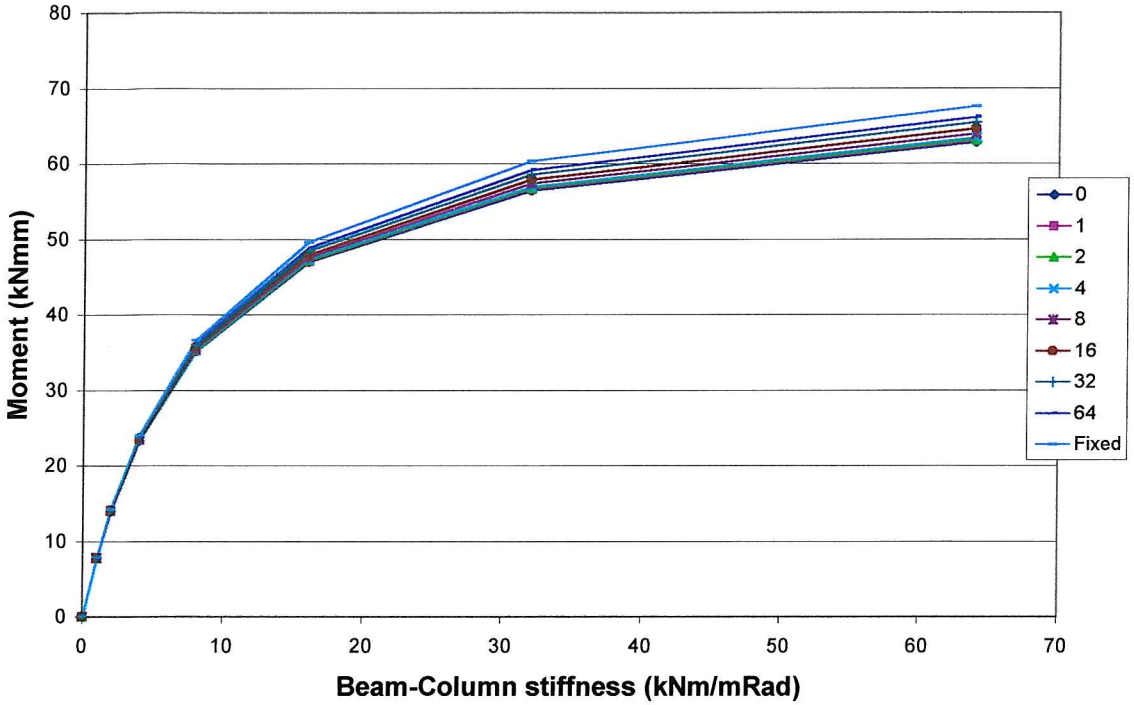

Figure 5.3 Bending Moments at the Top of the Column

Figure 5.3 shows that the beam-to-column stiffness has a large effect on the moments at the top of the column, but again the column base stiffness makes very little difference. This is also true for the mid-span moments, as shown in Figure 5.4 below.

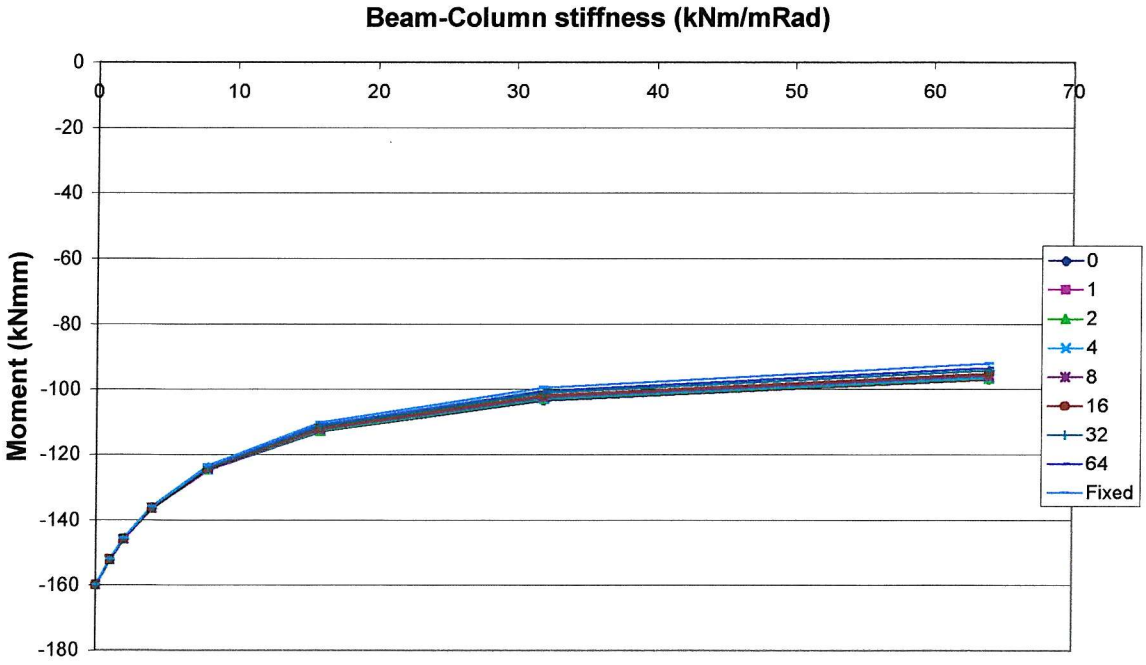

Figure 5.4 Bending Moments at Mid-Span

The column base rigidity does, however, affect the moments at the base of the column, as would be expected; this is shown in Figure 5.5 below.

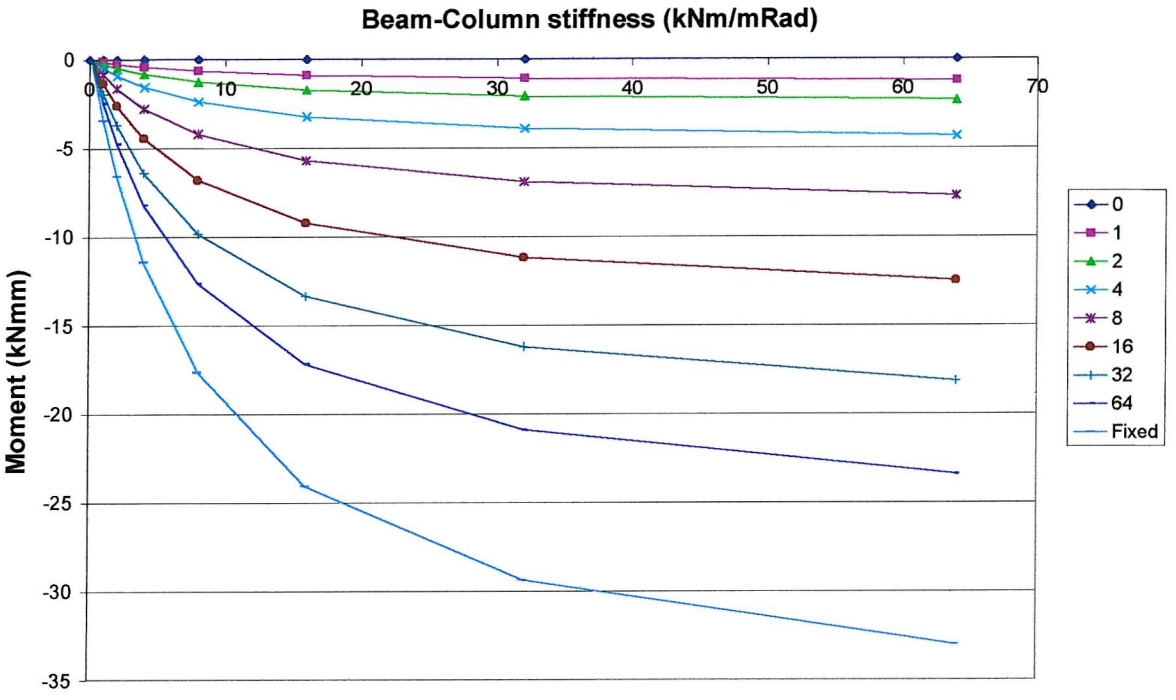

Figure 5.5 Moments at Column Base

5.2.2 Sway Analysis

For the sway analyses it is expected that there will be more influence from the column base connection, as shown in the research of Pertold **[38, 39]**. The same model is used as before, only this time the restraint at the top of the column is removed. The model is shown in Figure 5.6 below.

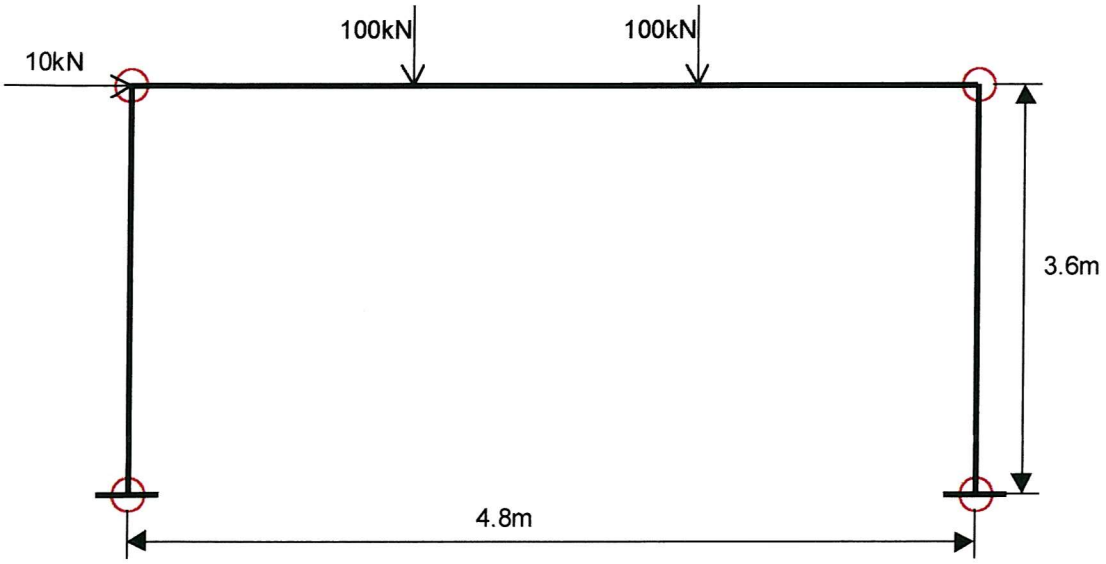

Figure 5.6 Sway Frame Model

The same cross-sections were used as in the previous model. The beam-to-column stiffnesses and column base stiffnesses were also kept the same as in the previous analyses. The deflections at the top of the column, the sway deflection, and the deflection at the mid-span were calculated.

The results of these analyses are shown in Table 5.3 and Table 5.4 below.

Table 5.3 Mid-Span Vertical Beam Deflection

	K Beam kNm/mRad								
K Column	0	1	2	4	8	16	32	64	Fixed
0	N/A	-12.78	-12.167	-11.244	-10.084	-8.9171	-7.979	-7.3512	-6.5637
1	-13.544	-12.78	-12.166	-11.241	-10.078	-8.9071	-7.9645	-7.3333	-6.541
2	-13.544	-12.78	-12.165	-11.239	-10.073	-8.8979	-7.9511	-7.3167	-6.5198
4	-13.544	-12.779	-12.164	-11.235	-10.064	-8.8812	-7.927	-7.2867	-6.4817
8	-13.544	-12.779	-12.162	-11.228	-10.049	-8.8538	-7.8872	-7.2373	-6.4186
16	-13.544	-12.778	-12.158	-11.219	-10.027	-8.8148	-7.8303	-7.1665	-6.3281
32	-13.544	-12.776	-12.154	-11.208	-10.002	-8.7692	-7.7635	-7.0831	-6.2212
64	-13.544	-12.775	-12.151	-11.198	-9.9784	-8.7267	-7.7011	-7.005	-6.1207
Fixed	-13.544	-12.773	-12.144	-11.18	-9.9365	-8.6499	-7.5878	-6.8628	-5.9368

Table 5.4 Horizontal Sway Deflection at Point of Applied Sway Load

K Column	K Beam kNm/mRad								
	0	1	2	4	8	16	32	64	Fixed
0	N/A	69.246	36.847	20.65	12.553	8.5068	6.4846	5.4739	4.4637
1	67.458	33.511	23.228	15.334	10.228	7.2815	5.6925	4.8664	4.0184
2	35.058	22.685	17.308	12.381	8.728	6.4221	5.1115	4.4104	3.6761
4	18.858	14.373	11.883	9.203	6.9077	5.2963	4.3164	3.7715	3.1845
8	10.758	8.9948	7.8584	6.4796	5.1454	4.1089	3.4329	3.0407	2.6043
16	6.7077	5.8902	5.317	4.5666	3.7755	3.1115	2.6524	2.376	2.0594
32	4.6827	4.2148	3.8718	3.4026	2.8816	2.4217	2.0909	1.8864	1.647
64	3.6702	3.3435	3.0984	2.7552	2.363	2.0065	1.744	1.579	1.3832
Fixed	2.6577	2.4487	2.2881	2.0577	1.7861	1.5312	1.3384	1.2149	1.0659

For the sway deflection the point where the loading was applied did not always give the largest deflection, as might have been expected. Where this was the case, the values are highlighted in the table above: these deflections are for the point where the loading was applied, but a larger deflection occurs elsewhere. This larger deflection is in the opposite column, where the top of the column bends outwards as shown in Figure 5.7 below.

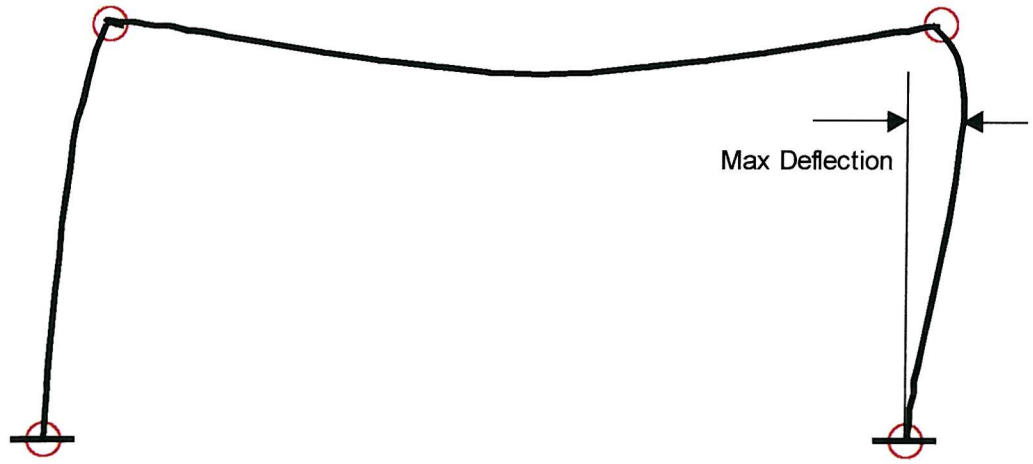

Figure 5.7 Deformed Shape of Sway Frame

The results for the sway deflections have been plotted on charts and these are shown below. The results are shown on four separate charts to demonstrate how the sway deflection and the beam deflection change with both the beam-to-column connection stiffness and the column base rotational stiffness.

Figures 5.8 and 5.9 show the vertical beam deflection at mid-span.

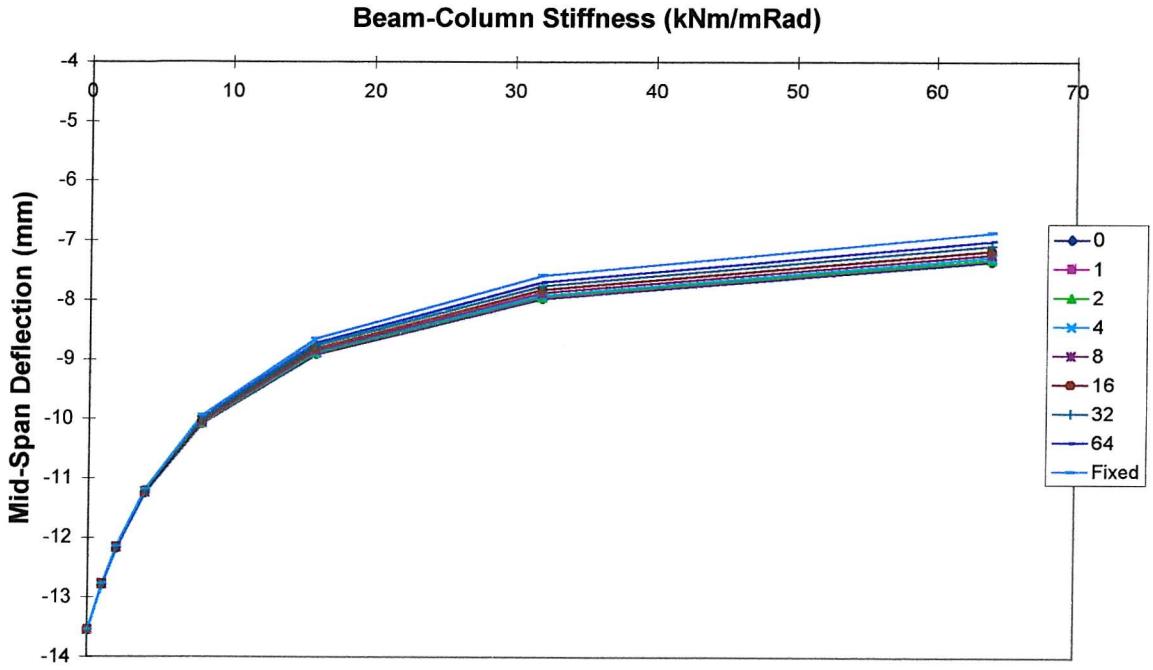

Figure 5.8 Mid-Span Beam Deflection v Beam-to-Column Stiffness

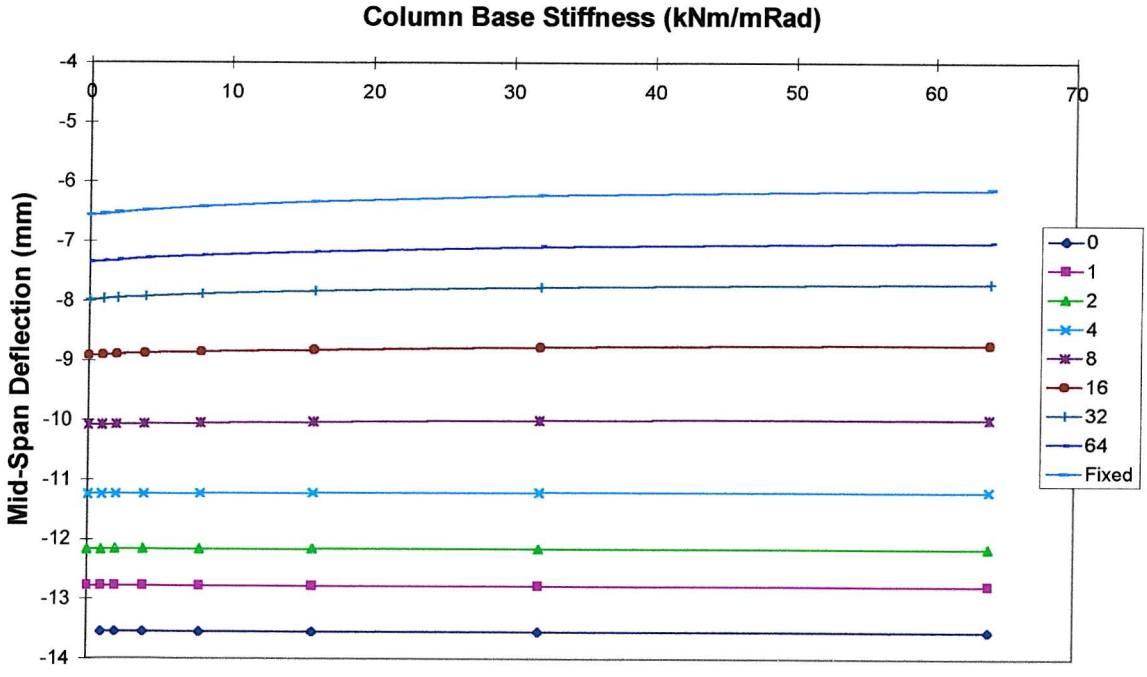

Figure 5.9 Mid-Span Beam Deflection v Column Base Stiffness

Both of these charts are plotted using the same set of results, but display them in a different way. Figure 5.8 shows how the beam-to-column stiffness affects the mid-span deflection, and each of the lines on the chart represents a column base stiffness in kNm/mRad. Figure 5.9, however, shows how the base stiffness affects the mid-span deflection; this time each line on the chart represents a beam-to-column stiffness in kNm/mRad. These charts show that the beam-to-column stiffness has a large influence over the mid-span deflection, especially at the lower stiffnesses. The column base rotational stiffness, however, has a very low influence on deflection. This is as would be expected, as the only loading on it from the beam is when the beam deflects, and therefore the columns get deflected inwards as the beam effectively shortens. There is no other sway loading applied to the column base from the beam loading. The results for this are very similar to those from the non-sway analyses of the deflections of the mid-span of the beam.

Figure 5.10 and Figure 5.11 show how the horizontal, sway, deflection is influenced by the beam-to-column connection stiffness and the column rotational stiffness. Again these results are plotted on two different charts.

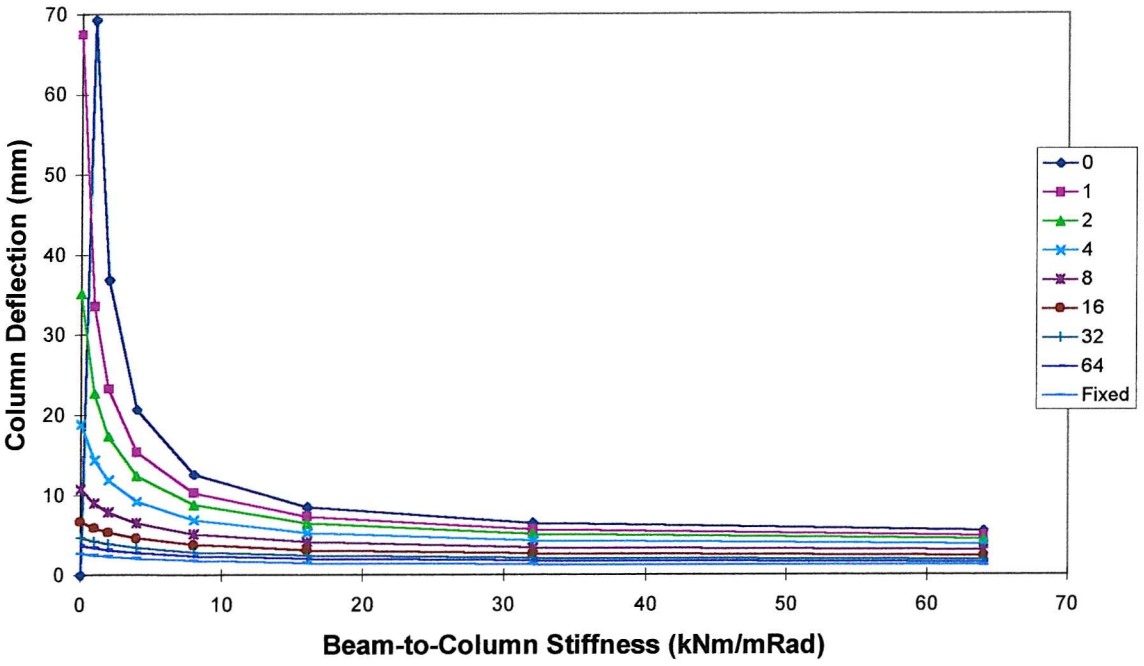

Figure 5.10 Sway Deflection v Beam-to-Column Stiffness

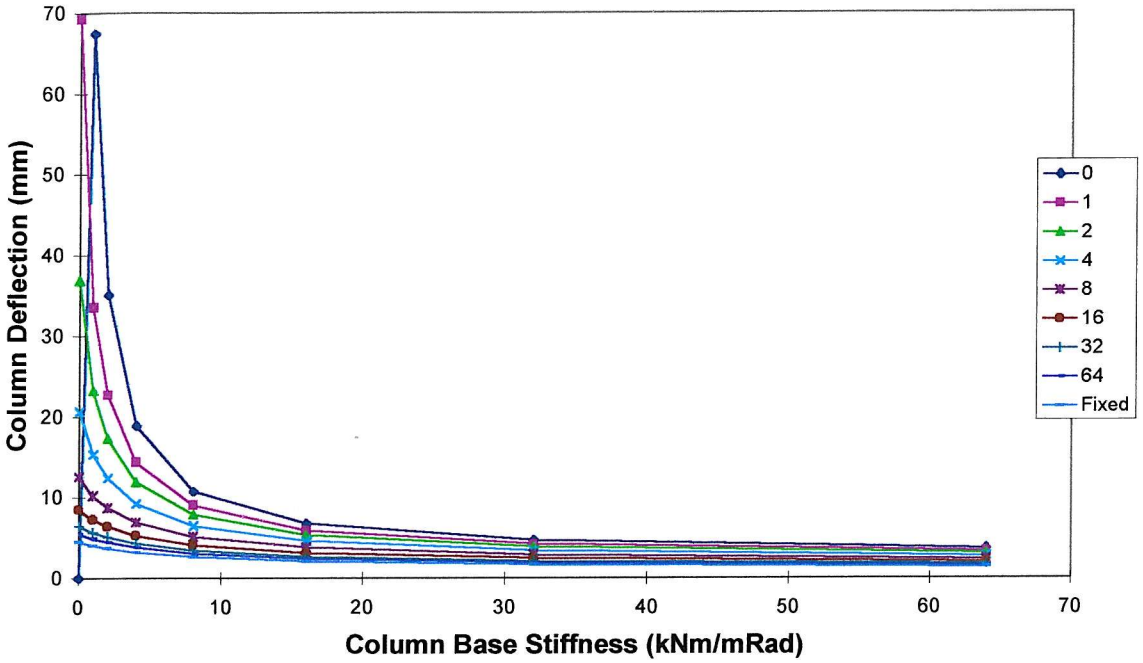

Figure 5.11 Sway Deflection v Column Base Stiffness

Figure 5.10 shows how the beam-to-column stiffness affects the column sway. Each of the lines on the chart represents a column base stiffness in kNm/mRad. Figure 5.11 shows how the column base rotational stiffness affects the column sway, and each line on the chart represents a beam-to-column stiffness in kNm/mRad. These charts show that whilst the vertical beam deflection is dependent only on the beam-to-column connection stiffness, the sway deflection is equally dependent on both the beam-to-column connection stiffness and the column base rotational stiffness. The charts also show that an increase in stiffness at the lower end of the scale of stiffnesses has the most dramatic effect on lowering the deflections; this is true for both sway and beam deflections.

As well as plotting the deflections, it is also possible to plot the beam-to-column connection, and column base rotations. This will be of more use as results can then be compared for different geometries. Figure 5.12 below plots the results for the column base rotations.

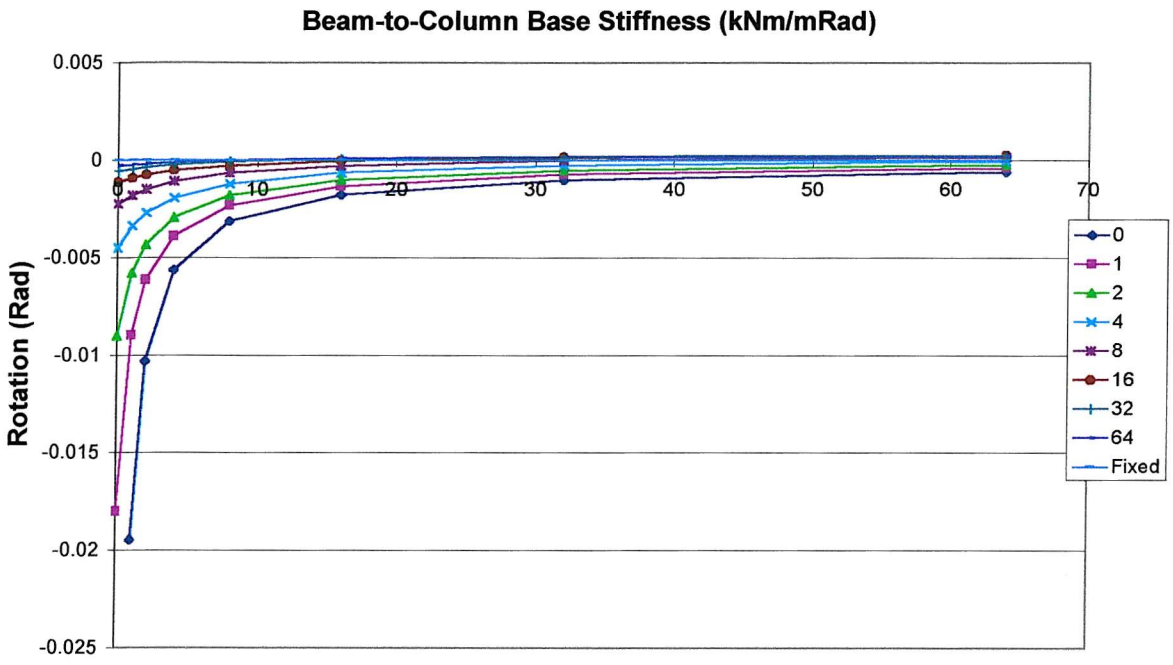

Figure 5.12 Column Base Rotation

Figure 5.12 shows how the beam-to-column stiffness affects the column base rotation under the sway loading. Each of the lines on the chart represents a different column base rotation stiffness in kNm/mRad. As the chart shows, the beam-to-column stiffness has a large influence over the rotation at the column base. The results show that the column base rotational stiffness influences the rotation by a similar amount. Figure 5.10 and Figure 5.11 above also show this trend.

The moments of the elements were also output from ANSYS. The results show the same trends as those for deflection, due to the model being elastic. The column base stiffness has very little influence on the bending moments at mid-span. However, it does have a large influence on the moments at the top of the column. Figure 5.13 below plots the bending moments at the top of the column.

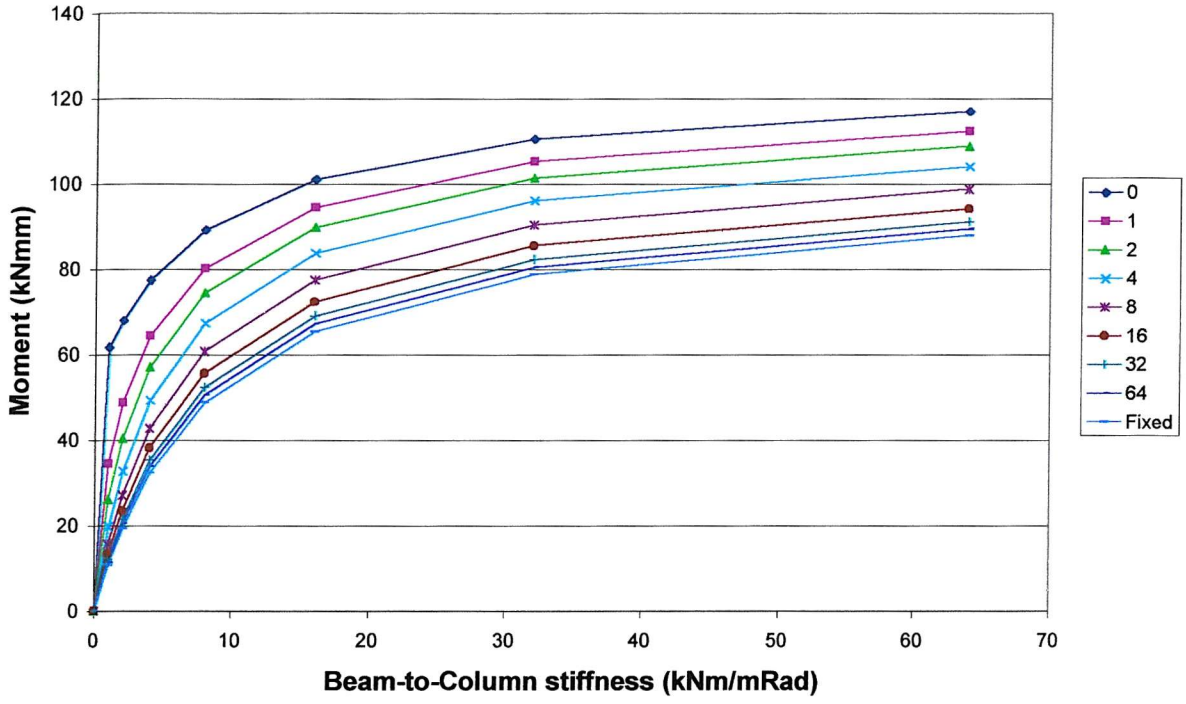

Figure 5.13 Bending Moments at the Top of the Column

Each of the lines on the chart in Figure 5.13 represents a different column base stiffness. The chart shows that for low base stiffnesses the moments at the beam-to-column connection are far greater, due to the moment being redistributed to the stiffest connection.

The three bending moment diagrams below show the three extreme cases for pinned and rigid connections. These show how the bending moments are distributed to the rigid connection. For the semi-rigid connections the bending moments are distributed to the stiffest connection, and the bending moment diagrams fall in between those cases that are shown in the figures below.

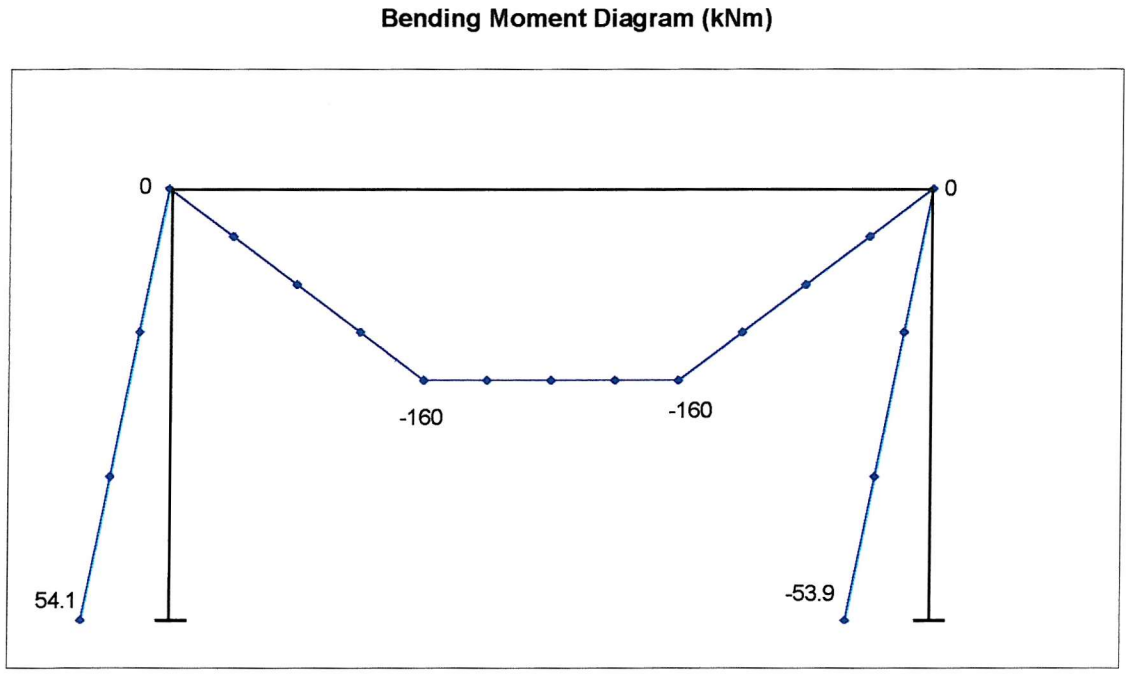

Figure 5.14 Column Base Fixed, Beam-to-Column Connection Pinned

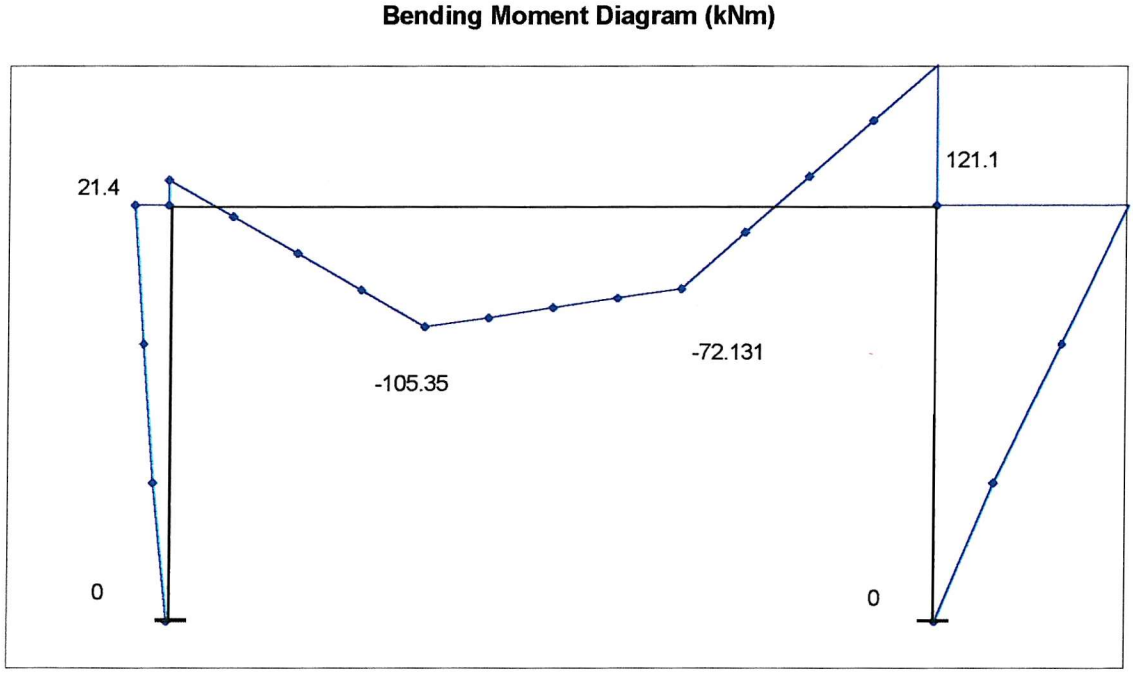

Figure 5.15 Column Base Pinned, Beam-to-Column Connection Fixed

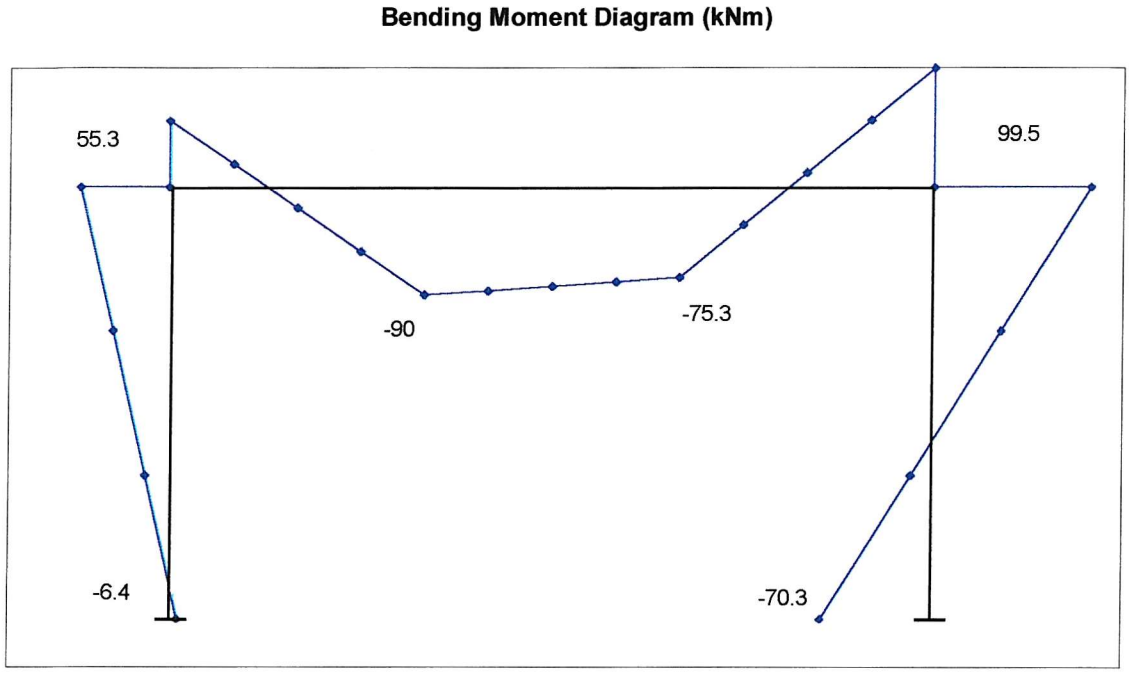

Figure 5.16 Column Base Fixed, Beam-to-Column Connection Fixed

5.3 Summary of Elastic Analysis

The vertical deflection of the beam is influenced mainly by the beam-to-column stiffness, with only a very small influence from the column base stiffness. The sway deflection, however, is influenced by both stiffnesses by a similar amount. This is also the case for bending moments, with the largest moments being carried by the stiffest connections, as expected.

5.4 Plastic Analysis

The plastic and non-linear analysis was carried out in two ways. Firstly the frames were analysed until a deflection limit had been reached, either at the top of the column in a sway frame analysis, or in the beam section in a non-sway analysis. The deflection limit was then removed, and the frames reanalysed to see how the beam-to-column connections affected the frames at higher loads, and how the frames would fail. Three

frames were analysed using different beam and column section sizes. The values used are shown in Tables 5.5 – 5.7 below.

Table 5.5 Section Properties Used in Frame 1

Frame 1	Height (m)	A(0) $x10^{-3}$ (m)	A(30) $x10^{-3}$ (m)	A(50) $x10^{-3}$ (m)	M_{pl} $x10^{3}$ Nm	L (m)	I_{xx} $x10^{-3}$ (m^4)
Beam UB457x191x89	0.463	48.4	7.61	3.18	553	4.8	0.41
Column UB457x191x89	0.463	48.4	7.61	3.18	553	3.6	0.41

Table 5.6 Section Properties Used in Frame 2

Frame 2	Height (m)	A(0) $x10^{-3}$ (m)	A(30) $x10^{-3}$ (m)	A(50) $x10^{-3}$ (m)	M_{pl} $x10^{3}$ Nm	L (m)	I_{xx} $x10^{-3}$ (m^4)
Beam UC254x254x89	0.260	55.6	7.07	0.871	338	4.8	0.143
Column UC254x254x89	0.260	55.6	7.07	0.871	338	3.6	0.143

Table 5.7 Section Properties Used in Frame 3

Frame 3	Height (m)	A(0) $x10^{-3}$ (m)	A(30) $x10^{-3}$ (m)	A(50) $x10^{-3}$ (m)	M_{pl} $x10^{3}$ Nm	L (m)	I_{xx} $x10^{-3}$ (m^4)
Beam UB457x191x89	0.463	48.4	7.61	3.18	553	4.8	0.41
Column UC254x254x89	0.260	55.6	7.07	0.871	338	3.6	0.143

The model used for the finite element analyses is shown in Figure 5.17 below.

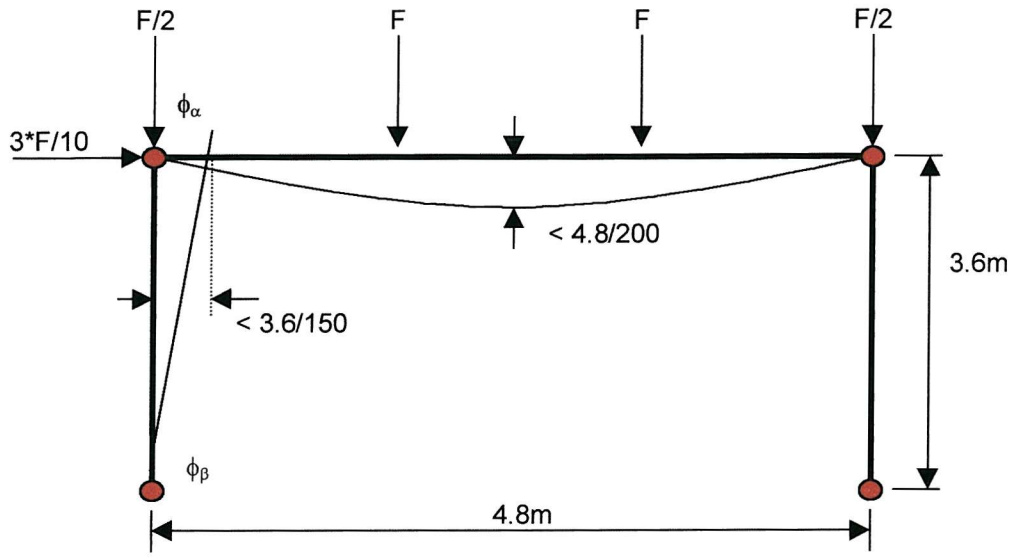

Figure 5.17 Single-storey Plastic Frame

The model for these analyses has the same geometry as was used in the elastic analyses. The columns were split into 6 elements, and the beam into 6 elements. A constraint was added to the top right of the model for the non-sway analyses. Due to the differences between the linear spring element used in the elastic analyses and the non-linear spring element used in the non-linear analyses, the property of the spring is no longer given as a stiffness, but as a rotation. The rotation then defines the moment-rotation behaviour of the beam-to-column and column base connection.

Pertold **[38, 39]** has already carried out much work into single-storey plastic analysis. The results of the analyses described here have been compared against his to make sure that they are consistent. The comparison showed that the two sets of analyses are very close. The small variation in results will be due to how the ANSYS solve options were set, and how the dimensions for the elements cross-section were input, as ANSYS gives different options for this.

The maximum sway and beam deflections were set as H/150 for the sway deflection, and L/200 for the beam deflection, as stipulated in BS 5950 **[41]**, and the analyses ran until this deflection was reached.

5.4.1 Non-Sway Analysis

The non-sway frame models were analysed until a deflection of L/200 had been reached. This occurred in the mid-span of the beam for all of the models. The tables below show the loading that was reached for each of the three frames analysed.

The values in the tables are the ANSYS load step at which the frame failed, with the strongest frame being the fully fixed case. The actual failure needs to be calculated from this figure; the maximum possible load applied to the frame; the ANSYS time step options; and the distribution of load on the frame, as shown in the diagram of the frame model above (Figure 5.17).

Table 5.8 Frame 1 Results

	Phi Beam-to-Column mRad										
Phi Colum	pinned	256	128	64	32	16	8	4	2	1	fixed
pinned	340.33	357.93	373.36	400.88	444.46	503.89	567.22	607.53	617.43	622.48	627.51
256	340.33	357.93	373.36	400.88	444.46	503.89	567.72	608.28	617.86	622.98	628.01
128	340.33	357.93	373.36	400.88	444.96	504.39	568.36	608.51	618.56	623.4	628.01
64	340.83	357.93	373.36	400.88	444.96	504.39	569.11	609.02	618.98	624.03	629.01
32	337.83	357.93	373.36	400.88	444.96	505.39	570.47	610.36	620.48	625.48	629.93
16	337.83	357.93	373.36	400.88	445.46	506.39	572.31	612.36	622.57	627.56	631.48
8	340.83	357.93	373.36	401.38	445.96	507.81	575.09	614.33	625.07	629.99	632.33
4	340.83	357.93	373.36	401.38	446.46	509.31	577.82	616.83	627.33	632.41	633.33
2	340.83	357.93	373.36	401.38	446.96	510.44	579.91	618.33	629.41	633.83	634.33
1	340.83	357.93	373.36	401.38	446.96	510.96	581.4	619.83	630.75	634.83	634.83
fixed	340.83	357.93	373.36	401.38	447.46	511.96	583.4	621.33	632.33	635.33	637.58

Table 5.9 Frame 2 Results

	Phi Beam-to-Column mRad										
Phi Colum	pinned	256	128	64	32	16	8	4	2	1	fixed
pinned	178.89	192.17	203.89	221.36	246.08	274.49	300.27	319.8	332.3	339.05	346.36
256	178.89	192.17	203.89	221.86	246.36	274.99	301.05	320.58	333.08	340.11	347.92
128	178.89	192.17	203.89	221.86	246.36	275.27	301.83	321.86	334.36	341.39	348.71
64	178.89	192.17	203.89	221.86	246.86	276.05	303.11	322.92	336.21	343.24	351.05
32	178.89	192.17	203.89	222.14	247.14	276.83	304.67	325.77	339.05	346.36	354.17
16	178.89	192.46	204.17	222.14	247.92	278.39	307.02	328.89	342.96	350.27	358.08
8	178.89	192.46	204.17	222.14	248.42	279.67	309.64	332.3	347.14	354.96	362.49
4	178.89	192.46	204.17	222.64	249.21	280.74	311.71	335.42	350.77	358.58	365.89
2	178.89	192.46	204.17	222.92	249.49	282.02	313.55	337.77	353.11	361.21	368.24
1	178.89	192.46	204.17	222.92	249.49	282.3	314.33	339.33	354.67	362.49	369.8
fixed	178.89	192.46	204.17	222.92	249.99	283.08	315.61	340.89	356.52	364.33	371.86

Table 5.10 Frame 3 Results

	Phi Beam-to-Column mRad										
Phi Colum	pinned	256	128	64	32	16	8	4	2	1	fixed
pinned	340.33	350.96	359.98	375.61	398.33	426.83	455.06	477.33	489.83	496.25	501.96
256	340.33	350.96	359.98	375.63	398.83	427.33	455.58	478.33	490.83	497.38	502.96
128	340.33	350.96	359.98	375.63	398.83	427.83	456.57	479.33	492.21	498.39	503.96
64	340.33	350.96	359.98	375.63	398.83	428.21	457.83	480.83	493.83	499.89	505.51
32	340.33	350.96	359.98	375.63	399.33	429.21	459.33	483.33	496.33	502.46	508.01
16	340.83	350.96	359.98	376.13	399.75	430.91	461.83	486.83	499.89	505.96	510.48
8	337.83	350.94	359.98	376.13	400.75	432.33	464.75	490.33	503.46	509.01	512.83
4	337.83	350.94	359.98	376.13	401.25	433.29	467.3	493.33	506.46	511.48	514.39
2	337.83	350.94	359.98	376.13	401.38	434.33	468.89	495.33	508.56	513.08	515.31
1	337.83	350.94	359.98	376.63	401.38	434.86	469.89	496.41	509.43	514.08	515.96
fixed	337.83	350.94	359.98	376.63	401.88	435.36	471.31	497.83	511.01	514.83	516.36

The results in the above tables show that the column base rigidity has very little influence over the load carried for the frame to reach the deflection limit. However, the beam-to-column connection can greatly increase the load carried by the frame, with up to twice the load being reached for a rigid frame, compared to that reached for a pinned frame. Frame 1 and Frame 3 have the same beam properties, so this shows that the column properties do have an influence over the load carried - Frame 1, with a stiffer column section, being able to carry a higher load until the deflection limit is reached.

As was shown in the elastic analysis earlier in this chapter, and in the East-Park Terrace analysis in Chapter 4, increasing the stiffness of the more flexible connections has a far greater impact than increasing the stiffness of the more rigid connections.

Dividing the load reached by the frames by the load reached by the fully-fixed frame gives a strength ratio. This was done for all the results to make it possible to compare the results for each frame further. The strength ratio results for Frame 3 have been shown in Figure 5.18 below.

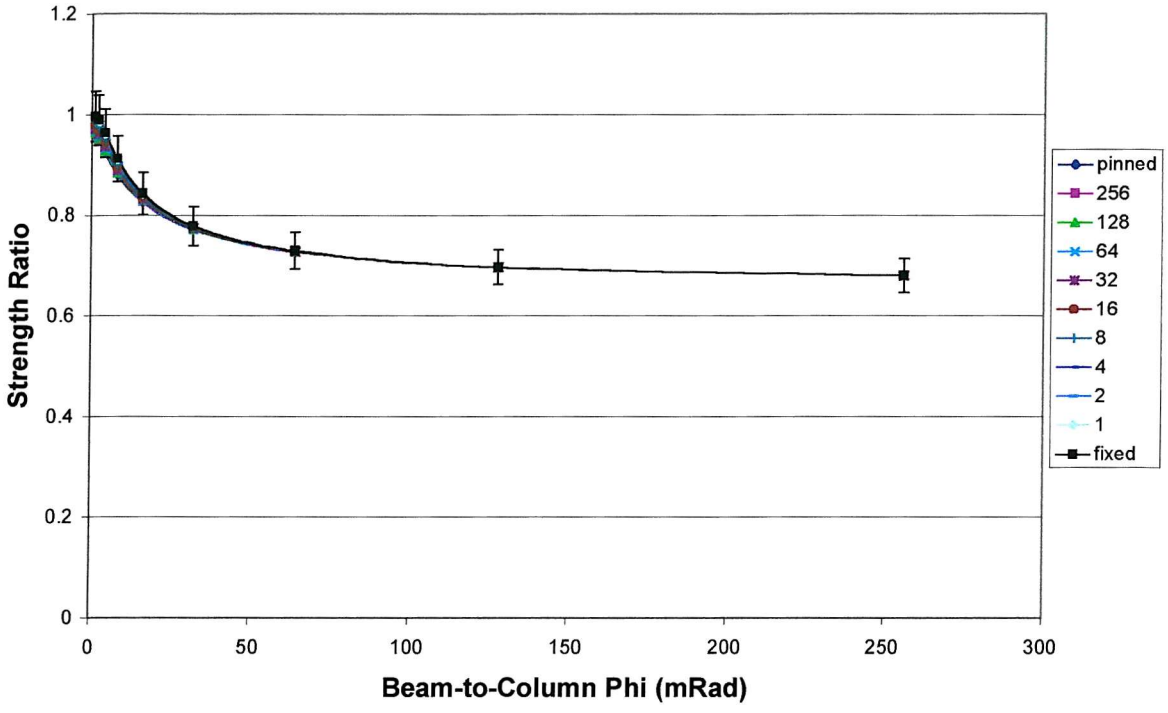

Figure 5.18 Strength Ratio Results for Frame 3 Non-Sway Frame

Each of the curves in Figure 5.18 shows the strength ratio of a frame with a different column base connection rotation, as shown in the legend. The horizontal axis of the chart shows the beam-to-column connection rotation of a frame, with 0 representing a fully fixed connection. The vertical axis plots the strength ratio of a frame, which is the strength of any frame divided by the strength of the fully-rigid connection case. As the previous tables showed, the column base rotation has only a very small impact on the strength, and hence on the strength ratio, of a non-sway frame. This is shown here by all the curves being very similar. The 'error' bars have been set at 5% on the case of fixed column bases, to show that all the results are within this.

5.4.2 Sway Analyses

The sway frame models were analysed until a deflection of H/150 had been reached. This occurred at the top of the column where the sway load was applied for all of the

models. The tables below show the loading that was reached for each of the three frames analysed.

Table 5.11 Frame 1 Results

	Phi Beam-to-Column mRad										
Phi Colum	pinned	256	128	64	32	16	8	4	2	1	fixed
pinned	0	23.705	44.918	82.893	141.67	219.52	302.61	369.02	400.77	407.3	411.62
256	24.205	48.622	70.78	109.52	170.3	250.77	336.21	400.27	423.42	427.61	430.83
128	47.054	71.882	95.108	134.64	197.14	279.96	368.24	427.61	441.67	445.3	448.38
64	89.102	115.11	139.33	181.24	246.86	333.86	422.92	465.61	472.14	475.27	477.07
32	160.42	189.33	215.11	260.42	332.02	421.08	494.33	511.36	515.83	515.83	515.06
16	268.24	300.27	328.74	378.11	439.33	500.33	547.83	556.39	557.97	557.83	557.76
8	344.36	360.83	375.33	402.33	445.33	505.83	561.08	582.33	590.33	594.58	599.26
4	344.36	361.33	376.61	403.33	447.84	509.83	570.07	595.33	604.88	609.46	613.68
2	344.36	361.33	376.61	404.08	449.26	512.58	575.71	602.83	611.88	616.43	620.96
1	344.36	361.33	377.11	404.58	450.39	513.83	579.26	606.33	615.33	619.43	623.46
fixed	344.36	361.33	377.13	405.25	450.96	516.08	582.28	609.89	618.33	621.94	625.83

Table 5.12 Frame 2 Results

	Phi Beam-to-Column mRad										
Phi Colum	pinned	256	128	64	32	16	8	4	2	1	fixed
pinned	0	13.922	25.629	44.918	71.081	100.41	126.55	145.3	157.02	163.55	170.58
256	14.188	28.9	41.715	61.97	89.602	120.58	147.92	168.24	180.46	187.49	194.02
128	27.477	42.783	55.864	77.088	106.42	139.05	167.96	189.05	201.83	208.86	214.83
64	50.258	66.776	80.692	104.02	135.42	171.08	202.61	225.77	239.33	244.52	249.49
32	85.498	104.02	119.8	145.58	181.24	221.36	257.8	281.52	289.83	292.17	294.02
16	131.52	152.61	170.58	200.27	240.89	276.05	303.89	321.36	328.11	329.96	329.36
8	178.39	192.17	203.89	222.14	247.92	278.39	307.8	326.83	335.42	338.55	340.88
4	178.89	192.46	204.17	222.92	249.21	280.74	310.42	331.24	340.11	343.74	346.83
2	178.89	192.46	204.17	223.42	249.99	282.02	312.77	333.86	343.24	347.14	350.33
1	178.89	192.46	204.17	223.42	250.27	282.3	313.55	335.42	345.3	348.71	352.33
fixed	178.89	192.46	204.17	223.71	250.77	283.08	315.11	336.99	347.14	350.77	354.14

Table 5.13 Frame 3 Results

	Phi Beam-to-Column mRad										
Phi Colum	pinned	256	128	64	32	16	8	4	2	1	fixed
pinned	0	14.188	26.553	48.122	79.991	118.74	156.52	186.21	205.74	217.17	228.11
256	14.188	29.4	42.783	65.475	98.712	140.11	180.46	211.99	232.8	244.8	254.96
128	27.477	43.283	57.165	80.692	115.89	159.36	201.83	235.42	257.3	269.02	279.17
64	50.258	67.077	82.393	107.62	146.08	193.24	240.11	277.33	301.55	310.92	318.74
32	85.498	104.72	121.36	150.27	193.24	247.14	301.05	343.24	362.77	368.74	373.42
16	131.52	153.39	172.92	206.24	256.52	319.8	380.74	413.55	418.86	418.24	417.46
8	179.96	204.96	227.33	265.89	324.21	393.46	440.42	448.33	449.88	449.83	449.36
4	220.58	247.92	272.92	315.89	378.33	428.83	455.77	463.39	465.96	466.33	466.83
2	248.42	277.61	304.67	349.49	399.01	430.83	459.25	467.46	470.83	472.83	474.33
1	265.11	295.58	322.92	369.08	400.01	431.83	460.93	469.33	473.33	474.83	476.83
fixed	283.86	315.89	344.52	376.58	400.26	432.83	462.51	471.83	475.33	477.33	478.83

As for the non-sway frames presented above, these results can also be divided by the strength of the fully fixed frame case to give a strength ratio. These have been plotted for Frame 3 and are shown in Figure 5.19 below.

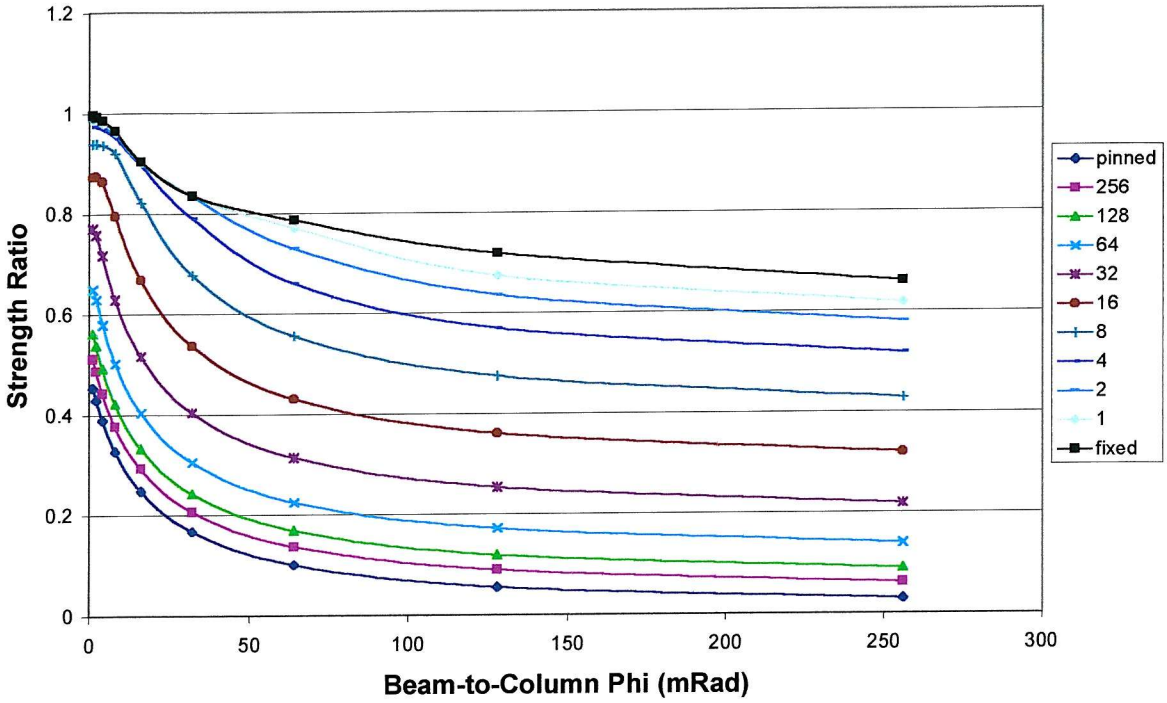

Figure 5.19 Load Factor Results for Frame 3 Sway Frame

The above tables and chart show that for the sway analysis the column base connection has a large influence. It can be seen from Tables 5.11-5.13 that the beam-to-column connection and the column base connection have a very similar influence over the strength of the frame. Plotting the results for Frame 3 as a surface plot can show this.

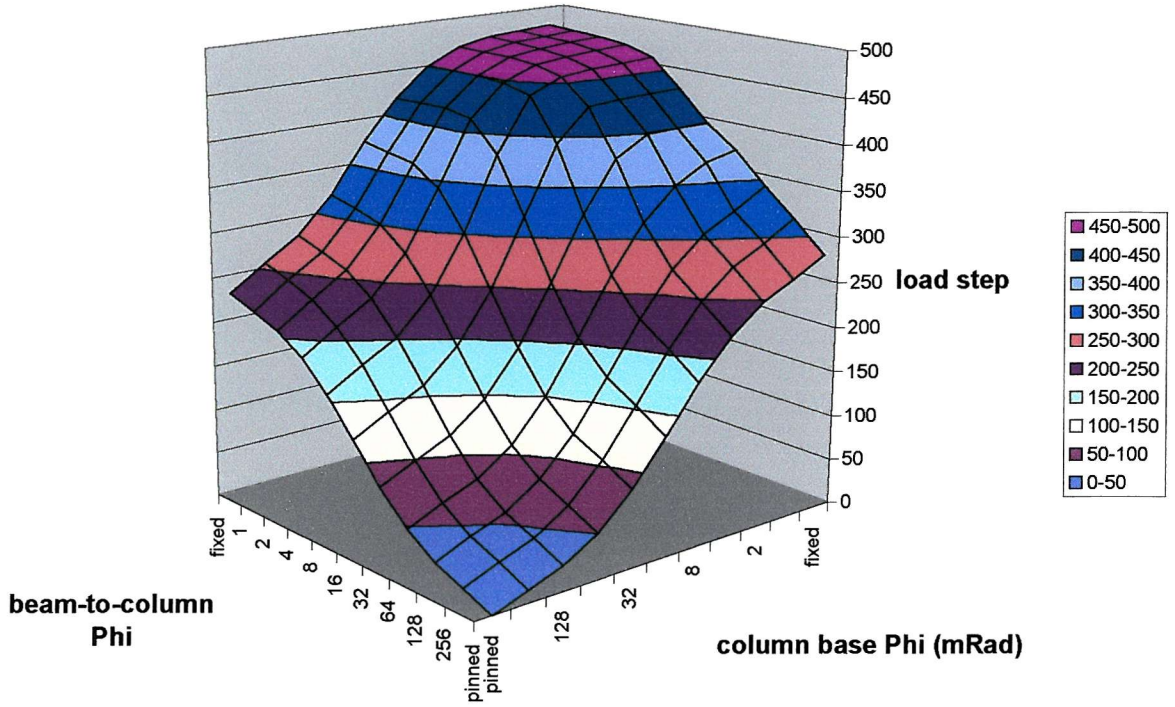

Figure 5.20 Load Step Results for Frame 3 Sway Frame

Here the ANSYS load step result is plotted with the beam-to-column connection rotation value, and the column base rotation value. The chart shows that the influence on strength from the beam-to-column connection is similar to that from the column base connection for a single storey frame of this geometry. The column base has a slightly greater influence on the strength than that of the beam-to-column connection, which is shown by the greater increase in strength along the axis for column base phi.

5.4.3 Collapse Analysis

The analyses described above do not show how the frames act over their full loading, right up to failure, only the loading that takes them up to the deflection constraints given in BS5950 **[41]**. In this section the analyses were carried on through to the failure load of the frame, to see how the semi-rigid frames behaved up to full plastic behaviour. The results presented here are for sway and non-sway frames with changing

beam-to-column connection stiffnesses. The column bases are either fully fixed, or pinned. Frame 3 has been used for these analyses.

The results from these analyses are shown in the graphs below. Figure 5.21 is the plot of a single storey sway frame, showing the deflection at the top of the column, where the sway load is applied.

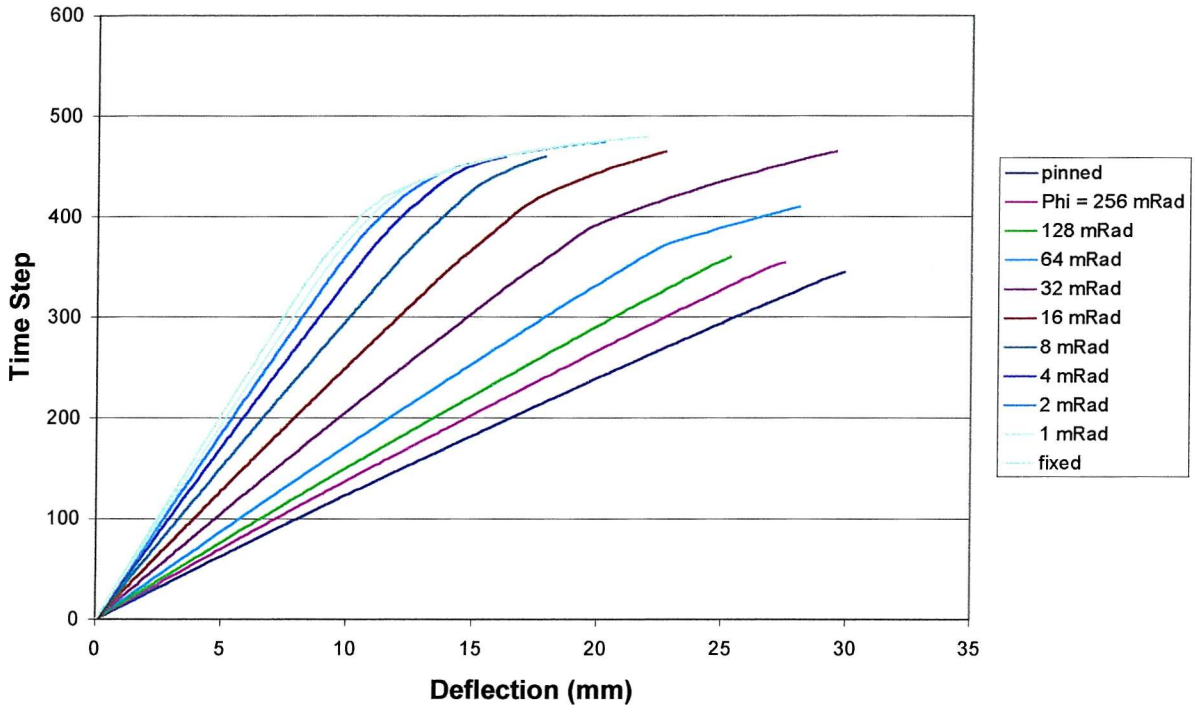

Figure 5.21 Load Deflection Curves at the Top of the Column

The frame used to plot the chart in Figure 5.21 had a fully fixed column base. Each curve plots the results for a different beam-to-column rotation, phi, which is shown in the legend. The chart shows that the frames with the least stiff connections obtained a greater deflection before failure, but they failed at a smaller loading. The chart does not show much in the way of formation of hinges for the more flexible connections: this is because the frames with the least stiff connections would have failed at the connection, as opposed to in the main steelwork.

The stress plot for the frame with beam-to-column connection of 1mRad, a stiff connection, is shown in Figure 5.22.

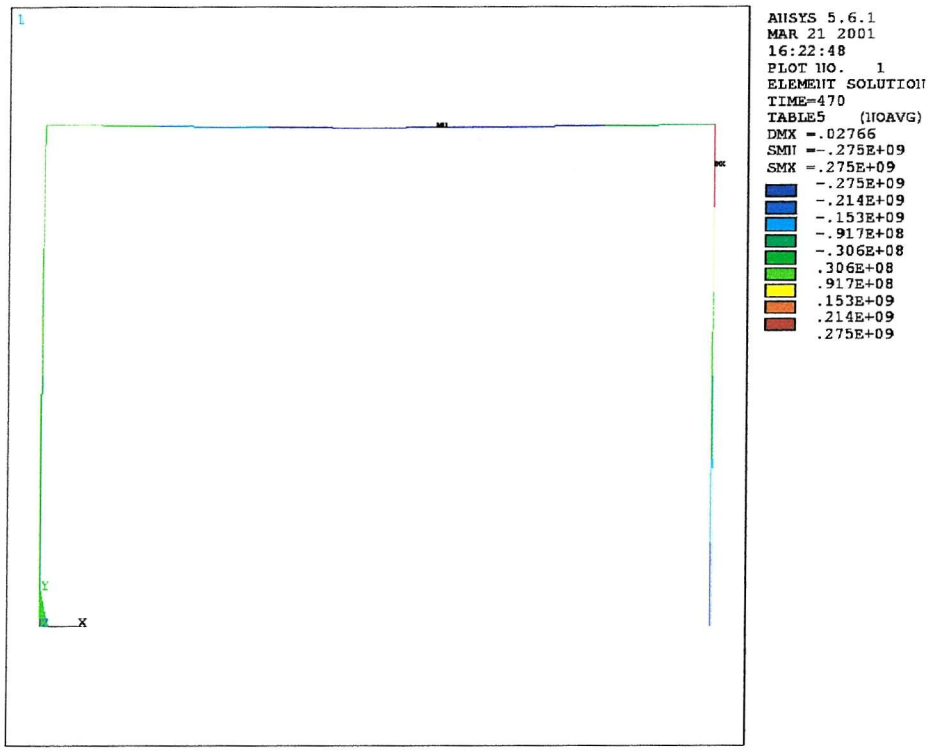

Figure 5.22 Stress Plot for Fixed Base Sway Frame, Phi = 1mRad

A yield stress of 275kN/mm^2 was used for the models, so it can be seen from Figure 5.22 that the frame collapsed with a plastic hinge forming at the mid-span of the beam, the top right corner of the frame and the right hand column base. The stresses can be outputted for any of 15 points throughout the beam element, as shown in Figure 5.23 below. For this plot the stresses were taken at position 5. A further hinge is required for the frame to fail; however, ANSYS is not able to find this, as an additional hinge would cause errors due to the very large deflections, and the solution cannot converge. A hinge forming at the base of the left hand column would cause a combined failure mechanism.

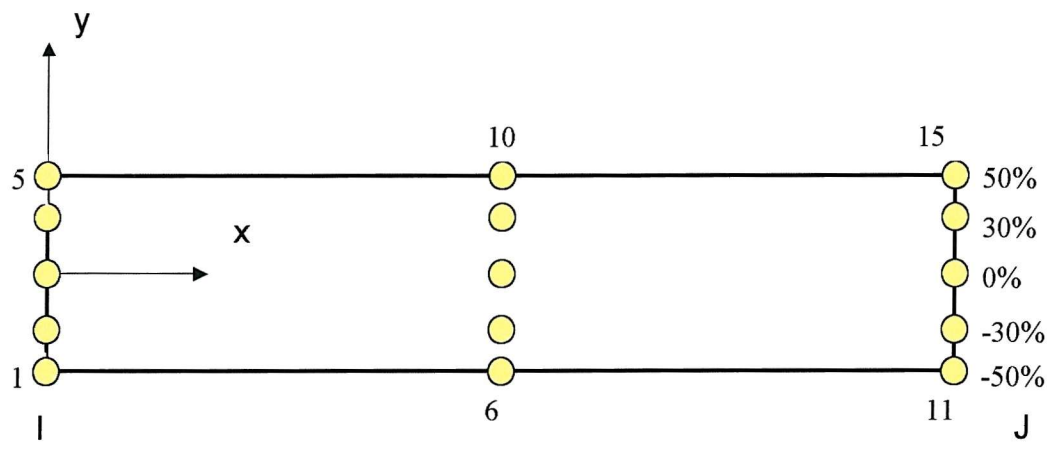

Figure 5.23 Output Points in BEAM23

Figure 5.24 shows the stress plot for a sway frame with a connection of 128mRad, a far more flexible connection.

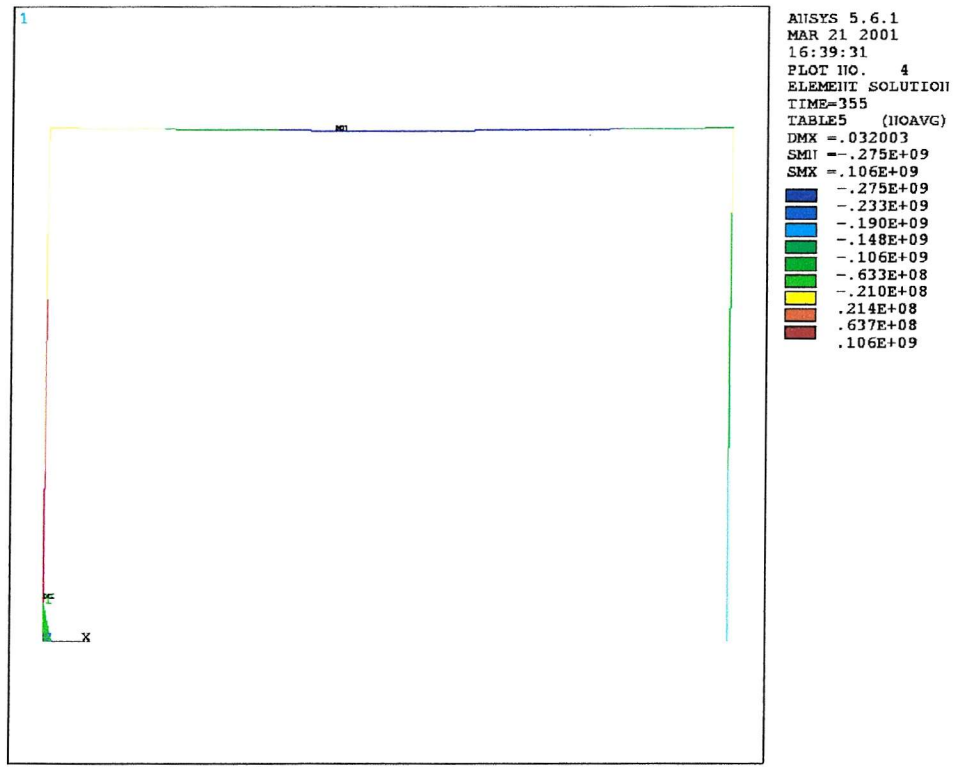

Figure 5.24 Stress Plot for Fixed Base Sway Frame, Phi = 128mRad

The stress plot shows that once again the centre of the beam has reached yield. However, there is no yielding at the top of the right hand column (as there was in the previous example with the stiff connection), which shows that this frame is failing with large rotations at the connection, rather than by yielding in the main column steel.

Figure 5.25 shows the load-deflection curves for a non-sway frame. This time the deflection has been plotted at the mid-span of the beam. As in the last case, the column base is fixed, and the beam-to-column connection stiffnesses have been varied.

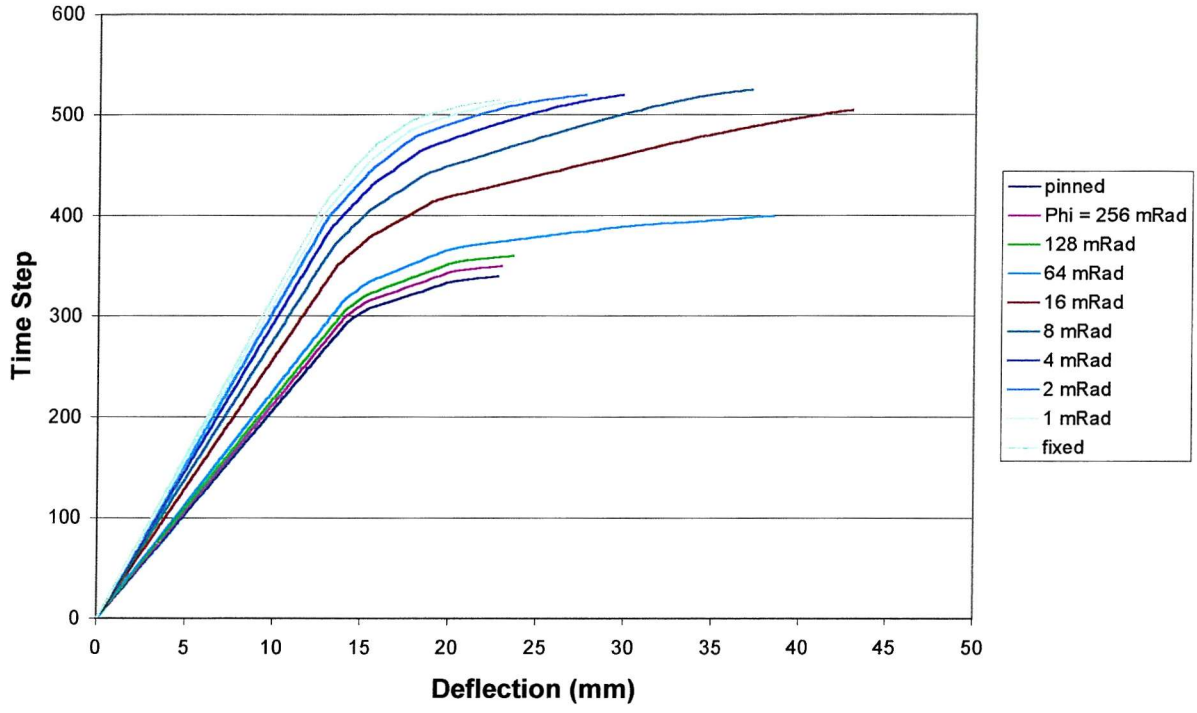

Figure 5.25 Load Deflection Curves at Mid-Span, Fixed Base

The results from this set of analyses showed that a far greater deflection was reached for the frame with beam-to-column phi of 32mRad, than for any of the other results. This was due to an error in the solving of the matrices for the model. Small pivot terms were present in the model, so mathematical manipulations had to be performed on both large and very small numbers, which can introduce large errors in the results. For this reason the result has been omitted from the above graph. Further inspection of this frame showed the column section near the beam-to-column connection was yielding at the same load that the beam-to-column connection was reaching its ultimate rotation.

This is probably the reason for the small pivot term errors, as there would be a large increase in the strains in the columns, and large increases in the rotation of the connections, for very small additions in load. The other analyses have been checked and there are no such errors in these.

The chart shows that the strength of the frame is increased with an increase in connection stiffness. The frames with a low connection stiffness fail at a low load, with low deflection values. This is due to the moment rotation limit of the beam-to-column connection being reached, and the frame failing with a beam mechanism. As the connection stiffness increases the maximum deflections of the frames also increase. This is due to the connections being able to redistribute more of the moment to the columns. The failure deflection and load of the frame continues to increase with beam-to-column stiffness up to the 16mRad connection. After this, the failure deflection of the frame reduces, with the failure load remaining constant. This is because these stiffer connections carry more moment over to the column, causing the column to yield near the connection. The failure loads remain constant for the frames with the stiffer connections, as the columns and beam fail at the same bending moment regardless of the beam-to-column connection, but the failure deflection decreases due to the stiffer connections. Figure 5.26 shows the stress plot for a frame with beam-to-column connections of 1mRad, and Figure 5.27 shows a stress plot for a frame with beam-to-column connections of 128mRad.

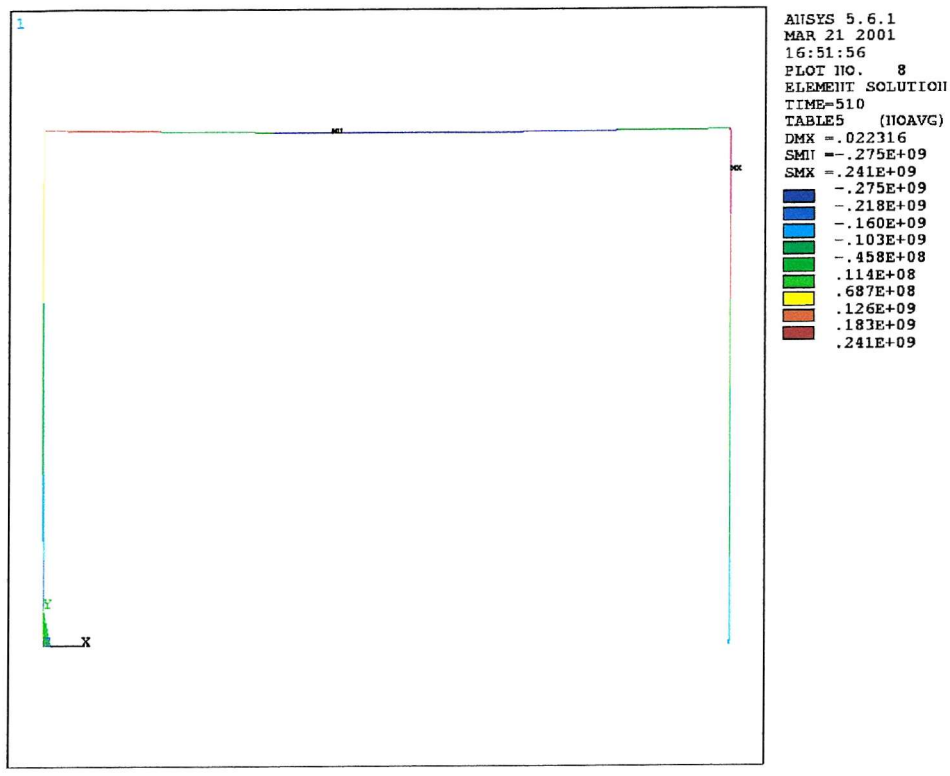

Figure 5.26 Stress Plot for Fixed Base Non-Sway Frame, Phi = 1mRad

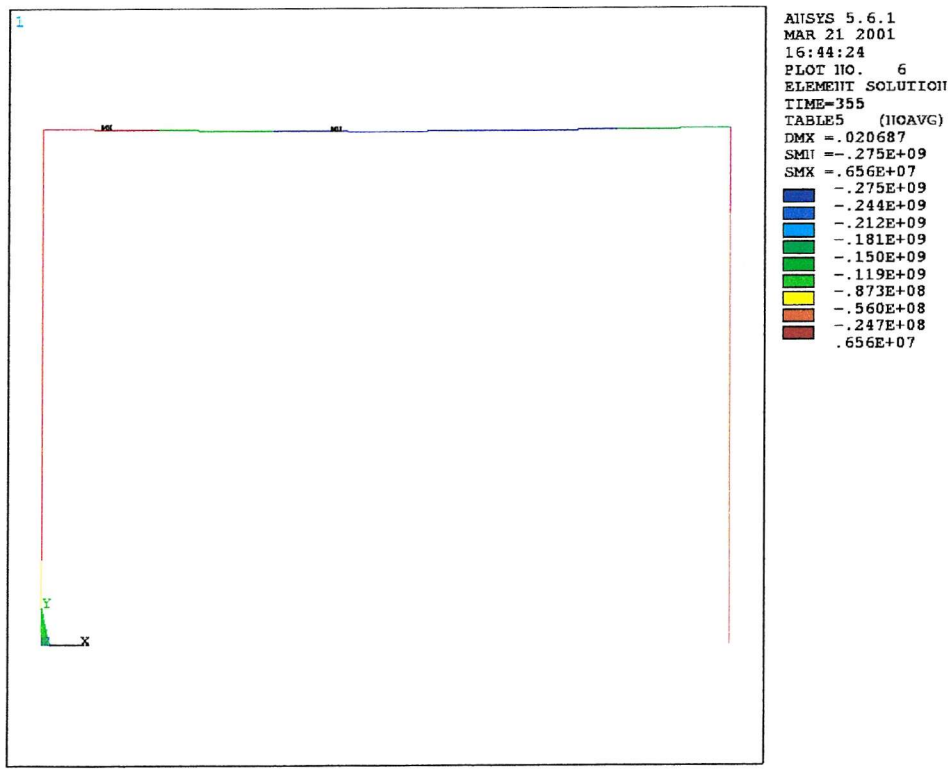

Figure 5.27 Stress Plot for Fixed Base Non-Sway Frame, Phi = 128mRad

Figure 5.27 shows that the stresses are very low in the column sections, compared to those in Figure 5.26 for the frame with the stiffer beam-to-column connections. This shows that the moments are not being transferred much from the beam to the columns for the frames with more flexible connections. The tops of the columns of the frame with stiffer connections, in Figure 5.26, are starting to reach the yield value used for the steel in the model.

The analyses shown in Figure 5.28 are similar to those shown previously, but in these analyses the column base connection is pinned.

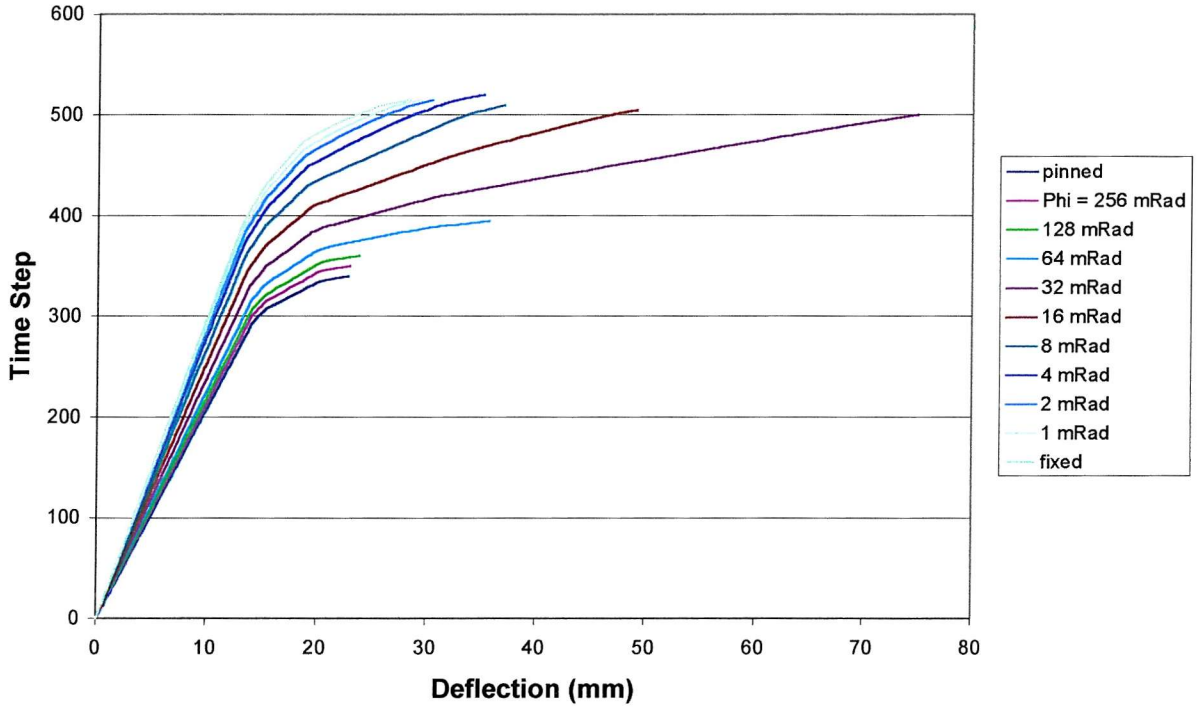

Figure 5.28 Load Deflection Curves at Mid-Span, Pinned Base

The results are similar to those in the previous analyses, as the column base only has a small influence on the strength of a frame in the non-sway case. The chart shows how the frame becomes stronger with stiffer beam-to-column connections, but only up to a rotation of 32mRad. With connection stiffness greater than this, the frame fails with a lower deflection.

The frames with more flexible connections fail at the connection; the frames with the stiffer connections fail with a plastic hinge forming in the steel section. This explains why in the last two figures there is an increase in deflection for the first few frames, as the load the frame can carry increases. This deflection then drops back as the frames start to fail with plastic hinges forming in the steel section, and the connections restrict the maximum deflection reached at failure. This is shown in more detail in the following chapter, on multi-storey frames.

5.5 Summary

Both the elastic and non-linear analyses have shown that for a non-sway frame nearly all the influence on strength and deflection is from the beam-to-column connection, with hardly any influence from the column base connection. For the sway frames, however, both the beam-to-column connection and the column base have a very similar influence for frames of the geometry used in this research. The collapse analysis has shown that the frames with the most flexible connections fail at a low load with a low deflection with failure occurring in the connection, whereas the stiffer frames fail in the steel sections.

The next chapter presents the research conducted on multi-storey frames. Chapter 7 then presents more discussion on the results found for the single storey frame and those found for the multi-storey frames.

Chapter 6

Multi-Storey Frame Analysis

6.1 Introduction

In this chapter finite element analysis is used to model multi-storey frames. The theories reported in the previous chapters on single-storey frames were adopted. The first sections of this chapter present the research on two-storey frames. The later sections present the work on five- and ten-storey frames that followed on from this.

6.2 Two-Storey Frame Analysis

The two-storey frame was analysed using both elastic and plastic models. These models use the same elements and techniques as those shown in Chapters 4 and 5.

6.2.1 Elastic Analysis

The model used for these analyses is shown in Figure 6.1 below. The frame's geometry is made up from two of the single-storey frames, one upon the other. The rigidities for column base, and beam-to-column rigidity are represented by a spring element, Combin14. The base rigidity is varied independently of the beam-to-column rigidity. The beam-to-column connections of the first storey, and the second storey can also be varied independently of each other if necessary. The beams and columns are modelled using Beam3, the 2D elastic beam element. All the section properties can be varied independently of each other. Both the element types used have been described in Chapter Three, along with any assumptions and restrictions of the elements.

The batch file system has again been utilised for these analyses, so that ANSYS can be used efficiently to output the results required for each set of analyses, with the analyses run for different column base, and beam-to-column connections.

For the elastic analyses the results are mainly focused on the deflections of the frame. The plastic analyses are used to identify the ultimate capacity of the frame, and the failure mechanism.

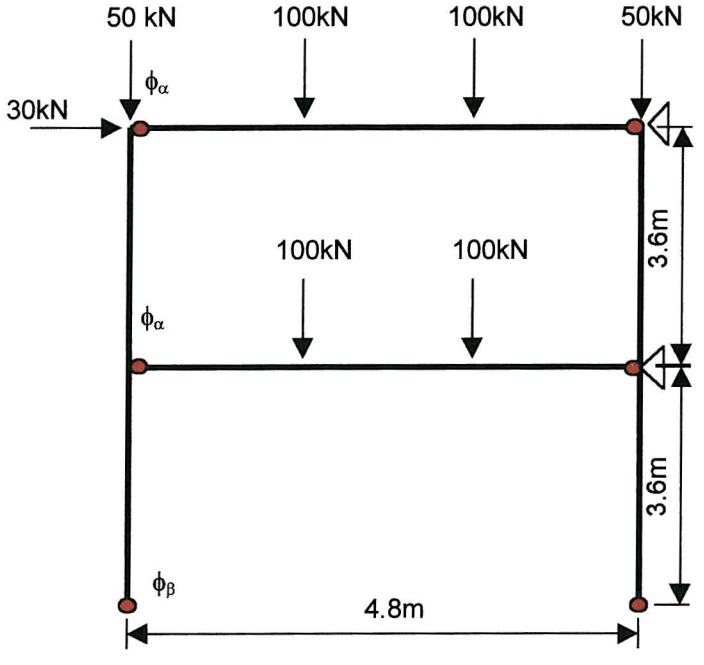

Figure 6.1 Non-Sway Elastic Model

The joint areas show the positions of the spring elements. The rotations of the elements are given by ϕ_β for the column base and ϕ_α for the beam-to-column connections. The columns are each made from six elements and the beams from twelve elements.

6.2.1.1 Non-Sway Analysis

The deflection results for the non-sway frames have been plotted for the beams. The results are shown in Tables 6.1 and 6.2 below. Table 6.1 shows the deflection results for the first storey beam, at mid-span. Table 6.2 shows the mid-span deflection, in mm, for the second storey beam.

Table 6.1 Deflections at Mid-Span of First Storey Beam

	K Beam kNmm/microRad								
K Column	0	1	2	4	8	16	32	64	Fixed
0	-5.0553	-4.9544	-4.8595	-4.6861	-4.3929	-3.957	-3.4195	-2.8909	-1.8623
1	-5.0553	-4.9544	-4.8595	-4.6861	-4.3928	-3.9569	-3.4193	-2.8906	-1.8616
2	-5.0553	-4.9544	-4.8595	-4.6861	-4.3928	-3.9568	-3.4191	-2.8903	-1.861
4	-5.0553	-4.9544	-4.8595	-4.6861	-4.3927	-3.9566	-3.4188	-2.8897	-1.8597
8	-5.0553	-4.9544	-4.8595	-4.686	-4.3926	-3.9563	-3.4181	-2.8886	-1.8573
16	-5.0553	-4.9544	-4.8595	-4.686	-4.3924	-3.9558	-3.417	-2.8866	-1.8531
32	-5.0553	-4.9544	-4.8595	-4.6859	-4.3921	-3.955	-3.4152	-2.8836	-1.8465
64	-5.0553	-4.9543	-4.8594	-4.6858	-4.3917	-3.9539	-3.4129	-2.8795	-1.8376
Fixed	-5.0553	-4.9543	-4.8593	-4.6853	-4.3904	-3.9502	-3.4046	-2.865	-1.8062

Table 6.2 Deflections at Mid-Span of Second Storey Beam

	K Beam kNmm/microRad								
K Column	0	1	2	4	8	16	32	64	Fixed
0	-5.2864	-5.1862	-5.093	-4.925	-4.6472	-4.2477	-3.7744	-3.3271	-2.499
1	-5.2864	-5.1862	-5.093	-4.925	-4.6472	-4.2477	-3.7745	-3.3272	-2.4993
2	-5.2864	-5.1862	-5.093	-4.925	-4.6472	-4.2477	-3.7746	-3.3273	-2.4995
4	-5.2864	-5.1862	-5.093	-4.925	-4.6472	-4.2478	-3.7747	-3.3275	-2.4998
8	-5.2864	-5.1862	-5.093	-4.925	-4.6473	-4.2479	-3.7749	-3.3279	-2.5006
16	-5.2864	-5.1862	-5.093	-4.925	-4.6473	-4.2481	-3.7753	-3.3286	-2.5019
32	-5.2864	-5.1862	-5.093	-4.9251	-4.6475	-4.2484	-3.776	-3.3296	-2.5039
64	-5.2864	-5.1862	-5.0931	-4.9251	-4.6476	-4.2488	-3.7769	-3.3311	-2.5066
Fixed	-5.2864	-5.1862	-5.0931	-4.9253	-4.6482	-4.2503	-3.7799	-3.3361	-2.5163

The results from these analyses are also shown in Figure 6.2 and Figure 6.3 below. The charts show the beam-to-column stiffness plotted against the deflections at the mid-span. Each line on the charts shows the results for a different column base connection. Figure 6.2 plots the deflections at the mid-span of the lower beam.

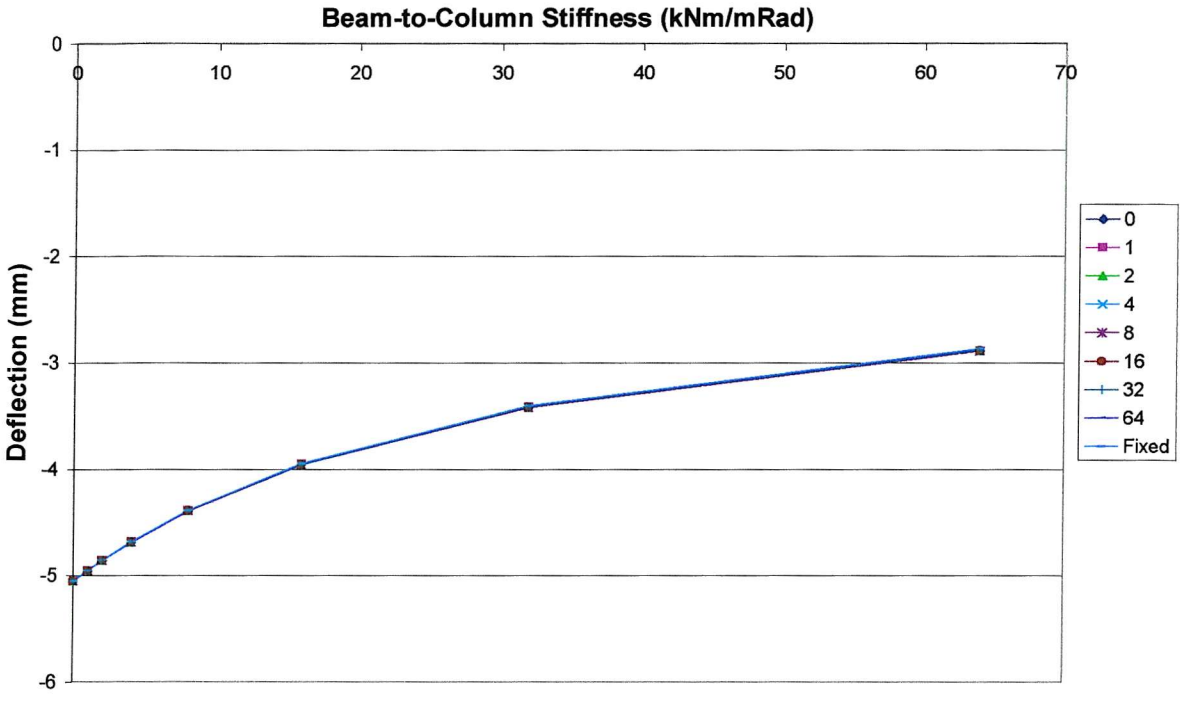

Figure 6.2 Non-Sway Vertical Deflections, First Storey Beam

The curves for each of the column base stiffnesses are almost identical, showing that the column base stiffness has very little effect on the mid-span deflection in a non-sway frame. This is even more pronounced than in the results for the single storey frame, where the column-base connection also has a very small influence over the mid-span deflections.

The trend of the column-base having virtually no influence on the mid-span beam deflection is again shown in the top storey beam deflections. The top storey deflections are shown in Figure 6.3 below.

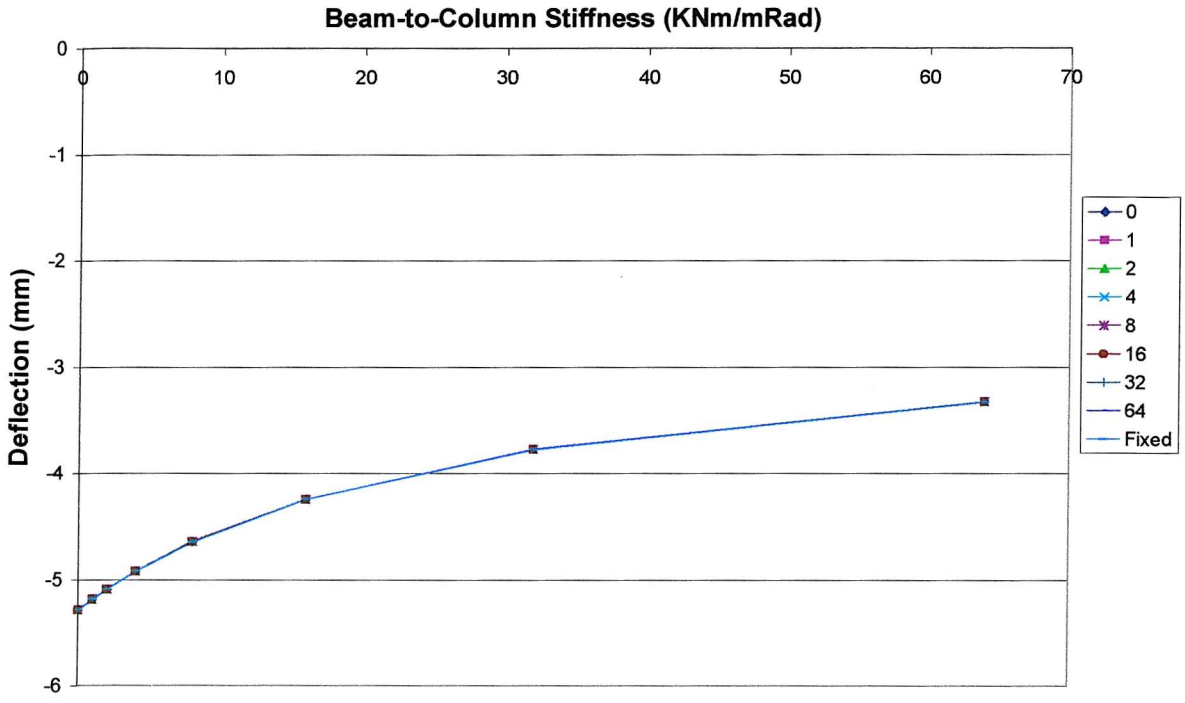

Figure 6.3 Non-Sway Vertical Deflections, Top Storey Beam

The top storey mid-span deflections are only very slightly influenced by the column-base stiffness.

The beam-to-column connections do have a large influence over the mid-span deflections, as would be expected in the light of the results of the single storey analyses. On the top storey the deflections are reduced by 53%, 5.29mm deflection reduced to 2.50mm, by going from a simple pinned beam-to-column connection to a fully fixed connection. The percentage reduction in the deflections on the first floor is 63%, 5.06mm deflection reduced to 1.85mm. The greatest reduction in deflection from the column-base was 3% by changing the column base to fixed, from pinned. For the case with fully rigid beam-to-column connections, at such small deflection values this 3% meant less than a 1mm reduction in deflection. Typical values for the reduction in deflection by changing the column base connection from pinned to fully fixed were less than 1%. So it is clear that for a non-sway frame, nearly all the influence on the deflection of the beams is from the beam-to-column connections. The column base rigidity can be neglected in the design of the beams in terms of deflection.

The next stage of the research is to see how the beam-to-column connections and column base rigidities affect the deflections of a sway frame.

6.2.1.2 Sway Analysis

The same model as used for the non-sway analyses is used for the sway analyses, except that the horizontal constraints are removed from each of the storey levels, allowing the frame to sway horizontally. All the loadings are the same as for the non-sway analyses.

For the sway analyses the deflections have been found for the horizontal deflection at the top of the column, where the sway load is applied. The results of these analyses are shown in Table 6.3 below.

Table 6.3 Horizontal Sway Deflections for Sway Frame

	K Beam kNm/mRad								
K Column	0	1	2	4	8	16	32	64	Fixed
0	N/A	398.28	203.84	106.57	57.843	33.354	20.966	14.652	8.098
1	799.82	262.82	160.21	92.606	53.07	31.482	20.081	14.139	7.8742
2	411.02	198.83	133.22	82.381	49.218	29.889	19.305	13.682	7.6711
4	216.62	137.15	101.58	68.409	43.384	27.322	18.01	12.904	7.3167
8	119.42	89.381	72.078	52.912	35.996	23.773	16.121	11.731	6.7622
16	70.819	58.287	49.862	39.241	28.5	19.778	13.844	10.259	6.0276
32	46.519	40.269	35.686	29.411	22.422	16.203	11.657	9.8404	5.2425
64	34.369	30.524	27.572	18.427	18.331	13.602	9.9692	7.5875	4.5743
Fixed	22.219	20.233	18.635	16.221	13.171	10.07	7.5328	5.7914	3.4976

Obviously many of the results given in the chart above are very large, and would never be encountered in a real design. However, these have still included these for completeness of the test results. As these are elastic analyses, all the results - even those for small stiffnesses - follow the same trends, as the charts below show.

The results from the elastic sway analyses are also shown in the figures below. Figures 6.4a and 6.4b show how the sway deflection varies with beam-to-column stiffness. Each curve on the charts represents a different column base rigidity. Both the charts show the same set of results, but with different scales for the y-axis, to show the results for higher beam-to-column stiffnesses in more detail.

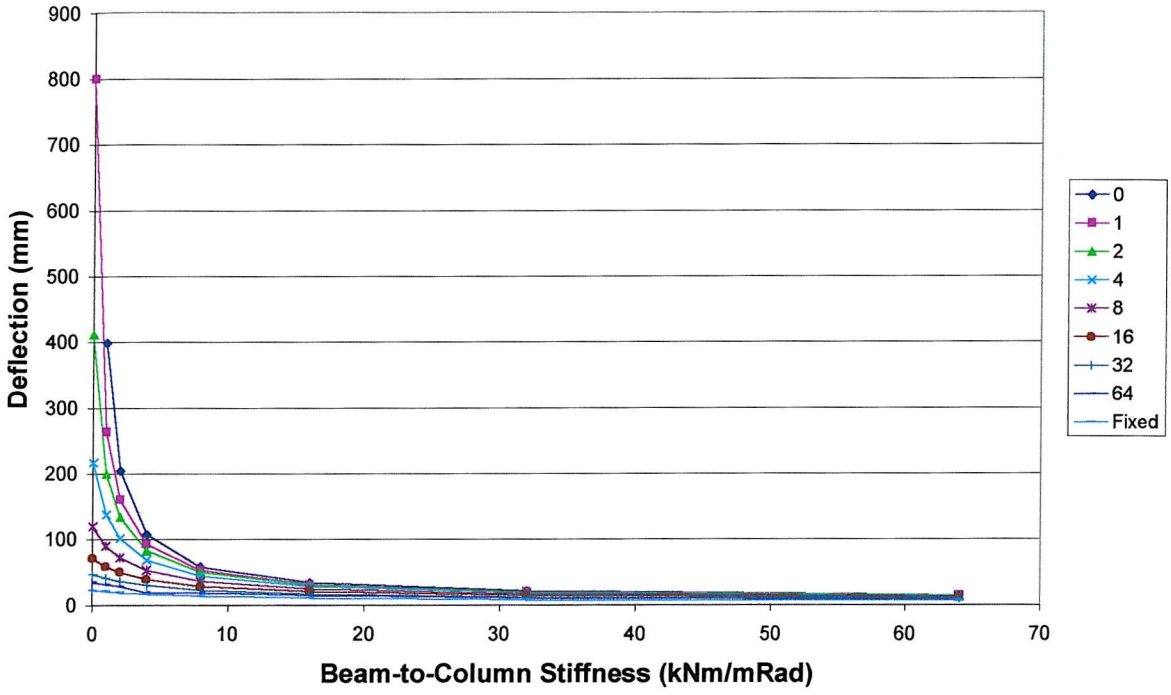

Figure 6.4a Two-Storey Sway Deflections

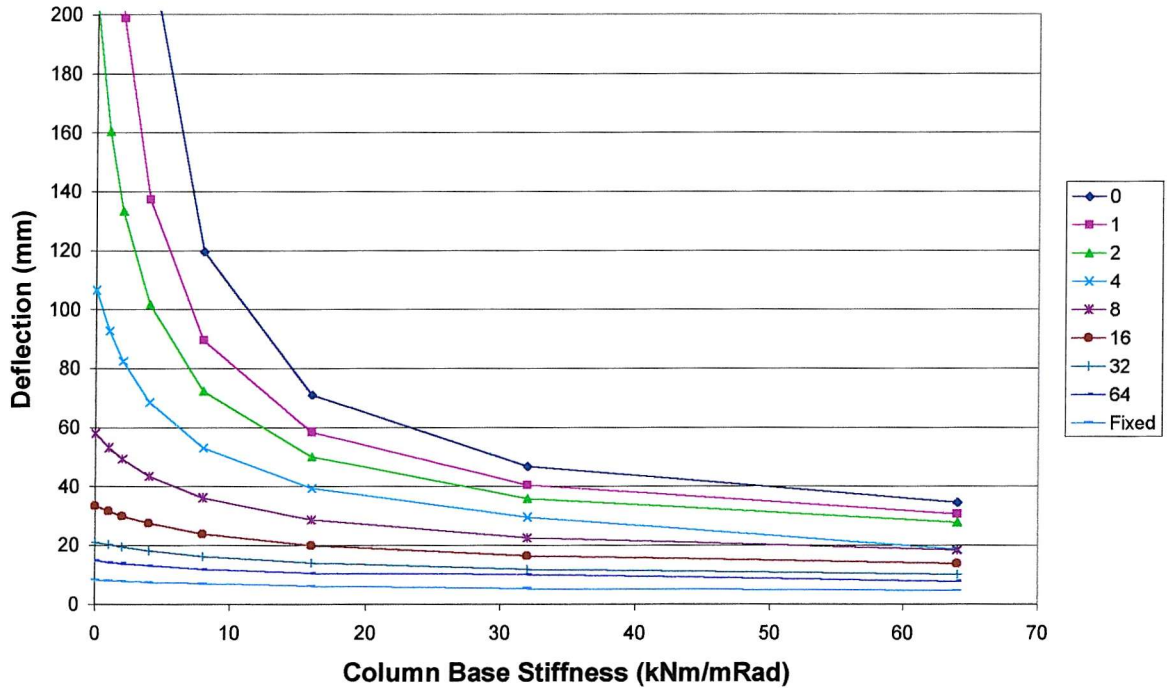

Figure 6.4b Two-Storey Sway Deflections

In contrast to the non-sway frame results, these charts shows that both the beam-to-column connections and the column base rigidity influence the sway deflections of the frame. The sway deflection reduces as the stiffness of the beam-to-column connection increases. A small increase in connection stiffness at a low beam-to-column stiffness causes a large decrease in sway connection. The decrease in sway deflection rapidly lessens as the connections become stiffer. The results show a very large decrease in deflection between a pinned connection and one where the connection stiffness is 10kNm/mRad. The reduction in deflection becomes much less after 30kNm/mRad, but as Figure 6.4b shows, there is still a large reduction in deflection at the stiffer end of the scale.

Figure 6.5 plots the same results, but this time the deflection has been plotted against column base stiffness, and each curve represents a different beam-to-column stiffness.

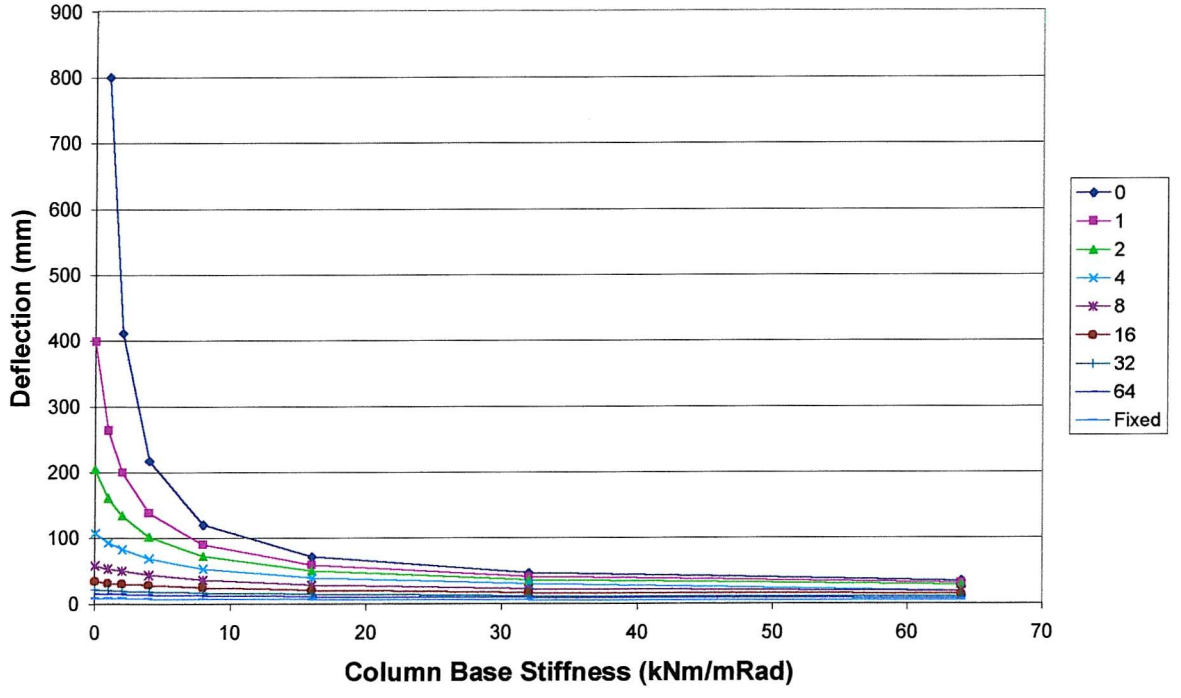

Figure 6.5 Two-Storey Sway Deflections

Comparing the chart in Figure 6.5 with that in Figure 6.4a shows that the curves are further spaced in the chart in Figure 6.5. Therefore the beam-to-column connection stiffness has a greater influence on the sway deflection than does the column base stiffness. As a further demonstration of this, the chart plotting deflection against beam-to-column stiffness also has a greater initial gradient than the chart plotting deflection against column base stiffness.

Comparing the two-storey elastic results with those from the single-storey elastic results shows that the trends are the same. The beam deflections in the non-sway frames are mainly dependent on the beam-to-column connection, with only very little influence on deflection from the column base rigidity, especially for the two-storey frame. The sway results show that for both the single- and two-storey frames the sway deflection is largely influenced by the beam-to-column connections and by the column base stiffness. For the two-storey frame, with the geometry used, the beam-to-column connection stiffness has more influence over the deflection than the column base stiffness. Comparing the results in Chapter Five for the single-storey frames we can see that these frames follow the same trend, with the beam-to-column stiffness having more effect on the sway deflection of the frame, than the column base stiffness.

So far only the deflections have been shown for an elastic model. Next, the frame was modelled with plastic elements to see how it behaved up to failure.

6.2.2 Plastic Analysis

The plastic model is similar to the elastic model described in the previous sections. This time, however, the plastic beam element Beam23 was used, and the non-linear spring element Combin39. The model used is shown in Figure 6.6 below.

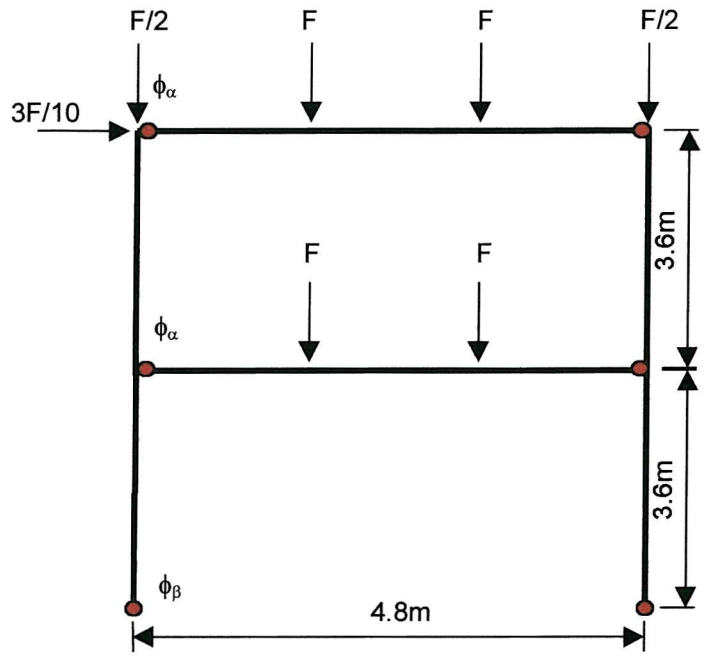

Figure 6.6 Plastic Non-Sway Two-Storey Model

The frame was loaded until a set deflection limit was reached. This deflection limit was set to that given in BS5950 **[41]** for serviceability, as L/200 for the beam deflection, and the height of storey under consideration/300 for the sway deflection. The deflection limit was set in ANSYS, and the load was applied using the load step options until this deflection was reached.

As with the single-storey analyses in Chapter 5, three different frames were analysed. The sections used for the frames are given in Tables 6.4 – 6.6 below.

Table 6.4 Section Properties Used in Frame 1

Frame 1	Height (m)	A(0) (m)	A(30) (m)	A(50) (m)	M_{pl} Nm	L (m)	I_{xx} (m^4)
Beam UB457x191x89	0.463	4.84e-2	7.61e-3	3.18e-3	5.53e5	4.8	4.1e-4
Column UB457x191x89	0.463	4.84e-2	7.61e-3	3.18e-3	5.53e5	3.6	4.1e-4

Table 6.5 Section Properties Used in Frame 2

Frame 2	Height (m)	A(0) (m)	A(30) (m)	A(50) (m)	M_{pl} Nm	L (m)	I_{xx} (m^4)
Beam UC254x254x89	0.260	5.56e-2	7.07e-3	8.71e-4	3.38e5	4.8	1.43e-4
Column UC254x254x89	0.260	5.56e-2	7.07e-3	8.71e-4	3.38e5	3.6	1.43e-4

Table 6.6 Section Properties Used in Frame 3

Frame 3	Height (m)	A(0) (m)	A(30) (m)	A(50) (m)	M_{pl} Nm	L (m)	I_{xx} (m^4)
Beam UB457x191x89	0.463	4.84e-2	7.61e-3	3.18e-3	5.53e5	4.8	4.1e-4
Column UC254x254x89	0.260	5.56e-2	7.07e-3	8.71e-4	3.38e5	3.6	1.43e-4

6.2.2.1 Non-Sway Analysis

For the non-sway analysis the top of the column, opposite from the sway load, was constrained in the UX direction. The results show the load step that was reached before the deflection limit was reached, in this case 24mm; the load is split into 1000 load steps in the solution parameters in ANSYS.

Table 6.7 below shows the results for the non-sway analyses for combinations of column base stiffness and beam-to-column stiffness between pinned and fully fixed, with the stiffness being doubled for each analysis. The values in the table are the load step, where the maximum is 1000, and F is 1000kN on the diagram above. The results for Frame 3 are shown here.

Table 6.7 Time Step Results for Non-Sway Frame

	Phi Beam-to-Column mRad										
Phi Colum	pinned	256	128	64	32	16	8	4	2	1	fixed
pinned	339.33	349.09	357.98	374	399.39	433.89	472.51	502.18	514.69	517.43	519.83
256	339.33	349.09	357.98	374	399.39	433.89	472.51	502.18	514.69	517.51	519.33
128	339.33	349.09	357.98	374	399.39	433.89	472.51	501.93	514.69	517.51	519.33
64	339.33	349.09	357.98	374	399.39	433.89	472.51	501.68	514.69	517.51	519.33
32	339.33	349.09	357.98	374	399.39	433.89	472.51	501.43	514.61	517.51	519.33
16	339.33	349.09	357.98	374	398.89	433.39	472.01	501.51	514.44	517.01	519.33
8	339.33	349.09	357.98	374	398.89	433.39	472.01	500.76	514.44	517.06	519.33
4	339.33	349.09	357.98	374	398.89	433.39	471.51	501.06	513.81	516.85	519.33
2	339.33	349.09	357.98	374	398.89	433.39	471.51	500.51	513.81	516.93	519.33
1	339.33	349.09	357.98	374	398.89	433.39	471.51	500.76	513.56	516.93	519.33
fixed	339.33	349.09	357.98	374	398.89	433.39	471.51	500.31	513.81	516.93	519.33

Table 6.8 shows the ratio of strength of each frame compared to that of the fully fixed frame. It is this ratio which will later be used to develop design equations similar to those developed by Pertold **[38,39]** for single storey frames. So it will be possible to design a semi-rigid frame by using the capacity of the frame as if it were fully fixed, and applying the appropriate load factor.

Table 6.8 Strength Ratio Results

	Phi Beam-to-Column mRad										
Phi Colum	pinned	256	128	64	32	16	8	4	2	1	fixed
pinned	0.6534	0.672193	0.689311	0.720159	0.769049	0.83548	0.909845	0.966977	0.991065	0.996341	1.000963
256	0.6534	0.672193	0.689311	0.720159	0.769049	0.83548	0.909845	0.966977	0.991065	0.996495	1
128	0.6534	0.672193	0.689311	0.720159	0.769049	0.83548	0.909845	0.966495	0.991065	0.996495	1
64	0.6534	0.672193	0.689311	0.720159	0.769049	0.83548	0.909845	0.966014	0.991065	0.996495	1
32	0.6534	0.672193	0.689311	0.720159	0.769049	0.83548	0.909845	0.965533	0.990911	0.996495	1
16	0.6534	0.672193	0.689311	0.720159	0.768086	0.834518	0.908883	0.965687	0.990584	0.995533	1
8	0.6534	0.672193	0.689311	0.720159	0.768086	0.834518	0.908883	0.964242	0.990584	0.995629	1
4	0.6534	0.672193	0.689311	0.720159	0.768086	0.834518	0.90792	0.96482	0.989371	0.995225	1
2	0.6534	0.672193	0.689311	0.720159	0.768086	0.834518	0.90792	0.963761	0.989371	0.995379	1
1	0.6534	0.672193	0.689311	0.720159	0.768086	0.834518	0.90792	0.964242	0.98889	0.995379	1
fixed	0.6534	0.672193	0.689311	0.720159	0.768086	0.834518	0.90792	0.963376	0.989371	0.995379	1

The results from Table 6.8 have been plotted in Figure 6.7 below.

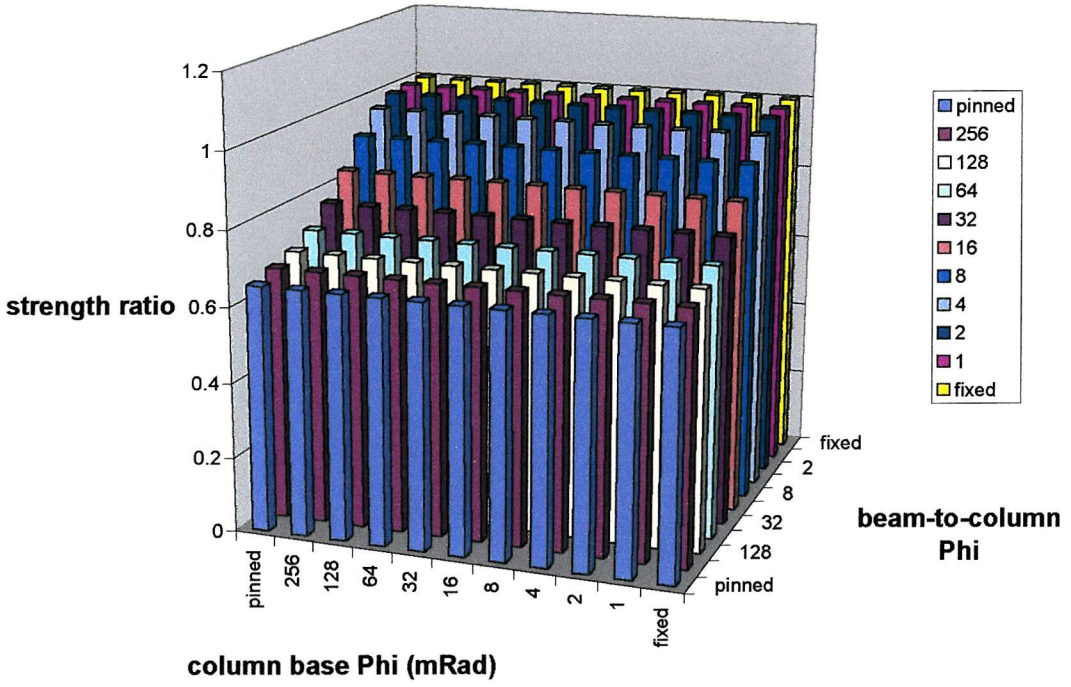

Figure 6.7 Ratio of Strength Against the Fully-Fixed Frame

The results show that the column-base stiffness has virtually no influence on the capacity of the non-sway frames. The frames will be reaching the deflection limit at the mid-span of the beams. The influence of capacity from the column base stiffness is even less than that for the single storey non-sway frame. The capacity of the frame is increased with increasing beam-to-column stiffness. The chart shows that the effect of the beam-to-column stiffness on strength becomes less for the stiffer connections.

6.2.2.2 Sway Analysis

The sway analysis was carried out in the same way as the non-sway analysis, with the sway constraint on the column removed. The same loading conditions were applied to the frame as before, and the same connection stiffnesses used. The deflection limit was again set to 24mm, which is H/300. The ultimate rotation of the connection, ϕ, has again been used to specify the stiffness of the connections.

Table 6.9 lists the load step results for the analyses of Frame 3.

Table 6.9 Time Step Results for Sway Frame

	Phi Beam-to-Column mRad										
Phi Colum	pinned	256	128	64	32	16	8	4	2	1	fixed
pinned	0	7.0938	13.422	24.629	42.215	65.174	90.803	114.33	131.24	142.17	154.96
256	3.5	10.891	17.984	29.9	48.122	72.683	100.41	125.27	144.02	155.74	169.52
128	6.25	14.188	21.781	34.24	53.461	79.491	108.82	135.42	154.96	167.46	182.3
64	10.891	19.434	27.477	41.147	61.97	90.303	122.14	151.83	173.42	187.49	203.39
32	16.586	26.553	35.24	50.258	73.484	105.22	141.39	174.49	199.49	215.61	233.86
16	22.781	33.672	43.283	59.869	85.998	122.14	163.27	201.55	230.74	249.21	270.58
8	27.977	39.579	50.258	68.378	97.31	136.99	182.8	226.05	259.36	276.83	304.67
4	31.748	43.851	55.063	74.285	104.72	147.64	197.14	244.52	280.74	289.33	329.17
2	34.24	46.486	57.966	78.088	109.52	154.17	206.52	256.24	292.96	294.02	343.24
1	35.308	48.122	59.568	79.991	112.43	158.08	211.21	262.77	301.83	297.92	351.55
fixed	36.375	49.69	61.47	81.893	115.11	161.99	217.17	269.8	301.83	302.33	360.42

Table 6.10 shows the capacity of each frame as a ratio of the fully fixed frame.

Table 6.10 Strength Ratio Results

	Phi Beam-to-Column mRad										
Phi Colum	pinned	256	128	64	32	16	8	4	2	1	fixed
pinned	0	0.019682	0.03724	0.068334	0.117127	0.180828	0.251937	0.317213	0.364131	0.394456	0.429943
256	0.009711	0.030218	0.049897	0.082959	0.133516	0.201662	0.278592	0.347567	0.399589	0.432107	0.47034
128	0.017341	0.039365	0.060432	0.095	0.14833	0.220551	0.301926	0.375728	0.429943	0.464625	0.505799
64	0.030218	0.05392	0.076236	0.114164	0.171938	0.250549	0.338882	0.421259	0.481161	0.520199	0.564314
32	0.046019	0.073672	0.097775	0.139443	0.203884	0.291937	0.392292	0.48413	0.553493	0.598219	0.648854
16	0.063207	0.093424	0.12009	0.166109	0.238605	0.338882	0.452999	0.559209	0.640198	0.691443	0.750735
8	0.077623	0.109814	0.139443	0.189718	0.269991	0.380084	0.507186	0.627185	0.719605	0.768076	0.845319
4	0.088086	0.121666	0.152775	0.206107	0.29055	0.409633	0.546973	0.678431	0.778925	0.802758	0.913296
2	0.095	0.128977	0.160829	0.216658	0.303868	0.427751	0.572998	0.710948	0.812829	0.81577	0.952333
1	0.097963	0.133516	0.165274	0.221938	0.311942	0.438599	0.586011	0.729066	0.83744	0.826591	0.97539
fixed	0.100924	0.137867	0.170551	0.227215	0.319377	0.449448	0.602547	0.748571	0.83744	0.838827	1

The results from Table 6.10 are plotted in Figure 6.8 below.

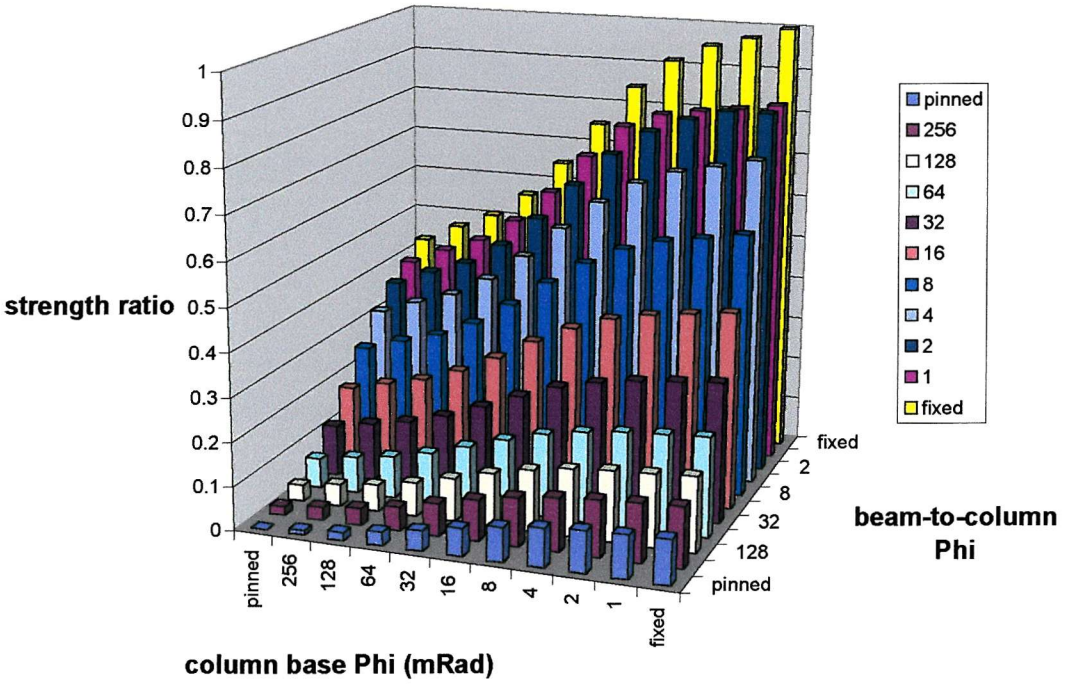

Figure 6.8 Ratio of Strength Against Fully-Fixed Frame

The chart shows that both the column base and the beam-to-column stiffness influence the capacity of the frame. This is consistent with the results from the single-storey frame.

The results show that the beam-to-column connection causes the greatest increase in strength. This was also shown in the elastic analyses, with the beam-to-column stiffness reducing the sway deflection more than the column-base stiffness.

The next analyses take the frames all the way to failure, by removing the deflection limit in ANSYS. The load deflection graphs for the frames can then be plotted for each frame, where the load is represented by the time step from ANSYS. The deflection is taken for the top of the column, where the sway loading is applied. The load step was set to remain constant during these analyses, and the deflection found for each time step. This was done for each frame, but due to the large amount of data that this gives, only the results for the fixed base models, and the fixed beam-to-column models have been shown. Figure 6.9 below shows the results for the fixed column base, with each curve representing a different beam-to-column stiffness, as shown in the legend.

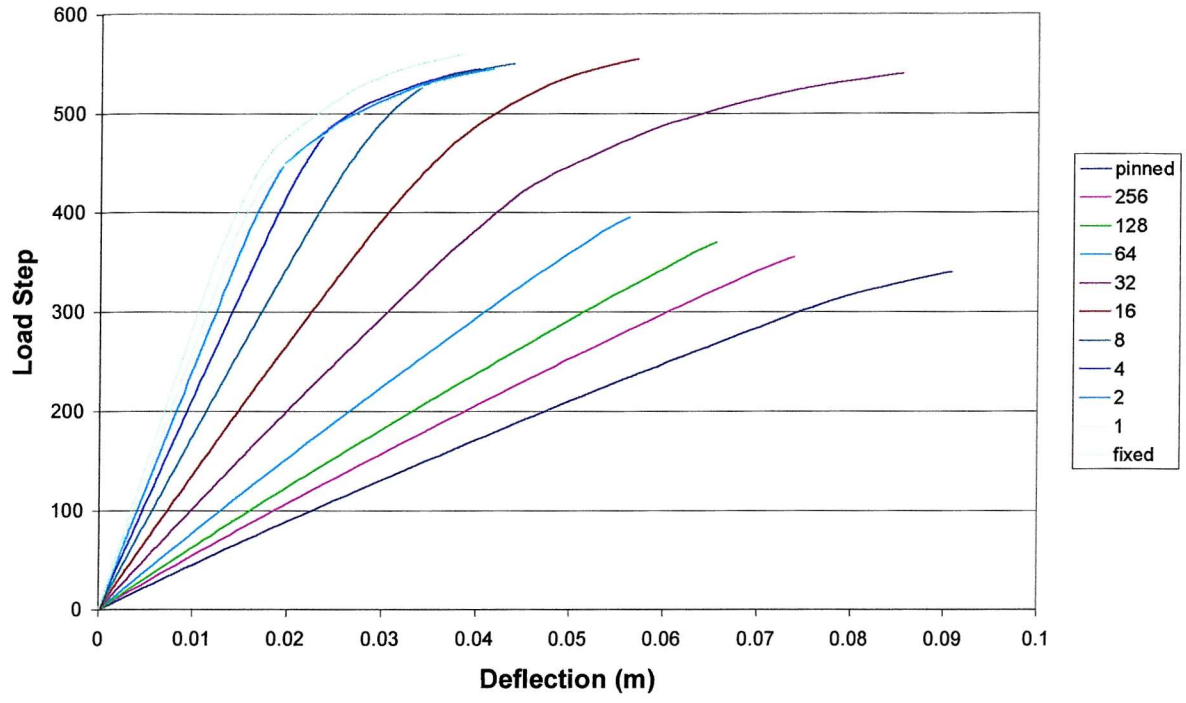

Figure 6.9 Load Deflection Curves for Fixed Base Frame

Figure 6.10 shows the load-deflection results for the frames with fixed beam-to-column connections, and each curve shows the results for a different column base stiffness.

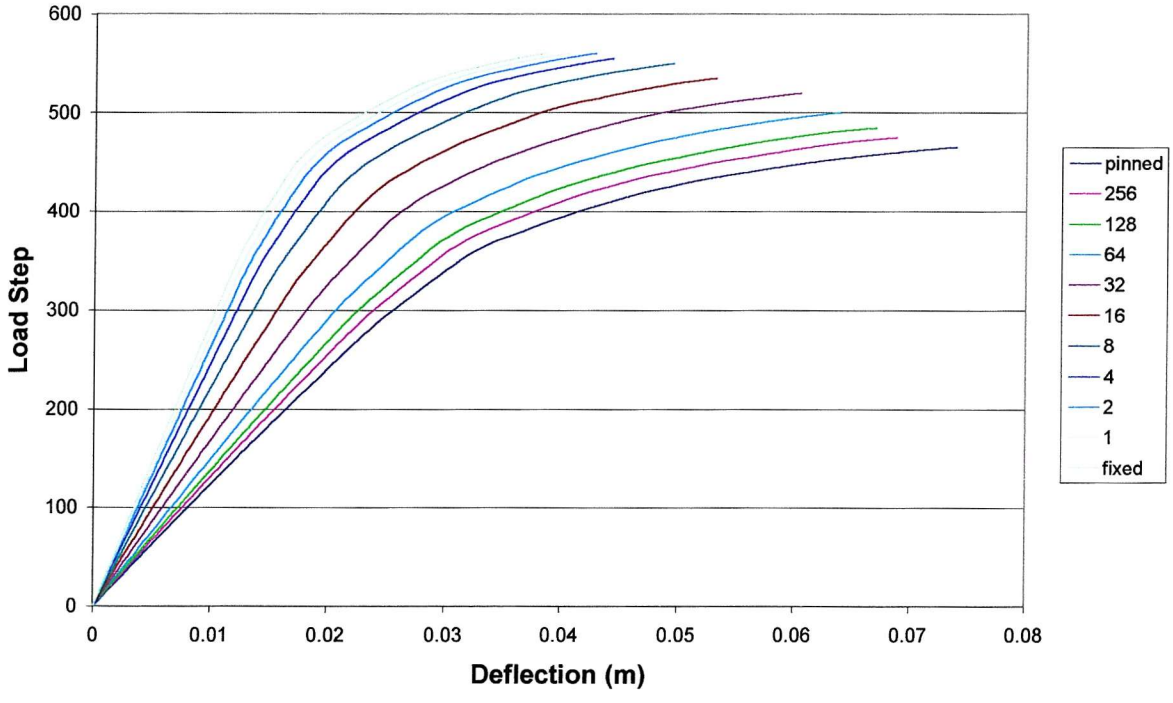

Figure 6.10 Load Deflection Curves for Fixed Beam-to-Column Connection

The chart for the frames with fully fixed base connections shows that the frames increase in collapse strength, as the beam-to-column connections become stiffer; this is as would be expected. There is also a reduction in flexibility, the sway deflection of the frame when it fails, for the four frames with the lowest beam-to-column rigidity. The flexibility increases again for the frame with a beam-to-column rotation of 32mRad, and then again decreases with increase in beam-to-column rigidity.

By using element tables in ANSYS it is possible to plot the stresses at 15 different points in each element, at each of the five integration points at each end of the element, and at the mid-length. This has been used this to find why the chart showing the results for the fixed base alters trends between the results for ϕ=64mRad, and ϕ=32mRad.

The results from the element tables are shown in the figures below. Figure 6.11 shows the stresses of the outermost fibre of the elements, at node j. This is plotted for frame 114, with a joint rotation of 64mRad.

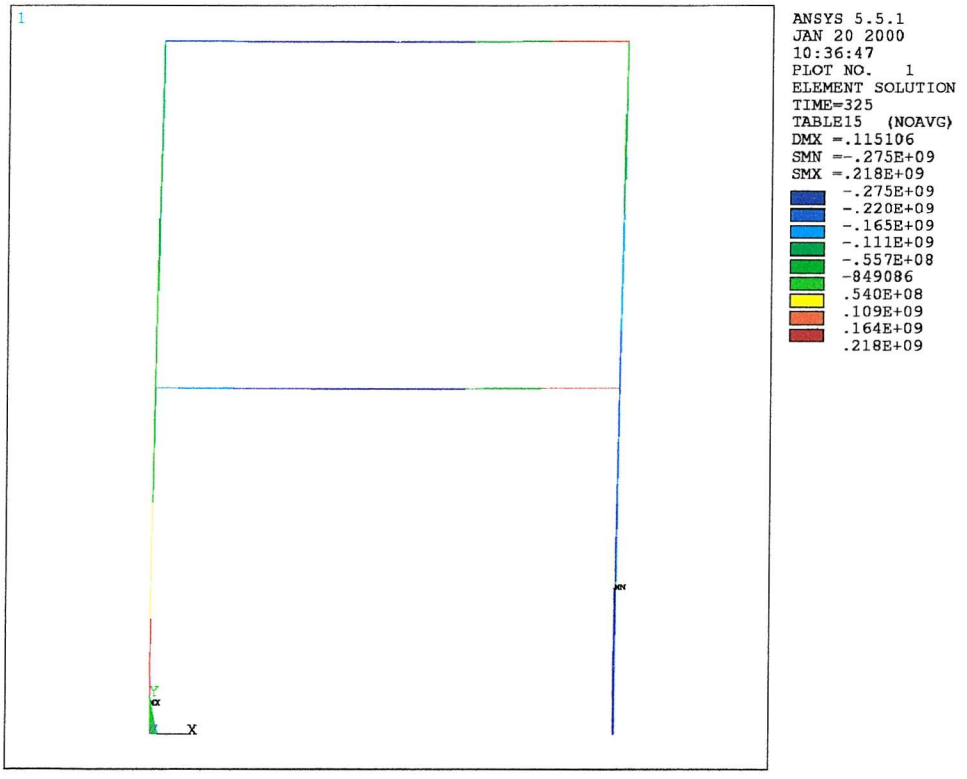

Figure 6.11 ANSYS Stress Plot, ϕ=64mRad

Figure 6.12 shows the stresses at the same points for the frame with a joint rotation of 32mRad.

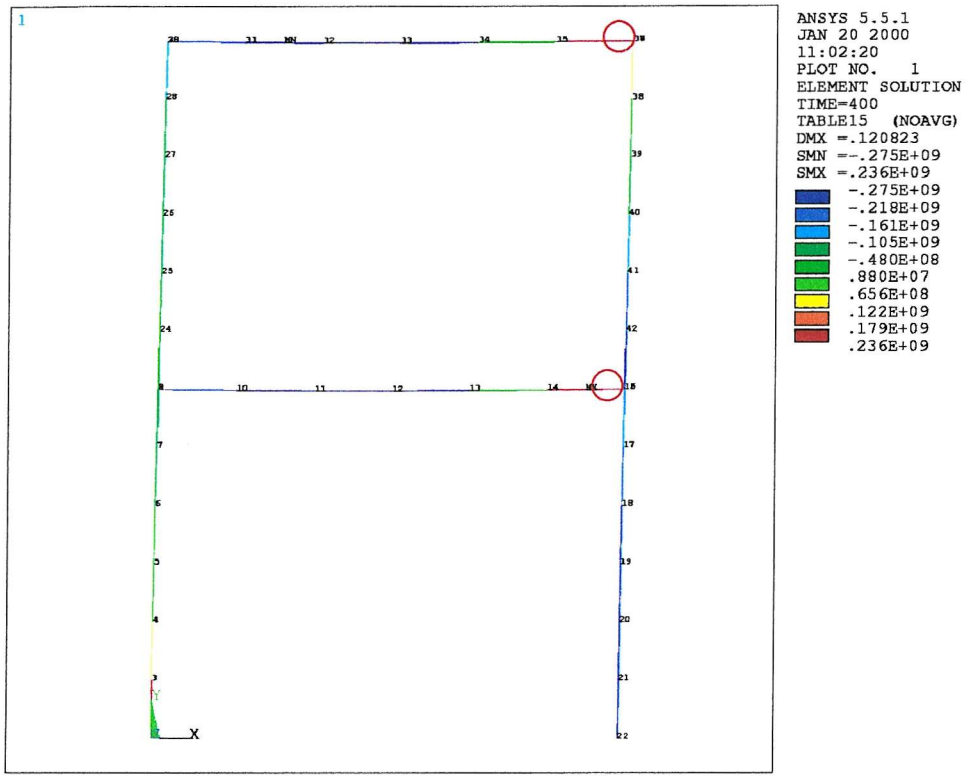

Figure 6.12 ANSYS Stress Plot, ϕ=32mRad

These figures show that the maximum material stress is reached in the outer fibres of the steel, in the second frame at the joints on the right-hand side. The red circles on the diagram show these points. Therefore a hinge has formed or is starting to form at this point. This has not happened in the first frame, although both show the last converged set of results for the frames, and therefore they are just about to fail.

The next two figures show the stresses at node j, for the innermost fibre. Figure 6.13 shows the frame with joint rotation of 64mRad. Figure 6.14 shows the frame with joint rotation of 32mRad.

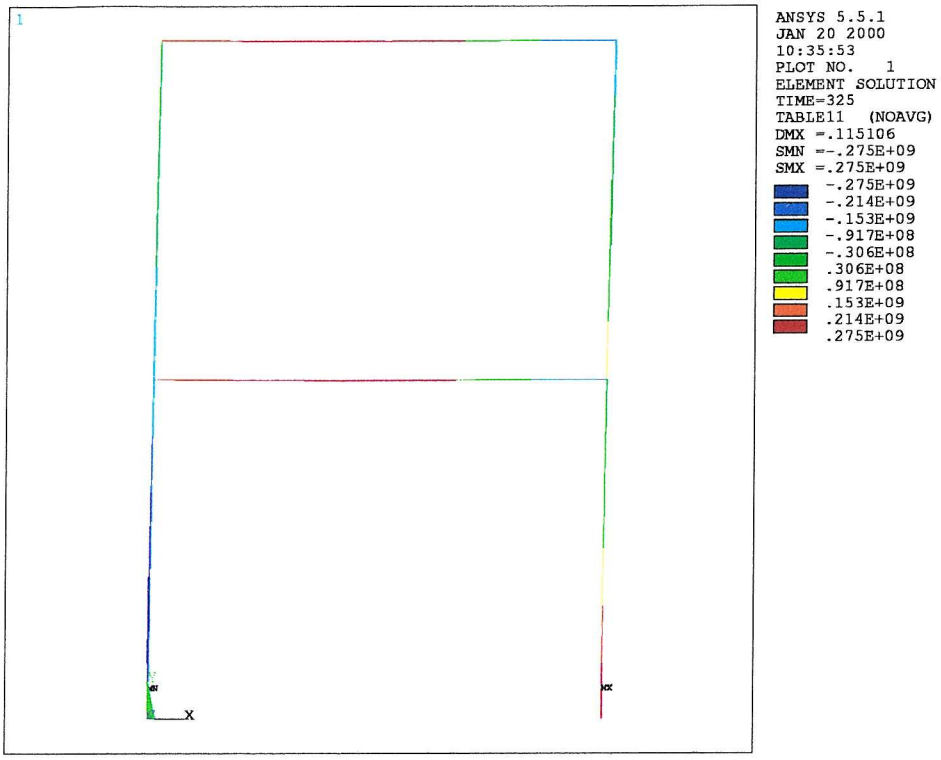

Figure 6.13 ANSYS Stress Plot, ϕ=64mRad

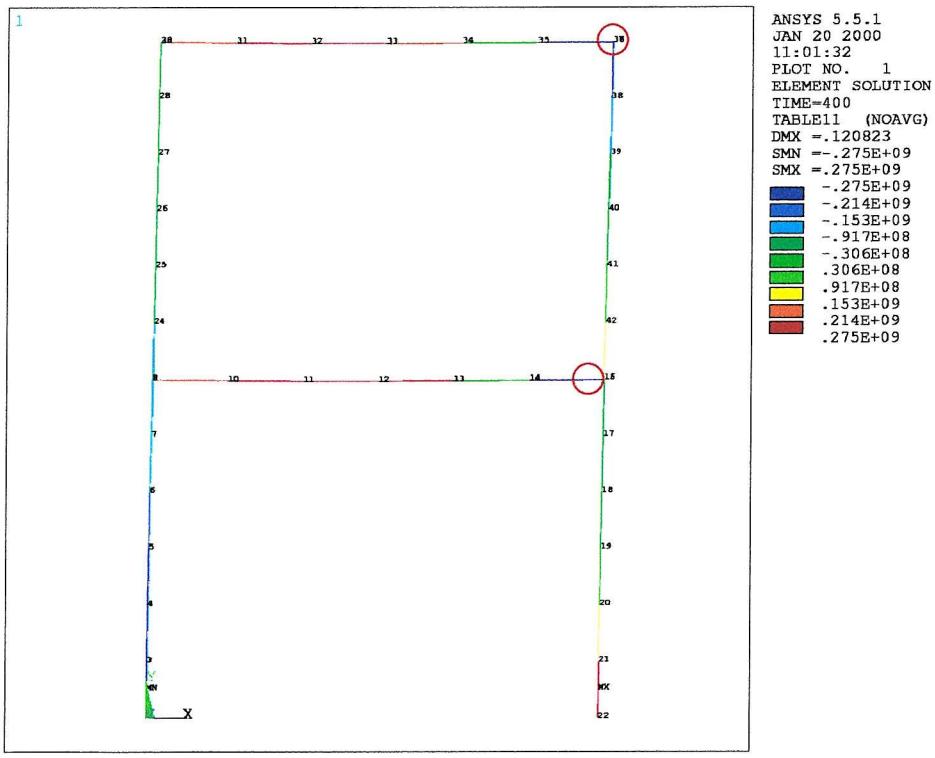

Figure 6.14 ANSYS Stress Plot, ϕ=32mRad

Red circles have again been used to show where the steel has reached its yield at the outer fibres by the connections on the right-hand side of the frame. These figures again show that a hinge is forming in the steel with the frame with the stiffer connections, by the two connections on the right-hand side. This means that the frame with the less stiff connections failed with hinges at the column bases and at the mid-spans of the beams; the connections on the right-hand side have failed due to excess rotation, and the steel by these has not reached yield.

The frame with the stiffer connections has failed with hinges at the column bases, in the mid-span of the beams and with hinges in the steel by the connections on the right-hand side. This explains the change in trend with the chart showing the load deflection results for the fixed base frame.

The chart showing the load deflection results for the frame with fixed beam-to-column connections, and varying column base stiffnesses is much more uniform. Each increase in column base stiffness gives an increase in collapse load, but a reduction in the deflection reached before failure.

6.2.3 Comparison of Results

Comparing the results shown here with those presented in the previous chapter on single-storey frames shows that the same trends are true for both sets of results. The column base has little effect on the non-sway deflections, or on the load to reach the deflection limit. For the sway frames, the column base has a large influence on the results – however, this influence is less for the two-storey frames. The sway behaviour of the sway frames with semi-rigid connections is influenced by the section properties of the beam and column sections, and by the stiffness and ultimate rotation capacity of the column base and beam-to-column connections. As the number of storeys of the frame increases, so does the number of beam-to-column connections, and therefore these play a increased role in the sway behaviour of multi-storey frames compared to the column base connections. This is shown in more detail in the following sections on five- and ten-storey frames. The load deflection curves, that plot the deflections up to failure, show the same trend in failure mechanism. The frames with the most flexible

connections fail at the connections, and the frames with the stiffer connections fail in the steel sections.

6.3 Five- and Ten-Storey Frame Analysis

The models for the five- and ten-storey models are an extension to the models for the single- and two-storey models discussed previously. For the analysis of these frames another column section was introduced, giving four different frame models. The sections used for these analyses are given in Tables 6.11 – 6.14 below.

Table 6.11 Section Properties Used in Frame 1

Frame 1	Height (m)	A(0) $x10^{-3}$ (m)	A(30) $x10^{-3}$ (m)	A(50) $x10^{-3}$ (m)	M_{pl} $x10^{3}$ Nm	L (m)	I_{xx} $x10^{-3}$ (m^4)
Beam UB457x191x89	0.463	48.4	7.61	3.18	553	4.8	0.41
Column UB457x191x89	0.463	48.4	7.61	3.18	553	3.6	0.41

Table 6.12 Section Properties Used in Frame 2

Frame 2	Height (m)	A(0) $x10^{-3}$ (m)	A(30) $x10^{-3}$ (m)	A(50) $x10^{-3}$ (m)	M_{pl} $x10^{3}$ Nm	L (m)	I_{xx} $x10^{-3}$ (m^4)
Beam UC254x254x89	0.260	55.6	7.07	0.871	338	4.8	0.143
Column UC254x254x89	0.260	55.6	7.07	0.871	338	3.6	0.143

Table 6.13 Section Properties Used in Frame 3

Frame 3	Height (m)	A(0) $x10^{-3}$ (m)	A(30) $x10^{-3}$ (m)	A(50) $x10^{-3}$ (m)	M_{pl} $x10^{3}$ Nm	L (m)	I_{xx} $x10^{-3}$ (m^4)
Beam UB457x191x89	0.463	48.4	7.61	3.18	553	4.8	0.41
Column UC254x254x89	0.260	55.6	7.07	0.871	338	3.6	0.143

Table 6.14 Section Properties Used in Frame 4

Frame 3	Height (m)	A(0) $x10^{-3}$ (m)	A(30) $x10^{-3}$ (m)	A(50) $x10^{-3}$ (m)	M_{pl} $x10^{3}$ Nm	L (m)	I_{xx} $x10^{-3}$ (m^4)
Beam UB457x191x89	0.463	48.4	7.61	3.18	553	4.8	0.41
Column UC305x305x198	0.3399	1.85	19.1	109	946	3.6	0.508

6.3.1 Plastic Analysis

As for the previous analyses for single- and two-storey frames, the models were loaded until a deflection limit was reached. This deflection limit was set to that given in BS5950 **[41]** for serviceability, as L/200 for the beam deflection, and the height of storey under consideration/300 for the sway deflection. The deflection limit was set in ANSYS, and the load was applied using the load step options until this deflection was reached.

6.3.1.1 Non-Sway Analysis

The analyses were run as described above, and the results for the non-sway five- and ten-storey frames are shown in Tables 6.15 and 6.16 below. These results show the load step that was reached for Frame 3 to reach the deflection limit.

Table 6.15 Load Step Results for Five-Storey Frame

	Phi Beam-to-Column mRad										
Phi Colum	pinned	256	128	64	32	16	8	4	2	1	fixed
pinned	312.77	321.08	328.11	340.11	357.3	378.39	399.49	416.67	426.55	430.74	434.64
256	312.77	321.08	328.11	340.11	357.3	378.39	399.49	416.67	426.55	430.74	434.36
128	312.77	321.08	328.11	340.11	357.3	378.39	399.49	416.67	426.55	430.74	434.36
64	312.77	321.08	328.11	340.11	357.3	378.39	399.49	416.67	426.55	430.74	434.36
32	312.77	321.08	328.11	340.11	357.3	378.39	399.49	416.67	426.55	430.46	434.36
16	312.77	321.08	328.11	340.11	357.3	378.39	399.49	416.67	426.55	430.46	433.86
8	312.77	321.08	328.11	340.11	357.3	378.39	399.49	416.67	426.05	430.46	433.86
4	312.77	321.08	328.11	340.11	357.3	378.39	399.49	416.67	426.05	429.96	433.86
2	312.77	321.08	328.11	340.11	357.3	378.39	399.49	416.67	426.05	429.96	433.86
1	312.77	321.08	328.11	340.11	357.3	378.39	399.49	416.67	426.05	429.96	433.86
fixed	312.77	321.08	328.11	340.11	357.3	378.39	399.49	416.39	426.05	429.96	433.86

Table 6.16 Load Step Results for Ten-Storey Frame

	Phi Beam-to-Column mRad										
Phi Colum	pinned	256	128	64	32	16	8	4	2	1	fixed
pinned	175.27	176.83	178.39	181.24	185.14	189.83	194.52	197.92	200.27	201.83	203.39
256	175.27	176.83	178.39	181.24	185.14	189.83	194.52	197.92	200.27	201.83	203.39
128	175.27	176.83	178.39	181.24	185.14	189.83	194.52	197.92	200.27	201.83	203.39
64	175.27	176.83	178.39	181.24	185.14	189.83	194.52	197.92	200.27	201.83	203.39
32	175.27	176.83	178.39	181.24	185.14	189.83	194.52	197.92	200.27	201.83	203.39
16	175.27	176.83	178.39	181.24	185.14	189.83	194.52	197.92	200.27	201.83	203.39
8	175.27	176.83	178.39	181.24	185.14	189.83	194.52	197.92	200.27	201.83	203.39
4	175.27	176.83	178.39	181.24	185.14	189.83	194.52	197.92	200.27	201.83	203.39
2	175.27	176.83	178.39	181.24	185.14	189.83	194.52	197.92	200.27	201.83	203.39
1	175.27	176.83	178.39	181.24	185.14	189.83	194.52	197.92	200.27	201.83	203.39
fixed	175.27	176.83	178.39	181.24	185.14	189.83	194.52	197.92	200.27	201.83	203.39

The results above show that the number of storeys of a frame decrease the load that can be applied to the beams before the deflection limit is reached. This will be due to the columns compressing under the loading applied. This is a problem of using a program such as ANSYS - it is not possible to output the relative deflections, only the absolute ones. This creates a difficulty for this type of analysis, as the results should be similar for all the non-sway analyses with the same beam and column sections. Figure 6.15 shows the vertical deflections for a ten-storey frame with a fixed column base and beam-to-column ultimate rotation of 16mRad. This figure shows that the vertical deflections in the top beams are higher than those in the lower beams, but this is only

due to the axial shortening of the columns – in reality, all the beam deflections would be the same.

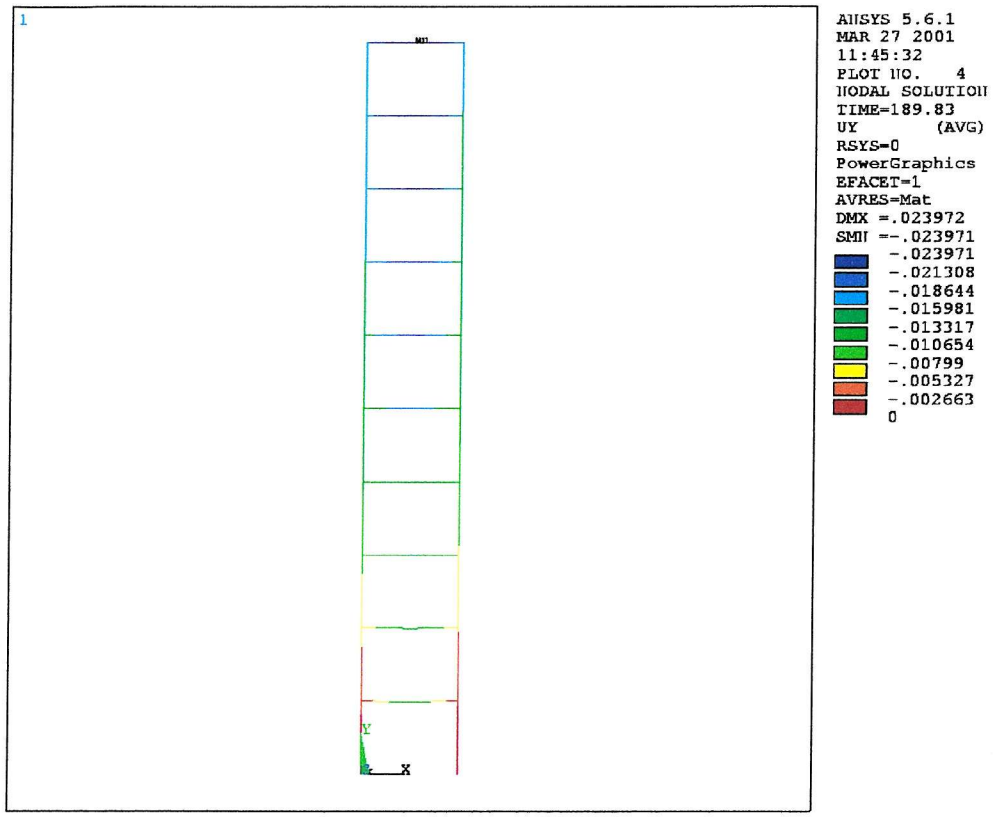

Figure 6.15 Vertical Deflections (Including Axial Shortning) for a Ten-Storey Frame

As for the single- and two-storey frames, the load reached by the frame is not affected by the column-base stiffness. Figure 6.16 and 6.17 below plot the results above as a strength factor.

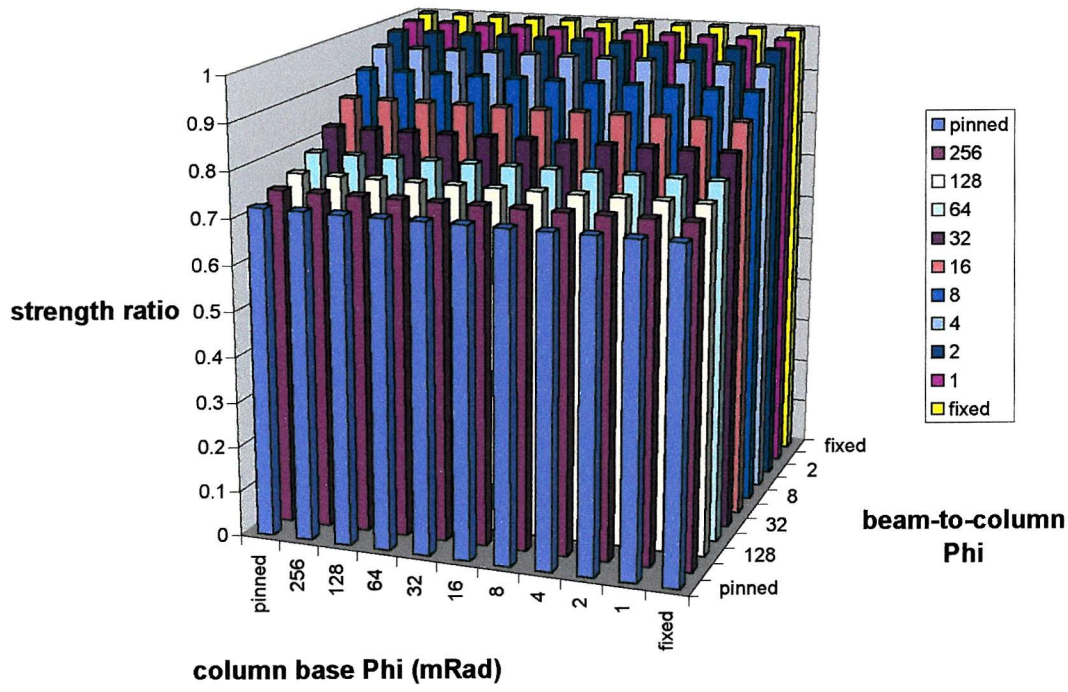

Figure 6.16 Ratio of Strength Against Fully-Fixed Frame for Five-Storey Frame

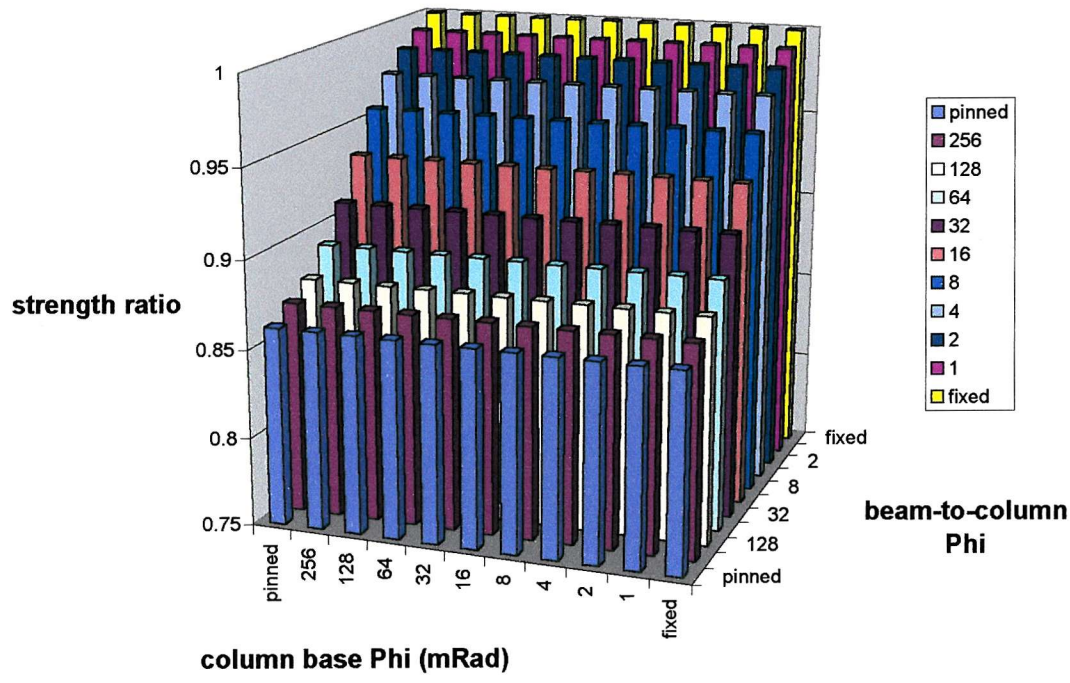

Figure 6.17 Ratio of Strength Against Fully-Fixed Frame for Ten-Storey Frame

The figures above show that the beam-to-column connection affects the strength ratio of the frame more for the ten-storey frame than for the five-storey frame, although this may be due to the problem discussed above. However, the graphs are following a similar trend. The strength ratio increases slightly as the beam-to-column connection becomes stiffer, with the greatest increase in strength ratio occurring over the mid-range of beam-to-column connection stiffnesses. Note that each value of phi is half that of the previous value, giving a logarithmic scale to the graphs.

6.3.1.2 Sway Analysis

As the structure becomes taller there will be more of an influence from the P-Δ effect. This is when the building has a sway deflection, and the vertical loading on the frame causes a moment to occur at the column base, therefore increasing the sway deflection beyond that from the sway loading alone. As the height of the building increases, the P-Δ effect becomes greater as the sway deflections are increasing, and as the vertical loading is greater due to the greater number of storeys.

The tables below show the load step reached for the five and ten-storey sway frames, using Frame 3.

Table 6.17 Load Step Results for Five-Storey Frame

	Phi Beam-to-Column mRad										
Phi Colum	pinned	256	128	64	32	16	8	4	2	1	fixed
pinned	0	18.484	24.629	34.74	51.559	75.086	103.52	131.52	154.17	169.02	187.77
256	15.637	22.281	28.477	39.011	55.864	79.991	109.52	139.05	162.77	178.39	198.71
128	18.484	25.129	31.324	41.715	59.068	83.595	114.33	144.8	169.8	186.21	207.3
64	22.281	28.9	35.24	45.986	63.572	89.102	121.36	153.39	179.96	197.92	220.58
32	26.053	33.172	39.511	50.258	68.679	95.608	129.67	164.33	192.96	212.49	237.49
16	29.4	36.375	42.783	54.262	73.484	101.62	137.49	174.49	205.46	226.83	253.39
8	31.748	39.011	45.418	57.466	77.088	105.92	143.24	182.3	215.11	237.77	265.11
4	33.172	40.647	47.054	59.068	79.289	108.82	147.14	186.99	221.36	244.8	272.64
2	34.172	41.147	48.122	60.369	80.491	110.73	149.49	190.11	224.99	249.21	276.83
1	34.24	41.715	48.622	60.67	81.192	111.23	150.27	191.67	226.83	251.05	278.89
fixed	34.74	42.215	49.19	61.47	81.893	112.43	151.83	193.24	228.89	253.39	280.74

Table 6.18 Load Step Results for Five-Storey Frame

Phi Colum	Phi Beam-to-Column mRad										
	pinned	256	128	64	32	16	8	4	2	1	fixed
pinned	0	21.332	27.477	36.875	51.86	72.382	95.608	118.74	136.21	144.8	150.08
256	18.484	25.129	30.824	40.079	54.762	75.086	99.212	122.92	141.39	151.05	157.61
128	20.832	27.477	32.748	42.215	56.665	77.588	102.12	125.77	144.8	155.74	162.64
64	24.205	30.324	35.308	44.851	59.568	79.991	105.22	129.96	149.49	161.21	169.8
32	27.053	32.748	37.943	47.054	62.271	83.095	108.82	134.64	154.96	167.46	176.83
16	28.9	34.74	40.079	49.19	64.373	85.998	111.93	138.55	159.64	172.92	182.02
8	30.324	35.808	41.147	50.758	65.975	87.699	114.33	140.89	162.77	176.05	184.64
4	30.824	36.875	42.215	51.559	66.776	88.9	115.89	142.46	164.33	178.11	186.21
2	31.324	36.875	42.215	51.86	67.077	89.102	116.39	143.74	165.89	179.17	186.99
1	31.324	37.443	42.783	51.86	67.577	89.602	116.67	144.02	166.39	179.67	186.99
fixed	31.748	37.443	42.783	52.36	67.878	90.102	117.17	144.8	166.67	179.96	187.49

The strength factors for the above results are plotted in Figure 6.18 and Figure 6.19 below.

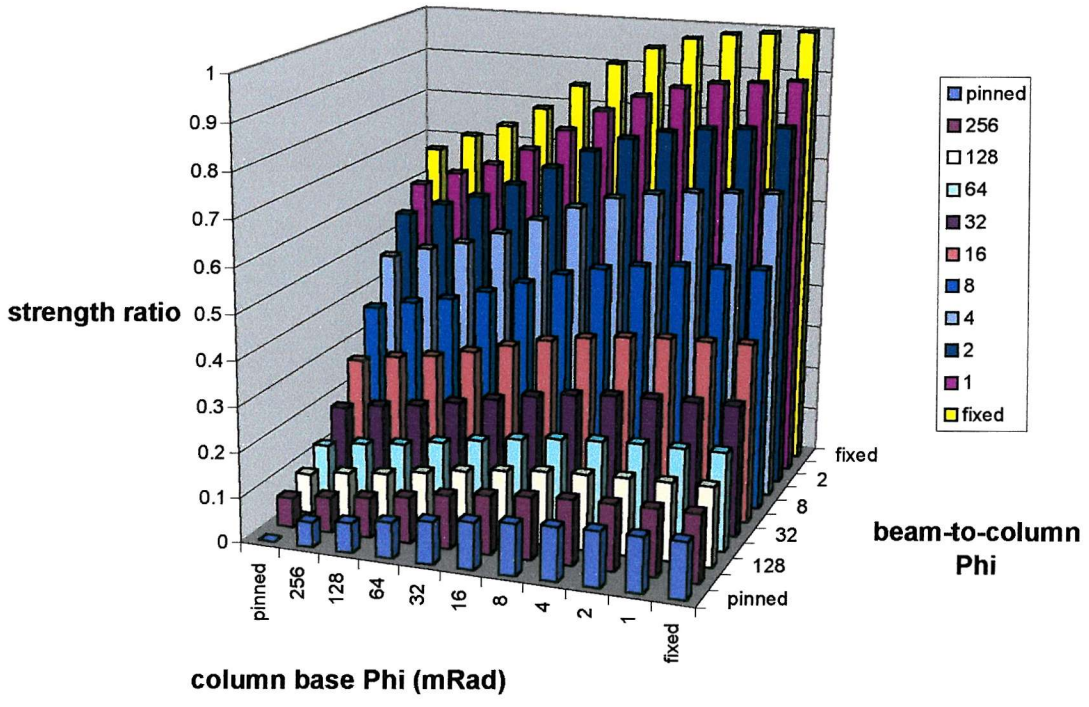

Figure 6.18 Ratio of Strength Against Fully-Fixed Frame for Five-Storey Frame

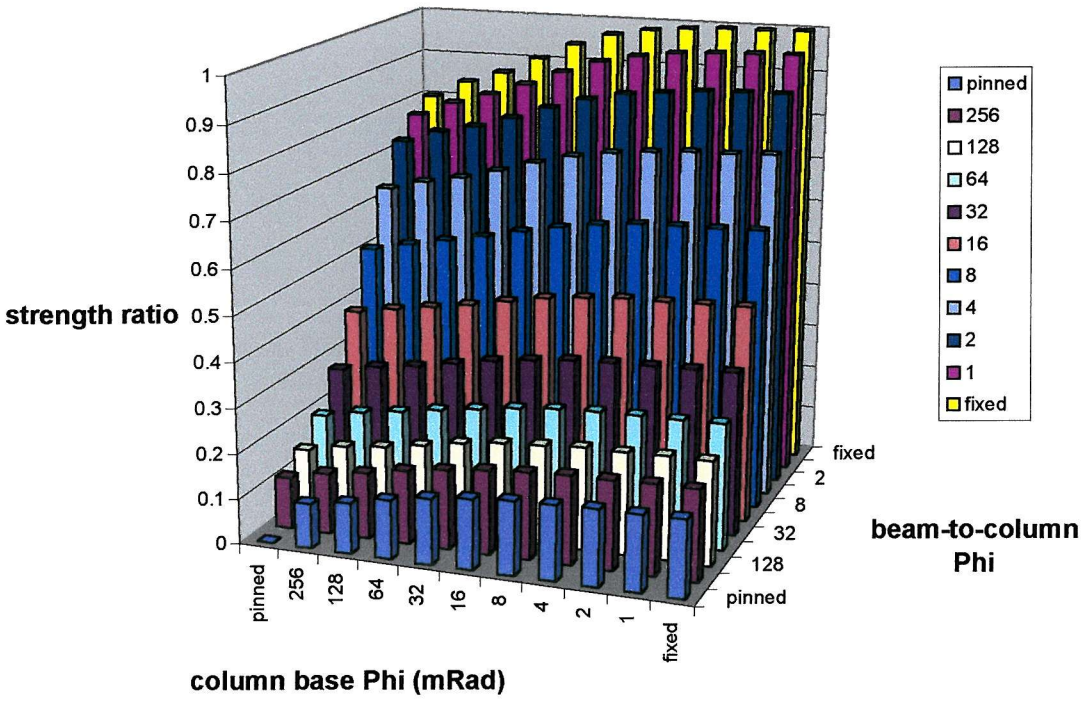

Figure 6.19 Ratio of Strength Against Fully-Fixed Frame for Ten-Storey Frame

The graphs above show that the same trends are followed for both the five- and ten-storey frames. These curves are also similar to those for the single- and two-storey frames. However, as the number of storeys in the frame increases, the beam-to-column connections have more influence on the load step at which the deflection limit is reached. The influence from the column base decreases. This is simply because there are more beam-to-column connections, and they have a cumulative effect on the sway behaviour of the frame, as discussed above.

To further show the effects that the storey number had on the loading to reach the deflection limit and the strength ratio, a set of frames was analysed from two storeys high through to ten storeys high. For these analyses the column base was kept fixed, and the beam-to-column connections were varied using the same values as for the previous analyses. The results from these analyses, using Frame 3, are shown in Figures 6.20 and 6.21 below.

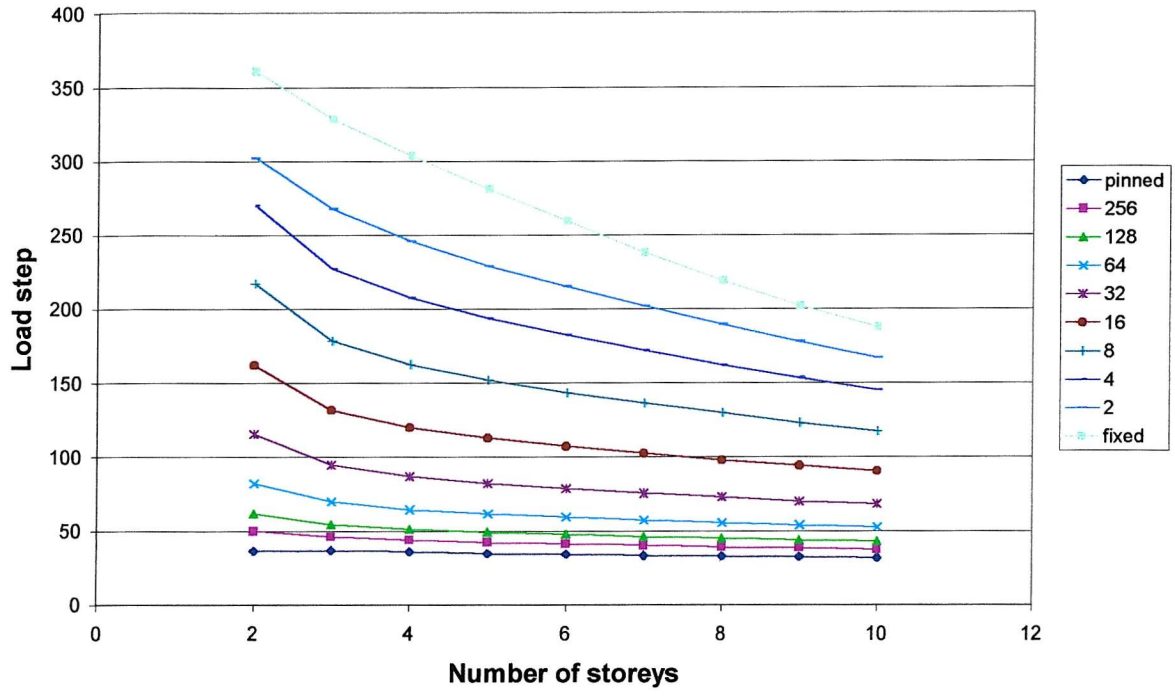

Figure 6.20 Load Step to Reach Deflection Limit Against Number of Storeys

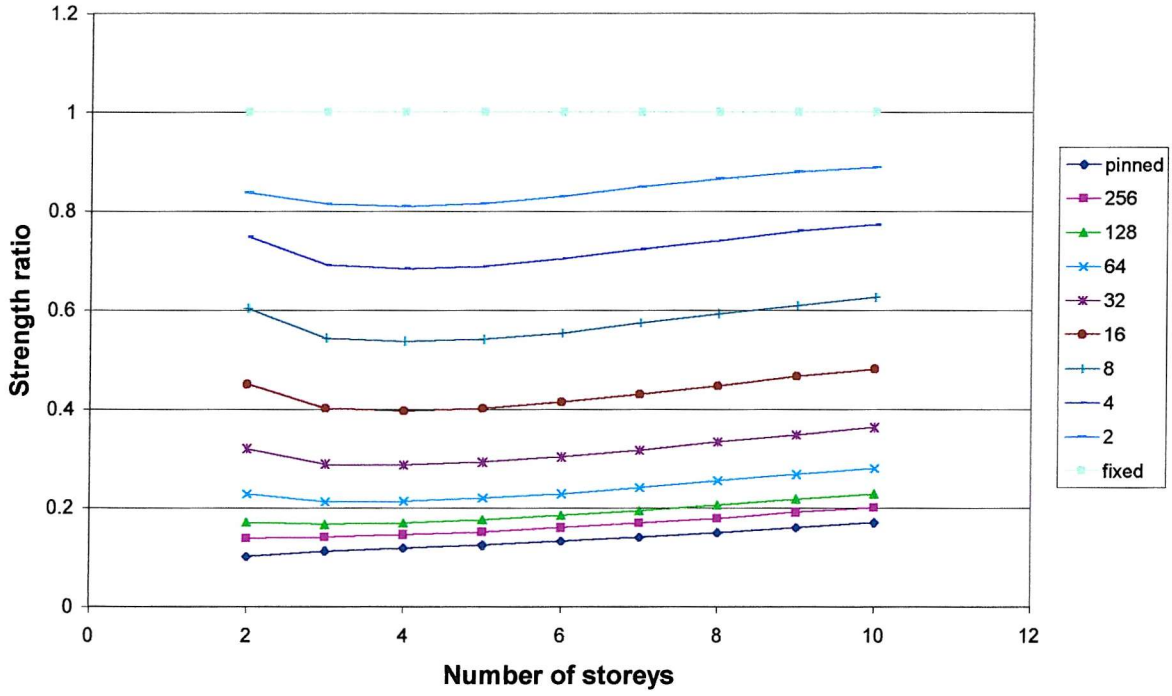

Figure 6.21 Strength Ratio Against a Fully Fixed Frame Against Number of Storeys

The results plotted in Figure 6.20 show that the strength of the frame decreases as the number of storeys increases. The strength of the frame decreases more sharply with storey height for the frames with the stiffest beam-to-column connections. Figure 6.21 shows the results for the strength ratio of the frames against the fully fixed frames. This graph shows that the strength ratio drops for frames with three to four storeys, with an ultimate beam-to-column rotation of less than 64mRad. In both the graphs above it is clear that there are trends occurring in the results. To show this trend the results for the strength ratios have been plotted against the ultimate rotation of the beam-to-column connections, phi, in Figure 6.22 below.

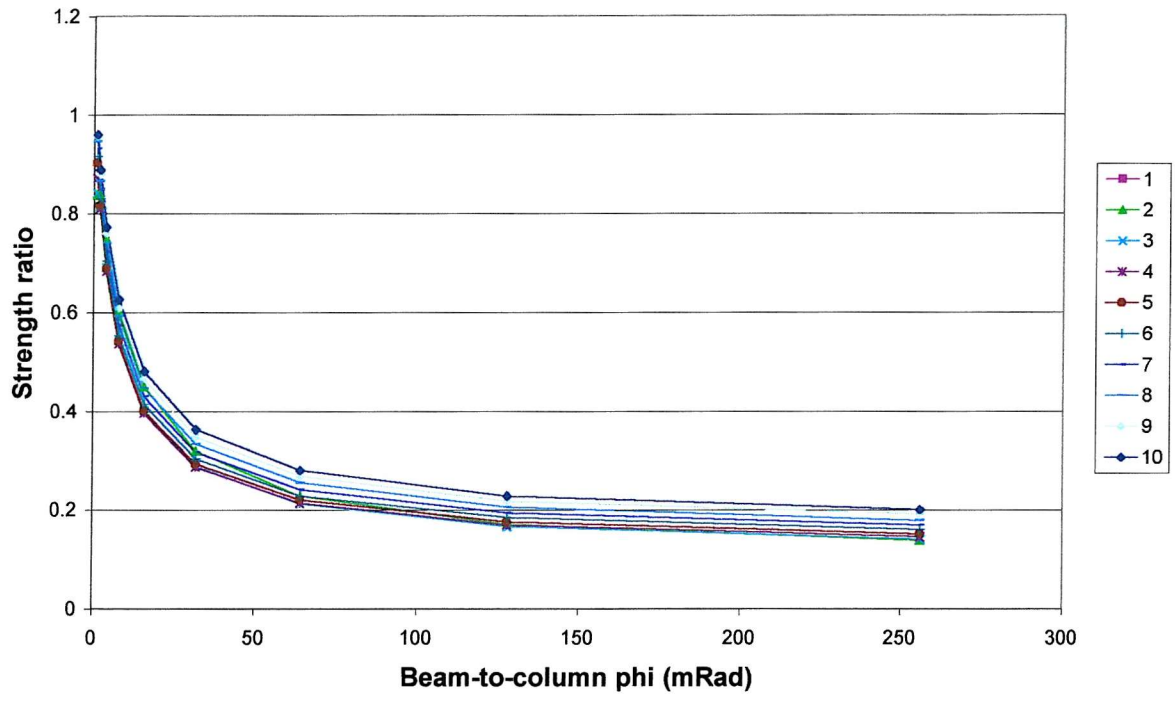

Figure 6.22 Strength Ratio Against Beam-to-Column Phi for Differing Number of Storeys

This figure shows that the strength ratio is dropping as the beam-to-column connections become less rigid. A very similar curve is plotted for each frame, regardless of the number of storeys. It is important to remember, however, that with increasing structure height the allowable sway deflection has also been increased.

The above analyses were repeated, this time with only a sway loading applied to the frame, with no vertical loading. This is to show how the second order effects affected the strengths found for the previous analyses.

The results for the load step applied to reach the deflection limit, and the strength ratio results are plotted in Figures 6.23 and 6.24 below.

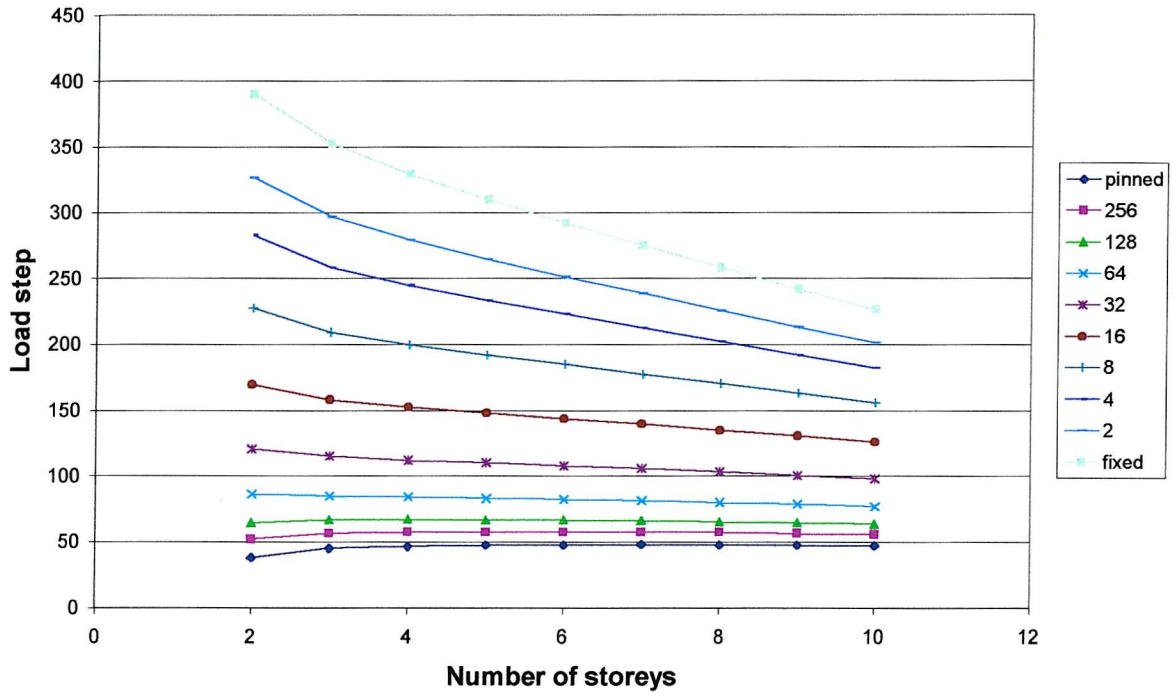

Figure 6.23 Load Step to Reach Deflection Limit Against Number of Storeys

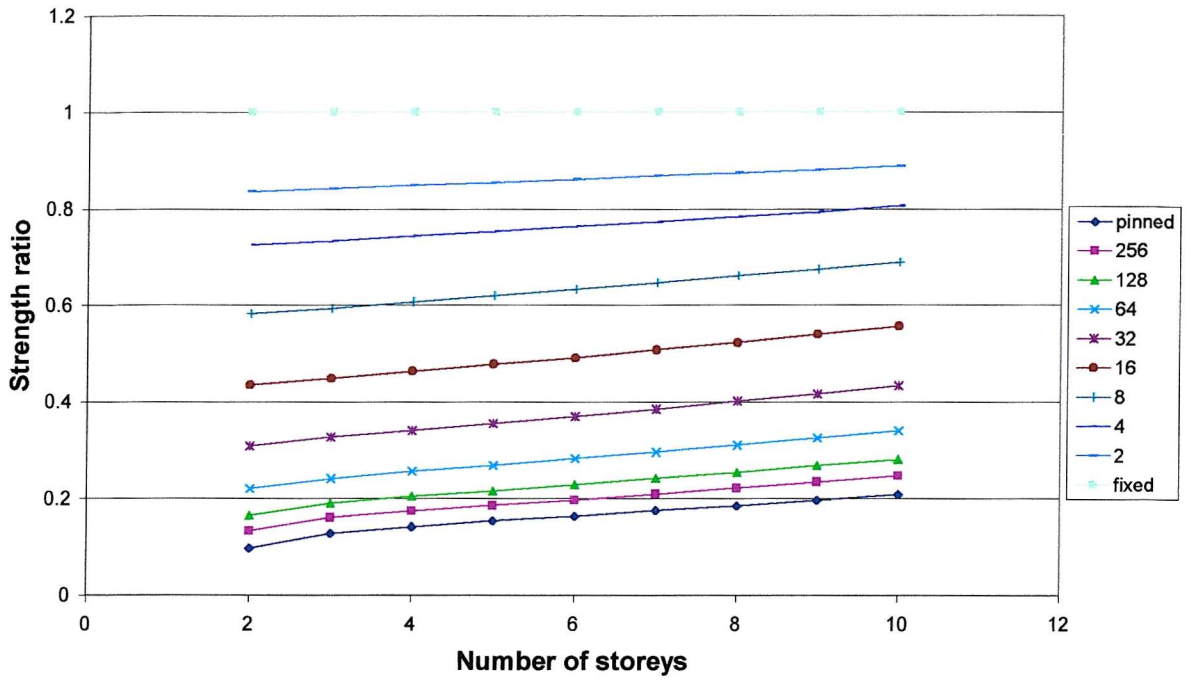

Figure 6.24 Strength Ratio Against a Fully Fixed Frame Against Number of Storeys

Figure 6.24 shows that the load step reached for these frames is greater than that reached by the frames with vertical as well as sway loading. The biggest differences between the load steps reached are for the frames with the most storeys. This is due to the P-Δ effect, which will increase with the sway deflection, which is greater for the frames with the higher storey numbers.

There is a big difference in the graphs of strength ratio. Figure 6.21 shows a dip in the strength ratio for frames with three or four storeys. There is no dip in Figure 6.24, the graph that shows the results for the frames with only sway loading. In fact the curves in this chart are almost linear, so the vertical loading must be causing these dips.

6.4 Summary

This chapter has shown that the same trends follow for the frames with multi-storeys, as for those with single-storeys. There are also trends relating the multi-storey frames

with differing numbers of storeys. The P-Δ effect has a big influence on the sway frames, which increases as the height of the frames increase. The beam-to-column connections have a greater influence over the strength of the sway frames than the column base stiffness does, due to the larger number of these connections.

Chapter 7 further discusses the results shown here, and develops on the trends introduced in this chapter.

Chapter 7

Analysis of FEM Results

7.1 Introduction

This chapter discusses the results in the previous two chapters, and uses analytical techniques to find the relationships between the strength ratio, and the factors that affect it. These factors are the stiffness and ultimate rotation of the connections, the beam properties, the column properties, and the number of storeys in the frame.

As all the frames analysed in this research are based on the same size frame, with the same values being used for the yield stress of steel, and for the Young's modulus, it is thought that it will be possible to create a general formula, or set of formulae to allow for the quick prediction of strength for these steel frames. These could then be further expanded upon to allow for the design of frames consisting of members with different properties.

Two different techniques have been trialled in this chapter, in the effort to create some general equations, which will specify the strength of a semi-rigid frame in relation to a fully-fixed frame (the strength ratio) for a frame consisting of any beam and column section, and any value of stiffness, or ultimate rotation, for the beam-to-column

connection. The methods used are curve fitting techniques, and dimensional analysis. The curve fitting is used as the previous chapters have shown that there are clear trends forming in the finite element analysis results. Dimensional analysis was tried, as it is a very strong tool that allows for equations to be formed that are dimensionless, and therefore can be applied to both physical models and real life situations. This technique is suitable for further examination of the numerical models produced in finite element analysis.

7.2 Curve Fitting

To fit curves to the data points, the least squares method was used. This is where the known data points are compared to those from a curve of an estimated function. The error between the two data sets is found and squared, and the errors are summed for all the data points. The curve is then adjusted until this error is at minimum value. For this technique to work there must be enough data points. Otherwise a curve may be found that does not properly represent the relationship. For the curve fitting, the frames with pinned and fully-fixed connections were ignored, as these did not have a value for the ultimate connection rotation. Only the frames with fixed column bases have been considered, to reduce the amount of data and variables.

7.2.1 One-Storey Frames

For the curve fitting analyses, various curves were tried. Also, some transformations were applied to the results before the curve fitting was conducted. This is shown in the following sections for the single storey sway and non-sway frames.

7.2.1.1 Non-Sway Frames

The first results shown here are for the single storey non-sway frame, with a fixed column base. These results are from frame 1. In Figure 7.1, the blue line, which has been plotted with 5% error bars, shows the strength ratio results for that frame. Two

different curves have been plotted with the results. The black line is a power curve in the form of $y = cx^b$, the green line is a logarithmic curve in the form of $y = c \ln(x) + b$. The equations found for each of these curves of best fit are shown on the figure.

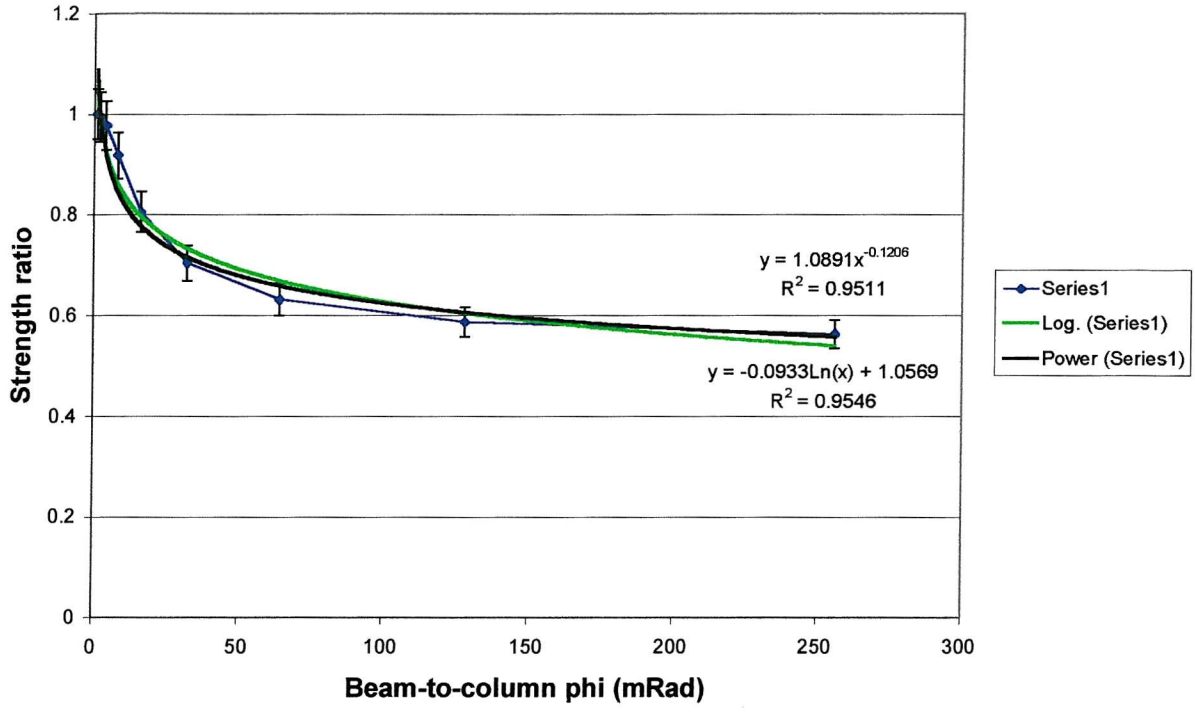

Figure 7.1 Non-Sway Single-Storey Frame – Curve Fitting

The error bars on the numerical results show that during most of the range of results both of the fitted curves fit closely to those from the finite element analyses. The values of R-squared given for each of the curves show that the logarithmic curve gives a better fit than the power curve. However, the power curve gives a more accurate interpretation of the results in the later stages of the curve, as it fits more closely to the results from the finite element analysis. It is during the first few values on the graph where the logarithmic curve is fitting more closely, and as there are more values at this end, it creates a smaller error value for that curve fit.

As it was possible to fit curves to the finite element analysis results, the theory was taken further. The bar charts plotted in the previous chapters effectively give a logarithmic axis, so it was then decided to see if this could be used. In the next figure

the values of Phi, the ultimate column rotation, have been transformed by taking the logarithm. Once again the values of strength ratio have been plotted.

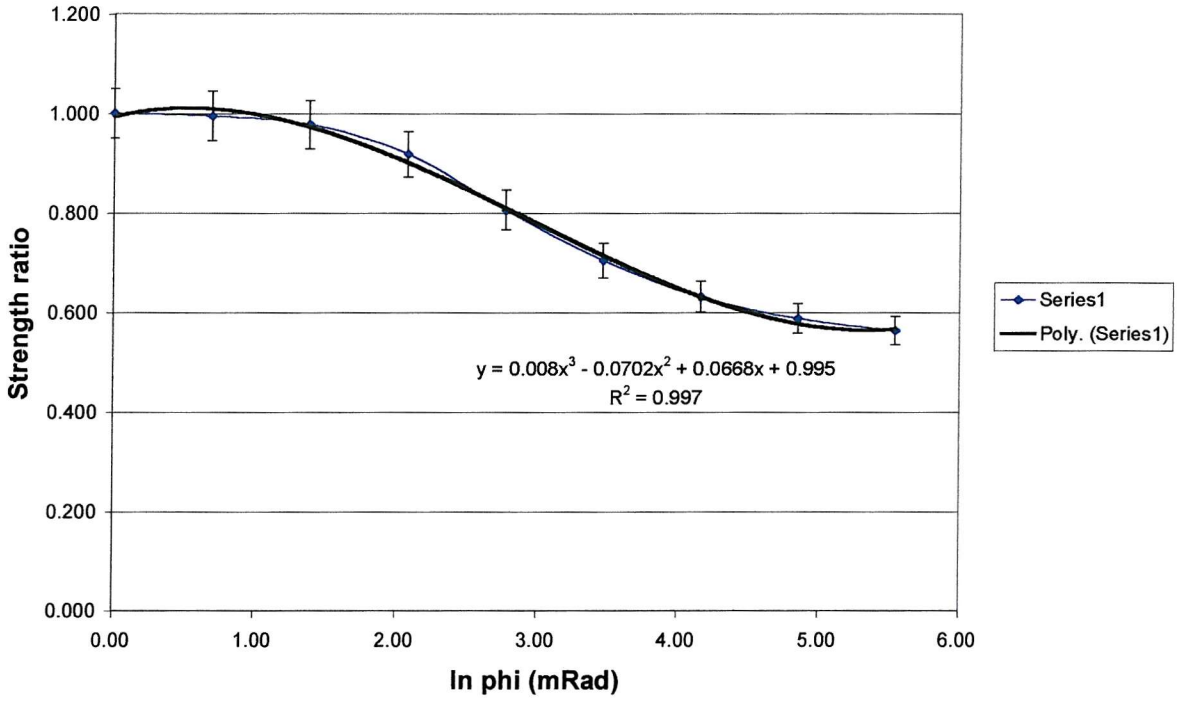

Figure 7.2 Non-Sway Single-Storey Frame – Curve Fitting

The results in Figure 7.2 show that the curve plotted here agrees much more closely than the curves plotted in the previous figure. However, this is a much more complex curve. The logarithm has been taken for the values of phi, and then a third order curve has been fitted to these results. This means that the equation is in the form $y = a\ \ln(x)^3 + b\ \ln(x)^2 + c\ \ln(x) + d$. The 5% error bars show that all the points for the curve fit lie very close to those from the finite element results.

The same approaches were applied to Frame 2 and Frame 3, and all the results are shown in Tables 7.1 – 7.3 below.

Table 7.1 Results for the Power Curve Fit

Frame No.	Equation of curve	R^2
Frame 1	$SR = 1.0891\phi^{-0.1206}$	0.9511
Frame 2	$SR = 1.0491\phi^{-0.1276}$	0.975
Frame 3	$SR = 1.0403\phi^{-0.0794}$	0.9704

Table 7.2 Results for the Logarithmic Curve Fit

Frame No.	Equation of curve	R^2
Frame 1	$SR = -0.0933Ln(\phi) + 1.0569$	0.9546
Frame 2	$SR = -0.0935Ln(\phi) + 1.0152$	0.9814
Frame 3	$SR = -0.0661Ln(\phi) + 1.0269$	0.9716

Table 7.3 Results for the Third Order Curve Fit using ln ϕ

Frame No.	Equation of curve	R^2
Frame 1	$Sr = 0.008(ln\phi)^3 - 0.0702(ln\phi)^2 + 0.0668(ln\phi) + 0.995$	0.997
Frame 2	$Sr = 0.0053(ln\phi)^3 - 0.046(ln\phi)^2 + 0.0084(ln\phi) + 0.978$	0.9997
Frame 3	$Sr = 0.0047(ln\phi)^3 - 0.0401(ln\phi)^2 + 0.0209(ln\phi) + 0.9964$	0.9991

Where:

Sr = Strength ratio

ϕ = Ultimate beam-to-column connection rotation

The logarithmic curve has given a better error value than the power curve in every case. However, there is only a very slight difference between these two. The curve fit that used the ln(ϕ) values is by far the best fit. The R – Squared value is very close to one, which is a perfect fit through the given points.

These results will be discussed in more detail later in this chapter, after the same analyses have been carried out on the sway frames, and multi-storey frames.

7.2.1.2 Sway Frames

The same approaches were used for the sway frames as for the non-sway frames above. Again the frames with fixed column bases have been used for the following curve fits.

Figure 7.3 below shows the curve fits using power and logarithmic curves for frame 1.

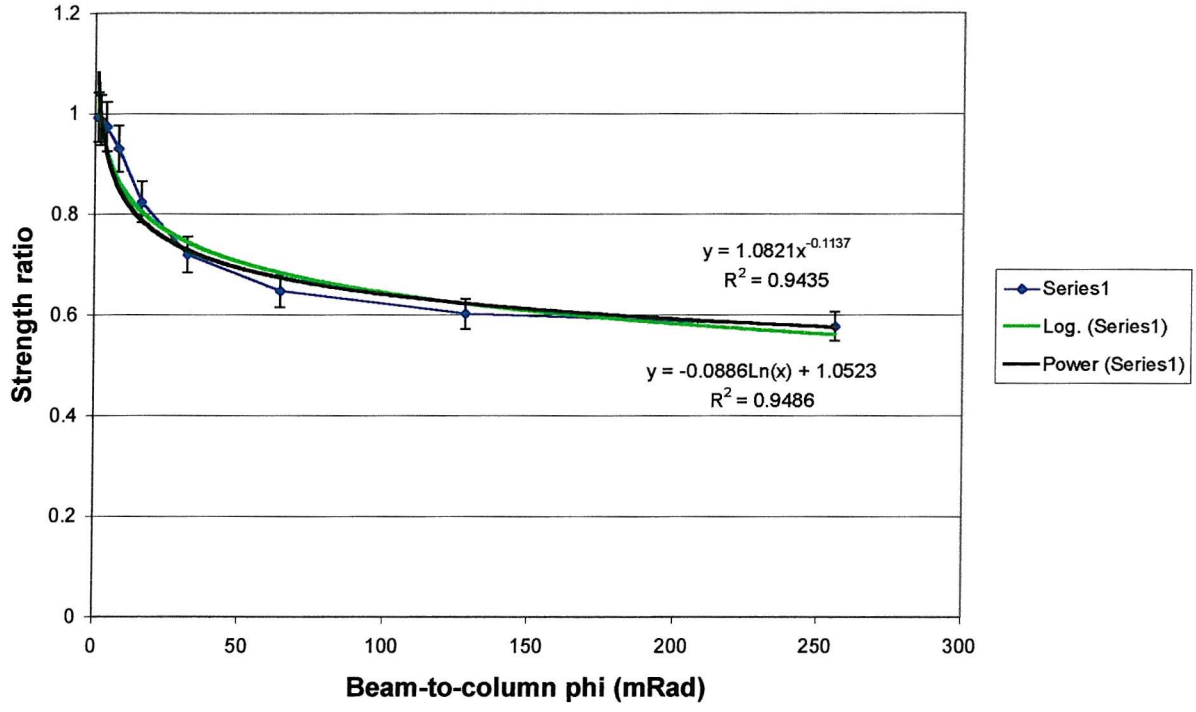

Figure 7.3 Sway Single-Storey Frame – Curve Fitting

The results for the sway frame with fixed column bases give a similar shaped curve to those from the non-sway analysis, and therefore the curves of best fit give a similar accuracy to before. The next graph, Figure 7.4, shows the results for a pinned base, and the associated curves of best fit.

This graph shows that although the curve fits are good for the frames with fixed bases, they are not as good for the frames with pinned bases. As the frames with other values for base stiffness all fall between those for fixed and pinned bases, the equations used for best fit curves will become less accurate as the column base connection becomes more flexible.

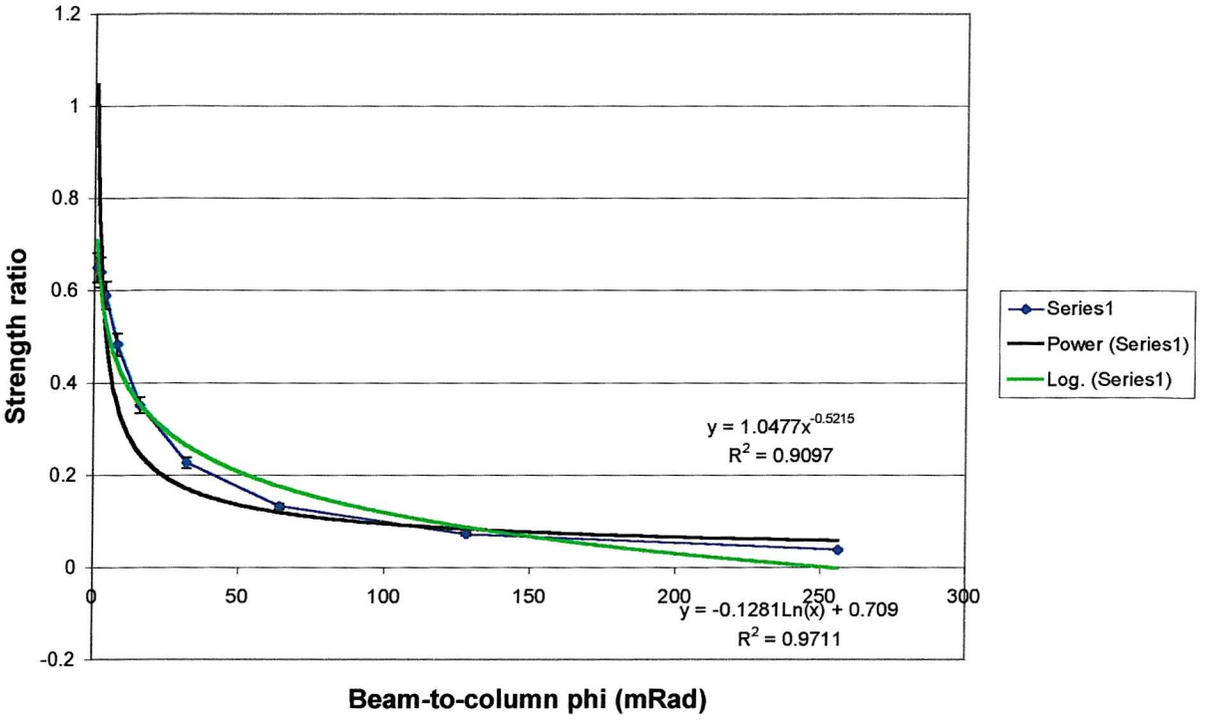

Figure 7.4 Sway Single-Storey Frame, Pinned Base – Curve Fitting

As for the non-sway frames in the previous section, the logarithm of the beam-to-column ultimate rotation was taken, and plotted with the strength ratio. This is shown in Figure 7.5 below for the frame with fixed column bases. Figure 7.6 plots the results for the frame with pinned column base connections, to see if this approach gives a better representation of the results from the finite element models.

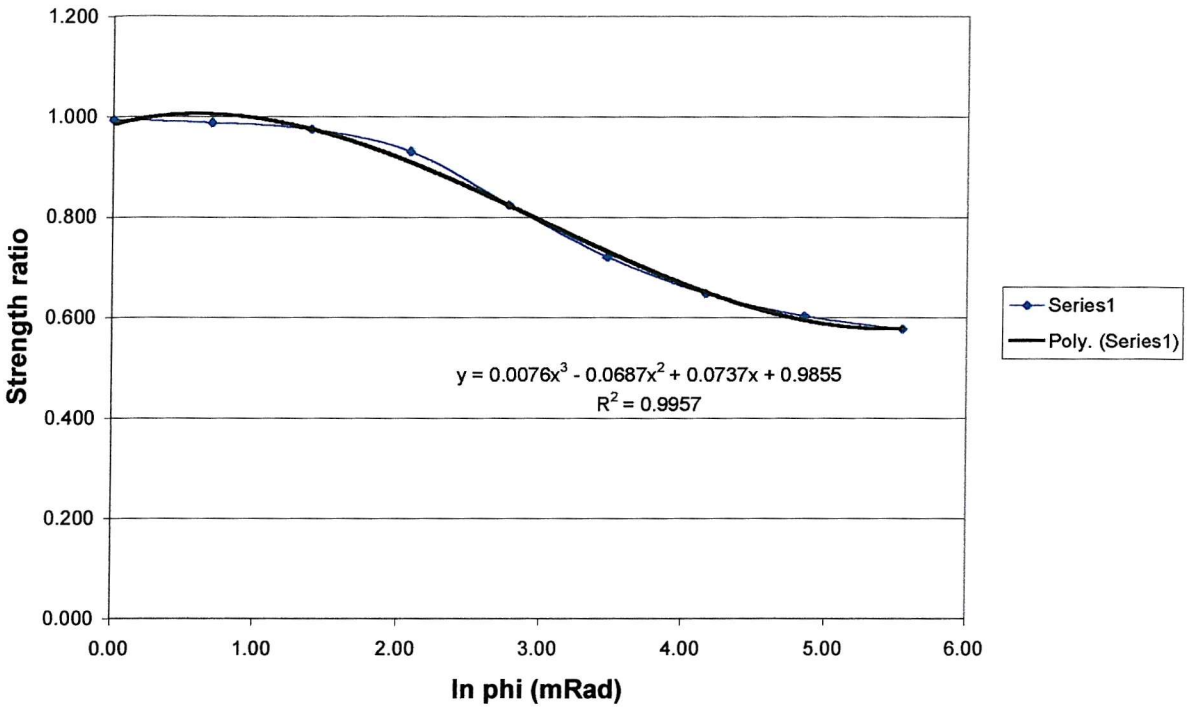

Figure 7.5 Sway Single-Storey Frame, Fixed Base – Curve Fitting

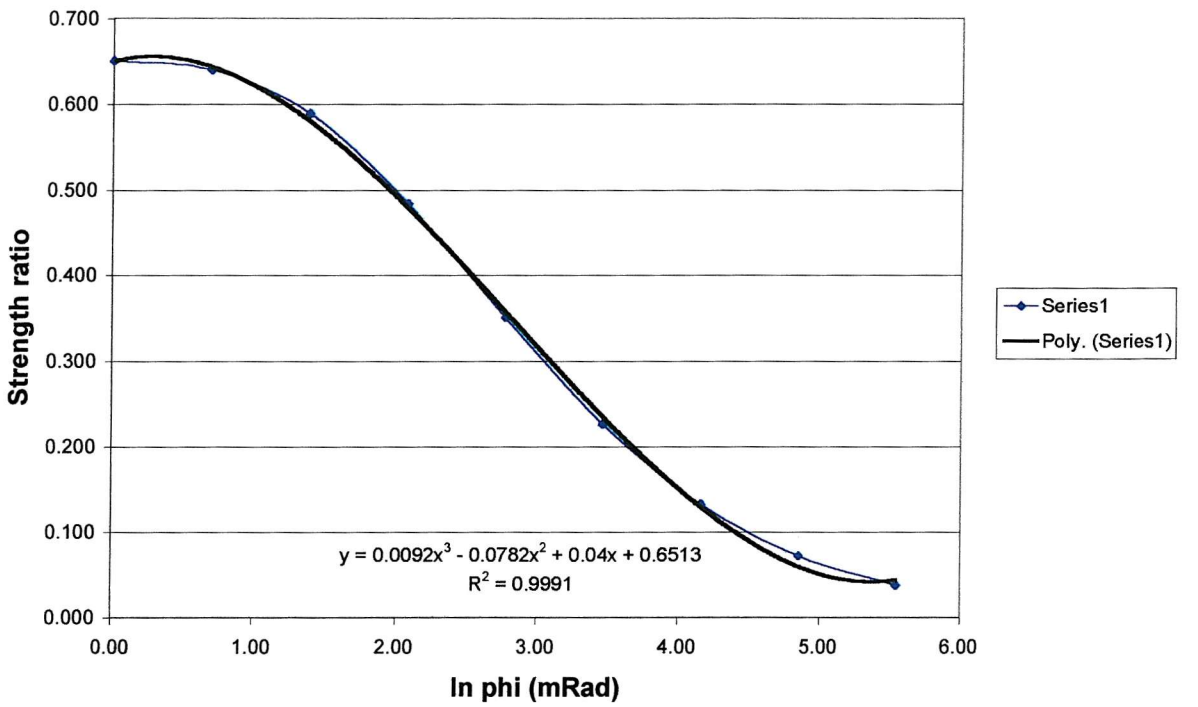

Figure 7.6 Sway Single-Storey Frame, Pinned Base – Curve Fitting

These figures show that this method is applicable to either fixed based, or pinned based frames. The curves also fit well to any of the values in between the two extremes.

Table 7.4 gives the equations of the lines of best fit for the three frames analysed.

Table 7.4 Results for the Third Order Curve Fit using ln ϕ

Frame No.	Equation of curve	R^2
Frame 1	$Sr = 0.0076(\ln\phi)^3 - 0.0687(\ln\phi)^2 + 0.0737(\ln\phi) + 0.9855$	0.9957
Frame 2	$Sr = 0.006(\ln\phi)^3 - 0.0541(\ln\phi)^2 + 0.0365(\ln\phi) + 0.9871$	0.9993
Frame 3	$Sr = 0.0024(\ln\phi)^3 - 0.0301(\ln\phi)^2 - 0.0333(\ln\phi) + 0.9925$	0.997

As the results gained by using the logarithm of the ultimate beam-to-column rotation, and then fitting a third order curve give better results than those from the other methods, only these will be considered from now on.

7.2.2 Two-Storey Frames

The same approaches have again been used to fit curves to the two-storey frame results. It will then be possible to see if there are any similarities with those from the single-storey frames.

The frames with fixed base connections have been used once more for the analyses in this section. The graphs shown are all for frame 1. Figure 7.7 plots the curve of best fit for the two-storey, non-sway frame, using the logarithm of phi, and the strength ratio.

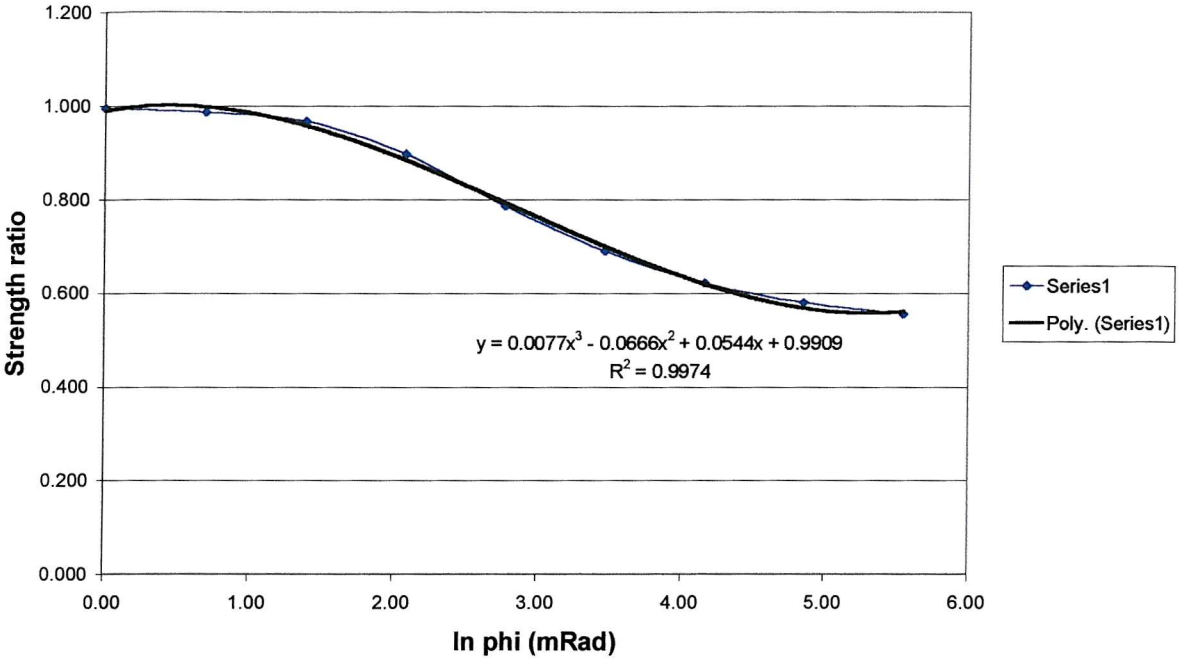

Figure 7.7 Non-Sway Two-Storey Frame – Curve Fitting

This graph shows that the curve still fits well for the two-storey frame, as it did for the single storey frame. Applying the method to each of the three frame sections gives the formulae in Table 7.5 below.

Table 7.5 Non-Sway Frame Results for the Third Order Curve Fit using ln ϕ

Frame No.	Equation of curve	R^2
Frame 1	$Sr = 0.0077(\ln\phi)^3 - 0.0666(\ln\phi)^2 + 0.0544(\ln\phi) + 0.9909$	0.9974
Frame 2	$Sr = 0.0057(\ln\phi)^3 - 0.0488(\ln\phi)^2 + 0.0102(\ln\phi) + 0.9762$	0.9997
Frame 3	$Sr = 0.005(\ln\phi)^3 - 0.0424(\ln\phi)^2 + 0.0226(\ln\phi) + 0.9954$	0.9987

Figure 7.7b plots the curve fit for the for the two-storey sway frame, using frame 1.

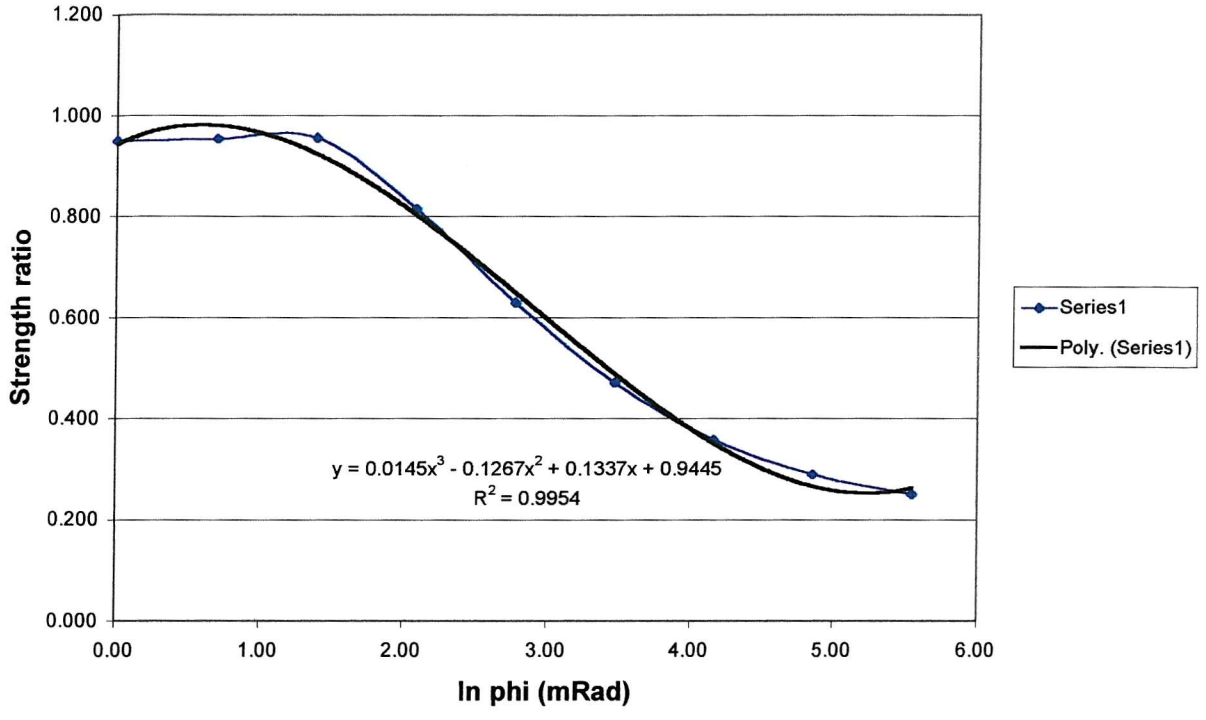

Figure 7.7b Sway Two-Storey Frame – Curve Fitting

The formulae found for each of the three frames are given in Table 7.6 below.

Table 7.6 Sway Frame Results for the Third Order Curve Fit using ln ϕ

Frame No.	Equation of curve	R^2
Frame 1	$Sr = 0.0145(\ln\phi)^3 - 0.1267(\ln\phi)^2 + 0.1337(\ln\phi) + 0.9445$	0.9954
Frame 2	$Sr = 0.0083(\ln\phi)^3 - 0.0698(\ln\phi)^2 - 0.0044(\ln\phi) + 0.9635$	0.9997
Frame 3	$Sr = 0.0106(\ln\phi)^3 - 0.0835(\ln\phi)^2 + 0.0122(\ln\phi) + 0.8504$	0.9973

So far, the curves fit well with the single and two-storey frames. The next section covers the higher structures with five and ten storeys. It will then be possible to see if trends are emerging which make it possible to form equations from these curve fits.

7.2.3 Five- and Ten-Storey Frames

The curve fitting analyses have been repeated for the five- and ten-storey frames. The analyses have been carried out for frames with fixed column base connections, and the graphs plotted are for frame 1. The five- and ten-storey frame analyses also included frame 4, the properties of which can be found in Chapter 6. The results are shown for the sway and non-sway frames.

Figures 7.8 and 7.9 show the curve fits for the analysis of the five-storey non-sway and sway frames.

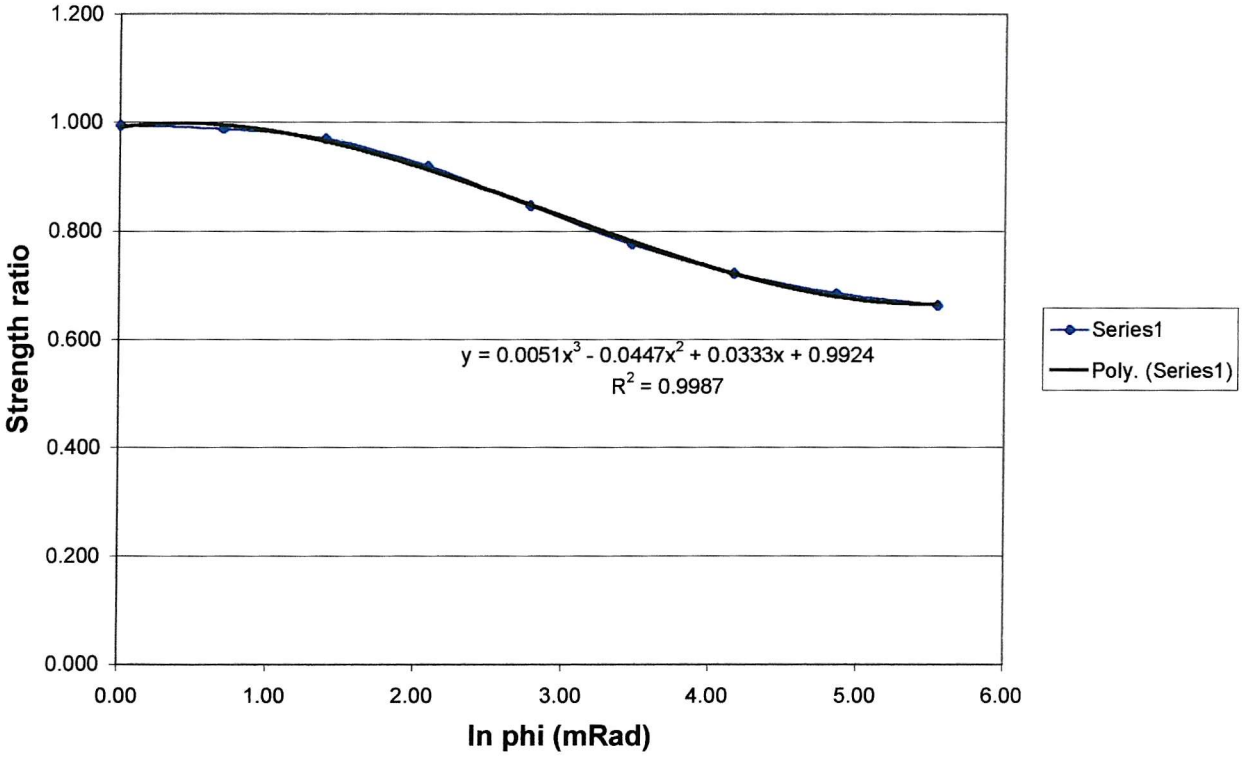

Figure 7.8 Non-Sway Five-Storey Frame – Curve Fitting

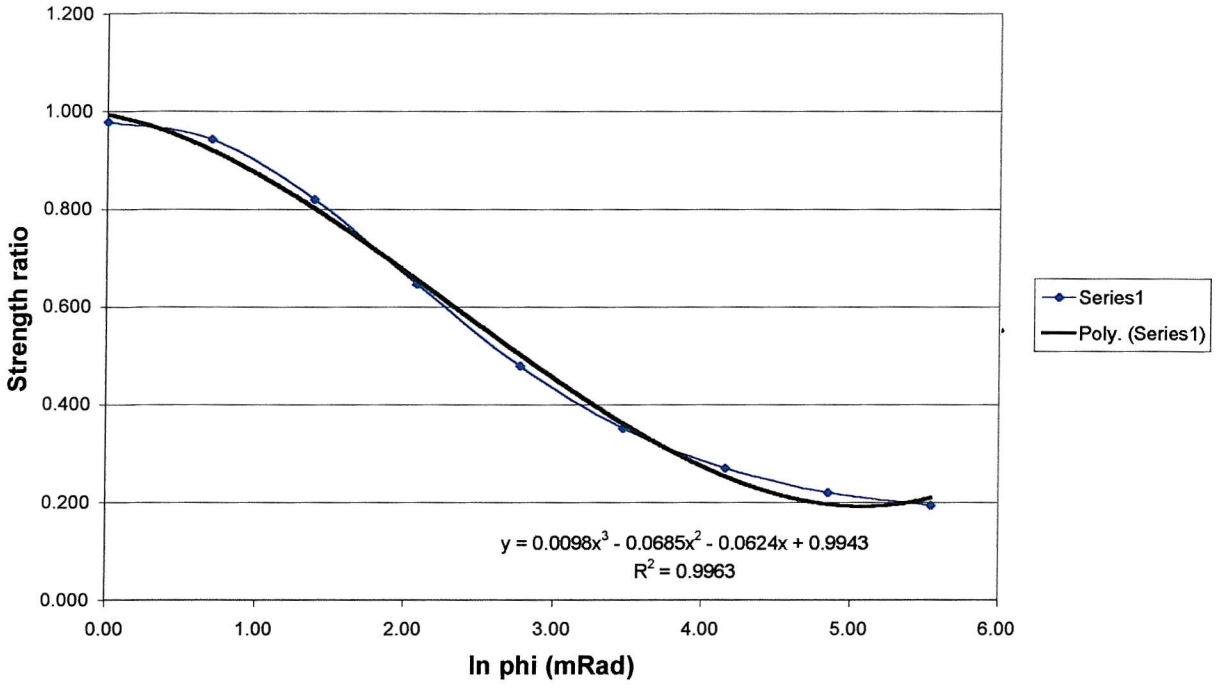

Figure 7.9 Sway Five-Storey Frame – Curve Fitting

The curves are still fitting to the finite element results for the strength ratio well, although for the sway frames the third order curve is starting to not fit as well as it did for the frames with a lower number of storeys. However, it is still giving a good representation of the curve.

Finally the third order curves have been fitted to the strength ratio results for the ten-storey frames. The curves for the non-sway and sway frames, for frame 1 are shown in Figures 7.10 and 7.11.

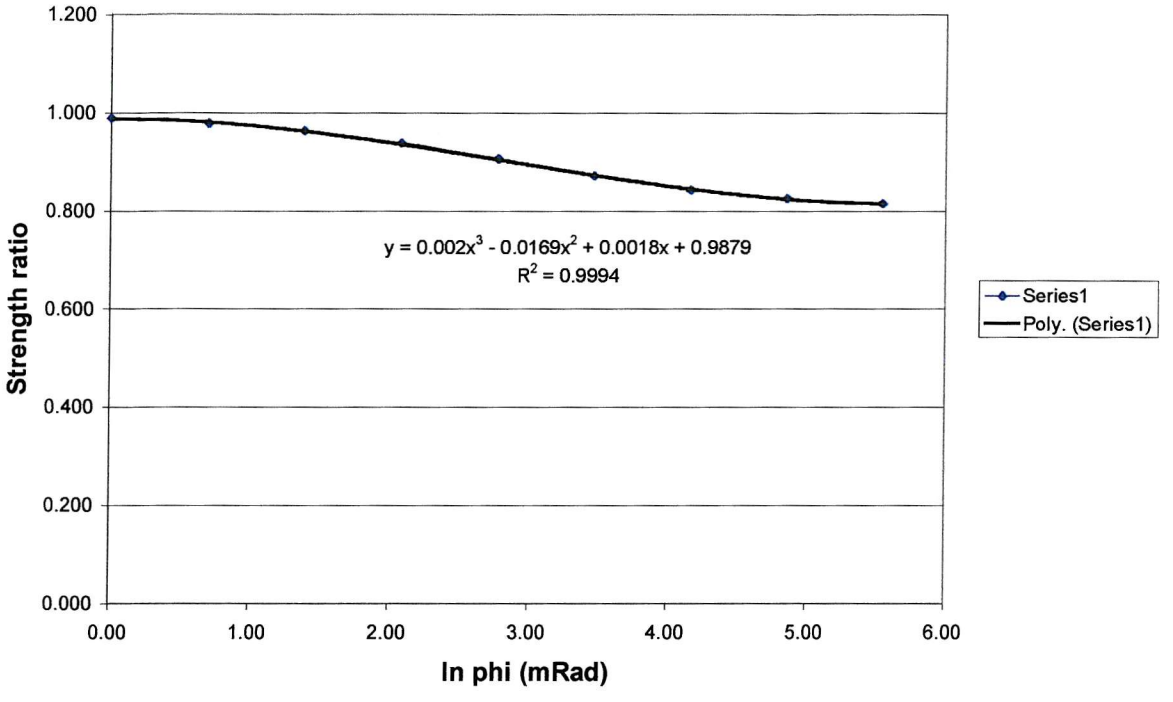

Figure 7.10 Non-Sway Ten-Storey Frame – Curve Fitting

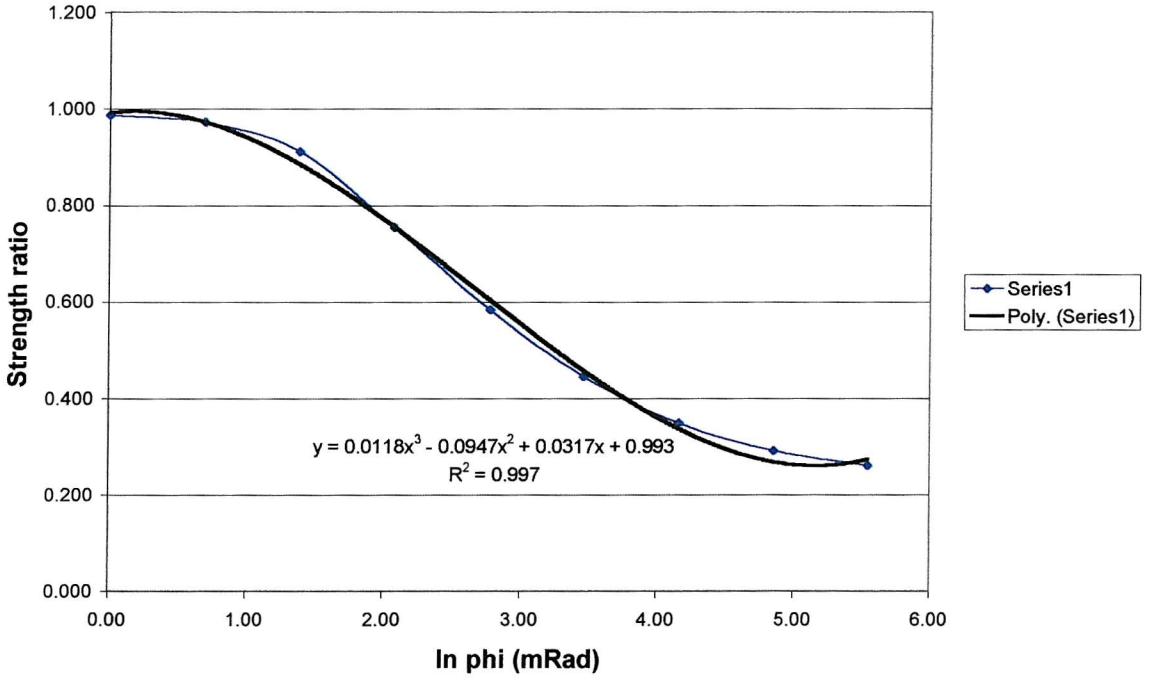

Figure 7.11 Sway Ten-Storey Frame – Curve Fitting

The curves are still giving a good representation of the finite element results, so these curves have been fitted to all the fixed frame results for the five- and ten-storey frames, and the results are shown below. The equations for the third order curves for the five-storey frames are given in Tables 7.7 and 7.8, and the equations for the third order curves for the ten-storey frames are given in Tables 7.9 and 7.10.

Table 7.7 Five-Storey Non-Sway Frame Results for the Third Order Curve Fit using ln ϕ

Frame No.	Equation of curve	R^2
Frame 1	$Sr = 0.0051(\ln\phi)^3 - 0.0447(\ln\phi)^2 + 0.0333x + 0.9924$	0.9987
Frame 2	$Sr = 0.0047(\ln\phi)^3 - 0.0418(\ln\phi)^2 + 0.0101x + 0.973$	0.9996
Frame 3	$Sr = 0.0031(\ln\phi)^3 - 0.0267(\ln\phi)^2 + 0.0078x + 0.9905$	0.9997
Frame 4	$Sr = 0.0064(\ln\phi)^3 - 0.0514(\ln\phi)^2 + 0.0061x + 0.9573$	0.9986

Table 7.8 Five-Storey Sway Frame Results for the Third Order Curve Fit using ln ϕ

Frame No.	Equation of curve	R^2
Frame 1	$Sr = 0.0098(\ln\phi)^3 - 0.0685(\ln\phi)^2 - 0.0624(\ln\phi) + 0.9943$	0.9963
Frame 2	$Sr = 0.0079(\ln\phi)^3 - 0.0584(\ln\phi)^2 - 0.0575(\ln\phi) + 0.9292$	0.9994
Frame 3	$Sr = 0.0058(\ln\phi)^3 - 0.0325(\ln\phi)^2 - 0.1336(\ln\phi) + 0.9109$	0.9986
Frame 4	$Sr = 0.01(\ln\phi)^3 - 0.0703(\ln\phi)^2 - 0.0513(\ln\phi) + 0.9323$	0.9937

Table 7.9 Ten-Storey Non-Sway Frame Results for the Third Order Curve Fit using ln ϕ

Frame No.	Equation of curve	R^2
Frame 1	$Sr = 0.002(\ln\phi)^3 - 0.0169(\ln\phi)^2 + 0.0018(\ln\phi) + 0.9879$	0.9994
Frame 2	$Sr = 0.0031(\ln\phi)^3 - 0.0293(\ln\phi)^2 + 0.014(\ln\phi) + 0.983$	0.9993
Frame 3	$Sr = 0.0013(\ln\phi)^3 - 0.0111(\ln\phi)^2 - 0.0002(\ln\phi) + 0.9915$	0.9995
Frame 4	$Sr = 0.0032(\ln\phi)^3 - 0.0256(\ln\phi)^2 - 0.0074(\ln\phi) + 0.978$	0.9997

Table 7.10 Ten-Storey Sway Frame Results for the Third Order Curve Fit using ln ϕ

Frame No.	Equation of curve	R^2
Frame 1	$Sr = 0.0118(\ln\phi)^3 - 0.0947(\ln\phi)^2 + 0.0317(\ln\phi) + 0.993$	0.997
Frame 2	$Sr = 0.008(\ln\phi)^3 - 0.0603(\ln\phi)^2 - 0.0465(\ln\phi) + 0.9352$	0.9994
Frame 3	$Sr = 0.007(\ln\phi)^3 - 0.0457(\ln\phi)^2 - 0.098(\ln\phi) + 0.9674$	0.9988
Frame 4	$Sr = 0.0061(\ln\phi)^3 - 0.034(\ln\phi)^2 - 0.1321(\ln\phi) + 0.9292$	0.9982

Although it has been shown that all the results follow the same trends, it would be very hard to form any actual design equations based on these results, especially with so few frames with differing beam and column sections analysed. To improve matters, many more five-storey frames were analysed, with different beam and column section properties.

7.2.4 Further Five-Storey Frame Analysis

The new frames were modelled using exactly the same methods as those described in Chapter 4 for the previous analyses. A selection of frames were made up by keeping the beam sections constant and changing the column constants, and then by keeping the column sections constant and changing the beam sections. The analyses were conducted both with the whole frame loaded, with no lateral restraint, giving a sway frame, and then with only the sway load applied, to rule out the P-Δ effect. The frames were also analysed with the lateral restraints giving a non-sway frame - in this case all the loading was applied.

Table 7.11 lists the beam sections that were used for the analyses. For these analyses the column section was kept constant, using UC 254x254x89kg/m.

Table 7.11 Beam Sections Used for the Five-Storey Analyses

	Height (m)	A(-50) $x10^{-3}$ (m^2)	A(-30) $x10^{-3}$ (m^2)	A(0) $x10^{-3}$ (m^2)	M_{pl} $x10^3$ Nm	I_{xx} $x10^{-3}$ (m^4)
Beam01 UB356x171x57	0.359	32.6	4.49	1.85	277.8	0.161
Beam02 UB406x178x74	0.413	40.9	6.21	2.67	412.5	0.273
Beam03 UB457x191x74	0.457	40.6	6.34	2.56	456.5	0.334
Beam04 UB457x152x82	0.465	41.0	7.53	3.10	495	0.362
Beam05 UB457x191x89	0.463	48.4	7.61	3.18	553	0.410
Beam06 UB533x210x92	0.533	49.3	7.88	3.66	651.8	0.554
Beam07 UB533x210x109	0.540	57.9	9.28	4.37	775.5	0.667
Beam08 UB610x229x125	0.612	67.2	10.2	5.66	1012	0.986
Beam09 UB686x254x125	0.678	64.4	10.7	5.98	1100	1.180
Beam10 UB686x254x140	0.684	73.8	11.6	6.61	1254	1.360

Table 7.12 shows the column section properties that were used for the analyses. For these frames the beam sections were kept constant, using UB 457x191x89kg/m.

Table 7.12 Column Sections Used for the Five-Storey Analyses

	Height (m)	A(-50) $x10^{-3}$ (m^2)	A(-30) $x10^{-3}$ (m^2)	A(0) $x10^{-3}$ (m^2)	M_{pl} $x10^3$ Nm	I_{xx} $x10^{-3}$ (m^4)
Column01 UC203x203x46	0.2032	29.7	3.38	0.712	136.7	0.0452
Column02 UC203x203x86	0.2223	47.4	8.33	0.868	269.2	0.0946
Column03 UC254x254x89	0.2604	55.6	7.07	0.871	338	0.143
Column04 305x305x97	0.3078	63.5	6.92	1.23	437	0.222
Column05 UC254x254x167	0.2891	85.0	17.7	1.17	666.6	0.299
Column06 UC356x368x153	0.362	99.9	11.1	1.95	814	0.485
Column07 UC305x305x198	0.3399	109	19.1	1.85	946	0.508
Column08 UC356x406x235	0.381	141	20.0	2.69	1290	0.791
Column09 UC305x305x283	0.3653	139	30.0	4.31	1403	0.788

As described in earlier chapters, these models were solved until a set deflection limit was reached. This gives the loading on the frame to reach that deflection limit. Dividing this value by the loading reached for the fully fixed frame gives the strength ratio. To reduce the large amount of data that these analyses would give, and the large amount of computer time it would take to solve so many models, only the cases with fully fixed column bases have been considered for these analyses.

The first results to be shown here are for the models with constant column sections, and changing beam sections.

Figure 7.12 plots the strength ratio for each value of phi, against the second moment of area of each beam section, for the non-sway frames.

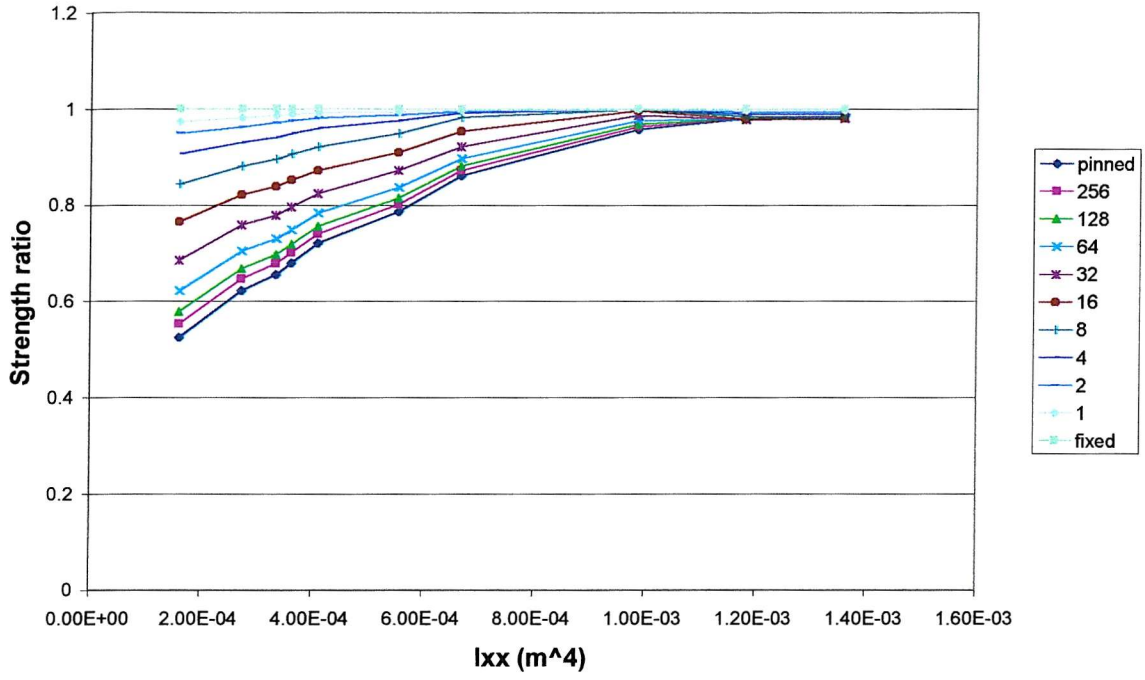

Figure 7.12 Non-Sway Frames Strength Ratio for Different Beam Sections

The strength ratio increases as the second moment of area of the beams increases. This is as expected, as it is the beam deflection limit upon which the models are dependent. The strength ratio is also greater for the stiffer connections - this has already been shown to be true in the previous chapters. The results obtained from the finite element models have not produced perfectly smooth curves due to rounding off errors in the solving routines. These errors will be compounded as the solving routine goes through many iterations for each load step.

Figure 7.13 plots the strength ratio results for the sway frame, with all the loading applied to the frame. These results will therefore be affected by the P-Δ effect. The strength ratio results for the frame with only the sway loading applied are shown in Figure 7.14.

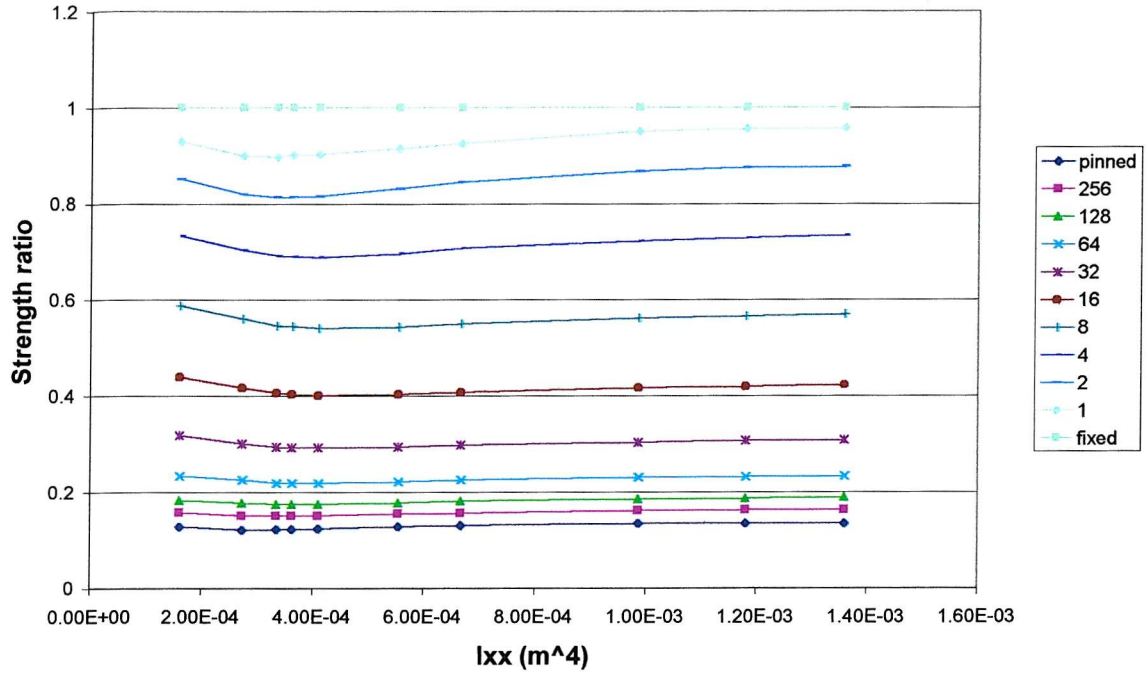

Figure 7.13 Sway Frames Strength Ratio for Different Beam Sections with Full Loading

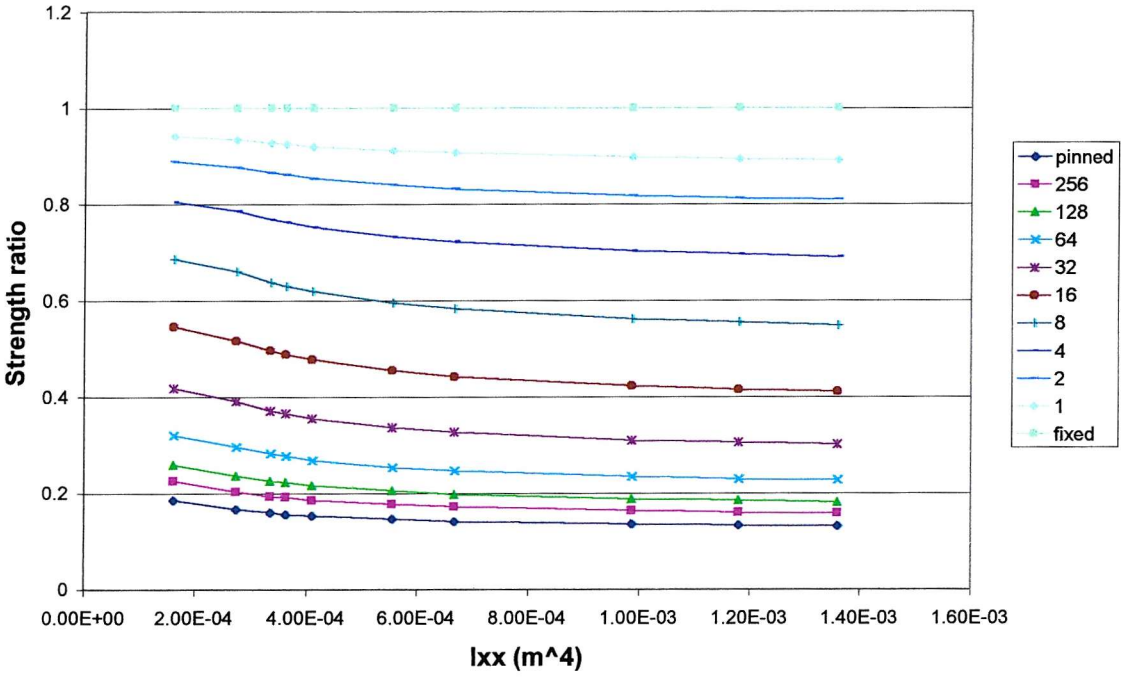

Figure 7.14 Sway Frames Strength Ratio for Different Beam Sections with Sway Loading Only

The load factor in the graph for the sway loading only (Figure 7.14) shows that the load factor decreases as the second moment of area for the beams increases. However, the loading reached by the frame does increase with an increase in the beam section. Although only the sway loading is applied to these frames, the beam sections still affect the loading reached by the frame. This is due to the bigger beam sections forming a stiffer connection with the column than the smaller beam sections. Also, the greater stiffness of the larger beam sections will add to the overall stiffness of the frames, as they can take larger moments that are distributed to them through the semi-rigid connections.

The graphs shown above for the sway frames are very different to each other. This is due to the second order effects in the frame with all the loading applied. The curves that this graph produces are far more complex than those for the sway only loading. Using this for practical frame design could be complex.

The next graphs show the results for the frames with changing column sections, and a constant beam section.

The graph in Figure 7.15 shows the strength ratio chart for the non-sway frames. It plots the strength ratio against the second moment of area for the column section.

The sway frame results are shown in Figures 7.16 and 7.17. Figure 7.16 shows the results for the frames with the full loading, whereas Figure 7.17 shows only the frames with the sway loading applied.

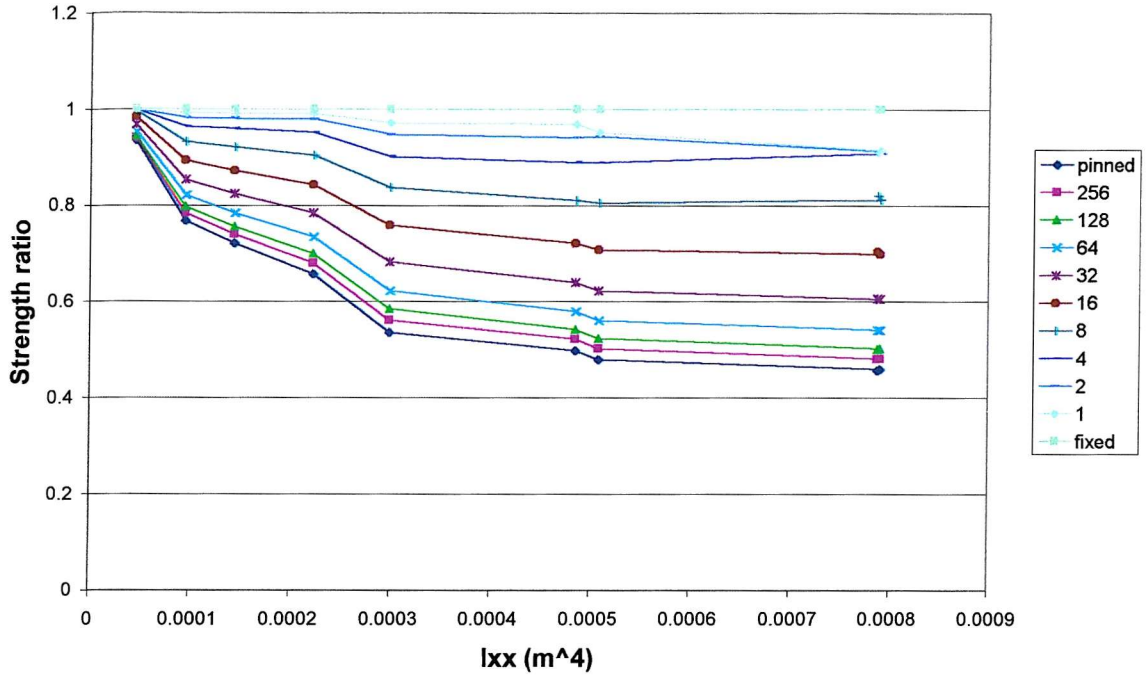

Figure 7.15 Non-Sway Frames Strength Ratio for Different Column Sections

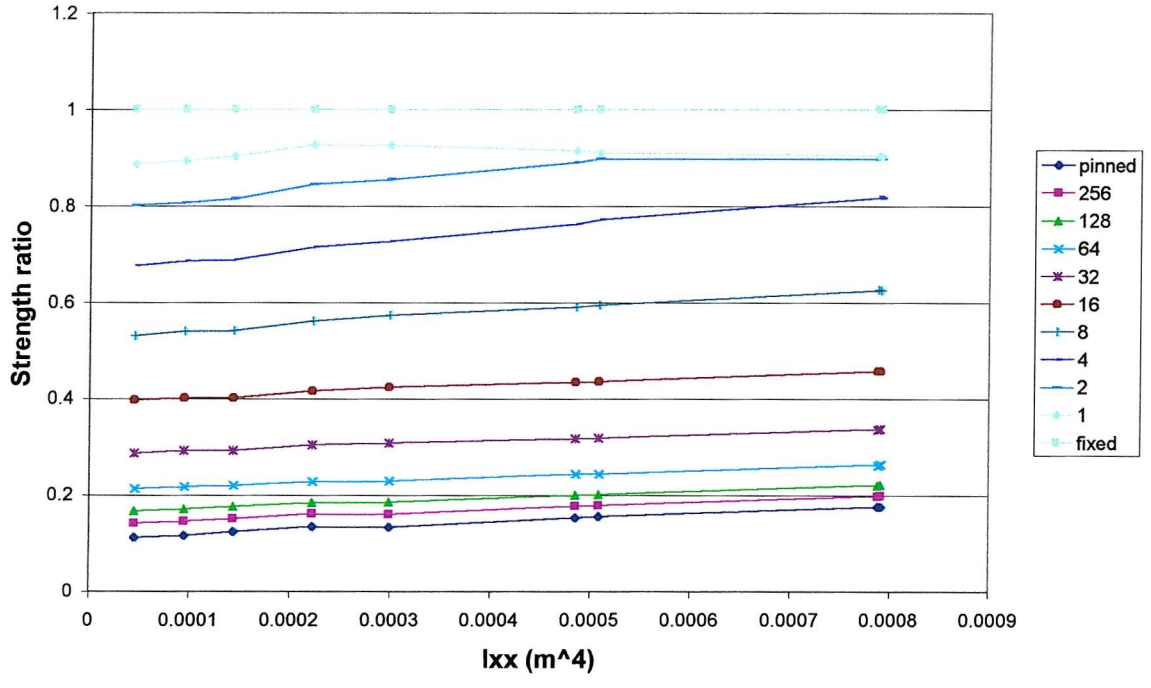

Figure 7.16 Sway Frames Strength Ratio for Different Column Sections with Full Loading

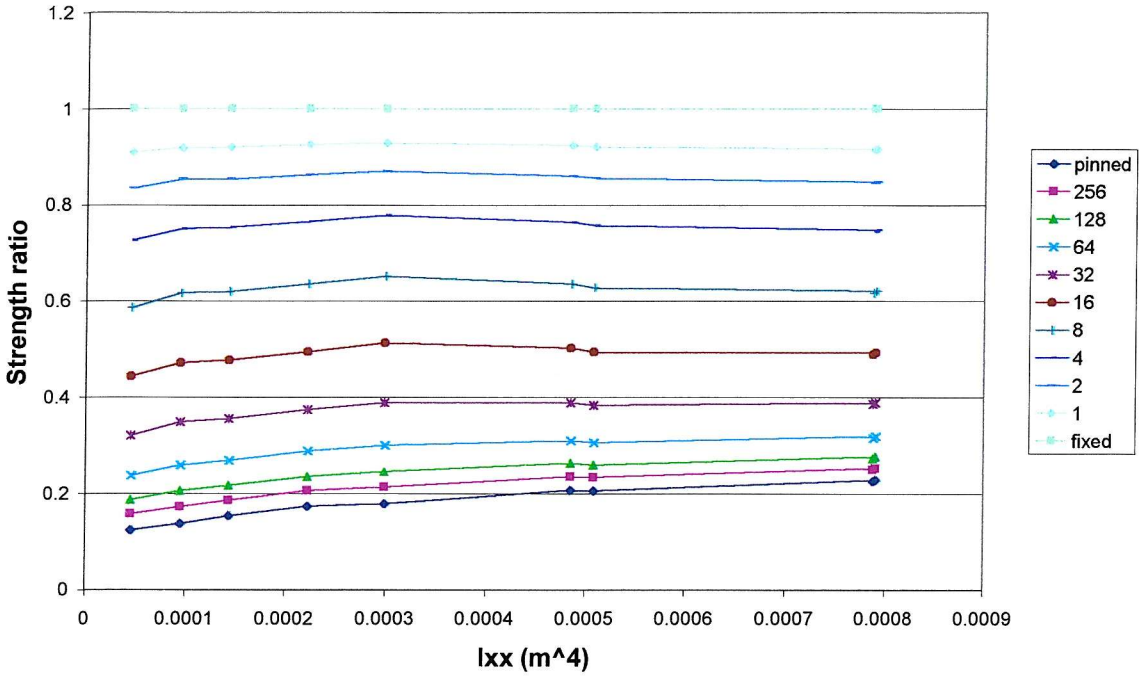

Figure 7.17 Sway Frames Strength Ratio for Different Column Sections with Sway Loading Only

The graph of the non-sway frame results shows that the strength ratio decreases with an increase in section size. However, the load reached by the frame before the deflection limit is reached does increase with column section size, as is expected. The decrease in strength ratio with increasing column section size is due to a far greater increase in load being carried by the frames with fixed connections and large column sections, over the frames with fixed connections and small column sections. It is these fixed frames that are used to calculate the strength ratio for the semi-rigid frames.

As for the previous analyses, when the column section remained constant and the beam sections were changed, the plots of the sway results show that the vertical loading has a large effect on the sway strength ratio. This is again due to the second order effects, showing how this complicates the analyses for the taller structures.

The next analyses used the same results as those discussed above. However, this time the beam section properties have been divided by those for the column to give a

dimensionless value, and this has been plotted with the strength ratio. The graphs from these analyses are shown below.

Figure 7.18 shows the strength ratio results for the non-sway frames when plotted against the second moment of area for the beam sections over the second moment of area for the column sections.

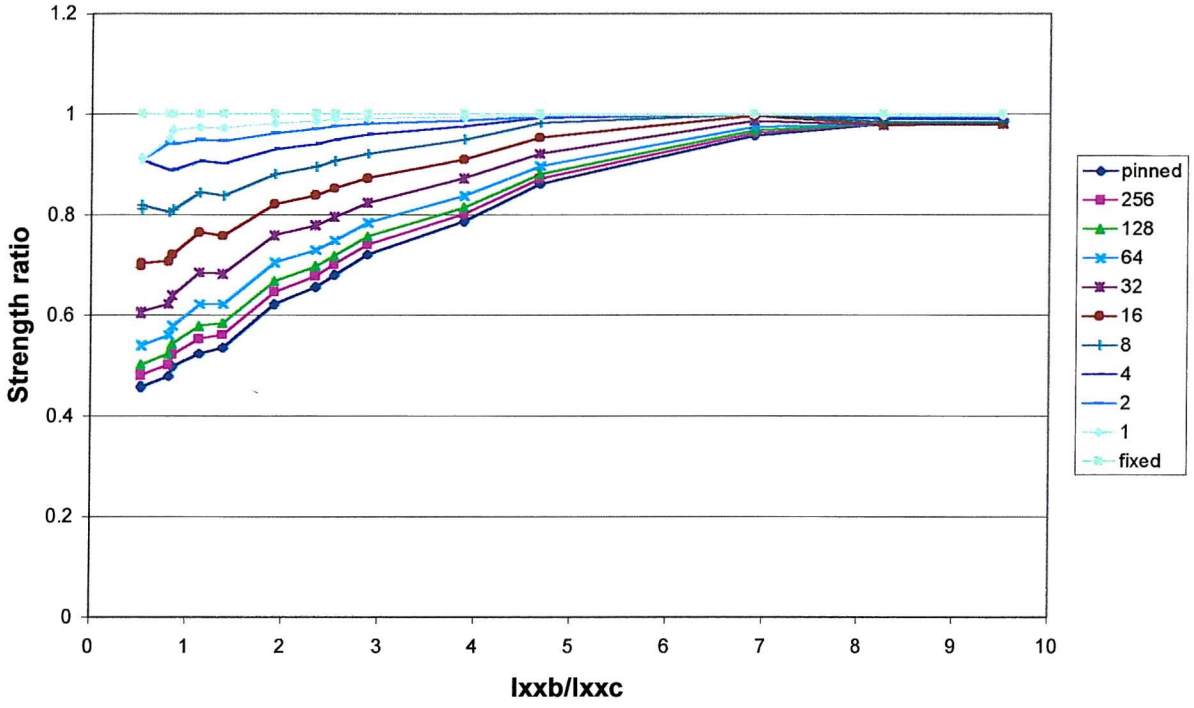

Figure 7.18 Strength Ratio for Non-Sway Frames Against I_{xx} Beam/I_{xx} Column

The same theory can be used to produce a plot of results where the plastic moment is used instead of the second moment of area. This is shown in Figure 7.19 below.

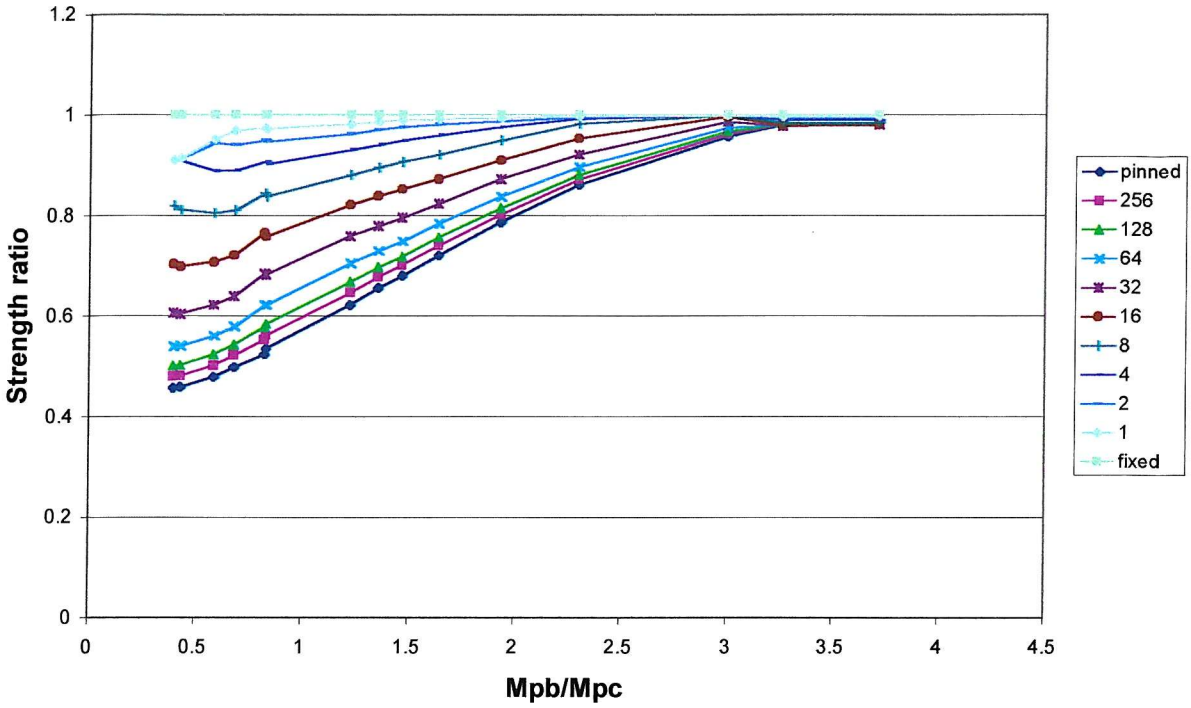

Figure 7.19 Strength Ratio for Non-Sway Frames Against I_{xx} Beam/I_{xx} Column

Both of the above charts form similarly shaped curves. The strength ratio is increasing as the beam/column property increases. The strength ratio also increases with the connection stiffness, as already stated. It is expected for the non-sway frames that the strength ratio would increase as the beam/column property increases, as it has already been shown that the beam section has a greater influence over the load to reach the deflection limit, than the column section does.

The same idea has been applied to the sway frames, both for the frames with full loading, and for those where just the sway loading is applied, with no vertical loading.

Figure 7.20 shows the results for the sway frame with full loading, with the second moment of area for the beam over the second moment of area for the column.

Figure 7.21 shows the results for the frame with sway loading only, and no vertical loading applied. Again the second moments of area are used for the horizontal axis.

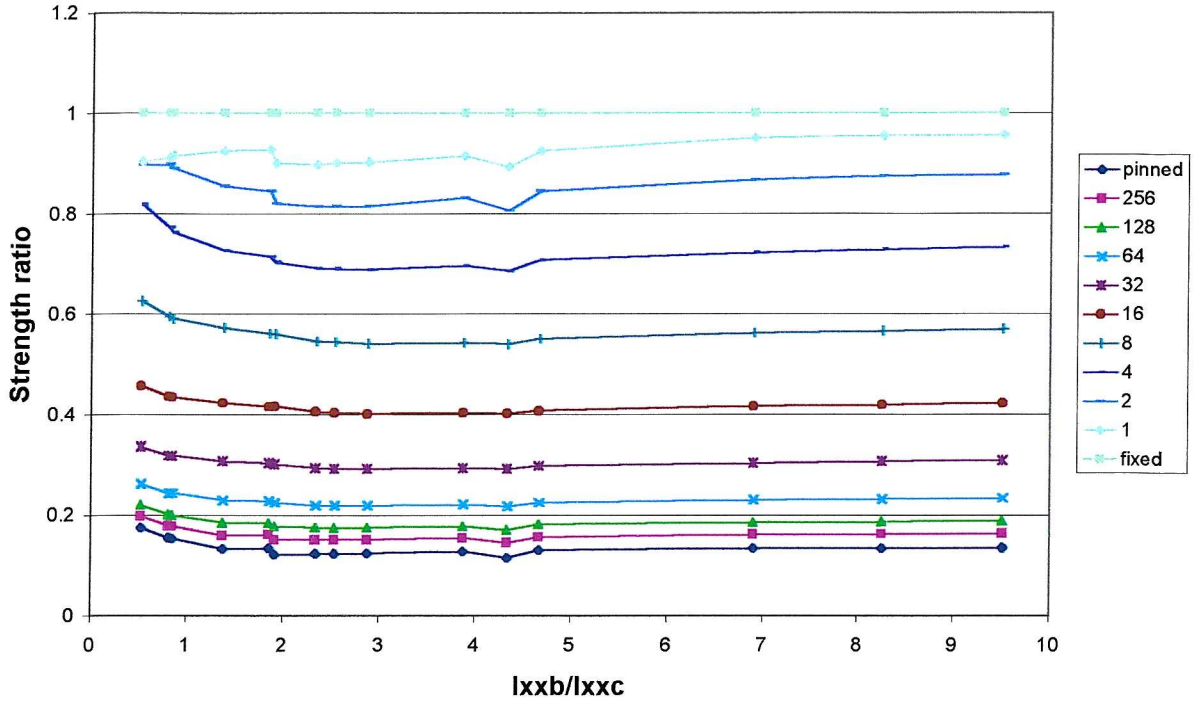

Figure 7.20 Strength Ratio for Sway Frames With Full Loading Against I_{xx} Beam/I_{xx} Column

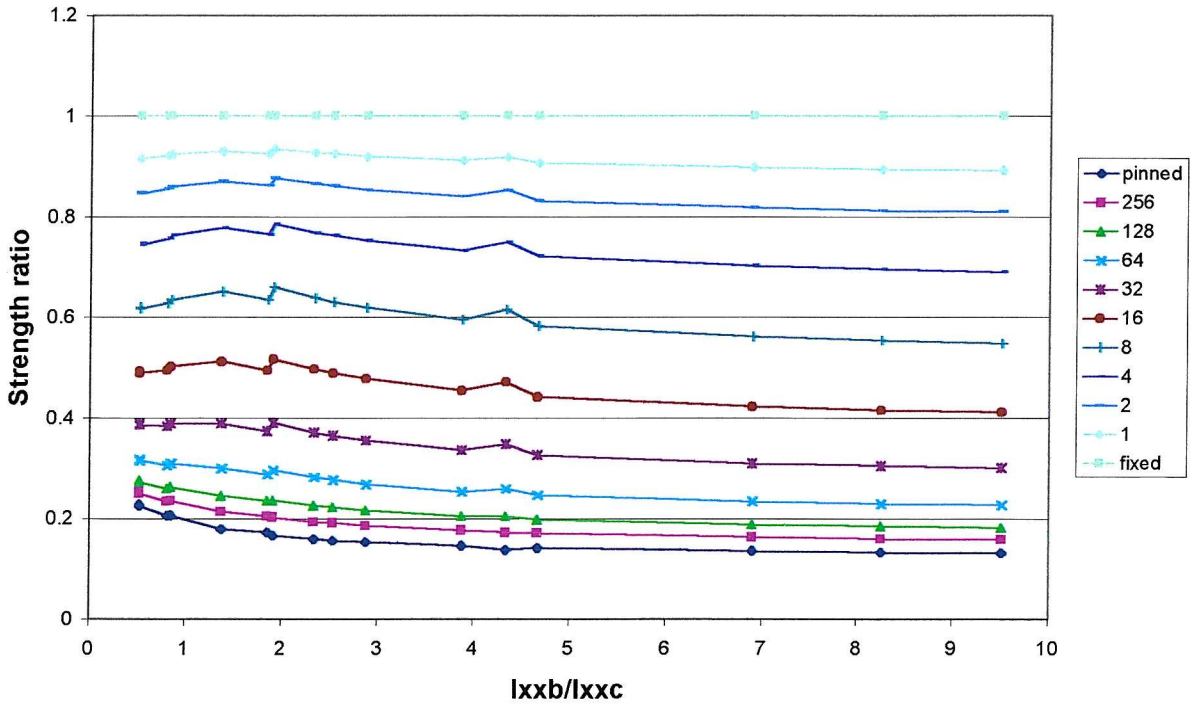

Figure 7.21 Strength Ratio for Sway Frames With Sway Loading Only Against I_{xx} Beam/I_{xx} Column

As before, the charts using the values of plastic moment for the beam and column instead of second moment of area, give graphs with similar curve patterns to those which use second moment of area.

The charts for the sway frames differ greatly from those for the non-sway frames, as the curves are much flatter in those for the sway frames. This is due to the column having a greater influence on the load reached by the frame, and hence the resulting load factor.

The curves for the frames with the full loading pattern applied are more horizontal than those for the frames with only sway loading applied.

In Chapter 6, the strength ratio was compared for frames with constant beam and column sections, but increasing numbers of storeys. For the sway frames, with only the sway loading applied, it was found that the relationship was linear. This next section takes this analysis a step further.

Curves have been fitted to the results from the analysis to give the equations of the lines, an example of which is shown in Figure 7.22 below. Only one of the lines has been shown on this graph for the sake of clarity. The example in the graph is of a chart with fixed base connections, and using frame 1, the section properties for which are given in Chapter 5 of this report.

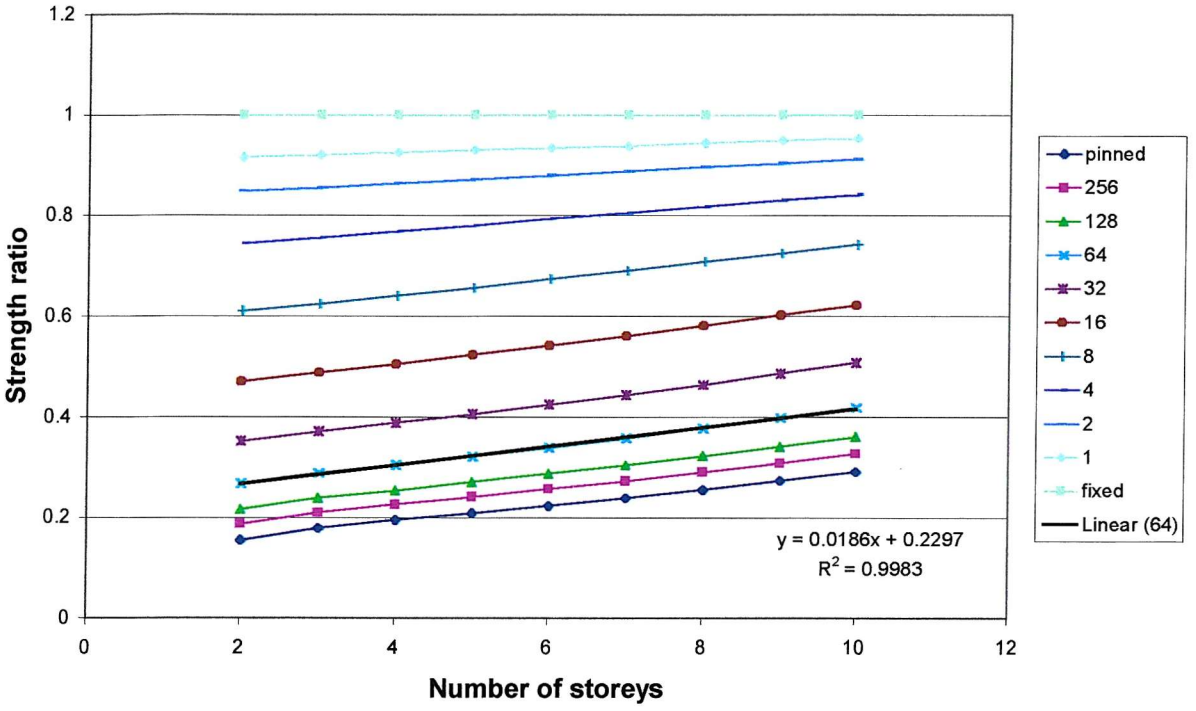

Figure 7.22 Plot of Strength Ratio Against Number of Storeys for a Non-Sway Frame

The linear relationship was found for each of the four sway frames, with each different beam-to-column connection. This gave a set of linear equations. The next step was to plot these linear equations to see if there were any relationships between them. For this the gradient of the line, and the y-axis intercept were separated and plotted separately against the beam-to-column ultimate rotation, phi.

This gave eight separate curves, one for the gradient, and intercept for each frame analysed.

The results for the linear curves for frame 1 are given in Table 7.13 below.

Table 7.13 Linear Curves for Frame 1, Sway Frame, With Sway Loading Only Applied

Beam-to-column phi	Gradient m	y-axis Intercept c
pinned	0.0163	0.1265
256	0.0169	0.1557
128	0.0176	0.1823
64	0.0186	0.2297
32	0.0193	0.3108
16	0.0190	0.4294
8	0.0167	0.5750
4	0.0124	0.7190
2	0.0080	0.8323
1	0.0047	0.9069
fixed	0	1

Plotting the gradient of these lines gives the graph in Figure 7.23 below.

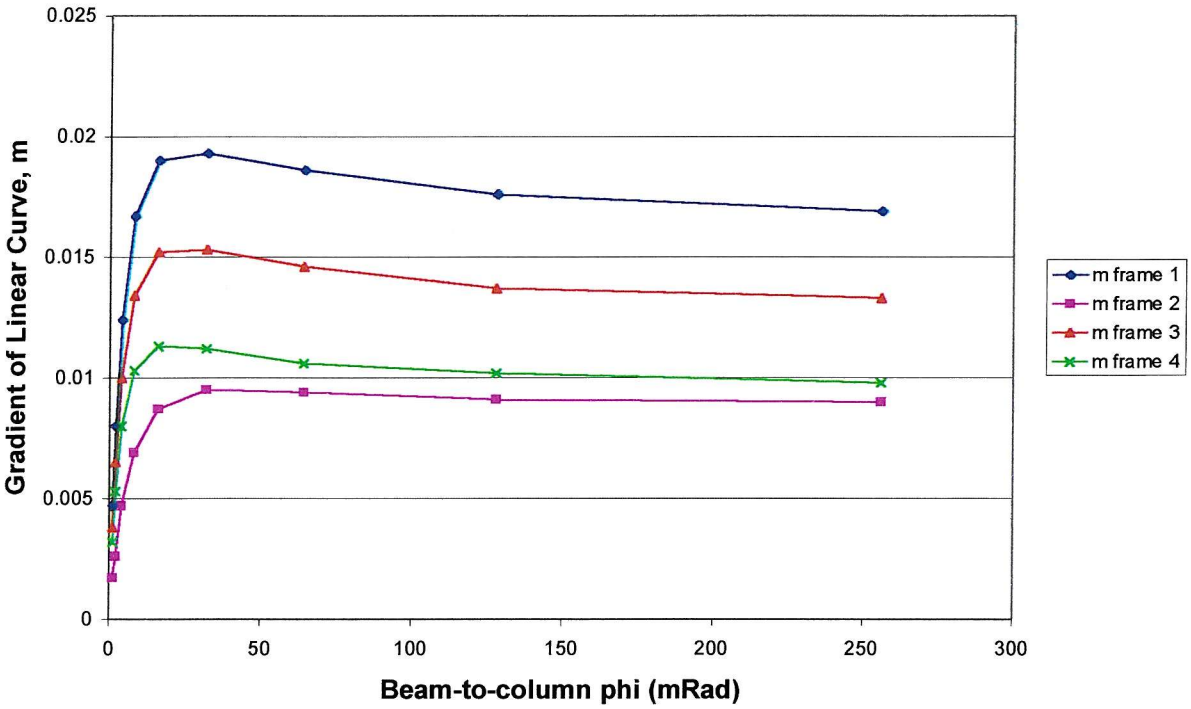

Figure 7.23 Plots of the Gradient of the Curve Fits Against Phi

The graph shows that the gradients for the curves increase greatly as the beam-to-column ultimate rotation increases, up to a value of 16mRad. After this point the curves flatten, and then begin to fall as the connections become more flexible. This shows the change in gradient better than Figure 7.22, as the curves look much more parallel in that graph. The gradient for the fully-fixed case is horizontal, by definition, and then the gradients increase as the beam-to-column connections become more flexible. For the most flexible connections, where phi is greater than 32mRad, the curves are almost parallel in Figure 7.22, and this is shown in Figure 7.23.

Figure 7.24 below shows the relationship of the y-axis intercept against beam-to-column connection ultimate rotation, phi.

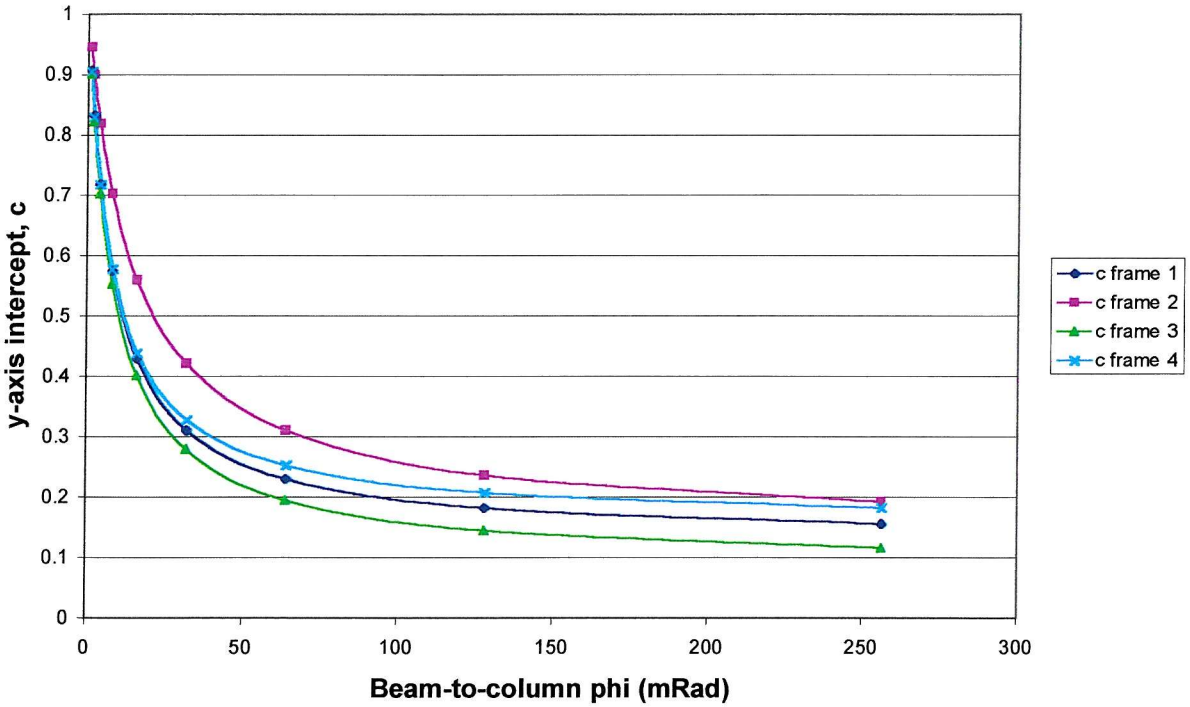

Figure 7.24 Plots of the Y-Axis intercept of the Curve Fits Against Phi

The curves in Figure 7.24 are much more simple than those for the gradient. The intercept decreases as the beam-to-column connection becomes more flexible. There is no stage at which the curve appears to change form as it did in the graph for gradient.

It does not seem possible to form any meaningful formulae from the above graphs to aid the design of semi-rigid frames. However, the graphs presented here do show some of the effects that these connections have on frameworks, and how the properties of the sections used, and the number of storeys of a frame affect the strength ratio of the framework.

7.3 Dimensional Analysis

The next analysis method tried was dimensional analysis. This is a powerful tool which has been used and refined by engineers for many years. The following sections have used the indicial method to find dimensionless groups.

The variables used in the dimensional analysis could include length of the beams and columns, second moment of area of the sections, plastic moment of the columns and ultimate beam-to-column rotation.

7.3.1 Theory of Dimensional Analysis

It is possible to reduce any physical quantity into three fundamental dimensions, mass, length and time.

$$J = f[M, L, T]$$

If the magnitude of J is compared for two similar systems, then

$$\frac{J''}{J'} = \frac{f[M,L,T]''}{f[M,L,T]'} = \lambda_J$$

This ratio must be dimensionless, which is true if the function is in the form of a product, and therefore

$$J = K[M^a, L^b, T^c]$$

where K is numeric and a, b, and c are indices whose magnitudes have to be determined. Dimensionless equations are completely general, and are frequently the basis for the representation of data.

For the dimensional analysis for this work the following variables were used:

Variable	Dimensions
E	$ML^{-1}T^{-2}$
I	L^4
Mp	ML^2T^{-2}
L	L
ϕ	*Dimensionless

As phi is dimensionless it means that it can occur anywhere in the final dimensionless group, and will therefore be omitted from the calculations to find the dimensionless groups.

Combining these terms to form a dimensionless group proved complicated, as there are many length terms involved. Also, it was further complicated by the fact that any other terms that could have been involved, were also all forms of length. The first attempt at forming a dimensionless group is shown below.

An indicial is applied to each of the variables, and shows that the final product must equal a dimensionless group.

$$\Pi = L^a Mp^b E^c I_{xx} = M^0 L^0 T^0$$

Then the dimensions for the variables are substituted into the equation.

$$\Pi = L^a (ML^2T^{-2})^b (ML^{-1}T^{-2})^c L^4 = M^0 L^0 T^0$$

The indices are then equated for each of the three dimensions.

M	$b + c = 0$
T	$-2b - 2c = 0$
L	$a + 2b - c + 4 = 0$

It is not possible to solve these equations, as the top two are identical. Therefore a different technique had to be applied.

As the problem is caused by there being too many terms involving length, for the next attempt the second moment of area was combined with the Young's modulus to give a stiffness. This gave the following list of variables and dimensions:

Variable	Dimensions
EI	ML^3T^{-2}
Mp	ML^2T^{-2}
L	L

Putting the terms equal to a dimensionless group gives:

$$\Pi = L^a Mp^b EI_{xx} = M^0 L^0 T^0$$

Then substituting in the dimensions:

$$\Pi = L^a (ML^2T^{-2})^b ML^3T^{-2} = M^0 L^0 T^0$$

Equating the variables for each of the three dimensions gives:

M	$b + 1 = 0$
L	$a + 2b + 3 = 0$
T	$-2b - 2 = 0$

Giving:

b = -1

a = -1

This gives:

$$\frac{EI}{MpL}$$

This dimensionless group was then applied to the finite element results. This was done by multiplying the value of Phi by the dimensionless group, to give a modified phi value. For the column base connections the values for the section properties for the columns were used in the dimensionless group, and for the beam-to-column connections the values for the beam properties were used in the dimensionless group to give the modified phi values.

This has been carried out for the five-storey sway frames, and the results are shown below for the frames with fixed column bases.

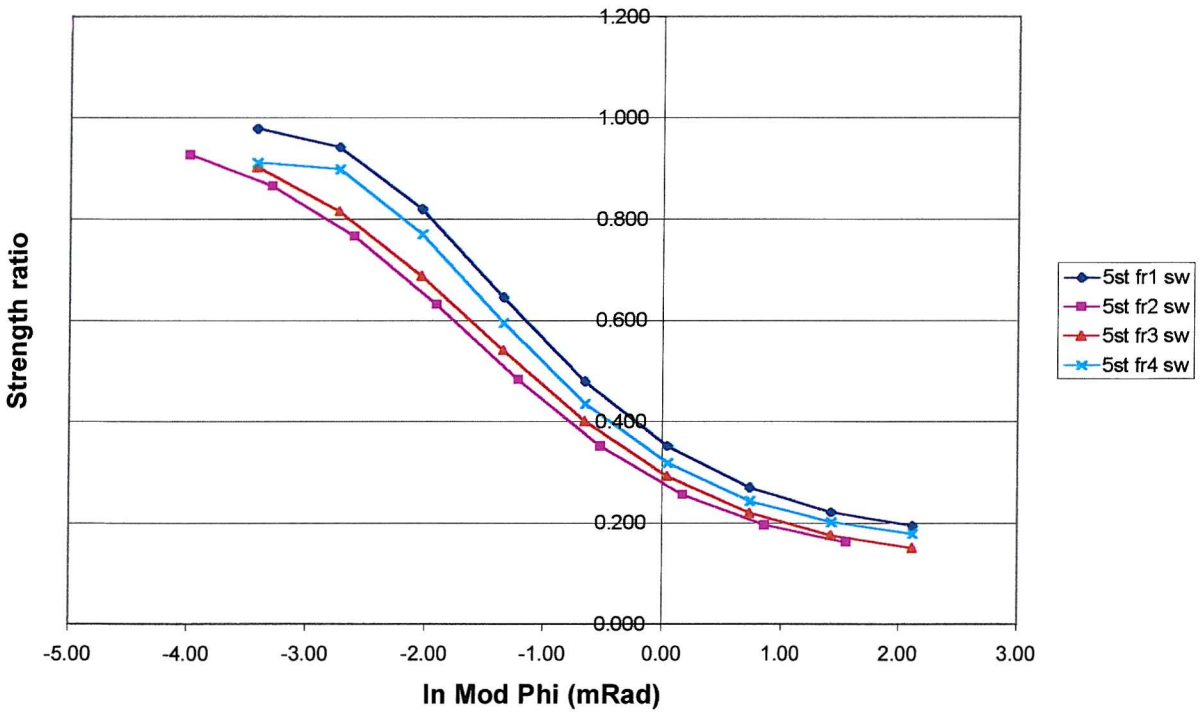

Figure 7.25 Sway Five-Storey Frame, Fixed Base – Mod Phi Curve Fit

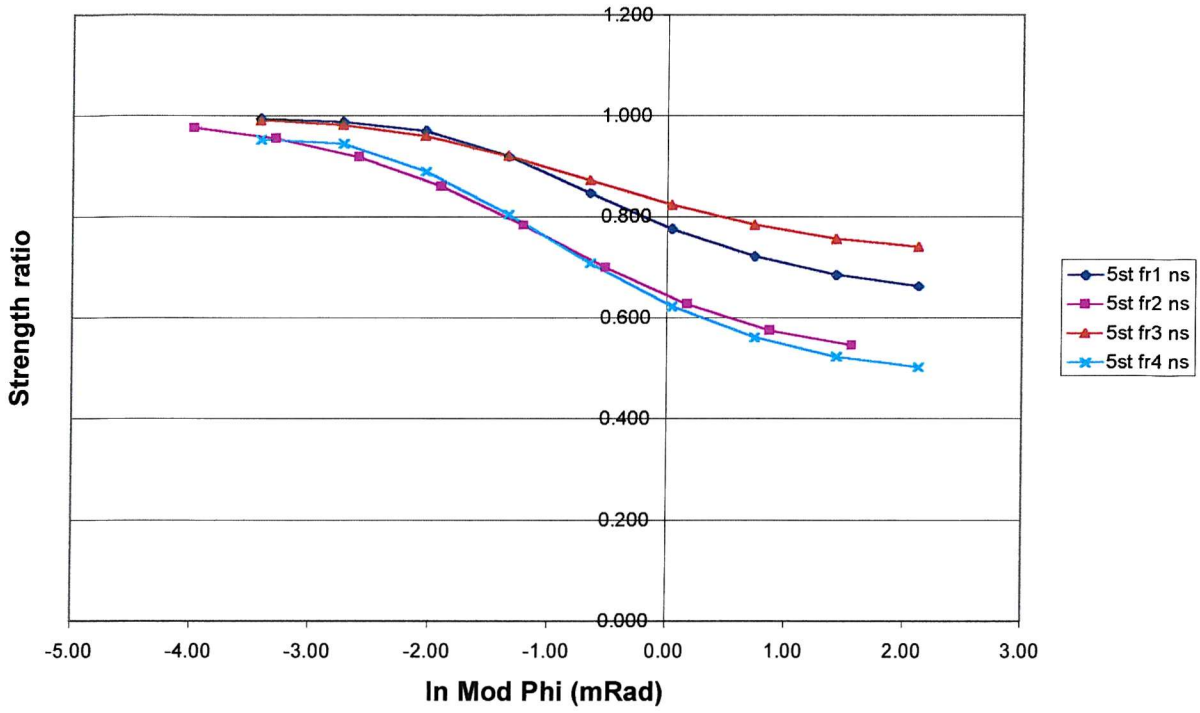

Figure 7.26 Non-Sway Five-Storey Frame, Fixed Base – Mod Phi Curve Fit

The graphs in Figures 7.25 and 7.26 show that the curves still follow the same trends as they did previously, which would be expected as the values of Phi have only been transformed by a constant value. However, as this value is different for each of the frames, the curves have changed in relation to each other. The curves are not similar enough to one another to make a general equation for these results.

The same analysis was conducted with changing column base ultimate rotation, and keeping the beam-to-column connections fixed. The results for the sway frames for these analyses are plotted in Figure 7.27.

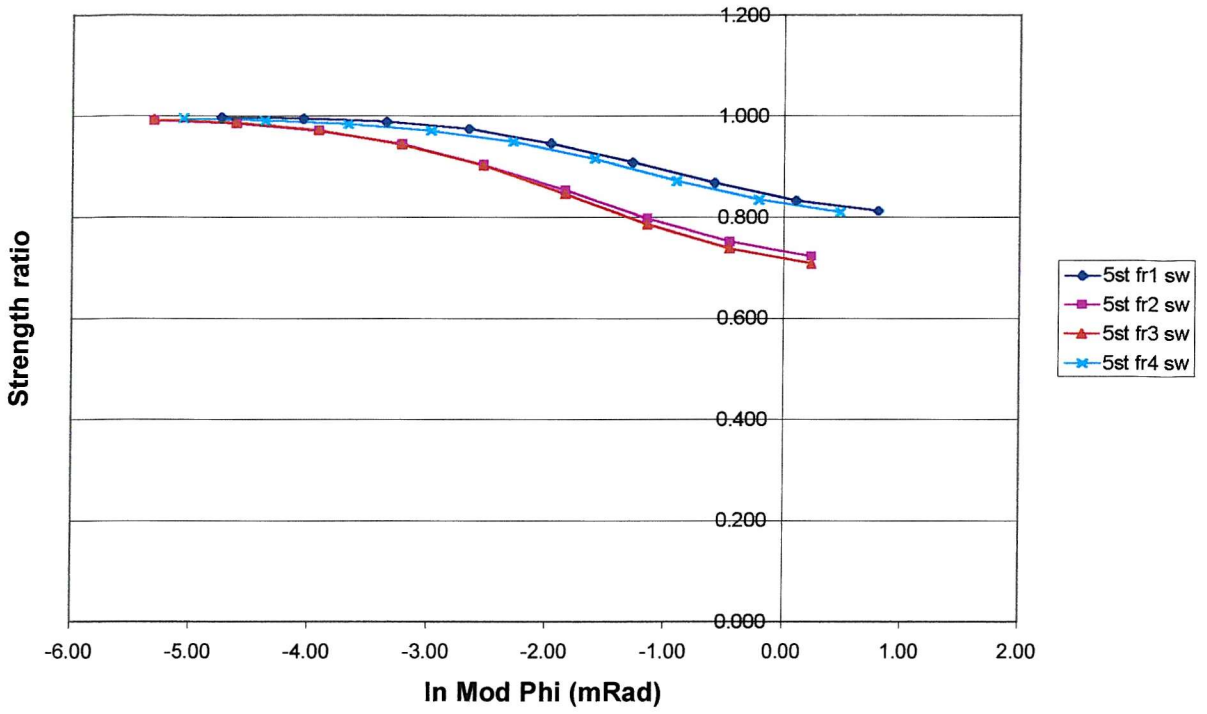

Figure 7.27 Sway Five-Storey Frame, Fixed Beam-to-Column Connections – Mod Phi Curve Fit

This graph again shows that the curves have kept the same form as before. The results in this case are much closer to each other. Frames 1 and 4 are very similar, as are frames 2 and 3. However, there is a large difference between these two sets of curves that would still make it implausible to form a general equation. Any changes that were made to one set of results to move them closer to the others, would have to be made to all the results, therefore moving them away.

7.4 Summary

The work in this chapter has shown that different methods can be used to analyse the results from the finite element models. Curve fitting has successfully shown a relationship for the strength ratio and the beam-to-column connections. This relationship was found to be a third order logarithmic curve. A dimensionless group was then found, but applying this to the finite element results did not result in any general equations for the frames that had been modelled.

Chapter 8

Conclusions and Further Work

8.1 Introduction

The previous chapters have reported an experiment on a building during the construction stages and later loading of the frame; this was used to verify finite element models to allow the analysis of frames with semi-rigid connections. The finite element models were then developed beyond the modelling of the actual structure, to allow for analysis of multi-storey sway and non-sway frames. Several beam-to-column sections were used to show how these affect the frame. A range of beam-to-column connection stiffnesses, and column base connection stiffnesses are used to see how these affect the strength and deflections of the frame. The connection stiffnesses were chosen to represent a range from pinned to fully fixed. The results show that this spread gives a good representation between these two points, with the results for the most flexible connections being close to those for the pinned connections, and the results for the most rigid connections being close to those for the fully fixed connections. The literature review at the beginning of the thesis shows some values of connection stiffness that were found by other researchers from their experimentation. These fit in well with those chosen for this research, although the stiffest values used here may not be found in actual structures. Finally, the results from the finite element models were analysed

to show how the beam-to-column connections, the column base connections, the sections used for the beams and columns, and the number of storeys for the multi-storey frames, affect the behaviour of the frames. Various trends have been found, and reported on. This chapter summarises the findings, and gives recommendations for further work that it is felt will further the knowledge, and widespread use of semi-rigid connections.

8.2 Conclusions of the Research and Discussion on Semi-Rigid Connections

The experiment that made up the first part of this research went very well, especially considering the harsh conditions on the building site. The information gained from the experiment was very useful in validating the initial finite element models. The models were compared to those from the building site, and the results between the two were found to be consistent. The finite element models were then expanded to allow for different sections, multi-storey frames, and sway behaviour.

The elastic modelling showed that the beam-to-column connection stiffness could drastically reduce the deflections of the beams. This was found to be especially true when pinned connections were changed for connections with a low stiffness value. As the stiffness of the beam-to-column connections increased, it was found that the effect of decreasing beam deflections became less. The same trend was found to be true when the column base connection stiffness was increased, with the most impact being found with increases in the low stiffness range. As the column base became stiffer, increasing the stiffness had an ever-decreasing effect. This, however, was only true for the sway frames - it was found that the column base connection stiffness had only a very small influence on the non-sway frames. The beam-to-column stiffness also decreased the bending moments experienced in the mid-span of the beams. However, this also caused an increase in moment at the beam ends, and in the supporting columns. So if the connection stiffnesses were used in design, the columns would have to undergo careful design to make sure they could carry both the axial loads and the extra bending moments. As discussed in the literature review, the connections in use do behave semi-rigidly, so there could be higher bending moments in the supporting columns than expected at the moment.

Non-linear models were developed, that allowed for material non-linearity, and connection non-linearity. As these models were run using several small load-steps, they also allowed for any geometric non-linearity from the sway deflections in the columns. The non-linear models were analysed in two ways. First, they were analysed until a deflection limit had been reached. At this point the frame would have failed the serviceability criteria for design, or would have failed due to the ultimate load of the frame being reached. Secondly, some of the frames were solved with no deflection limit. This allowed the analysis to run until the ultimate load had been applied, and the frame had failed either due to yielding in the main steel sections, or the connections failing.

The first analyses, where a deflection limit was applied, were used to find the strength ratio for the frame. This was defined as being the load step reached for any frame, over the load factor reached for the fully fixed frame. These strength ratios were used to compare the results for frames with different connections, different section properties and different numbers of storeys. Curve fitting techniques were used to show trends for each of these changes. By changing the connection stiffness it was found that the strength ratio changed with a third-order logarithmic relationship. Increasing the number of storeys of the frame produced an almost linear relationship for the sway frames, especially when only the sway loading was applied, with no vertical loading on the frame. The vertical loading introduced second-order effects, which became more pronounced as the number of storeys increased (it would also increase as the storey height increased). The relationships have been shown in more detail in Chapter 7 of this thesis.

The second group of analyses, with no deflection limit being applied to the frames so that the behaviour of the frame could be analysed up to the ultimate load, showed that the connection stiffness had a large influence on the collapse behaviour of the frame. The frames with the most flexible connections failed at the connections, with no yielding occurring in the sections. The frames with the stiffer connections failed with plastic hinges occurring in the steel sections. The plastic hinges occurred in the sections, near to the connections, where the bending moments would have been at their greatest.

The work detailed in this thesis has shown that semi-rigid connections can be used to improve the efficiency of frameworks. The frameworks can be designed using connections that are currently in use, but taking into account their inherent stiffness makes frame design more efficient. This efficiency is in the form of savings on steel costs, and a reduction in the beam depth required, which allows either an increase in the ceiling height within buildings, a shortening of buildings, or more space for services in the service space between the floors of buildings.

The main drawback to the use of semi-rigid connections is an increase in the time of the designer. The connections would have to be detailed by the designer, which is currently the job of the contractor. The columns would have to undergo more rigorous design, because of the moments that are carried over to them from the beams due to the semi-rigid behaviour of the connections. Unless a straightforward design approach can be established, this increase in costs could outweigh the savings from the quantity of steel being used. Further work is needed to resolve this situation.

8.3 Recommendations for Further Work

Semi-rigid connections in design affect the rest of the frame, its strength, overall rigidity, and collapse behaviour. For these reasons, it is very important that the full effects of semi-rigid connections are thoroughly understood. The research in this thesis shows the effects of changing connection stiffness on single- and multi-storey, single bay frames. To reduce the amount of data that could be produced using the analysis techniques used here, only one size of frame was analysed. Further work could usefully be done to analyse frames with different beam and column lengths, and also frames with multi-bays.

The work presented by other researchers, which is reviewed in Chapter 2, shows that there is great further potential for research on semi-rigid connections. The work that has been done so far is mainly either concerned with how to model a single connection, or based on a few frames with similar initial stiffness values. The literature review has showed that different connections have different initial stiffnesses, and these change

depending on the construction of each connection, and the section sizes of the beams and columns.

More work needs to be done, following on from the work in this thesis, to find formulae or design principles that could be used when designing structures that make full use of the existing connections' behaviour. Unless specific design codes are written, the use of semi-rigid connections could be prohibited by the cost of the design of the frame. If design codes were available, savings in steel costs could be made without excessive cost in design time, resulting in an overall cost reduction for the project.

The use of computers in design is now widespread, and these could be used for the effective design of frames with semi-rigid connections. Currently programs that solve problems using finite elements are prohibitively expensive, and require fast computers for a complete analysis of a structure, along with the experience to know how to use the program accurately. A more simplistic program could be used, and adapted, to allow for the moment distribution of the connections. The computer program would need a database of connection types, and the formulae required to work out the initial stiffness, and ultimate rotation of the different connection types depending on the section sizes of the beam and columns, and the detailing of the connection. The program would have to solve the problem using load steps set by the designer, so the moments and deflections could be calculated at each stage, and the correct stage on the moment-rotation curve for the connections would be used for the next load step in the analysis. This would further reduce design time, making the use of semi-rigid connections more cost-effective, and bringing them into more widespread use.

References:

1. Howlett J. H., Jenkins W. M., (eds.), Joints in Structural Steelwork, the Design and Performance of Semi-Rigid and Rigid Steel Joints in Steel and Composite Structures and their Influence on Structural Behaviour: Proceedings of the International Conference, 1981.

2. Eurocode No. 3, Design of Steel Structures, Part 1.1 General Rules and Rules for Buildings. DD ENV 1993-1-1, April 1992, European Committee for Standardisation (CEN).

3. Owens G. W., Knowles P. R., The Steel Designers' Manual, The Steel Construction Institute, 1992.

4. Lloyd. R. M., Wright. H. D., In Situ Testing of a Composite Floor System. The Structural Engineer, 1992, Vol. 70, pp. 211-219.

5. Kim S.E., Chen W.F., Practical Advanced Analysis for Semi-Rigid Frame Design. Engineering Journal, 1996, fourth quarter, pp. 129-141.

6. Kishi N., Chen W.F., Moment-rotation Relations of Semi-Rigid Connections with Angles. ASCE Journal of Structural Engineering, 1990, Vol. 116, No. 7, pp. 1813-1834.

7. Moore D. B., Nethercot D. A., Kirby, P.A., Testing steel frames at full-scale. The Structural Engineer, 1993, Vol. 71, pp. 418-427.

8. Moore D. B., Nethercot D. A., Testing steel frames at full-scale: appraisal of results and implications for design. The Structural Engineer, 1993, Vol. 71, pp. 428-435.

9. Li T. Q., Moore D. B., Nethercot D. A., Choo B. S., The Experimental Behaviour of a Full-Scale, Semi-Rigidly Connected Composite Frame: Overall Considerations. Journal of Constructional Steel Research, 1996, Vol. 39, No. 3, pp. 167-191.

10. Li T. Q., Moore D. B., Nethercot D. A., Choo B. S., The Experimental Behaviour of a Full-Scale, Semi-Rigidly Connected Composite Frame: Detailed Appraisal. Journal of Constructional Steel Research, 1996, Vol. 39, No. 3, pp. 193-220.

11. Jaspart J., Maquoi R., Guidelines for the Design of Braced Frames with Semi-Rigid Connections. Journal of Constructional Steel Research, 1990, Vol. 16, No. 4, pp. 319-328.

12. Snijder H., Bijlaard F. S. K., Stark J. W. B., Use of the Elastic Effective Length for Stability Checks of Columns and Consequences for Checks on Beams in Braced Frames. Proceedings of the Michael R. Horne Conference, Granada, London, 1983.

13. Liew R. J. Y., White D. W., Chen W. F., Limit States Design of Semi-Rigid Frames Using Advanced Analysis: Part 1: Connection Modelling and Classification. Journal of Constructional Steel Research, 1993, Vol. 26, No. 1, pp. 1-27.

14. Liew R. J. Y., White D. W., Chen W. F., Limit States Design of Semi-Rigid Frames Using Advanced Analysis: Part 2: Analysis and Design. Journal of Constructional Steel Research, 1993, Vol. 26, No. 1, pp. 29-57.

15. Kishi N., Chen W. R., Goto Y., Matsuoka K. G., Design Aid of Semi-Rigid Connections for Frame Analysis. Engineering Journal, 1993, Vol. 30, No. 3, pp. 90-107.

16. Christopher J. E., Bjorhovde R., Response Characteristics of Frames with Semi-Rigid Connections. Journal of Constructional Steel Research, 1998, Vol. 46, No. 1-3, pp. 253-254.

17. Liew R. J. Y., Yu C. H., Ng Y. H., Shanmugam N. E., Testing of Semi-Rigid Unbraced Frames for Calibration of Second-Order Inelastic Analysis. Journal of Constructional Steel Research, 1997, Vol. 41, No. 2/3, pp. 159-195.

18. Yu C. H., Liew R. J. Y., Shanmugam N. E., Ng Y. H., Collapse Behaviour of Sway Frames with End-Plate Connections. Journal of Constructional Steel Research, 1998, Vol. 48, No. 2/3, pp. 169-188.

19. Johnson R.P., Hope-Gill M., Semi-Rigid Joints in Composite Frames. IABSE, 1972, pp. 133-144.

20. Wong C. W., Mak W. H., System Identification of Semi-Rigid Connections in Steel Frame Structures. Proceedings of SPIE - The International Society for Optical Engineering, 1993, Vol. 1923, Part 1, pp. 267-273

21. loannides S. A., Tarpy T. S., Practical Application of Semi-Rigid Beam to Column End-Plate Connectors. Applied Mathematical Modelling, 1980, Vol. 4, No. 1, pp. 23-27.

22. Cunningham R., Some Aspects of Semi-Rigid Connections in Structural Steelwork. The Structural Engineer, 1990, Vol. 68, No. 5/6, pp. 85-91.

23. Kishi N., Chen W. R., Goto Y., Matsuoka K. G., Behaviour of Tall Frame Combining Rigid and Semi-Rigid Connections. Proceedings of the Structures Congress, 1994, pp. 1185-1190.

24. Kishi N., Chen W. R., Goto Y., Matsuoka K. G., Behaviour of Tall Buildings with Mixed Use of Rigid and Semi-Rigid Connections. Computers and Structures, 1996, Vol. 61, No. 6, pp. 1193-1206.

25. Li G. Q., Mativo J., Approximate Estimation of the Maximum Load of Semi-Rigid Steel Frames. Journal of Constructional Steel Research, 2000, Vol. 54, No. 2, pp. 213-225.

26. Gibbons C., Kirby P. A., Nethercot D. A., Calculation of Serviceability Deflections for Non-Sway Frames with Semi-Rigid Connections. Proceedings of the Institution of Civil Engineers, Structures and Buildings, 1996, Vol. 116, No. 2, pp. 186-193.

27. Anderson D., Benterkia Z., Analysis of Semi-Rigid Steel Frames and Criteria for their Design, Journal of Constructional Steel Research, 1991, Vol. 18, No. 3, pp. 227-237.

28. Ahmed, Kirby P. A., Maximum Connection Rotations in Non-Sway Semi-Rigid Frames, Journal of Constructional Steel Research, 1996, Vol. 40. No. 1, pp. 1-15.

29. Li T. Q., Choo B. S., Nethercot D. A., Connection Element Method for the Analysis of Semi-Rigid Frames. Journal of Constructional Steel Research, 1995, Vol. 32, pp. 143-171.

30. Yau C. Y., Chan S. L., Inelastic and Stability Analysis of Flexibly Connected Steel Frames by Spring-in-Series Model. Journal of Structural Engineering, 1994, Vol. 120, No. 10, pp. 2803-2819.

31. Vogel, U., Stahlbau, 1985, Vol. 54, No.10. pp. 295-301.

32. Li T. Q., Choo B. S., Nethercot D. A., Determination of Rotation Capacity Requirements for Steel and Composite Beams. Journal of Constructional Steel Research, 1995, Vol. 32, No. 3, pp. 303-332.

33. Bjorhovde R., Colson A., Brozzetti J., Classification System for Beam-to-Column Connections. Journal of Structural Engineering, 1990, Vol. 166, No. 11, pp. 3059-3076.

34. Aristizabal-Ochoa, J., Stability of Columns Under Uniform Axial Load With Semi-Rigid Connections. Journal of Structural Engineering, 1993, Vol. 120, No. 11, pp. 3212-3221.

35. Stojadinovic B., Spacone E., Goel S. C., Kwon M., Influence of Semi-Rigid Column Base Models on the Response of Steel MRF Buildings. Unpublished manuscript.

36. Mei-xin Y., Nethercot D.A., Li. T. Q., Nonlinear Finite-Element Analysis of Composite Frames. Proceedings of the Institution of Civil Engineers, Structures and Bridges, 1996, 116, May, pp. 244-247.

37. Rodrigues F. C., Saldanha A. C., Pfeil M. S., Non-Linear Analysis of Steel Plane Frames with Semi-Rigid Connections. Journal of Constructional Steel Research, 1998, Vol. 26, No. 1-3, pp. 94-97.

38. Pertold. J., Xiao. R. Y., Frame Analysis with Semi-Rigid Connections Rigidity Factor Method Part I Non-sway Mode. Unpublished manuscript, attached as Appendix E.

39. Pertold. J., Xiao. R. Y., Frame Analysis with Semi-Rigid Connections Rigidity Factor Method Part II Sway Mode. Unpublished manuscript, attached as Appendix F.

40. British Standards Institution, Specification for Metal Props and Struts, BS 4074, (1982), BSI, London.

41. British Standards Institution, Part 1: Code of Practice for Design in Simple and Continuous Construction: Hot Rolled Sections, BS 5950 (1990), BSI, London.

Appendix A

Single-Storey Model And Results

A.1 The Model

The following text shows the finite element model that was used for the single storey plastic modelling. For each frame the geometry file would be called, followed by one set of stiffness files. The solution parameters were then loaded, and the model solved. For the next frame the same geometry file would then be loaded followed by the next set of stiffness files.

The geometry file:

```
/PREP7
!     material property
UIMP,1,EX, , ,2.1e11,
UIMP,1,DENS, , , ,
UIMP,1,ALPX, , , ,
UIMP,1,REFT, , , ,
UIMP,1,NUXY, , ,0.3,
UIMP,1,PRXY, , , ,
UIMP,1,GXY, , ,8.07692e10,
UIMP,1,MU, , , ,
UIMP,1,DAMP, , , ,
UIMP,1,KXX, , , ,
UIMP,1,C, , , ,
UIMP,1,ENTH, , , ,
```

```
UIMP,1,HF, , , ,
UIMP,1,EMIS, , , ,
UIMP,1,QRATE, , , ,
UIMP,1,MURX, , , ,
UIMP,1,MGXX, , , ,
UIMP,1,RSVX, , , ,
UIMP,1,PERX, , , ,
UIMP,1,VISC, , , ,
UIMP,1,SONC, , , ,
!*       data table yield stress Fy=275 MPa, E=0 after plasticity
TB,BKIN,1, , , ,
TBMODIF,2,1,2.75e8

!     FIRST STOREY
!     beam elements are r=1
!     column elements are r=2
!     base springs are r=3
!     beam-column are r=4
!*               BEAM
ET,1,BEAM23
TYPE,1,
MAT,1,
REAL,1,
ESYS,0,
KEYOPT,1,2,0
KEYOPT,1,4,1
KEYOPT,1,6,4
KEYOPT,1,10,0
!*
!     section properties
R,1,0.463,4.84e-2,7.61e-3,3.18e-3, , ,
RMORE, ,

!*             COLUMN
ET,2,BEAM23
KEYOPT,2,2,0
KEYOPT,2,4,1
KEYOPT,2,6,4
KEYOPT,2,10,0
!*
!     section properties
R,2,0.260,5.56e-2,7.07e-3,8.71e-4, , ,
RMORE, ,
!*

!*          BASE SPRING
ET,3,COMBIN39
KEYOPT,3,1,0
KEYOPT,3,2,0
KEYOPT,3,3,6
KEYOPT,3,4,0
KEYOPT,3,6,0
!
!     rigidity
R,3,154.88e-3,3.3665e5,500,3.3665e8,,,
RMORE,,,,,,,
!*

!           BEAM TO COLUMN SPRING
ET,4,COMBIN39
KEYOPT,4,1,0
```

```
KEYOPT,4,2,0
KEYOPT,4,3,6
KEYOPT,4,4,0
KEYOPT,4,6,0

!     rigidity
R,4,269.18e-3,3.3665e5,500,3.3665e8,,,
RMORE,,,,,,,

N,1,,,,,,,
N,2,,,,,,,
N,8,0,3.6,,,,,
N,9,0,3.6,,,,,
N,15,4.8,3.6,,,,,
N,16,4.8,3.6,,,,,
N,22,4.8,0,,,,,
N,23,4.8,0,,,,,
FILL,2,8,5, ,1,1,1,1,
FILL,9,15,5, ,1,1,1,1,
FILL,16,22,5, ,1,1,1,1,


!     COLUMNS
TYPE,2
REAL,2
E,2,3
E,3,4
E,4,5
E,5,6
E,6,7
E,7,8

E,16,17
E,17,18
E,18,19
E,19,20
E,20,21
E,21,22

!     BEAM
TYPE,1
REAL,1
E,9,10
E,10,11
E,11,12
E,12,13
E,13,14
E,14,15

!     BASE
TYPE,3
REAL,3
E,1,2
E,22,23

!     BEAM-COLUMN
TYPE,4
REAL,4
E,8,9
E,15,16
```

```
!     COUPLED RESTRICTIONS
CP,1,UX,8,9
CP,2,UY,8,9
CP,3,UX,15,16
CP,4,UY,15,16

!     BC'S
D,1, , , , , ,ALL
D,23, , , , , ,ALL

D,2, , , , , ,UX,UY
D,22, , , , , ,UX,UY

!     Restraint for non-sway frames
!D,15, , , , , ,UX

/SOLU
F,9,FY,-500e3
F,15,FY,-500e3
F,11,FY,-1000e3
F,13,FY,-1000e3
F,9,FX,300e3

FINISH
```

A set of stiffness files:

```
!Column base stiffness
/PREP7
R,3,32e-3,338.25e3,1,338.25e3,,,
RMORE, , , , , , ,
FINISH

!Beam-to-column stiffnesses
/PREP7
R,4,32e-3,338.25e3,1,338.25e3,,,
RMORE, , , , , , ,
FINISH
```

The solution parameters:

```
/SOLU
!*                          Analysis options
NLGEOM,1
NROPT,FULL, ,ON
LUMPM,0
EQSLV,FRONT,1e-08,0,
SSTIF
PSTRES
TOFFST,0,

!*                        Time and time step options
```

```
TIME,1000
!*                  ON-automatic  OFF- not automatic time step
AUTOTS,ON
!*    for automatic step size
DELTIM,1,0.5,50,OFF
!PRED,ON

!DELTIM,1

KBC,0
!*                        max. no. of iterations
NEQIT,80,
!*                        do not terminate analyses after non converging
solution
!*                 if UX,UY,ROTZ if higher than 0.024 than stop. (10m)
NCNV,2,0.024,0,0,0,

CNVTOL,F, ,0.001,2,-1,

!*                           output controls
OUTRES,ALL,ALL,
OUTPR,BASIC,NONE,
/STAT,SOLU
SOLVE
```

A.2 The Results

The following lists all the single storey frame results. The results are given as tables as they were in the main text of the thesis. The title of each frame gives the frame number, and the sway/non-sway behaviour of the frame. The strength ratio is the value given in the tables.

Table A.1 Frame 1, Non-Sway, Strength Ratio

	Phi Beam-to-Column mRad										
Phi Column	pinned	256	128	64	32	16	8	4	2	1	fixed
pinned	0.533784	0.561388	0.585589	0.628752	0.697105	0.790317	0.889645	0.952869	0.968396	0.976317	0.984206
256	0.533784	0.561388	0.585589	0.628752	0.697105	0.790317	0.890429	0.954045	0.969071	0.977101	0.98499
128	0.533784	0.561388	0.585589	0.628752	0.697889	0.791101	0.891433	0.954406	0.970168	0.97776	0.98499
64	0.534568	0.561388	0.585589	0.628752	0.697889	0.791101	0.89261	0.955206	0.970827	0.978748	0.986559
32	0.529863	0.561388	0.585589	0.628752	0.697889	0.792669	0.894743	0.957307	0.97318	0.981022	0.988002
16	0.529863	0.561388	0.585589	0.628752	0.698673	0.794238	0.897629	0.960444	0.976458	0.984284	0.990433
8	0.534568	0.561388	0.585589	0.629537	0.699457	0.796465	0.901989	0.963534	0.980379	0.988096	0.991766
4	0.534568	0.561388	0.585589	0.629537	0.700242	0.798817	0.906271	0.967455	0.983924	0.991891	0.993334
2	0.534568	0.561388	0.585589	0.629537	0.701026	0.80059	0.909549	0.969808	0.987186	0.994118	0.994903
1	0.534568	0.561388	0.585589	0.629537	0.701026	0.801405	0.911886	0.97216	0.989288	0.995687	0.995687
fixed	0.534568	0.561388	0.585589	0.629537	0.70181	0.802974	0.915022	0.974513	0.991766	0.996471	1

Table A.2 Frame 2, Non-Sway, Strength Ratio

	Phi Beam-to-Column mRad										
Phi Column	pinned	256	128	64	32	16	8	4	2	1	fixed
pinned	0.481068	0.516781	0.548298	0.595278	0.661754	0.738154	0.807481	0.860001	0.893616	0.911768	0.931426
256	0.481068	0.516781	0.548298	0.596622	0.662507	0.739499	0.809579	0.862099	0.895713	0.914618	0.935621
128	0.481068	0.516781	0.548298	0.596622	0.662507	0.740252	0.811676	0.865541	0.899156	0.918061	0.937745
64	0.481068	0.516781	0.548298	0.596622	0.663852	0.742349	0.815119	0.868391	0.904131	0.923036	0.944038
32	0.481068	0.516781	0.548298	0.597375	0.664605	0.744447	0.819314	0.876056	0.911768	0.931426	0.952428
16	0.481068	0.51756	0.549051	0.597375	0.666703	0.748642	0.825633	0.884446	0.922283	0.941941	0.962943
8	0.481068	0.51756	0.549051	0.597375	0.668047	0.752084	0.832679	0.893616	0.933523	0.954553	0.974802
4	0.481068	0.51756	0.549051	0.59872	0.670172	0.754962	0.838246	0.902006	0.943285	0.964288	0.983946
2	0.481068	0.51756	0.549051	0.599473	0.670925	0.758404	0.843194	0.908326	0.949578	0.97136	0.990265
1	0.481068	0.51756	0.549051	0.599473	0.670925	0.759157	0.845291	0.912521	0.953773	0.974802	0.99446
fixed	0.481068	0.51756	0.549051	0.599473	0.672269	0.761254	0.848733	0.916716	0.958748	0.97975	1

Table A.3 Frame 3, Non-Sway, Strength Ratio

	Phi Beam-to-Column mRad										
Phi Column	pinned	256	128	64	32	16	8	4	2	1	fixed
pinned	0.659094	0.679681	0.697149	0.727419	0.771419	0.826613	0.881284	0.924413	0.948621	0.961054	0.972112
256	0.659094	0.679681	0.697149	0.727458	0.772387	0.827582	0.882291	0.92635	0.950558	0.963243	0.974049
128	0.659094	0.679681	0.697149	0.727458	0.772387	0.82855	0.884209	0.928286	0.95323	0.965199	0.975986
64	0.659094	0.679681	0.697149	0.727458	0.772387	0.829286	0.886649	0.931191	0.956368	0.968104	0.978988
32	0.659094	0.679681	0.697149	0.727458	0.773356	0.831222	0.889554	0.936033	0.961209	0.973081	0.983829
16	0.660063	0.679681	0.697149	0.728426	0.774169	0.834515	0.894395	0.942811	0.968104	0.979859	0.988613
8	0.654253	0.679642	0.697149	0.728426	0.776106	0.837265	0.90005	0.949589	0.975017	0.985766	0.993164
4	0.654253	0.679642	0.697149	0.728426	0.777074	0.839124	0.904989	0.955399	0.980827	0.990549	0.996185
2	0.654253	0.679642	0.697149	0.728426	0.777326	0.841138	0.908068	0.959273	0.984894	0.993648	0.997967
1	0.654253	0.679642	0.697149	0.729394	0.777326	0.842164	0.910005	0.961364	0.986579	0.995584	0.999225
fixed	0.654253	0.679642	0.697149	0.729394	0.778294	0.843133	0.912755	0.964114	0.989639	0.997037	1

Table A.4 Frame 1, Sway, Strength Ratio

	Phi Beam-to-Column mRad										
Phi Column	pinned	256	128	64	32	16	8	4	2	1	fixed
pinned	0	0.037878	0.071773	0.132453	0.226371	0.350766	0.483534	0.589649	0.640382	0.650816	0.657719
256	0.038677	0.077692	0.113098	0.175	0.272119	0.4007	0.537223	0.639583	0.676574	0.683269	0.688414
128	0.075187	0.114859	0.151971	0.215138	0.315006	0.447342	0.588403	0.683269	0.705735	0.711535	0.716457
64	0.142374	0.183932	0.222632	0.289599	0.394452	0.533468	0.675775	0.743988	0.754422	0.759423	0.7623
32	0.256332	0.302526	0.34372	0.416119	0.530527	0.672834	0.789879	0.817091	0.824233	0.824233	0.823003
16	0.428615	0.479795	0.525286	0.604174	0.701996	0.799466	0.875366	0.889043	0.891568	0.891344	0.891232
8	0.550245	0.576562	0.599732	0.642874	0.711583	0.808255	0.896537	0.930492	0.943275	0.950066	0.957544
4	0.550245	0.577361	0.601777	0.644472	0.715594	0.814646	0.910902	0.951265	0.966524	0.973843	0.980586
2	0.550245	0.577361	0.601777	0.645671	0.717863	0.81904	0.919914	0.963249	0.97771	0.98498	0.992218
1	0.550245	0.577361	0.602576	0.646469	0.719668	0.821038	0.925587	0.968841	0.983222	0.989774	0.996213
fixed	0.550245	0.577361	0.602608	0.64754	0.720579	0.824633	0.930412	0.97453	0.988016	0.993784	1

Table A.5 Frame 2, Sway, Strength Ratio

	Phi Beam-to-Column mRad										
Phi Column	pinned	256	128	64	32	16	8	4	2	1	fixed
pinned	0	0.039312	0.07237	0.126837	0.200714	0.283532	0.357345	0.41029	0.443384	0.461823	0.481674
256	0.040063	0.081606	0.117792	0.174987	0.253013	0.340487	0.417688	0.475066	0.509572	0.529423	0.547862
128	0.077588	0.120808	0.157746	0.217677	0.300503	0.392641	0.474276	0.533828	0.569916	0.589767	0.606624
64	0.141916	0.188558	0.227853	0.293726	0.382391	0.483086	0.572118	0.637516	0.675806	0.690461	0.704495
32	0.241424	0.293726	0.338284	0.41108	0.511775	0.625064	0.727961	0.79494	0.818405	0.825013	0.830237
16	0.371379	0.430931	0.481674	0.565511	0.680211	0.779494	0.858107	0.907438	0.926498	0.931722	0.930028
8	0.503727	0.542639	0.575733	0.627266	0.700062	0.786102	0.869148	0.922884	0.94714	0.955978	0.962557
4	0.505139	0.543457	0.576523	0.629469	0.703705	0.792737	0.876546	0.935336	0.960383	0.970633	0.979358
2	0.505139	0.543457	0.576523	0.63088	0.705907	0.796352	0.883182	0.942735	0.969221	0.980234	0.989242
1	0.505139	0.543457	0.576523	0.63088	0.706698	0.797142	0.885384	0.94714	0.975038	0.984667	0.994889
fixed	0.505139	0.543457	0.576523	0.631699	0.70811	0.799345	0.889789	0.951573	0.980234	0.990484	1

Table A.6 Frame 3, Sway, Strength Ratio

	Phi Beam-to-Column mRad										
Phi Column	pinned	256	128	64	32	16	8	4	2	1	fixed
pinned	0	0.029631	0.055454	0.100499	0.167055	0.247979	0.32688	0.388885	0.429672	0.453543	0.47639
256	0.029631	0.0614	0.089349	0.13674	0.206152	0.292609	0.376877	0.442725	0.486185	0.511246	0.532465
128	0.057384	0.090393	0.119385	0.168519	0.242027	0.332811	0.421507	0.491657	0.537351	0.561828	0.583025
64	0.10496	0.140085	0.172072	0.224756	0.305077	0.403567	0.501451	0.579183	0.629764	0.649333	0.665664
32	0.178556	0.2187	0.253451	0.313827	0.403567	0.516133	0.62872	0.716831	0.757618	0.770085	0.779859
16	0.27467	0.320343	0.36113	0.430717	0.535722	0.667878	0.795147	0.863668	0.874757	0.873462	0.871833
8	0.375833	0.428043	0.474761	0.555291	0.677088	0.821711	0.919784	0.936303	0.93954	0.939436	0.938454
4	0.460665	0.517762	0.569973	0.659712	0.790113	0.895579	0.951841	0.967755	0.973122	0.973895	0.974939
2	0.518806	0.579767	0.63628	0.729883	0.833302	0.899756	0.959109	0.976255	0.983293	0.987469	0.990602
1	0.553662	0.617296	0.674394	0.770795	0.83539	0.901844	0.962617	0.98016	0.988514	0.991646	0.995823
fixed	0.59282	0.659712	0.719504	0.786459	0.835913	0.903933	0.965917	0.985381	0.992691	0.996867	1

Appendix B

Two-Storey Model And Results

B.1 The Model

The following text shows the finite element model that was used for the two-storey plastic modelling. For each frame the geometry file would be called, followed by one set of stiffness files. The solution parameters were then loaded, and the model solved. For the next frame the same geometry file would then be loaded followed by the next set of stiffness files.

The geometry file:

```
/PREP7
!      material property
UIMP,1,EX, , ,2.1e11,
UIMP,1,DENS, , , ,
UIMP,1,ALPX, , , ,
UIMP,1,REFT, , , ,
UIMP,1,NUXY, , ,0.3,
UIMP,1,PRXY, , , ,
UIMP,1,GXY, , ,8.07692e10,
UIMP,1,MU, , , ,
UIMP,1,DAMP, , , ,
UIMP,1,KXX, , , ,
UIMP,1,C, , , ,
UIMP,1,ENTH, , , ,
```

```
UIMP,1,HF, , , ,
UIMP,1,EMIS, , , ,
UIMP,1,QRATE, , , ,
UIMP,1,MURX, , , ,
UIMP,1,MGXX, , , ,
UIMP,1,RSVX, , , ,
UIMP,1,PERX, , , ,
UIMP,1,VISC, , , ,
UIMP,1,SONC, , , ,
!*       data table yield stress Fy=275 MPa, E=0 after plasticity
TB,BKIN,1, , , ,
TBMODIF,2,1,2.75e8

!     FIRST STOREY
!     beam elements are r=1
!     column elements are r=2
!     base springs are r=3
!     beam-column are r=4

!*                BEAM
ET,1,BEAM23
TYPE,1,
MAT,1,
REAL,1,
ESYS,0,
KEYOPT,1,2,0
KEYOPT,1,4,1
KEYOPT,1,6,4
KEYOPT,1,10,0
!*
!     section properties
R,1,0.463,4.84e-2,7.61e-3,3.18e-3, , ,
RMORE, ,

!*              COLUMN
ET,2,BEAM23
KEYOPT,2,2,0
KEYOPT,2,4,1
KEYOPT,2,6,4
KEYOPT,2,10,0
!*
!     section properties
R,2,0.260,5.56e-2,7.07e-3,8.71e-4, , ,
RMORE, ,
!*
!*           BASE SPRING
ET,3,COMBIN39
KEYOPT,3,1,0
KEYOPT,3,2,0
KEYOPT,3,3,6
KEYOPT,3,4,0
KEYOPT,3,6,0
!
!     rigidity
R,3,154.88e-3,3.3665e5,500,3.3665e8,,,
RMORE,,,,,,,
!*

!           BEAM TO COLUMN SPRING
ET,4,COMBIN39
KEYOPT,4,1,0
```

```
KEYOPT,4,2,0
KEYOPT,4,3,6
KEYOPT,4,4,0
KEYOPT,4,6,0

!     rigidity
R,4,269.18e-3,3.3665e5,500,3.3665e8,,,
RMORE,,,,,,,

N,1,,,,,,,
N,2,,,,,,,
N,8,0,3.6,,,,,
N,9,0,3.6,,,,,
N,15,4.8,3.6,,,,,
N,16,4.8,3.6,,,,,
N,22,4.8,0,,,,,
N,23,4.8,0,,,,,
FILL,2,8,5, ,1,1,1,1,
FILL,9,15,5, ,1,1,1,1,
FILL,16,22,5, ,1,1,1,1,

!     COLUMNS
TYPE,2
REAL,2
E,2,3
E,3,4
E,4,5
E,5,6
E,6,7
E,7,8

E,16,17
E,17,18
E,18,19
E,19,20
E,20,21
E,21,22

!     BEAM
TYPE,1
REAL,1
E,9,10
E,10,11
E,11,12
E,12,13
E,13,14
E,14,15

!     BASE
TYPE,3
REAL,3
E,1,2
E,22,23

!     BEAM-COLUMN
TYPE,4
REAL,4
E,8,9
E,15,16
```

```
!     COUPLED RESTRICTIONS
CP,1,UX,8,9
CP,2,UY,8,9
CP,3,UX,15,16
CP,4,UY,15,16

!     BC'S
D,1, , , , , ,ALL
D,23, , , , , ,ALL

D,2, , , , , ,UX,UY
D,22, , , , , ,UX,UY

!     FOR NON-SWAY ADD...
D,15, , , , , ,UX

/SOLU
!F,9,FY,-500e3
!F,15,FY,-500e3
F,11,FY,-1000e3
F,13,FY,-1000e3
!F,9,FX,-300e3


!     SECOND STOREY
/PREP7
!     beam elements are r=5
!     column elements are r=6
!     beam-column are r=7

!*                BEAM
ET,5,BEAM23
TYPE,1,
MAT,1,
REAL,5,
ESYS,0,
KEYOPT,5,2,0
KEYOPT,5,4,1
KEYOPT,5,6,4
KEYOPT,5,10,0
!*
!     section properties
R,5,0.463,4.84e-2,7.61e-3,3.18e-3, , ,
RMORE, ,

!*              COLUMN
ET,6,BEAM23
KEYOPT,6,2,0
KEYOPT,6,4,1
KEYOPT,6,6,4
KEYOPT,6,10,0
!*
!     section properties
R,6,0.260,5.56e-2,7.07e-3,8.71e-4, , ,
RMORE, ,
!*

!           BEAM TO COLUMN SPRING
ET,7,COMBIN39
KEYOPT,7,1,0
KEYOPT,7,2,0
```

```
KEYOPT,7,3,6
KEYOPT,7,4,0
KEYOPT,7,6,0

!     rigidity
R,7,269.18e-3,3.3665e5,500,3.3665e8,,,
RMORE,,,,,,,

N,29,0,7.2,
N,30,0,7.2,
N,36,4.8,7.2,
N,37,4.8,7.2,
FILL,8,29,5,24,1,1,1,1,
FILL,30,36,5,31,1,1,1,1,
FILL,37,15,5,38,1,1,1,1,


!     Columns
TYPE,6
REAL,6
E,8,24
E,24,25
E,25,26
E,26,27
E,27,28
E,28,29

E,37,38
E,38,39
E,39,40
E,40,41
E,41,42
E,42,16

!     Beam
TYPE,5
REAL,5
E,30,31
E,31,32
E,32,33
E,33,34
E,34,35
E,35,36

!     Beam-column
TYPE,7
REAL,7
E,29,30
E,36,37

!     COUPLED RESTRICTIONS
CP,5,UX,29,30
CP,6,UY,29,30
CP,7,UX,36,37
CP,8,UY,36,37

!     FOR NON-SWAY ADD...
D,36, , , , , ,UX

F,30,FY,-500e3
F,36,FY,-500e3
```

```
F,32,FY,-1000e3
F,34,FY,-1000e3
F,30,FX,300e3

FINISH
```

A set of stiffness files:

```
!Column base stiffness
/PREP7
R,3,32e-3,338.25e3,1,338.25e3,,,
RMORE, , , , , , ,
FINISH

!Beam-to-column stiffnesses
/PREP7
R,4,32e-3,338.25e3,1,338.25e3,,,
RMORE, , , , , , ,
FINISH

!Beam-to-column stiffnesses
/PREP7
R,7,32e-3,338.25e3,1,338.25e3,,,
RMORE, , , , , , ,
FINISH
```

The solution parameters:

```
/SOLU
!*                          Analysis options
NLGEOM,1
NROPT,FULL, ,ON
LUMPM,0
EQSLV,FRONT,1e-08,0,
SSTIF
PSTRES
TOFFST,0,

!*                        Time and time step options
TIME,1000
!*                  ON-automatic  0FF- not automatic time step
AUTOTS,ON
!*   for automatic step size
DELTIM,1,0.5,50,OFF
!PRED,ON

!DELTIM,1

KBC,0
!*                        max. no. of iterations
NEQIT,80,
```

```
!*                          do not terminate analyses after non converging
solution
!*                  if UX,UY,ROTZ if higher than 0.024 than stop. (10m)
NCNV,2,0.024,0,0,0,

CNVTOL,F, ,0.001,2,-1,

!*                              output controls
OUTRES,ALL,ALL,
OUTPR,BASIC,NONE,
/STAT,SOLU
SOLVE
```

B.2 The Results

The following lists all the two-storey frame results. The results are given as tables as they were in the main text of the thesis. The title of each frame gives the frame number, and the sway/non-sway behaviour of the frame. The strength ratio is the value given in the tables.

Table B.1 Frame 1, Non-Sway, Strength Ratio

	Phi Beam-to-Column mRad										
Phi Column	pinned	256	128	64	32	16	8	4	2	1	fixed
pinned	0.531124	0.556449	0.579865	0.621907	0.690385	0.788023	0.898746	0.969024	0.987431	0.995962	1.000329
256	0.531124	0.556449	0.579865	0.621907	0.690385	0.788023	0.898746	0.969024	0.987431	0.995179	1.000329
128	0.531124	0.556449	0.579865	0.621907	0.690385	0.788023	0.897964	0.969024	0.987431	0.995179	1.000329
64	0.531124	0.556449	0.579865	0.621907	0.690385	0.788023	0.897964	0.968602	0.987431	0.995179	1.000329
32	0.531124	0.556449	0.579865	0.621907	0.690385	0.788023	0.897964	0.968602	0.987431	0.995179	1.000329
16	0.531124	0.556449	0.579865	0.621907	0.690385	0.78724	0.897964	0.967819	0.987384	0.995179	1.000329
8	0.531124	0.556449	0.579865	0.621907	0.690385	0.78724	0.897964	0.967819	0.987384	0.995304	1.000329
4	0.531124	0.556449	0.579865	0.621907	0.690385	0.78724	0.897478	0.967819	0.986602	0.994522	0.999859
2	0.531124	0.556449	0.579865	0.621907	0.690385	0.78724	0.897478	0.967819	0.986602	0.994522	0.999859
1	0.531124	0.556449	0.579865	0.621907	0.690385	0.78724	0.896586	0.967037	0.986602	0.994522	1
fixed	0.531124	0.556449	0.579865	0.621907	0.690385	0.78724	0.896586	0.967037	0.986602	0.994522	1

Table B.2 Frame 2, Non-Sway, Strength Ratio

	Phi Beam-to-Column mRad										
Phi Column	pinned	256	128	64	32	16	8	4	2	1	fixed
pinned	0.464205	0.498944	0.530237	0.583202	0.659683	0.751557	0.844152	0.918575	0.962401	0.983298	1.004917
256	0.464205	0.498944	0.530237	0.583202	0.659683	0.751557	0.844152	0.918575	0.962401	0.981962	1.004917
128	0.464205	0.498944	0.530237	0.582454	0.659683	0.751557	0.844152	0.918575	0.961065	0.981962	1.004917
64	0.464205	0.498944	0.530237	0.582454	0.659683	0.751557	0.844152	0.918575	0.961065	0.981962	1.004169
32	0.464205	0.498944	0.530237	0.582454	0.659683	0.75022	0.843403	0.917239	0.961065	0.981187	1.004169
16	0.464205	0.498944	0.530237	0.582454	0.658347	0.75022	0.843403	0.917239	0.960316	0.981187	1.002833
8	0.464205	0.498944	0.530237	0.582454	0.658347	0.75022	0.842067	0.916491	0.95898	0.979851	1.002084
4	0.464205	0.498944	0.530237	0.582454	0.658347	0.75022	0.842067	0.915155	0.95898	0.979103	1.000748
2	0.464205	0.498944	0.530237	0.582454	0.658347	0.75022	0.842067	0.915155	0.958232	0.979103	1.000748
1	0.464205	0.498944	0.530237	0.582454	0.658347	0.75022	0.841319	0.915155	0.958232	0.977766	1.000748
fixed	0.464205	0.498944	0.530237	0.582454	0.658347	0.749472	0.841319	0.91438	0.956896	0.977766	1

Table B.3 Frame 3, Non-Sway, Strength Ratio

	Phi Beam-to-Column mRad										
Phi Column	pinned	256	128	64	32	16	8	4	2	1	fixed
pinned	0.6534	0.672193	0.689311	0.720159	0.769049	0.83548	0.909845	0.966977	0.991065	0.996341	1.000963
256	0.6534	0.672193	0.689311	0.720159	0.769049	0.83548	0.909845	0.966977	0.991065	0.996495	1
128	0.6534	0.672193	0.689311	0.720159	0.769049	0.83548	0.909845	0.966495	0.991065	0.996495	1
64	0.6534	0.672193	0.689311	0.720159	0.769049	0.83548	0.909845	0.966014	0.991065	0.996495	1
32	0.6534	0.672193	0.689311	0.720159	0.769049	0.83548	0.909845	0.965533	0.990911	0.996495	1
16	0.6534	0.672193	0.689311	0.720159	0.768086	0.834518	0.908883	0.965687	0.990584	0.995533	1
8	0.6534	0.672193	0.689311	0.720159	0.768086	0.834518	0.908883	0.964242	0.990584	0.995629	1
4	0.6534	0.672193	0.689311	0.720159	0.768086	0.834518	0.90792	0.96482	0.989371	0.995225	1
2	0.6534	0.672193	0.689311	0.720159	0.768086	0.834518	0.90792	0.963761	0.989371	0.995379	1
1	0.6534	0.672193	0.689311	0.720159	0.768086	0.834518	0.90792	0.964242	0.98889	0.995379	1
fixed	0.6534	0.672193	0.689311	0.720159	0.768086	0.834518	0.90792	0.963376	0.989371	0.995379	1

Table B.4 Frame 1, Sway, Strength Ratio

	Phi Beam-to-Column mRad										
Phi Column	pinned	256	128	64	32	16	8	4	2	1	fixed
pinned	0	0.023037	0.045025	0.083435	0.143654	0.227508	0.321705	0.408175	0.473022	0.514705	0.563562
256	0.011365	0.036533	0.059096	0.098209	0.161459	0.247589	0.345857	0.435963	0.503913	0.547138	0.595008
128	0.022514	0.04784	0.070772	0.111995	0.177093	0.266108	0.368033	0.460669	0.531149	0.575915	0.621255
64	0.040286	0.067673	0.091877	0.135145	0.203218	0.298541	0.40608	0.505455	0.579572	0.62588	0.669124
32	0.067673	0.097221	0.123075	0.16997	0.245494	0.347952	0.465294	0.574927	0.656771	0.699443	0.743241
16	0.102498	0.134157	0.164232	0.216065	0.298541	0.413788	0.545596	0.667582	0.750968	0.784924	0.82971
8	0.137321	0.172344	0.205589	0.262471	0.354119	0.482291	0.629971	0.767946	0.842063	0.843051	0.899202
4	0.165221	0.203218	0.238319	0.300083	0.399893	0.53941	0.701557	0.846687	0.889932	0.88839	0.943968
2	0.184216	0.224583	0.261483	0.32633	0.431338	0.579018	0.751957	0.896099	0.919262	0.917721	0.970215
1	0.196087	0.236778	0.274824	0.341766	0.449858	0.602735	0.78184	0.924895	0.937248	0.933157	0.985098
fixed	0.207961	0.250672	0.289272	0.358764	0.47148	0.629971	0.815815	0.956321	0.954779	0.949601	1

Table B.5 Frame 2, Sway, Strength Ratio

	Phi Beam-to-Column mRad										
Phi Column	pinned	256	128	64	32	16	8	4	2	1	fixed
pinned	0	0.030133	0.054889	0.098569	0.158759	0.229212	0.29853	0.352107	0.38783	0.408241	0.431654
256	0.014867	0.046262	0.074484	0.118839	0.183854	0.259833	0.33255	0.390808	0.428638	0.449919	0.475448
128	0.026548	0.060267	0.088489	0.136981	0.204409	0.284925	0.363172	0.424407	0.464362	0.487767	0.514315
64	0.046262	0.08255	0.11279	0.165708	0.237295	0.326595	0.411222	0.477572	0.522131	0.54749	0.575227
32	0.070453	0.110666	0.145442	0.201996	0.284925	0.382729	0.477572	0.552035	0.601776	0.63168	0.664854
16	0.096767	0.140906	0.179318	0.2441	0.334674	0.444822	0.552035	0.638306	0.694716	0.727891	0.766545
8	0.118839	0.168121	0.208946	0.27812	0.378481	0.498938	0.618384	0.714638	0.777674	0.816286	0.859443
4	0.134857	0.186267	0.23049	0.301933	0.409099	0.538739	0.666978	0.771047	0.84071	0.880554	0.923711
2	0.145442	0.19746	0.242821	0.317666	0.426514	0.561974	0.698029	0.806346	0.877241	0.922479	0.959009
1	0.149979	0.201996	0.249626	0.326595	0.438875	0.575227	0.714638	0.824144	0.900476	0.94359	0.978931
fixed	0.154511	0.208946	0.256431	0.334674	0.449919	0.591836	0.733328	0.847379	0.923711	0.965636	1

Table B.6 Frame 3, Sway, Strength Ratio

	Phi Beam-to-Column mRad										
Phi Column	pinned	256	128	64	32	16	8	4	2	1	fixed
pinned	0	0.019682	0.03724	0.068334	0.117127	0.180828	0.251937	0.317213	0.364131	0.394456	0.429943
256	0.009711	0.030218	0.049897	0.082959	0.133516	0.201662	0.278592	0.347567	0.399589	0.432107	0.47034
128	0.017341	0.039365	0.060432	0.095	0.14833	0.220551	0.301926	0.375728	0.429943	0.464625	0.505799
64	0.030218	0.05392	0.076236	0.114164	0.171938	0.250549	0.338882	0.421259	0.481161	0.520199	0.564314
32	0.046019	0.073672	0.097775	0.139443	0.203884	0.291937	0.392292	0.48413	0.553493	0.598219	0.648854
16	0.063207	0.093424	0.12009	0.166109	0.238605	0.338882	0.452999	0.559209	0.640198	0.691443	0.750735
8	0.077623	0.109814	0.139443	0.189718	0.269991	0.380084	0.507186	0.627185	0.719605	0.768076	0.845319
4	0.088086	0.121666	0.152775	0.206107	0.29055	0.409633	0.546973	0.678431	0.778925	0.802758	0.913296
2	0.095	0.128977	0.160829	0.216658	0.303868	0.427751	0.572998	0.710948	0.812829	0.81577	0.952333
1	0.097963	0.133516	0.165274	0.221938	0.311942	0.438599	0.586011	0.729066	0.83744	0.826591	0.97539
fixed	0.100924	0.137867	0.170551	0.227215	0.319377	0.449448	0.602547	0.748571	0.83744	0.838827	1

Appendix C

Five-Storey Model And Results

C.1 The Model

The following text shows the finite element model that was used for the five-storey plastic modelling. For each frame the geometry file would be called, followed by one set of stiffness files. The solution parameters were then loaded, and the model solved. For the next frame the same geometry file would then be loaded followed by the next set of stiffness files.

The geometry file:

```
/PREP7
!,material property
UIMP,1,EX, , ,2.10E+11,
UIMP,1,DENS, , , ,
UIMP,1,ALPX, , , ,
UIMP,1,REFT, , , ,
UIMP,1,NUXY, , ,0.3,
UIMP,1,PRXY, , , ,
UIMP,1,GXY, , ,8.08E+10,
UIMP,1,MU, , , ,
UIMP,1,DAMP, , , ,
UIMP,1,KXX, , , ,
UIMP,1,C, , , ,
UIMP,1,ENTH, , , ,
```

```
UIMP,1,HF, , , ,
UIMP,1,EMIS, , , ,
UIMP,1,QRATE, , , ,
UIMP,1,MURX, , , ,
UIMP,1,MGXX, , , ,
UIMP,1,RSVX, , , ,
UIMP,1,PERX, , , ,
UIMP,1,VISC, , , ,
UIMP,1,SONC, , , ,
!*       data table yield stress Fy=275 MPa, E=0 after plasticity
TB,BKIN,1, , ,
TBMODIF,2,1,2.75E+08

!,FIRST STOREY
!,beam elements are r=,1
!,column elements are r=,2
!,base springs are r=,3
!,beam-column are r=,4
!*                BEAM
ET,1,BEAM23
TYPE,1,
MAT,1,
REAL,1,
ESYS,0,
KEYOPT,1,2,0
KEYOPT,1,4,1
KEYOPT,1,6,4
KEYOPT,1,10,0
!*
!,section properties
R,1,0.463,4.84E-02,7.61E-03,3.18E-03, , ,
RMORE, ,,,,,,,

!*              COLUMN
ET,2,BEAM23,,,,,,
KEYOPT,2,2,0,,,,,
KEYOPT,2,4,1,,,,,
KEYOPT,2,6,4,,,,,
KEYOPT,2,10,0,,,,,
!*
!,section properties
R,2,0.260,5.56e-2,7.07e-3,8.71e-4
RMORE,
!*

!* ,,BASE SPRING
ET,3,COMBIN39
KEYOPT,3,1,0
KEYOPT,3,2,0
KEYOPT,3,3,6
KEYOPT,3,4,0
KEYOPT,3,6,0
!
!,rigidity
R,3,1.55E-01,3.37E+05,500,3.37E+08,,,
RMORE
!*
!
!,,BEAM TO COLUMN SPRING
ET,4,COMBIN39
KEYOPT,4,1,0
```

```
KEYOPT,4,2,0
KEYOPT,4,3,6
KEYOPT,4,4,0
KEYOPT,4,6,0
!
!,rigidity
R,4,2.69E-01,3.37E+05,500,3.37E+08
RMORE
!
N,1,,,,,,,
N,2,,,,,,,
N,8,0,3.6,,,,,
N,9,0,3.6,,,,,
N,15,4.8,3.6,,,,,
N,16,4.8,3.6,,,,,
N,22,4.8,0,,,,,,
N,23,4.8,0,,,,,
FILL,2,8,5, ,1,1,1,1,
FILL,9,15,5, ,1,1,1,1,
FILL,16,22,5, ,1,1,1,1,


!,COLUMNS,,,,,,,,
TYPE,2,,,,,,,,
REAL,2,
E,2,3
E,3,4
E,4,5
E,5,6
E,6,7
E,7,8

E,16,17
E,17,18
E,18,19
E,19,20
E,20,21
E,21,22

!,BEAM,
TYPE,1,
REAL,1,
E,9,10
E,10,11
E,11,12
E,12,13
E,13,14
E,14,15

!,BASE,
TYPE,3,
REAL,3,
E,1,2
E,22,23

!,BEAM-COLUMN,
TYPE,4,,,,,,,
REAL,4,,,,,,,
E,8,9,,,,,,
E,15,16,,,,,,
```

```
!,COUPLED RESTRICTIONS,,,,,,
CP,1,UX,8,9,,,,
CP,2,UY,8,9,,,,
CP,3,UX,15,16,,,,
CP,4,UY,15,16,,,,

!,BC'S
D,1, , , , , ,ALL,
D,23, , , , , ,ALL,
!
D,2, , , , , ,UX,UY
D,22, , , , , ,UX,UY
!,,,,,,,,
!,FOR NON-SWAY ADD...
D,15, , , , , ,UX,

/SOLU
!F,9,FY,-5.00E+05
!F,15,FY,-5.00E+05
F,11,FY,-1.00E+06
F,13,FY,-1.00E+06
!F,9,FX,-3.00E+05

!*****************************************************************
!,SECOND STOREY
/PREP7
!,beam elements are r=,5
!,column elements are r=,6
!,beam-column are r=,7
!
!*      BEAM
!
!,section properties
R,5,0.463,4.84E-02,7.61E-03,3.18E-03, , ,
RMORE,
!
!*    Column
!,section properties
R,6,0.260,5.56e-2,7.07e-3,8.71e-4
RMORE,
!*
!
!,beam to column rigidity
R,7,2.69E-01,3.37E+05,500,3.37E+08,,,
RMORE
!
N,29,0,7.2
N,30,0,7.2
N,36,4.8,7.2
N,37,4.8,7.2
FILL,9,29,5,24,1,1,1,1
FILL,30,36,5,31,1,1,1,1
FILL,37,15,5,38,1,1,1,1
!
!
!,Columns
TYPE,2
REAL,6
E,8,24
E,24,25
E,25,26
```

```
E,26,27
E,27,28
E,28,29
!,,
E,37,38
E,38,39
E,39,40
E,40,41
E,41,42
E,42,16
!,,
!,,
!,Beam,
TYPE,1,
REAL,5,
E,30,31
E,31,32
E,32,33
E,33,34
E,34,35
E,35,36
!,,
!,Beam-column,
TYPE,4,
REAL,7,
E,29,30
E,36,37
!,,
!,,
!,COUPLED RESTRICTIONS,
CP,5,UX,29,30,,,
CP,6,UY,29,30,,,
CP,7,UX,36,37,,,
CP,8,UY,36,37,,,
!,,,,,,,
!,FOR NON-SWAY ADD...
D,36, , , , , ,UX
!,,,,,,,
!F,30,FY,-5.00E+05,,,,
!F,36,FY,-5.00E+05,,,,
F,32,FY,-1.00E+06,,,,
F,34,FY,-1.00E+06,,,,
!F,30,FX,-3.00E+05,,,,
!
!*****************************************************************
!,Third STOREY
/PREP7
!,beam elements are r=,8
!,column elements are r=,9
!,beam-column are r=,10
!
!*                BEAM
!*
!,section properties,,,,,,,,
R,8,0.463,4.84E-02,7.61E-03,3.18E-03, , ,
RMORE,
!,,,,,,,,,
!*    Column
!,section properties
R,9,0.260,5.56e-2,7.07e-3,8.71e-4
RMORE,
```

```
!*
!
!,rigidity
R,10,2.69E-01,3.37E+05,500,3.37E+08,,,
RMORE
!
N,48,0,10.8
N,49,0,10.8
N,55,4.8,10.8
N,56,4.8,10.8
FILL,30,48,5,43,1,1,1,1,
FILL,49,55,5,50,1,1,1,1,
FILL,56,36,5,57,1,1,1,1,
!
!
!,Columns
TYPE,2
REAL,9
E,30,43
E,43,44
E,44,45
E,45,46
E,46,47
E,47,48
!
E,56,57
E,57,58
E,58,59
E,59,60
E,60,61
E,61,37
!
!
!,Beam
TYPE,1
REAL,8
E,49,50
E,50,51
E,51,52
E,52,53
E,53,54
E,54,55
!
!,Beam-column
TYPE,4
REAL,10
E,48,49
E,55,56
!
!
!,COUPLED RESTRICTIONS
CP,9,UX,48,49
CP,10,UY,48,49
CP,11,UX,55,56
CP,12,UY,55,56
!,,,,,,,,,
!,FOR NON-SWAY ADD...
D,55, , , , , ,UX,,
!
!F,49,FY,-5.00E+05
!F,55,FY,-5.00E+05
```

```
F,51,FY,-1.00E+06
F,53,FY,-1.00E+06
!F,49,FX,-3.00E+05
!
!*****************************************************************
!,forth STOREY
/PREP7
!,beam elements are r=,11
!,column elements are r=,12
!,beam-column are r=,13
!
!*                BEAM
!*
!,section properties,,,,,,,,
R,11,0.463,4.84E-02,7.61E-03,3.18E-03, , ,
RMORE,
!
!*    Column
!,section properties
R,12,0.260,5.56e-2,7.07e-3,8.71e-4
RMORE,
!*
!
!,rigidity
R,13,2.69E-01,3.37E+05,500,3.37E+08,,,
RMORE
!
N,67,0,14.4
N,68,0,14.4
N,74,4.8,14.4
N,75,4.8,14.4
FILL,49,67,5,62,1,1,1,1,
FILL,68,74,5,69,1,1,1,1,
FILL,75,55,5,76,1,1,1,1,
!
!
!,Columns
TYPE,2
REAL,12
E,49,62
E,62,63
E,63,64
E,64,65
E,65,66
E,66,67
!
E,75,76
E,76,77
E,77,78
E,78,79
E,79,80
E,80,56
!
!
!,Beam
TYPE,1
REAL,11
E,68,69
E,69,70
E,70,71
E,71,72
```

```
E,72,73
E,73,74
!
!,Beam-column
TYPE,4
REAL,13
E,67,68
E,74,75
!
!
!,COUPLED RESTRICTIONS
CP,13,UX,67,68
CP,14,UY,67,68
CP,15,UX,74,75
CP,16,UY,74,75
!
!,FOR NON-SWAY ADD...
D,74, , , , , ,UX,,
!
!F,68,FY,-5.00E+05
!F,74,FY,-5.00E+05
F,70,FY,-1.00E+06
F,72,FY,-1.00E+06
!F,68,FX,-3.00E+05
!
!*****************************************************************
!,fifth STOREY
/PREP7
!,beam elements are r=,14
!,column elements are r=,15
!,beam-column are r=,16
!
!*                BEAM
!*
!,section properties
R,14,0.463,4.84E-02,7.61E-03,3.18E-03, , ,
RMORE,
!,,,,,,,,,
!*    Column
!,section properties
R,15,0.260,5.56e-2,7.07e-3,8.71e-4
RMORE,
!*
!
!,rigidity
R,16,2.69E-01,3.37E+05,500,3.37E+08,,,
RMORE
!
N,86,0,18
N,87,0,18
N,93,4.8,18
N,94,4.8,18
FILL,68,86,5,81,1,1,1,1,
FILL,87,93,5,88,1,1,1,1,
FILL,94,74,5,95,1,1,1,1,
!
!
!,Columns
TYPE,2
REAL,15
E,68,81
```

```
E,81,82
E,82,83
E,83,84
E,84,85
E,85,86
!
E,94,95
E,95,96
E,96,97
E,97,98
E,98,99
E,99,75
!
!
!,Beam
TYPE,1
REAL,14
E,87,88
E,88,89
E,89,90
E,90,91
E,91,92
E,92,93
!
!,Beam-column
TYPE,4
REAL,16
E,86,87
E,93,94
!
!
!,COUPLED RESTRICTIONS
CP,17,UX,86,87
CP,18,UY,86,87
CP,19,UX,93,94
CP,20,UY,93,94
!
!,FOR NON-SWAY ADD...
D,93, , , , , ,UX,,
!
F,87,FY,-5.00E+05
F,93,FY,-5.00E+05
F,89,FY,-1.00E+06
F,91,FY,-1.00E+06
F,87,FX,3.00E+05
```

A set of stiffness files:

```
!Column base stiffness
/PREP7
R,3,32e-3,338.25e3,1,338.25e3,,,
RMORE,
FINISH

!Beam-to-column stiffnesses
/PREP7
R,4,32e-3,338.25e3,1,338.25e3,,,
RMORE,
FINISH
```

```
!Beam-to-column stiffnesses
/PREP7
R,7,32e-3,338.25e3,1,338.25e3,,,
RMORE,
FINISH

!Beam-to-column stiffnesses
/PREP7
R,10,32e-3,338.25e3,1,338.25,,,
RMORE,
FINISH

!Beam-to-column stiffnesses
/PREP7
R,13,32e-3,338.25e3,1,338.25,,,
RMORE,
FINISH

!Beam-to-column stiffnesses
/PREP7
R,16,32e-3,338.25e3,1,338.25,,,
RMORE,
FINISH
```

The solution parameters:

```
/SOLU
!*                        Analysis options
NLGEOM,1
NROPT,FULL, ,ON
LUMPM,0
EQSLV,FRONT,1e-08,0,
SSTIF
PSTRES
TOFFST,0,

!*                       Time and time step options
TIME,1000
!*                 ON-automatic  OFF- not automatic time step
AUTOTS,ON
!*   for automatic step size
DELTIM,1,0.5,50,OFF
!PRED,ON

!DELTIM,1

KBC,0
!*                       max. no. of iterations
NEQIT,80,
!*                       do not terminate analyses after non converging
solution
!*                 if UX,UY,ROTZ if higher than 0.024 than stop. (10m)
NCNV,2,0.024,0,0,0,

CNVTOL,F, ,0.001,2,-1,

!*                         output controls
OUTRES,ALL,ALL,
```

```
OUTPR,BASIC,NONE,
/STAT,SOLU
SOLVE
```

C.2 The Results

The following lists all the five-storey frame results. The results are given as tables as they were in the main text of the thesis. The title of each frame gives the frame number, and the sway/non-sway behaviour of the frame. The strength ratio is the value given in the tables.

Table C.1 Frame 1, Non-Sway, Strength Ratio

	Phi Beam-to-Column mRad										
Phi Column	pinned	256	128	64	32	16	8	4	2	1	fixed
pinned	0.635931	0.662363	0.685176	0.721713	0.775715	0.846614	0.919688	0.970518	0.987618	0.993961	1.000691
256	0.635931	0.662363	0.685176	0.721713	0.775715	0.846614	0.919688	0.970518	0.987618	0.993961	1.000854
128	0.635931	0.662363	0.685176	0.721713	0.775715	0.846614	0.919688	0.970518	0.987984	0.993961	1.000691
64	0.635931	0.662363	0.685176	0.721713	0.775715	0.846614	0.919688	0.970762	0.987984	0.993961	1.000854
32	0.635931	0.662363	0.685176	0.721713	0.775715	0.846614	0.919688	0.970742	0.987414	0.993961	1.001342
16	0.635931	0.662363	0.685176	0.721713	0.775715	0.846614	0.919688	0.970254	0.988085	0.994978	1.000407
8	0.635931	0.662363	0.685176	0.721713	0.775715	0.846614	0.919688	0.970966	0.988248	0.994978	1.000366
4	0.635931	0.662363	0.685176	0.721713	0.775715	0.846614	0.919688	0.970254	0.988248	0.994978	1.000895
2	0.635931	0.662363	0.685176	0.721713	0.775715	0.846614	0.919688	0.970274	0.988248	0.994978	1.000386
1	0.635931	0.662363	0.685176	0.721713	0.775715	0.846614	0.919688	0.970518	0.988248	0.993961	1
fixed	0.635931	0.662363	0.685176	0.721713	0.775715	0.846614	0.919688	0.970518	0.988248	0.994734	1

Table C.2 Frame 2, Non-Sway, Strength Ratio

	Phi Beam-to-Column mRad										
Phi Column	pinned	256	128	64	32	16	8	4	2	1	fixed
pinned	0.509684	0.545654	0.575584	0.627345	0.699487	0.782899	0.860305	0.918275	0.95519	0.976279	1
256	0.509684	0.545654	0.575584	0.627345	0.699487	0.782899	0.860305	0.918275	0.95519	0.976279	1
128	0.509684	0.545654	0.575584	0.627345	0.699487	0.782899	0.860305	0.918275	0.95519	0.976279	1
64	0.509684	0.545654	0.575584	0.627345	0.699487	0.782899	0.860305	0.918275	0.95519	0.976279	1
32	0.509684	0.545654	0.575584	0.627345	0.699487	0.782899	0.860305	0.918275	0.95519	0.976279	1
16	0.509684	0.545654	0.575584	0.627345	0.699487	0.782899	0.860305	0.918275	0.95519	0.976279	1
8	0.509684	0.545654	0.575584	0.627345	0.699487	0.782899	0.860305	0.918275	0.95519	0.976279	1
4	0.509684	0.545654	0.575584	0.627345	0.699487	0.782899	0.860305	0.918275	0.95519	0.976279	1
2	0.509684	0.545654	0.575584	0.627345	0.699487	0.782899	0.860305	0.918275	0.95519	0.976279	1
1	0.509684	0.545654	0.575584	0.627345	0.699487	0.782899	0.860305	0.918275	0.95519	0.976279	1
fixed	0.509684	0.545654	0.575584	0.627345	0.699487	0.782899	0.860305	0.918275	0.95519	0.976279	1

Table C.3 Frame 3, Non-Sway, Strength Ratio

	Phi Beam-to-Column mRad										
Phi Column	pinned	256	128	64	32	16	8	4	2	1	fixed
pinned	0.720901	0.740054	0.756258	0.783916	0.823538	0.872148	0.920781	0.960379	0.983151	0.992809	1.001798
256	0.720901	0.740054	0.756258	0.783916	0.823538	0.872148	0.920781	0.960379	0.983151	0.992809	1.001152
128	0.720901	0.740054	0.756258	0.783916	0.823538	0.872148	0.920781	0.960379	0.983151	0.992809	1.001152
64	0.720901	0.740054	0.756258	0.783916	0.823538	0.872148	0.920781	0.960379	0.983151	0.992809	1.001152
32	0.720901	0.740054	0.756258	0.783916	0.823538	0.872148	0.920781	0.960379	0.983151	0.992163	1.001152
16	0.720901	0.740054	0.756258	0.783916	0.823538	0.872148	0.920781	0.960379	0.983151	0.992163	1
8	0.720901	0.740054	0.756258	0.783916	0.823538	0.872148	0.920781	0.960379	0.981999	0.992163	1
4	0.720901	0.740054	0.756258	0.783916	0.823538	0.872148	0.920781	0.960379	0.981999	0.991011	1
2	0.720901	0.740054	0.756258	0.783916	0.823538	0.872148	0.920781	0.960379	0.981999	0.991011	1
1	0.720901	0.740054	0.756258	0.783916	0.823538	0.872148	0.920781	0.960379	0.981999	0.991011	1
fixed	0.720901	0.740054	0.756258	0.783916	0.823538	0.872148	0.920781	0.959734	0.981999	0.991011	1

Table C.4 Frame 4, Non-Sway, Strength Ratio

	Phi Beam-to-Column mRad										
Phi Column	pinned	256	128	64	32	16	8	4	2	1	fixed
pinned	0.479521	0.502174	0.523499	0.561394	0.622795	0.708077	0.805149	0.888828	0.944696	0.951963	1
256	0.479521	0.502174	0.523499	0.561394	0.622795	0.708077	0.805149	0.888828	0.944696	0.951963	1
128	0.479521	0.502174	0.523499	0.561394	0.622795	0.708077	0.805149	0.888828	0.944696	0.951963	1
64	0.479521	0.502174	0.523499	0.561394	0.622795	0.708077	0.805149	0.888828	0.944696	0.952555	1
32	0.479521	0.502174	0.523499	0.561394	0.622795	0.708077	0.805149	0.888828	0.944696	0.952555	1
16	0.479521	0.502174	0.523499	0.561394	0.622795	0.708077	0.805149	0.888987	0.944696	0.952555	1
8	0.479521	0.502174	0.523499	0.561394	0.622795	0.708077	0.805149	0.888741	0.944696	0.952555	1
4	0.479521	0.502174	0.523499	0.561394	0.622795	0.708077	0.805149	0.888741	0.944696	0.952555	1
2	0.479521	0.502174	0.523499	0.561394	0.622795	0.708077	0.805149	0.888741	0.944696	0.952555	1
1	0.479521	0.502174	0.523499	0.561394	0.622795	0.708077	0.805149	0.889492	0.944696	0.952555	1
fixed	0.479521	0.502174	0.523499	0.561394	0.622795	0.708077	0.805149	0.889492	0.944696	0.952555	1

Table C.5 Frame 1, Sway, Strength Ratio

	Phi Beam-to-Column mRad										
Phi Column	pinned	256	128	64	32	16	8	4	2	1	fixed
pinned	0	0.086769	0.109538	0.150491	0.21862	0.321025	0.446992	0.575091	0.678947	0.740878	0.78734
256	0.075096	0.099415	0.122764	0.163626	0.233119	0.335183	0.464074	0.595698	0.701085	0.765148	0.812621
128	0.08561	0.109538	0.132887	0.174569	0.243521	0.348001	0.479024	0.61278	0.720298	0.786493	0.833119
64	0.100782	0.125683	0.148301	0.18989	0.259936	0.365848	0.501735	0.639154	0.75233	0.818525	0.867966
32	0.118295	0.143926	0.167181	0.20877	0.28238	0.391484	0.5324	0.677581	0.796387	0.863347	0.908634
16	0.135806	0.161436	0.185515	0.22847	0.303998	0.419224	0.566564	0.719533	0.8455	0.911695	0.946623
8	0.148301	0.174569	0.200014	0.244888	0.323157	0.442729	0.596463	0.756594	0.886851	0.945858	0.975293
4	0.157058	0.183326	0.20877	0.256104	0.335948	0.459045	0.617809	0.784361	0.916724	0.965071	0.988466
2	0.161436	0.18907	0.213969	0.261303	0.343737	0.468337	0.630627	0.800678	0.931673	0.972259	0.994971
1	0.163626	0.191257	0.217254	0.265954	0.348001	0.473968	0.637022	0.80997	0.938096	0.975758	0.997868
fixed	0.165815	0.194269	0.220536	0.269237	0.352264	0.479024	0.645577	0.819891	0.94236	0.978655	1

Table C.6 Frame 2, Sway, Strength Ratio

	Phi Beam-to-Column mRad										
Phi Column	pinned	256	128	64	32	16	8	4	2	1	fixed
pinned	0	0.079046	0.105913	0.156378	0.229747	0.328999	0.437485	0.53182	0.595524	0.636749	0.682509
256	0.061196	0.094735	0.122686	0.173145	0.248616	0.352585	0.464011	0.560118	0.63086	0.673322	0.722261
128	0.07159	0.105913	0.134164	0.184476	0.261196	0.366731	0.482291	0.584287	0.658009	0.700942	0.751531
64	0.086502	0.117097	0.147992	0.198304	0.280059	0.390318	0.513539	0.61967	0.696349	0.742344	0.797527
32	0.100324	0.131219	0.16182	0.217167	0.300701	0.416843	0.545972	0.659187	0.742344	0.792933	0.852768
16	0.108857	0.145047	0.17609	0.229747	0.319564	0.442203	0.577214	0.696349	0.783746	0.838987	0.903357
8	0.117097	0.153433	0.184476	0.242326	0.333716	0.456938	0.598469	0.726855	0.818905	0.875795	0.944759
4	0.120041	0.156378	0.189918	0.248616	0.341378	0.468145	0.612603	0.745289	0.838987	0.898763	0.97073
2	0.122686	0.159323	0.192862	0.251961	0.346095	0.475218	0.622615	0.754476	0.852768	0.912603	0.984511
1	0.122686	0.16182	0.192862	0.251961	0.347868	0.478163	0.626737	0.760718	0.857362	0.920141	0.990813
fixed	0.12563	0.16182	0.195359	0.254906	0.350813	0.482291	0.63086	0.765371	0.8649	0.926384	1

Table C.7 Frame 3, Sway, Strength Ratio

	Phi Beam-to-Column mRad										
Phi Column	pinned	256	128	64	32	16	8	4	2	1	fixed
pinned	0	0.06584	0.087729	0.123744	0.183654	0.267457	0.36874	0.468476	0.549156	0.602052	0.668839
256	0.055699	0.079365	0.101435	0.138958	0.198988	0.284929	0.390112	0.495298	0.579789	0.635428	0.707808
128	0.06584	0.08951	0.111577	0.148589	0.210401	0.297767	0.407245	0.51578	0.60483	0.663283	0.738406
64	0.079365	0.102942	0.125525	0.163803	0.226444	0.317383	0.432286	0.546377	0.64102	0.704994	0.785709
32	0.092801	0.118159	0.140739	0.17902	0.244636	0.340557	0.461886	0.585346	0.687326	0.756892	0.845943
16	0.104723	0.129568	0.152394	0.193282	0.261751	0.361972	0.489741	0.621536	0.731852	0.807972	0.902579
8	0.113087	0.138958	0.16178	0.204695	0.274589	0.377289	0.510223	0.649355	0.766225	0.84694	0.944326
4	0.118159	0.144785	0.167607	0.210401	0.282429	0.387618	0.524115	0.666061	0.788488	0.871981	0.971148
2	0.121721	0.146566	0.171411	0.215035	0.28671	0.394422	0.532486	0.677175	0.801418	0.88769	0.986073
1	0.121963	0.148589	0.173192	0.216107	0.289207	0.396203	0.535264	0.682731	0.807972	0.894244	0.99341
fixed	0.123744	0.15037	0.175216	0.218957	0.291704	0.400477	0.540821	0.688324	0.81531	0.902579	1

Table C.8 Frame 4, Sway, Strength Ratio

	Phi Beam-to-Column mRad										
Phi Column	pinned	256	128	64	32	16	8	4	2	1	fixed
pinned	0	0.079204	0.098966	0.134087	0.194529	0.286167	0.40724	0.535554	0.643974	0.712006	0.781332
256	0.075753	0.096338	0.114943	0.150761	0.211203	0.30539	0.430072	0.562665	0.674693	0.743373	0.810248
128	0.08777	0.107532	0.127372	0.162572	0.223942	0.320495	0.447004	0.583692	0.699352	0.766875	0.834883
64	0.102593	0.123666	0.14335	0.179477	0.242239	0.341522	0.473444	0.615059	0.736155	0.801203	0.871686
32	0.119963	0.140342	0.160719	0.197775	0.264469	0.367476	0.504835	0.654823	0.781332	0.844576	0.916216
16	0.132931	0.155163	0.176699	0.215605	0.283692	0.390978	0.535554	0.693939	0.821096	0.876452	0.949387
8	0.142193	0.165582	0.186657	0.227876	0.298149	0.409045	0.56019	0.725307	0.85362	0.891557	0.971085
4	0.148908	0.171837	0.193373	0.235068	0.307194	0.421698	0.575318	0.745177	0.873491	0.899954	0.983738
2	0.151457	0.175542	0.197775	0.239463	0.312607	0.428267	0.58434	0.75783	0.886144	0.905367	0.990955
1	0.15331	0.176699	0.200088	0.241777	0.315082	0.431899	0.589776	0.764423	0.891557	0.907842	0.995744
fixed	0.155163	0.178321	0.201709	0.243396	0.318043	0.435508	0.595189	0.770483	0.898797	0.910803	1

Appendix D

Ten-Storey Model And Results

D.1 The Model

The following text shows the finite element model that was used for the ten-storey plastic modelling. For each frame the geometry file would be called, followed by one set of stiffness files. The solution parameters were then loaded, and the model solved. For the next frame the same geometry file would then be loaded followed by the next set of stiffness files.

The geometry file:

```
/PREP7
!
!,material property
!
UIMP,1,EX, , ,2.10E+11,
UIMP,1,DENS, , , ,
UIMP,1,ALPX, , , ,
UIMP,1,REFT, , , ,
UIMP,1,NUXY, , ,0.3,
UIMP,1,PRXY, , , ,
UIMP,1,GXY, , ,8.08E+10,
UIMP,1,MU, , , ,
UIMP,1,DAMP, , , ,
UIMP,1,KXX, , , ,
```

```
UIMP,1,C, , , ,
UIMP,1,ENTH, , , ,
UIMP,1,HF, , , ,
UIMP,1,EMIS, , , ,
UIMP,1,QRATE, , , ,
UIMP,1,MURX, , , ,
UIMP,1,MGXX, , , ,
UIMP,1,RSVX, , , ,
UIMP,1,PERX, , , ,
UIMP,1,VISC, , , ,
UIMP,1,SONC, , , ,
!*       data table yield stress Fy=275 MPa, E=0 after plasticity
TB,BKIN,1, , ,
TBMODIF,2,1,2.75E+08,,
!
!,FIRST STOREY
!
!,beam elements are r=,1
!,column elements are r=,2
!,base springs are r=,3
!,beam-column are r=,4
!
!
!*                BEAM
ET,1,BEAM23,,,
TYPE,1,
MAT,1,
REAL,1,
ESYS,0,
KEYOPT,1,2,0,,,,,
KEYOPT,1,4,1,,,,,
KEYOPT,1,6,4,,,,,
KEYOPT,1,10,0,,,,,
!*
!,section properties
R,1,0.463,4.84E-02,7.61E-03,3.18E-03, , ,
RMORE,
!
!
!*              COLUMN
ET,2,BEAM23,,,,,,
KEYOPT,2,2,0,,,,,
KEYOPT,2,4,1,,,,,
KEYOPT,2,6,4,,,,,
KEYOPT,2,10,0,,,,,
!*
!,section properties
R,2,0.260,5.56e-2,7.07e-3,8.71e-4, , ,
RMORE, ,,,,,,,
!*
!,,,,,,,,
!* ,,BASE SPRING
ET,3,COMBIN39,,,,,,
KEYOPT,3,1,0,,,,,
KEYOPT,3,2,0,,,,,
KEYOPT,3,3,6,,,,,
KEYOPT,3,4,0,,,,,
KEYOPT,3,6,0,,,,,
!
!,rigidity
R,3,1.55E-01,3.37E+05,500,3.37E+08,,,
```

```
RMORE
*
!
!,,BEAM TO COLUMN SPRING
ET,4,COMBIN39,,,,,,
KEYOPT,4,1,0,,,,,
KEYOPT,4,2,0,,,,,
KEYOPT,4,3,6,,,,,
KEYOPT,4,4,0,,,,,
KEYOPT,4,6,0,,,,,
!
!,rigidity
R,4,2.69E-01,3.37E+05,500,3.37E+08,,,
RMORE,
!
N,1,,,,,,,
N,2,,,,,,,
N,8,0,3.6,,,,,
N,9,0,3.6,,,,,
N,15,4.8,3.6,,,,,
N,16,4.8,3.6,,,,,
N,22,4.8,0,,,,,,
N,23,4.8,0,,,,,
FILL,2,8,5, ,1,1,1,1,
FILL,9,15,5, ,1,1,1,1,
FILL,16,22,5, ,1,1,1,1,
!
!
!,COLUMNS
TYPE,2,
REAL,2,
E,2,3
E,3,4
E,4,5
E,5,6
E,6,7
E,7,8
!,,
E,16,17
E,17,18
E,18,19
E,19,20
E,20,21
E,21,22
!,,
!,BEAM,
TYPE,1,
REAL,1,
E,9,10
E,10,11
E,11,12
E,12,13
E,13,14
E,14,15
!,,
!,BASE,
TYPE,3,
REAL,3,
E,1,2
E,22,23
!,,
```

```
!,BEAM-COLUMN,
TYPE,4,,,,,,
REAL,4,,,,,,
E,8,9,,,,,
E,15,16,,,,,
!,,,,,,,,
!,COUPLED RESTRICTIONS
CP,1,UX,8,9,,,,
CP,2,UY,8,9,,,,
CP,3,UX,15,16,,,,
CP,4,UY,15,16,,,,
!,,,,,,,,
!,BC'S,,,,,,,
D,1, , , , , ,ALL,
D,23, , , , , ,ALL,
!,,,,,,,,
D,2, , , , , ,UX,UY
D,22, , , , , ,UX,UY
!,,,,,,,,
!,FOR NON-SWAY ADD...
!D,15, , , , , ,UX,
!
/SOLU
!F,9,FY,-5.00E+05,,,,,
!F,15,FY,-5.00E+05,,,,,
F,11,FY,-1.00E+06,,,,,
F,13,FY,-1.00E+06,,,,,
!F,9,FX,-3.00E+05,,,,,
!
!*****************************************************************
!,SECOND STOREY
/PREP7
!,beam elements are r=,5
!,column elements are r=,6
!,beam-column are r=,7
!
!*      BEAM
!
!,section properties
R,5,0.463,4.84E-02,7.61E-03,3.18E-03, , ,
RMORE,
!
!*    Column
!,section properties
R,6,0.260,5.56e-2,7.07e-3,8.71e-4, , ,
RMORE,
!*
!
!,beam to column rigidity
R,7,2.69E-01,3.37E+05,500,3.37E+08,
RMORE,
!
N,29,0,7.2,,,,,
N,30,0,7.2,,,,,
N,36,4.8,7.2,,,,,
N,37,4.8,7.2,,,,,
FILL,9,29,5,24,1,1,1,1
FILL,30,36,5,31,1,1,1,1
FILL,37,15,5,38,1,1,1,1
!
!
```

```
!,Columns
TYPE,2,,,,,,
REAL,6,,,,,,
E,8,24,,,,,
E,24,25
E,25,26
E,26,27
E,27,28
E,28,29
!,,
E,37,38
E,38,39
E,39,40
E,40,41
E,41,42
E,42,16
!,,
!,,
!,Beam,
TYPE,1,
REAL,5,
E,30,31
E,31,32
E,32,33
E,33,34
E,34,35
E,35,36
!,,
!,Beam-column,
TYPE,4,
REAL,7,
E,29,30
E,36,37
!
!
!,COUPLED RESTRICTIONS,
CP,5,UX,29,30,,,
CP,6,UY,29,30,,,
CP,7,UX,36,37,,,
CP,8,UY,36,37,,,
!
!,FOR NON-SWAY ADD...
!D,36, , , , , ,UX
!
!F,30,FY,-5.00E+05,,,,
!F,36,FY,-5.00E+05,,,,
F,32,FY,-1.00E+06,,,,
F,34,FY,-1.00E+06,,,,
!F,30,FX,-3.00E+05,,,,
!
!*****************************************************************
!,Third STOREY
/PREP7
!,beam elements are r=,8,,,,,,,
!,column elements are r=,9,,,,,,,
!,beam-column are r=,10,,,,,,,
!,,,,,,,,,
!*                BEAM
!*
!,section properties,,,,,,,,
R,8,0.463,4.84E-02,7.61E-03,3.18E-03, , ,
```

```
RMORE,
!
!*    Column
!,section properties
R,9,0.260,5.56e-2,7.07e-3,8.71e-4, , ,
RMORE,
!*
!
!,rigidity
R,10,2.69E-01,3.37E+05,500,3.37E+08,,,
RMORE,
!
N,48,0,10.8
N,49,0,10.8
N,55,4.8,10.8
N,56,4.8,10.8
FILL,30,48,5,43,1,1,1,1,
FILL,49,55,5,50,1,1,1,1,
FILL,56,36,5,57,1,1,1,1,
!
!
!,Columns
TYPE,2
REAL,9
E,30,43
E,43,44
E,44,45
E,45,46
E,46,47
E,47,48
!
E,56,57
E,57,58
E,58,59
E,59,60
E,60,61
E,61,37
!
!
!,Beam
TYPE,1
REAL,8
E,49,50
E,50,51
E,51,52
E,52,53
E,53,54
E,54,55
!
!,Beam-column
TYPE,4,
REAL,10,
E,48,49,
E,55,56,
!
!
!,COUPLED RESTRICTIONS
CP,9,UX,48,49
CP,10,UY,48,49
CP,11,UX,55,56
CP,12,UY,55,56
```

```
!
!,FOR NON-SWAY ADD...
!D,55, , , , , ,UX,,
!
!F,49,FY,-5.00E+05
!F,55,FY,-5.00E+05
F,51,FY,-1.00E+06
F,53,FY,-1.00E+06
!F,49,FX,-3.00E+05
!
!*****************************************************************
!,forth STOREY
/PREP7
!,beam elements are r=,11
!,column elements are r=,12
!,beam-column are r=,13
!
!*                BEAM
!*
!,section properties
R,11,0.463,4.84E-02,7.61E-03,3.18E-03, , ,
RMORE,
!
!*    Column
!,section properties,,,,,,,,
R,12,0.260,5.56e-2,7.07e-3,8.71e-4, , ,
RMORE,
!*
!
!,rigidity
R,13,2.69E-01,3.37E+05,500,3.37E+08,,,
RMORE
!
N,67,0,14.4,,,,,,
N,68,0,14.4,,,,,,
N,74,4.8,14.4,,,,,,
N,75,4.8,14.4,,,,,,
FILL,49,67,5,62,1,1,1,1,
FILL,68,74,5,69,1,1,1,1,
FILL,75,55,5,76,1,1,1,1,
!
!
!,Columns
TYPE,2,,,,,,,,
REAL,12,,,,,,,,
E,49,62,,,,,,,
E,62,63,,,,,,,
E,63,64,,,,,,,
E,64,65,,,,,,,
E,65,66,,,,,,,
E,66,67,,,,,,,
!,,,,,,,,,
E,75,76,,,,,,,
E,76,77,,,,,,,
E,77,78,,,,,,,
E,78,79,,,,,,,
E,79,80,,,,,,,
E,80,56,,,,,,,
!,,,,,,,,,
!,,,,,,,,,
!,Beam,,,,,,,,
```

```
TYPE,1,,,,,,,
REAL,11,,,,,,,
E,68,69,,,,,,
E,69,70,,,,,,
E,70,71,,,,,,
E,71,72,,,,,,
E,72,73,,,,,,
E,73,74,,,,,,
!
!,Beam-column
TYPE,4,,,,,,,
REAL,13,,,,,,,
E,67,68,,,,,,
E,74,75,,,,,,
!
!
!,COUPLED RESTRICTIONS
CP,13,UX,67,68,,,,
CP,14,UY,67,68,,,,
CP,15,UX,74,75,,,,
CP,16,UY,74,75,,,,
!
!,FOR NON-SWAY ADD...
!D,74, , , , , ,UX,,
!,,,,,,,,,
!F,68,FY,-5.00E+05,,,,,
!F,74,FY,-5.00E+05,,,,,
F,70,FY,-1.00E+06,,,,,
F,72,FY,-1.00E+06,,,,,
!F,68,FX,-3.00E+05,,,,,
!,,,,,,,,,
!*****************************************************************
!,fifth STOREY
/PREP7
!,beam elements are r=,14
!,column elements are r=,15
!,beam-column are r=,16
!
!*                BEAM
!*
!,section properties,,,,,,,
R,14,0.463,4.84E-02,7.61E-03,3.18E-03, , ,
RMORE,
!
!*    Column
!,section properties
R,15,0.260,5.56e-2,7.07e-3,8.71e-4, , ,
RMORE,
!*
!
!,rigidity
R,16,2.69E-01,3.37E+05,500,3.37E+08,,,
RMORE,
!
N,86,0,18,,,,,
N,87,0,18,,,,,
N,93,4.8,18,,,,,
N,94,4.8,18,,,,,
FILL,68,86,5,81,1,1,1,1,
FILL,87,93,5,88,1,1,1,1,
FILL,94,74,5,95,1,1,1,1,
```

```
!
!
!,Columns
TYPE,2,,,,,,,,
REAL,15,,,,,,,,
E,68,81,,,,,,,
E,81,82,,,,,,,
E,82,83,,,,,,,
E,83,84,,,,,,,
E,84,85,,,,,,,
E,85,86,,,,,,,
!
E,94,95,,,,,,,
E,95,96,,,,,,,
E,96,97,,,,,,,
E,97,98,,,,,,,
E,98,99,,,,,,,
E,99,75,,,,,,,
!
!
!,Beam
TYPE,1,,,,,,,,
REAL,14,,,,,,,,
E,87,88,,,,,,,
E,88,89,,,,,,,
E,89,90,,,,,,,
E,90,91,,,,,,,
E,91,92,,,,,,,
E,92,93,,,,,,,
!
!,Beam-column
TYPE,4,,,,,,,,
REAL,16,,,,,,,,
E,86,87,,,,,,,
E,93,94,,,,,,,
!
!
!,COUPLED RESTRICTIONS
CP,17,UX,86,87,,,,,
CP,18,UY,86,87,,,,,
CP,19,UX,93,94,,,,,
CP,20,UY,93,94,,,,,
!
!,FOR NON-SWAY ADD...
!D,93, , , , , ,UX,,
!
!F,87,FY,-5.00E+05,,,,,,
!F,93,FY,-5.00E+05,,,,,,
F,89,FY,-1.00E+06,,,,,,
F,91,FY,-1.00E+06,,,,,,
!F,87,FX,-3.00E+05,,,,,,
!
!*****************************************************************
!,sixth STOREY
/PREP7
!,beam elements are r=,17
!,column elements are r=,18
!,beam-column are r=,19
!
!*                BEAM
!*
```

```
!,section properties
R,17,0.463,4.84E-02,7.61E-03,3.18E-03, , ,              ,
RMORE,
!
!*    Column
!,section properties
R,18,0.260,5.56e-2,7.07e-3,8.71e-4, , ,
RMORE,
!*
!
!,rigidity
R,19,2.69E-01,3.37E+05,500,3.37E+08,,,
RMORE,
!
N,105,0,21.6,,,,,
N,106,0,21.6,,,,,
N,112,4.8,21.6,,,,,
N,113,4.8,21.6,,,,,
FILL,87,105,5,100,1,1,1,1
FILL,106,112,5,107,1,1,1,1
FILL,113,93,5,114,1,1,1,1
!
!
!,Columns
TYPE,2,,,,,,
REAL,18,,,,,,
E,87,100,,,,,
E,100,101,,,,,
E,101,102,,,,,
E,102,103,,,,,
E,103,104,,,,,
E,104,105,,,,,
!
E,113,114,,,,,
E,114,115,,,,,
E,115,116,,,,,
E,116,117,,,,,
E,117,118,,,,,
E,118,94,,,,,
!
!
!,Beam
TYPE,1,,,,,,
REAL,17,,,,,,
E,106,107,,,,,
E,107,108,,,,,
E,108,109,,,,,
E,109,110,,,,,
E,110,111,,,,,
E,111,112,,,,,
!
!,Beam-column
TYPE,4,,,,,,
REAL,19,,,,,,
E,105,106,,,,,
E,112,113,,,,,
!
!
!,COUPLED RESTRICTIONS
CP,21,UX,105,106,,,
CP,22,UY,105,106,,,
```

```
CP,23,UX,112,113
CP,24,UY,112,113
!
!,FOR NON-SWAY ADD...
!D,112, , , , , ,UX,
!
!F,106,FY,-5.00E+05
!F,112,FY,-5.00E+05
F,108,FY,-1.00E+06
F,110,FY,-1.00E+06
!F,106,FX,-3.00E+05
!
!*****************************************************************
!,seventh STOREY
/PREP7
!,beam elements are r=,20
!,column elements are r=,21
!,beam-column are r=,22
!
!*                BEAM
!*
!,section properties
R,20,0.463,4.84E-02,7.61E-03,3.18E-03, , ,
RMORE,
!
!*    Column
!,section properties
R,21,0.260,5.56e-2,7.07e-3,8.71e-4, , ,
RMORE,
!*
!
!,rigidity
R,22,2.69E-01,3.37E+05,500,3.37E+08,,,
RMORE
!
N,124,0,25.2
N,125,0,25.2
N,131,4.8,25.2
N,132,4.8,25.2
FILL,106,124,5,119,1,1,1,1
FILL,125,131,5,126,1,1,1,1
FILL,132,112,5,133,1,1,1,1
!
!
!,Columns
TYPE,2
REAL,21
E,106,119,,,,,
E,119,120,,,,,
E,120,121,,,,,
E,121,122,,,,,
E,122,123,,,,,
E,123,124,,,,,
!
E,132,133,,,,,
E,133,134,,,,,
E,134,135,,,,,
E,135,136,,,,,
E,136,137,,,,,
E,137,113,,,,,
!
```

```
!
!,Beam
TYPE,1
REAL,20
E,125,126,,,,,
E,126,127,,,,,
E,127,128,,,,,
E,128,129,,,,,
E,129,130,,,,,
E,130,131,,,,,
!
!,Beam-column
TYPE,4,,,,,,
REAL,22,,,,,,
E,124,125,,,,,
E,131,132,,,,,
!
!
!,COUPLED RESTRICTIONS
CP,25,UX,124,125,,,,
CP,26,UY,124,125,,,,
CP,27,UX,131,132,,,,
CP,28,UY,131,132,,,,
!
!,FOR NON-SWAY ADD...
!D,131, , , , , ,UX,
!
!F,125,FY,-5.00E+05,,,,,
!F,131,FY,-5.00E+05,,,,,
F,127,FY,-1.00E+06,,,,,
F,129,FY,-1.00E+06,,,,,
!F,125,FX,-3.00E+05,,,,,
!
!*****************************************************************
!,eight STOREY
/PREP7
!,beam elements are r=,23
!,column elements are r=,24
!,beam-column are r=,25
!
!*                BEAM
!*
!,section properties
R,23,0.463,4.84E-02,7.61E-03,3.18E-03, , ,
RMORE,
!
!*    Column
!,section properties
R,24,0.260,5.56e-2,7.07e-3,8.71e-4, , ,
RMORE,
!*
!
!,rigidity
R,25,2.69E-01,3.37E+05,500,3.37E+08,,,
RMORE
!
N,143,0,28.8,,,,,
N,144,0,28.8,,,,,
N,150,4.8,28.8,,,,,
N,151,4.8,28.8,,,,,
FILL,125,143,5,138,1,1,1,1
```

```
FILL,144,150,5,145,1,1,1,1
FILL,151,131,5,152,1,1,1,1
!
!
!,Columns
TYPE,2
REAL,24
E,125,138,,,,,
E,138,139,,,,,
E,139,140,,,,,
E,140,141,,,,,
E,141,142,,,,,
E,142,143,,,,,
!
E,151,152,,,,,
E,152,153,,,,,
E,153,154,,,,,
E,154,155,,,,,
E,155,156,,,,,
E,156,132,,,,,
!
!
!,Beam
TYPE,1
REAL,23
E,144,145,,,,,
E,145,146,,,,,
E,146,147,,,,,
E,147,148,,,,,
E,148,149,,,,,
E,149,150,,,,,
!
!,Beam-column
TYPE,4,,,,,,
REAL,25,,,,,,
E,143,144,,,,,
E,150,151,,,,,
!
!
!,COUPLED RESTRICTIONS
CP,29,UX,143,144,,,,
CP,30,UY,143,144,,,,
CP,31,UX,150,151,,,,
CP,32,UY,150,151,,,,
!
!,FOR NON-SWAY ADD...
!D,150, , , , , ,UX,
!
!F,144,FY,-5.00E+05,,,,,
!F,150,FY,-5.00E+05,,,,,
F,146,FY,-1.00E+06,,,,,
F,148,FY,-1.00E+06,,,,,
!F,144,FX,-3.00E+05,,,,,
!
!*****************************************************************
!,nineth STOREY
/PREP7
!,beam elements are r=,26
!,column elements are r=,27
!,beam-column are r=,28
!
```

```
!*                BEAM
!*
!,section properties
R,26,0.463,4.84E-02,7.61E-03,3.18E-03, , ,
RMORE,
!
!*    Column
!,section properties
R,27,0.260,5.56e-2,7.07e-3,8.71e-4, , ,
RMORE,
!*
!
!,rigidity
R,28,2.69E-01,3.37E+05,500,3.37E+08,,,
RMORE,
!
N,162,0,32.4,,,,,
N,163,0,32.4,,,,,
N,169,4.8,32.4,,,,,
N,170,4.8,32.4,,,,,
FILL,144,162,5,157,1,1,1,1
FILL,163,169,5,164,1,1,1,1
FILL,170,150,5,171,1,1,1,1
!
!
!,Columns
TYPE,2
REAL,27
E,144,157,,,,,,
E,157,158,,,,,,
E,158,159,,,,,,
E,159,160,,,,,,
E,160,161,,,,,,
E,161,162,,,,,,
!
E,170,171,,,,,,
E,171,172,,,,,,
E,172,173,,,,,,
E,173,174,,,,,,
E,174,175,,,,,,
E,175,151,,,,,,
!
!
!,Beam
TYPE,1,,,,,,,
REAL,26,,,,,,,
E,163,164,,,,,,
E,164,165,,,,,,
E,165,166,,,,,,
E,166,167,,,,,,
E,167,168,,,,,,
E,168,169,,,,,,
!
!,Beam-column
TYPE,4,,,,,,,
REAL,28,,,,,,,
E,162,163,,,,,,
E,169,170,,,,,,
!
!
!,COUPLED RESTRICTIONS
```

```
CP,33,UX,162,163,,,,
CP,34,UY,162,163,,,,
CP,35,UX,169,170,,,,
CP,36,UY,169,170,,,,
!
!,FOR NON-SWAY ADD...
!D,169, , , , , ,UX,
!
!F,163,FY,-5.00E+05,,,,,
!F,169,FY,-5.00E+05,,,,,
F,165,FY,-1.00E+06,,,,,
F,167,FY,-1.00E+06,,,,,
!F,163,FX,-3.00E+05,,,,,
!
!*****************************************************************
!,tenth STOREY
/PREP7
!,beam elements are r=,29
!,column elements are r=,30
!,beam-column are r=,31
!
!*                BEAM
!*
!,section properties
R,29,0.463,4.84E-02,7.61E-03,3.18E-03, , ,
RMORE,
!
!*    Column
!,section properties
R,30,0.260,5.56e-2,7.07e-3,8.71e-4, , ,
RMORE,
!*
!
!,rigidity
R,31,2.69E-01,3.37E+05,500,3.37E+08,,,
RMORE
!
N,181,0,36,,,,,
N,182,0,36,,,,,
N,188,4.8,36,,,,,
N,189,4.8,36,,,,,
FILL,163,181,5,176,1,1,1,1
FILL,182,188,5,183,1,1,1,1
FILL,189,169,5,190,1,1,1,1
!
!
!,Columns
TYPE,2
REAL,30
E,163,176,,,,,,
E,176,177,,,,,,
E,177,178,,,,,,
E,178,179,,,,,,
E,179,180,,,,,,
E,180,181,,,,,,
!
E,189,190,,,,,,
E,190,191,,,,,,
E,191,192,,,,,,
E,192,193,,,,,,
E,193,194,,,,,,
```

```
E,194,170,,,,,
!
!
!,Beam
TYPE,1
REAL,29
E,182,183,,,,,
E,183,184,,,,,
E,184,185,,,,,
E,185,186,,,,,
E,186,187,,,,,
E,187,188,,,,,
!
!,Beam-column
TYPE,4
REAL,31
E,181,182,,,,,
E,188,189,,,,,
!
!
!,COUPLED RESTRICTIONS
CP,37,UX,181,182,,,,
CP,38,UY,181,182,,,,
CP,39,UX,188,189,,,,
CP,40,UY,188,189,,,,
!
!,FOR NON-SWAY ADD...
!D,188, , , , , ,UX,
!
F,182,FY,-5.00E+05,,,,
F,188,FY,-5.00E+05,,,,
F,184,FY,-1.00E+06,,,,
F,186,FY,-1.00E+06,,,,
F,182,FX,3.00E+05,,,,

FINISH
```

A set of stiffness files:

```
!Column base stiffness
/PREP7
R,3,32e-3,338.25e3,1,338.25e3,,,
RMORE, , , , , , ,
FINISH

!Beam-to-column stiffnesses
/PREP7
R,4,32e-3,338.25e3,1,338.25e3,,,
RMORE, , , , , , ,
FINISH

!Beam-to-column stiffnesses
/PREP7
R,7,32e-3,338.25e3,1,338.25e3,,,
RMORE, , , , , , ,
FINISH

!Beam-to-column stiffnesses
```

```
/PREP7
R,10,32e-3,338.25e3,1,338.25,,,
RMORE, , , , , , ,
FINISH

!Beam-to-column stiffnesses
/PREP7
R,13,32e-3,338.25e3,1,338.25,,,
RMORE, , , , , , ,
FINISH

!Beam-to-column stiffnesses
/PREP7
R,16,32e-3,338.25e3,1,338.25,,,
RMORE, , , , , , ,
FINISH

/prep7,,,,,
r,19,3.20E-02,338250,1,338250

/prep7,,,,,
r,22,3.20E-02,338250,1,338250

/prep7,,,,,
r,25,3.20E-02,338250,1,338250

/prep7,,,,,
r,28,3.20E-02,338250,1,338250

/prep7,,,,,
r,31,3.20E-02,338250,1,338250
```

The solution parameters:

```
/SOLU
!*                          Analysis options
NLGEOM,1
NROPT,FULL, ,ON
LUMPM,0
EQSLV,FRONT,1e-08,0,
SSTIF
PSTRES
TOFFST,0,

!*                        Time and time step options
TIME,1000
!*                  ON-automatic  0FF- not automatic time step
AUTOTS,ON
!*   for automatic step size
DELTIM,1,0.5,50,OFF
!PRED,ON

!DELTIM,1

KBC,0
!*                        max. no. of iterations
NEQIT,80,
!*                        do not terminate analyses after non converging
solution
```

```
!*                  if UX,UY,ROTZ if higher than 0.024 than stop. (10m)
NCNV,2,0.024,0,0,0,

CNVTOL,F, ,0.001,2,-1,

!*                              output controls
OUTRES,ALL,ALL,
OUTPR,BASIC,NONE,
/STAT,SOLU
SOLVE
```

D.2 The Results

The following lists all the ten-storey frame results. The results are given as tables as they were in the main text of the thesis. The title of each frame gives the frame number, and the sway/non-sway behaviour of the frame. The strength ratio is the value given in the tables.

Table D.1 Frame 1, Non-Sway, Strength Ratio

	Phi Beam-to-Column mRad										
Phi Column	pinned	256	128	64	32	16	8	4	2	1	fixed
pinned	0.800955	0.81515	0.825842	0.843585	0.87202	0.906324	0.938308	0.963194	0.978662	0.989354	1
256	0.800955	0.81515	0.825842	0.843585	0.87202	0.906324	0.938308	0.963194	0.978662	0.989354	1
128	0.800955	0.81515	0.825842	0.843585	0.87202	0.906324	0.938308	0.963194	0.978662	0.989354	1
64	0.800955	0.81515	0.825842	0.843585	0.87202	0.906324	0.938308	0.963194	0.978662	0.989354	1
32	0.800955	0.81515	0.825842	0.843585	0.87202	0.906324	0.938308	0.963194	0.978662	0.989354	1
16	0.800955	0.81515	0.825842	0.843585	0.87202	0.906324	0.938308	0.963194	0.978662	0.989354	1
8	0.800955	0.81515	0.825842	0.843585	0.87202	0.906324	0.938308	0.963194	0.978662	0.989354	1
4	0.800955	0.81515	0.825842	0.843585	0.87202	0.906324	0.938308	0.963194	0.978662	0.989354	1
2	0.800955	0.81515	0.825842	0.843585	0.87202	0.906324	0.938308	0.963194	0.978662	0.989354	1
1	0.800955	0.81515	0.825842	0.843585	0.87202	0.906324	0.938308	0.963194	0.978662	0.989354	1
fixed	0.800955	0.81515	0.825842	0.843585	0.87202	0.906324	0.938308	0.963194	0.978662	0.989354	1

Table D.2 Frame 2, Non-Sway, Strength Ratio

	Phi Beam-to-Column mRad										
Phi Column	pinned	256	128	64	32	16	8	4	2	1	fixed
pinned	0.64878	0.68094	0.709648	0.749258	0.806008	0.865847	0.914845	0.952698	0.974623	0.985828	1
256	0.64878	0.68094	0.709648	0.749258	0.806008	0.865847	0.914845	0.952698	0.974623	0.985828	1
128	0.64878	0.68094	0.709648	0.749258	0.806008	0.865847	0.914845	0.952698	0.974623	0.985828	1
64	0.64878	0.68094	0.709648	0.749258	0.806008	0.865847	0.914845	0.952698	0.974623	0.985828	1
32	0.64878	0.68094	0.709648	0.749258	0.806008	0.865847	0.914845	0.952698	0.974623	0.985828	1
16	0.64878	0.68094	0.709648	0.749258	0.806008	0.865847	0.914845	0.952698	0.974623	0.985828	1
8	0.64878	0.68094	0.709648	0.749258	0.806008	0.865847	0.914845	0.952698	0.974623	0.985828	1
4	0.64878	0.68094	0.709648	0.749258	0.806008	0.865847	0.914845	0.952698	0.974623	0.985828	1
2	0.64878	0.68094	0.709648	0.749258	0.806008	0.865847	0.914845	0.952698	0.974623	0.985828	1
1	0.64878	0.68094	0.709648	0.749258	0.806008	0.865847	0.914845	0.952698	0.974623	0.985828	1
fixed	0.64878	0.68094	0.709648	0.749258	0.806008	0.865847	0.914845	0.952698	0.974623	0.985828	1

Table D.3 Frame 3, Non-Sway, Strength Ratio

	Phi Beam-to-Column mRad										
Phi Column	pinned	256	128	64	32	16	8	4	2	1	fixed
pinned	0.861743	0.869413	0.877083	0.891096	0.910271	0.93333	0.956389	0.973106	0.98466	0.99233	1
256	0.861743	0.869413	0.877083	0.891096	0.910271	0.93333	0.956389	0.973106	0.98466	0.99233	1
128	0.861743	0.869413	0.877083	0.891096	0.910271	0.93333	0.956389	0.973106	0.98466	0.99233	1
64	0.861743	0.869413	0.877083	0.891096	0.910271	0.93333	0.956389	0.973106	0.98466	0.99233	1
32	0.861743	0.869413	0.877083	0.891096	0.910271	0.93333	0.956389	0.973106	0.98466	0.99233	1
16	0.861743	0.869413	0.877083	0.891096	0.910271	0.93333	0.956389	0.973106	0.98466	0.99233	1
8	0.861743	0.869413	0.877083	0.891096	0.910271	0.93333	0.956389	0.973106	0.98466	0.99233	1
4	0.861743	0.869413	0.877083	0.891096	0.910271	0.93333	0.956389	0.973106	0.98466	0.99233	1
2	0.861743	0.869413	0.877083	0.891096	0.910271	0.93333	0.956389	0.973106	0.98466	0.99233	1
1	0.861743	0.869413	0.877083	0.891096	0.910271	0.93333	0.956389	0.973106	0.98466	0.99233	1
fixed	0.861743	0.869413	0.877083	0.891096	0.910271	0.93333	0.956389	0.973106	0.98466	0.99233	1

Table D.4 Frame 4, Non-Sway, Strength Ratio

	Phi Beam-to-Column mRad										
Phi Column	pinned	256	128	64	32	16	8	4	2	1	fixed
pinned	0.674504	0.691633	0.706861	0.733517	0.774719	0.828005	0.883217	0.927684	0.960041	0.978388	1
256	0.674504	0.691633	0.706861	0.733517	0.774719	0.828005	0.883217	0.927684	0.960041	0.978388	1
128	0.674504	0.691633	0.706861	0.733517	0.774719	0.828005	0.883217	0.927684	0.960041	0.978388	1
64	0.674504	0.691633	0.706861	0.733517	0.774719	0.828005	0.883217	0.927684	0.960041	0.978388	1
32	0.674504	0.691633	0.706861	0.733517	0.774719	0.828005	0.883217	0.927684	0.960041	0.978388	1
16	0.674504	0.691633	0.706861	0.733517	0.774719	0.828005	0.883217	0.927684	0.960041	0.978388	1
8	0.674504	0.691633	0.706861	0.733517	0.774719	0.828005	0.883217	0.927684	0.960041	0.978388	1
4	0.674504	0.691633	0.706861	0.733517	0.774719	0.828005	0.883217	0.927684	0.960041	0.978388	1
2	0.674504	0.691633	0.706861	0.733517	0.774719	0.828005	0.883217	0.927684	0.960041	0.978388	1
1	0.674504	0.691633	0.706861	0.733517	0.774719	0.828005	0.883217	0.927684	0.960041	0.978388	1
fixed	0.674504	0.691633	0.706861	0.733517	0.774719	0.828005	0.883217	0.927684	0.960041	0.978388	1

Table D.5 Frame 1, Sway, Strength Ratio

	Phi Beam-to-Column mRad										
Phi Column	pinned	256	128	64	32	16	8	4	2	1	fixed
pinned	0	0.161393	0.197847	0.255355	0.349166	0.480962	0.636879	0.782009	0.851442	0.877771	0.89569
256	0.143182	0.17832	0.212488	0.27	0.362431	0.494218	0.649861	0.797596	0.869132	0.894867	0.914156
128	0.156511	0.19068	0.222252	0.28098	0.371129	0.502903	0.660602	0.808292	0.885222	0.907711	0.925081
64	0.173438	0.207606	0.239338	0.29425	0.385318	0.517118	0.676144	0.826164	0.904694	0.928418	0.942268
32	0.19068	0.224848	0.255355	0.310271	0.401792	0.535585	0.694017	0.849842	0.930429	0.949582	0.964483
16	0.205321	0.239338	0.27	0.324912	0.418266	0.551172	0.715455	0.87256	0.951136	0.967866	0.98007
8	0.215084	0.248032	0.279609	0.335896	0.42925	0.56548	0.729716	0.890433	0.962198	0.976139	0.987064
4	0.219966	0.255355	0.284641	0.343219	0.437025	0.574896	0.740458	0.901129	0.967272	0.98071	0.992869
2	0.224848	0.259016	0.288303	0.34688	0.440234	0.579741	0.747589	0.90698	0.969694	0.98487	0.995429
1	0.224848	0.259016	0.290588	0.34688	0.44252	0.582027	0.751154	0.908306	0.97198	0.98487	0.997714
fixed	0.227134	0.261302	0.291964	0.349166	0.445724	0.583307	0.75344	0.911871	0.97198	0.987155	1

Table D.6 Frame 2, Sway, Strength Ratio

	Phi Beam-to-Column mRad										
Phi Column	pinned	256	128	64	32	16	8	4	2	1	fixed
pinned	0	0.115101	0.152292	0.211997	0.297336	0.41659	0.542113	0.649581	0.724896	0.771969	0.824544
256	0.091341	0.133493	0.167166	0.223156	0.314074	0.431494	0.560936	0.669995	0.74922	0.796333	0.852754
128	0.10518	0.140929	0.174602	0.234308	0.322443	0.444048	0.575848	0.688817	0.768051	0.81514	0.87164
64	0.115101	0.152292	0.185761	0.245467	0.335264	0.456602	0.594679	0.707648	0.792414	0.843351	0.902045
32	0.126056	0.163247	0.19692	0.256626	0.347551	0.475433	0.613502	0.730397	0.819058	0.87164	0.932686
16	0.129974	0.170684	0.204161	0.263866	0.359831	0.487979	0.62684	0.753138	0.839433	0.895933	0.957135
8	0.133493	0.174602	0.208079	0.268318	0.364282	0.494256	0.640169	0.764133	0.856673	0.912076	0.975551
4	0.137411	0.174602	0.211997	0.272236	0.368733	0.500533	0.645663	0.773544	0.866076	0.920461	0.987775
2	0.137411	0.17852	0.211997	0.272236	0.368733	0.504451	0.649581	0.777463	0.87164	0.926573	0.993888
1	0.140929	0.17852	0.211997	0.272236	0.372651	0.504451	0.651164	0.781381	0.87164	0.930491	0.997806
fixed	0.140929	0.17852	0.21532	0.276687	0.372651	0.50681	0.651164	0.782964	0.877126	0.932686	1

Table D.7 Frame 3, Sway, Strength Ratio

	Phi Beam-to-Column mRad										
Phi Column	pinned	256	128	64	32	16	8	4	2	1	fixed
pinned	0	0.113777	0.146552	0.196677	0.276601	0.386058	0.509937	0.633314	0.726492	0.772308	0.800469
256	0.098587	0.134028	0.164403	0.213766	0.29208	0.40048	0.529159	0.655608	0.75412	0.805643	0.840632
128	0.11111	0.146552	0.174665	0.225159	0.302229	0.413825	0.544669	0.670809	0.772308	0.830658	0.86746
64	0.1291	0.161737	0.188319	0.239218	0.317713	0.426641	0.561203	0.693157	0.797323	0.859833	0.905648
32	0.14429	0.174665	0.202373	0.250968	0.33213	0.443197	0.580404	0.718118	0.826497	0.893168	0.943144
16	0.154142	0.18529	0.213766	0.262361	0.343341	0.45868	0.596992	0.738973	0.851459	0.922289	0.970825
8	0.161737	0.190986	0.219462	0.270724	0.351885	0.467753	0.609793	0.751453	0.868153	0.938983	0.984799
4	0.164403	0.196677	0.225159	0.274996	0.356158	0.474159	0.618113	0.759827	0.876473	0.949971	0.993173
2	0.16707	0.196677	0.225159	0.276601	0.357763	0.475236	0.62078	0.766654	0.884794	0.955624	0.997333
1	0.16707	0.199707	0.228188	0.276601	0.36043	0.477903	0.622273	0.768148	0.887461	0.958291	0.997333
fixed	0.169332	0.199707	0.228188	0.279268	0.362035	0.48057	0.62494	0.772308	0.888954	0.959838	1

Table D.8 Frame 4, Sway, Strength Ratio

	Phi Beam-to-Column mRad										
Phi Column	pinned	256	128	64	32	16	8	4	2	1	fixed
pinned	0	0.111127	0.13242	0.172824	0.238128	0.336021	0.461444	0.592736	0.70178	0.772995	0.859792
256	0.103618	0.126338	0.147728	0.186512	0.250392	0.349352	0.477026	0.61054	0.719584	0.794445	0.88204
128	0.114169	0.13708	0.156852	0.195639	0.260085	0.359066	0.487338	0.621678	0.734368	0.810825	0.897621
64	0.126338	0.147728	0.168261	0.207045	0.270924	0.371628	0.501496	0.639482	0.754394	0.833101	0.917647
32	0.138504	0.159134	0.179667	0.217596	0.282615	0.384959	0.518502	0.659507	0.777439	0.859792	0.942145
16	0.145447	0.168261	0.188794	0.226438	0.292893	0.396895	0.532659	0.677311	0.798918	0.88204	0.963595
8	0.151434	0.172824	0.193357	0.23328	0.299729	0.405811	0.543769	0.690671	0.814471	0.899843	0.977752
4	0.153713	0.176528	0.197063	0.236704	0.304572	0.410255	0.550463	0.698761	0.824185	0.908759	0.988862
2	0.154571	0.177385	0.199342	0.238128	0.306566	0.412477	0.554109	0.703205	0.830053	0.915425	0.993334
1	0.155995	0.178809	0.200199	0.239553	0.30799	0.414699	0.556331	0.706224	0.833101	0.917647	0.99698
fixed	0.156852	0.179667	0.200199	0.240125	0.30856	0.416123	0.557129	0.708475	0.835323	0.919869	1

Appendix E

Frame Analysis with Semi-Rigid Connections
Rigidity Factor Method
Part I Non-Sway Mode

Pertold J, Xiao R Y
Department of Civil & Environmental Engineering
University of Southampton
Southampton, UK

ABSTRACT

In this paper, the influence of rigidity of beam-column and column base connection on the overall non-sway frame behaviour has been studied. The calculation of one storey one bay frame was modelled by use of finite element method (FEM). The plastic load capacity of the frame with semi-rigid beam-column and base connections (semi-rigid frame) was calculated for four different beam and column profiles, each for 121 combinations of connection rigidity. The design model for plastic load capacity calculation of semi-rigid frame has been proposed based on the FEM results, these in turn were calibrated with experimental results[1,2]. The rigidity factor K was defined as a ratio between the plastic load capacity of semi-rigid and rigid frame for serviceability and ultimate limit state. Formula for the frame rigidity factor K was proposed as a function of connection rigidity, frame geometry, member section and material characteristics. The capacity of semi-rigid frame can be obtained by multiplying the load capacity of the frame with all connections rigid by the rigidity factor K. Using this factor, there is no need to conduct FEM calculation. The results show that the difference between rigid and semi-rigid frame load capacity is influenced with the base rigidity by 5% only and with the beam-column connection rigidity by 95%. Comparison of plastic load capacity calculated from the proposed rigidity factor method with values calculated by FEM yields maximum error of 7% for all 484 calculated frames.

INTRODUCTION

Traditionally, the connections in framed structures are classified into two types, perfectly pinned and perfectly rigid-plastic. The Eurocode introduce a criteria for classification of the connection as a rigid, pinned or semi-rigid[8]. However, in the real structures, perfectly pinned and rigid connections do not exist, all the connections are semi-rigid. M–ϕ characteristics for semi-rigid connection and for its various simplifications are shown in Figure 1.

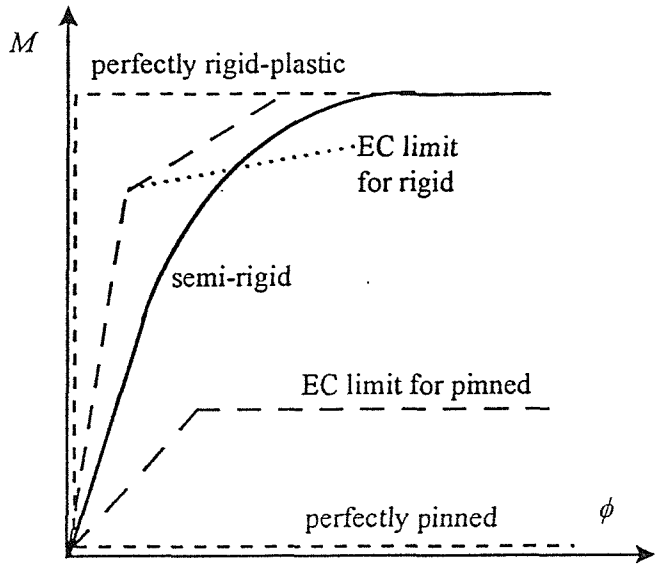

Figure 1. Moment - rotation characteristic for different connections.

Because of the rigid connections are typically complicated to fabricate and the production cost is high, in most cases the connections has been conservatively designed as perfectly pinned. The experimental results show, that the simplification of semi-rigid connection behaviour to pinned or rigid model is for some connection types very inaccurate and can lead to an over conservative design of the frame. If the real semi-rigid property of the connection is taken into account, the frame design becomes more precise and the cost of the structure consequently reduced. The beam-column connection rigidity has been studied in recent years[3-5]. The connections were classified in terms of strength, stiffness and ductility, using test and theoretical data. Some special cases were also classified, such as connections with softening-stiffening characteristics, connections with low ductility, and connections with properties that vary as a function of the applied load sense. The classification system is arranged such that new connection types can easily fit into the current data base. The experimental work for steel columns and concrete bases within the past 15 years has revealed the semi-rigidity of the column bases[6,7].

In this paper the influence of column-beam and base connections rigidity on the overall frame behaviour is expressed by use of frame rigidity factor K. Proposed analytical model represents very accurate simplification of reality.

To develop this method, four steps have been carried out:

1) Plastic load capacity calculation for semi-rigid frame by use of FEM. The results are presented for various combinations of plastic connection rotations ϕ_α, ϕ_β and different member sections.
2) Definition of modified plastic rotations Φ_α and Φ_β as a function of frame geometry, member section and material characteristics for beam-column and base connections respectively.
3) Definition of connection rigidity coefficients α_α and β_α for beam-column and base connections respectively as a function of Φ_α and Φ_β to fit the best the FEM results.
4) Definition of frame rigidity factor K_α as a function of α_α and β_α.

NUMERICAL SIMULATION BY USE OF FEM PROGRAMME

In order to check the accuracy of FEM model, the experimentally tested semi-rigid frame[1,2] has been modelled by FEM program ANSYS 5.3. A good agreement of numerical with experimental data was

found. In numerical analysis the semi-rigid full strength connections were modelled by use of non-linear spring elements COMBIN39 of zero size. Beam and column members were modelled by plastic beam elements BEAM23. Local buckling was not taken into account, shear deflection was not included. The numerical model has yielded similar results like previously reported simulation[14], when FEM program ABAQUS was used, beams were modelled by elements B22 and connections were modelled by a two-node nonlinear spring element SPRING2 of zero size.

After a good agreement with experimentally tested frame was reached, another frame models were prepared in order to study the behaviour of semi-rigid frame. One bay, one storey non-sway semi-rigid frame was modelled by use of FEM program ANSYS 5.3. The geometry of the frame is shown in Figure 2. Four different frame models were prepared, each one with different profile of the beam and column section. These models were labelled A, B, C, and D. Details for the models are summarised in Tables 1, 2, 3 and 4. As it can be seen from Figure 2, the ratio of vertical and horizontal load was equal to 10 and the serviceability limit state for vertical deflection L/200 was considered[8].

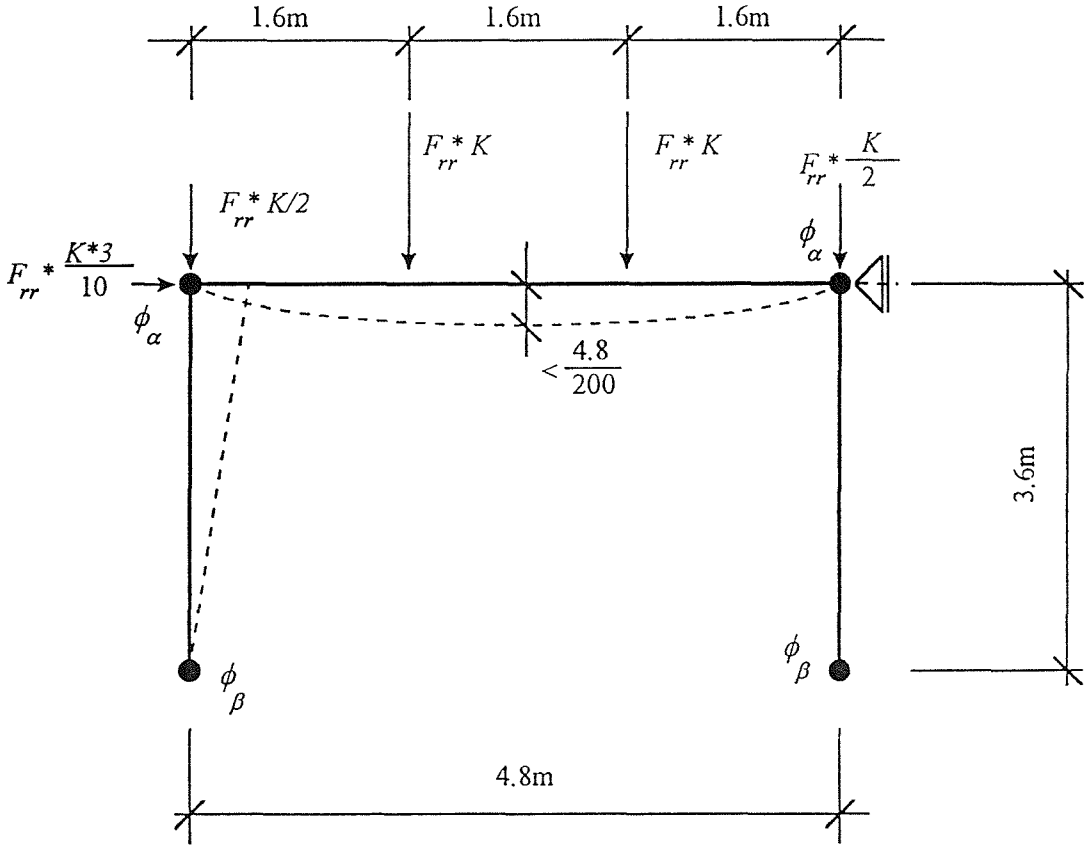

Figure 2. Geometry of FEM model of the non-sway semi-rigid frame.

Where:

ϕ_α is the plastic rotation at M_{pl} for beam-column connection,

ϕ_β is the plastic rotation at M_{pl} for column base connection,

K is the frame rigidity factor,

$F_{r,r}$ is the plastic load capacity of frame with rigid beam-column and base connections at serviceability or ultimate limit state.

Semi-rigid, full strength connections were modelled by use of non-linear spring elements COMBIN39 of zero size, beam and column members were modelled each by 6 plastic beam elements BEAM23. Local buckling has not been taken into account, shear deflection has not been included. The connection rigidity was modelled as a bilinear as shown in Figure 3.

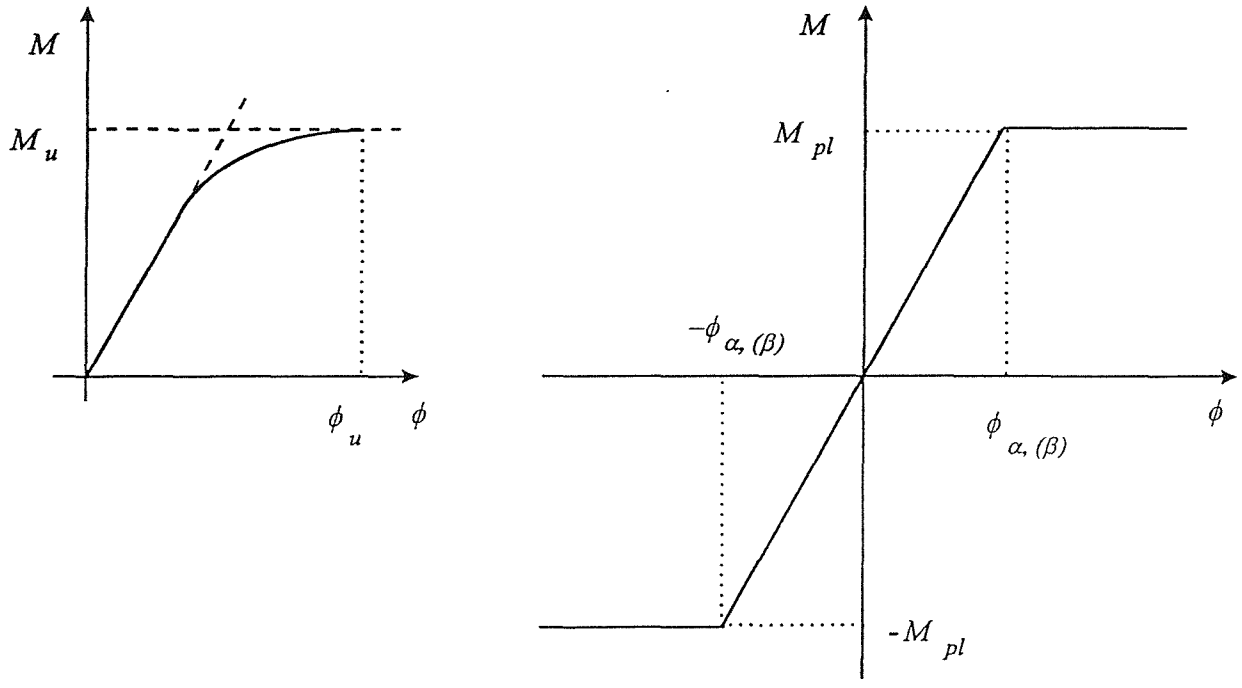

(a) from tests *(b) from FEM model*

Figure 3. Connection M-φ characteristics

Where:

M_{pl} is the plastic moment of designed connection,
M_u is the connection ultimate moment from experiments,
ϕ_u is the plastic rotation at M_{pl} from experiments.

For all the numerical models material with the modulus of elasticity E as $2.1 \cdot 10^5$ N/mm^2 and yield stress R_y as 275 N/mm^2 was used.

For frame analyses, section sizes HE300B, UC 254x254x89 and UB 457x191x89 were used. These are the representative section sizes for common design practise. Tables 1 through 4 summarise the input values for FEM analysis of frames A, B, C and D.

Table 1.: Section properties and geometry of frame A. Input data for the FEM model.

FRAME A	*A(0)*	*A(30)*	*A(50)*	*Mpl*	*L*	*Iy*	*A*	*rz*
	(m^2)	(m^2)	(m^2)	(Nm)	(m)	(m^4)	(m^2)	(m)
beam **HE300B**	7.41E-02	9.24E-03	9.79E-04	5.14E+05	4.80E+00	2.52E-04	1.49E-02	1.26E-01
column **HE300B**	7.41E-02	9.24E-03	9.79E-04	5.14E+05	3.60E+00	2.52E-04	1.49E-02	1.26E-01

Table 2.: Input data for FEM model of frame B. Section properties and frame geometry.

FRAME B	$A(0)$	$A(30)$	$A(50)$	M_{pl}	L	I_y	A	r_z
	(m^2)	(m^2)	(m^2)	(Nm)	(m)	(m^4)	(m^2)	(m)
beam UC 254x254x89	5.56E+04	7.07E+03	8.71E+02	3.37E+05	4.80E+00	1.43E-04	1.13E-02	1.08E-01
column UC 254x254x89	5.56E+04	7.07E+03	8.71E+02	3.37E+05	3.60E+00	1.43E-04	1.13E-02	1.08E-01

Table 3.: Input data for FEM model of frame C. Section properties and frame geometry.

FRAME C	$A(0)$	$A(30)$	$A(50)$	M_{pl}	L	I_y	A	r_z
	(m^2)	(m^2)	(m^2)	(Nm)	(m)	(m^4)	(m^2)	(m)
beam UB 457x191x89	4.84E+04	7.61E+03	3.18E+03	5.54E+05	4.80E+00	4.10E-04	1.14E-02	1.77E-01
column UB 457x191x89	4.84E+04	7.61E+03	3.18E+03	5.54E+05	3.60E+00	4.10E-04	1.14E-02	1.77E-01

Table 4. Input data for FEM model of frame D. Section properties and frame geometry

FRAME D	$A(0)$	$A(30)$	$A(50)$	M_{pl}	L	I_y	A	r_z
	(m^2)	(m^2)	(m^2)	(Nm)	(m)	(m^4)	(m^2)	(m)
beam UB 457x191x89	4.84E+04	7.61E+03	3.18E+03	5.54E+05	4.80E+00	4.10E-04	1.14E-02	1.77E-01
column UC 254x254x89	5.56E+04	7.07E+03	8.71E+02	3.37E+05	3.60E+00	1.43E-04	1.13E-02	1.08E-01

Where:

A(0), A(30), A(50) are the geometry input values used for BEAM23 element,
$M_{pl,Rd}$ is the plastic moment of member section,
L is the member length,
I_y is the second moment of area of member section,
A is the area of member section,
r_z is the radius of gyration of member section.

FEM RESULTS

After each FEM analysis the full history of load-deflection response of the frame was obtained. The plastic load capacities of the frames A, B, C and D are summarised in Tables 6, 7, 8 and 9. These values were calculated for the whole range of modified plastic rotations going from pinned ($\Phi_{\alpha(\beta)} = 50$) to rigid ($\Phi_{\alpha(\beta)} = 0.5$). The definition of $\Phi_{\alpha(\beta)}$ will be described later. In addition, the plastic load capacity of the frame with pinned and rigid connections has been calculated without use of spring elements. In all analysed frame models the calculation was stopped when either the ultimate or serviceability limit state was reached. The influence of plastic rotations was expressed by the frame rigidity factor K. This factor represent the ratio of plastic load capacity of semi-rigid and rigid frame and is calculated in Tables 6, 7, 8 and 9. By definition it has the value of 1 for frame with rigid connections. The minimum value of K is for the frame with pinned connections. Frame rigidity factor K for all the other connections lays in between of these two limits.

Plastic load capacity of the frame with various plastic rotations was labelled in accordance with the Table 5.

Table 5. Indexes i, j of plastic load capacity F_{ij} for the semi-rigid frame

Base rigidity \ Beam-Column rigidity	pinned $\Phi_\alpha > 50$	semirigid Φ_α	rigid $\Phi_\alpha < 0.5$
pinned $\Phi_\beta > 2.5$	F_{pp}	$F_{\Phi\alpha, p}$	F_{rp}
semirigid Φ_β	$F_{p, \Phi\beta}$	$F_{\Phi\alpha, \Phi\beta}$	$F_{r, \Phi\beta}$
rigid $\Phi_\beta < 0.5$	F_{pr}	$F_{\Phi\alpha, r}$	F_{rr}

Where:

Φ_α is the modified plastic rotation of beam-column connection,

Φ_β is the modified plastic rotation of base connection.

Table 6. Plastic load capacities F and rigidity factors K and K_a for frame A. Values of Φ_α, Φ_β and α_α, β_α have been calculated by analytical model described further in this paper.

FRAME A

Base ϕ_β (mrad)	Beam-Column Φ_β (rad)	ϕ_α (mrad) / Φ_α (rad) / β_α (1)	pinned	313.67	156.83	78.42	39.21	19.60	9.80	4.90	2.45	1.23	rigid
			pinned	53.53	26.76	13.38	6.69	3.35	1.67	0.84	0.42	0.21	rigid
		α_α (1)	0.000	0.036	0.073	0.185	0.345	0.524	0.696	0.834	0.910	1.000	1.000
pinned	pinned	0.000	F= 301 K= 0.50 Ka= 0.50	F= 315 K= 0.52 Ka= 0.52	F= 328 K= 0.54 Ka= 0.54	F= 353 K= 0.58 Ka= 0.59	F= 388 K= 0.64 Ka= 0.67	F= 435 K= 0.72 Ka= 0.75	F= 483 K= 0.80 Ka= 0.84	F= 524 K= 0.87 Ka= 0.90	F= 551 K= 0.91 Ka= 0.94	F= 564 K= 0.93 Ka= 0.98	F= 579 K= 0.96 Ka= 0.98
268.86	0.00	0.000	F= 301 K= 0.50 Ka= 0.50	F= 315 K= 0.52 Ka= 0.52	F= 330 K= 0.55 Ka= 0.54	F= 352 K= 0.58 Ka= 0.59	F= 388 K= 0.64 Ka= 0.67	F= 435 K= 0.72 Ka= 0.75	F= 483 K= 0.80 Ka= 0.84	F= 524 K= 0.87 Ka= 0.90	F= 552 K= 0.91 Ka= 0.94	F= 566 K= 0.94 Ka= 0.98	F= 580 K= 0.96 Ka= 0.98
134.43	30.59	0.000	F= 300 K= 0.50 Ka= 0.50	F= 315 K= 0.52 Ka= 0.52	F= 330 K= 0.55 Ka= 0.54	F= 352 K= 0.58 Ka= 0.59	F= 388 K= 0.64 Ka= 0.67	F= 436 K= 0.72 Ka= 0.75	F= 485 K= 0.80 Ka= 0.84	F= 526 K= 0.87 Ka= 0.90	F= 554 K= 0.92 Ka= 0.94	F= 568 K= 0.94 Ka= 0.98	F= 580 K= 0.96 Ka= 0.98
67.21	15.29	0.000	F= 301 K= 0.50 Ka= 0.50	F= 315 K= 0.52 Ka= 0.52	F= 329 K= 0.54 Ka= 0.54	F= 352 K= 0.58 Ka= 0.59	F= 389 K= 0.64 Ka= 0.67	F= 436 K= 0.72 Ka= 0.75	F= 486 K= 0.80 Ka= 0.84	F= 527 K= 0.87 Ka= 0.90	F= 555 K= 0.92 Ka= 0.94	F= 570 K= 0.94 Ka= 0.98	F= 583 K= 0.96 Ka= 0.98
33.61	7.65	0.170	F= 301 K= 0.50 Ka= 0.50	F= 315 K= 0.52 Ka= 0.52	F= 329 K= 0.54 Ka= 0.54	F= 352 K= 0.58 Ka= 0.59	F= 389 K= 0.64 Ka= 0.67	F= 436 K= 0.72 Ka= 0.76	F= 488 K= 0.81 Ka= 0.84	F= 530 K= 0.88 Ka= 0.90	F= 560 K= 0.93 Ka= 0.94	F= 574 K= 0.95 Ka= 0.98	F= 586 K= 0.97 Ka= 0.98
16.80	3.82	0.438	F= 301 K= 0.50 Ka= 0.51	F= 315 K= 0.52 Ka= 0.53	F= 330 K= 0.55 Ka= 0.54	F= 352 K= 0.58 Ka= 0.60	F= 389 K= 0.64 Ka= 0.67	F= 439 K= 0.73 Ka= 0.76	F= 491 K= 0.81 Ka= 0.84	F= 536 K= 0.89 Ka= 0.91	F= 564 K= 0.93 Ka= 0.95	F= 579 K= 0.96 Ka= 0.99	F= 593 K= 0.98 Ka= 0.99
8.40	1.91	0.634	F= 301 K= 0.50 Ka= 0.51	F= 315 K= 0.52 Ka= 0.53	F= 330 K= 0.55 Ka= 0.55	F= 354 K= 0.58 Ka= 0.60	F= 391 K= 0.65 Ka= 0.68	F= 441 K= 0.73 Ka= 0.76	F= 495 K= 0.82 Ka= 0.85	F= 541 K= 0.89 Ka= 0.91	F= 570 K= 0.94 Ka= 0.95	F= 584 K= 0.97 Ka= 0.99	F= 597 K= 0.99 Ka= 0.99
4.20	0.96	0.771	F= 301 K= 0.50 Ka= 0.51	F= 315 K= 0.52 Ka= 0.53	F= 330 K= 0.55 Ka= 0.55	F= 354 K= 0.58 Ka= 0.60	F= 392 K= 0.65 Ka= 0.68	F= 442 K= 0.73 Ka= 0.77	F= 498 K= 0.82 Ka= 0.85	F= 546 K= 0.90 Ka= 0.92	F= 576 K= 0.95 Ka= 0.95	F= 588 K= 0.97 Ka= 1.00	F= 601 K= 0.99 Ka= 1.00
2.10	0.48	0.864	F= 301 K= 0.50 Ka= 0.52	F= 315 K= 0.52 Ka= 0.53	F= 330 K= 0.55 Ka= 0.55	F= 353 K= 0.58 Ka= 0.61	F= 392 K= 0.65 Ka= 0.68	F= 444 K= 0.73 Ka= 0.77	F= 501 K= 0.83 Ka= 0.85	F= 549 K= 0.91 Ka= 0.92	F= 580 K= 0.96 Ka= 0.95	F= 592 K= 0.98 Ka= 1.00	F= 604 K= 1.00 Ka= 1.00
1.05	0.24	0.925	F= 301 K= 0.50 Ka= 0.52	F= 315 K= 0.52 Ka= 0.53	F= 330 K= 0.55 Ka= 0.55	F= 353 K= 0.58 Ka= 0.61	F= 392 K= 0.65 Ka= 0.68	F= 445 K= 0.73 Ka= 0.77	F= 502 K= 0.83 Ka= 0.85	F= 552 K= 0.91 Ka= 0.92	F= 582 K= 0.96 Ka= 0.96	F= 594 K= 0.98 Ka= 1.00	F= 605 K= 1.00 Ka= 1.00
rigid	rigid	1.000	F= 301 K= 0.50 Ka= 0.52	F= 314 K= 0.52 Ka= 0.54	F= 330 K= 0.55 Ka= 0.55	F= 354 K= 0.59 Ka= 0.61	F= 392 K= 0.65 Ka= 0.68	F= 446 K= 0.74 Ka= 0.77	F= 504 K= 0.83 Ka= 0.85	F= 555 K= 0.92 Ka= 0.92	F= 584 K= 0.97 Ka= 0.96	F= 597 K= 0.99 Ka= 1.00	F= 605 K= 1.00 Ka= 1.00

Table 7. Plastic load capacities F and rigidity factors K and K_a for frame B. Values of Φ_α, Φ_β and α_α, β_α have been calculated by analytical model described further in this paper.

FRAME B

Base ϕ_β (mrad)	Beam-Column Φ_β (rad)	ϕ_α (mrad) / Φ_α (rad) / β_α(1) / α (1)	pinned	538.36	269.18	134.59	67.29	33.65	16.82	8.41	4.21	2.10	rigid
			pinned	92.16	46.08	23.04	11.52	5.76	2.88	1.44	0.72	0.36	rigid
			0.000	0.000	0.036	0.092	0.217	0.383	0.563	0.730	0.856	0.916	1.000
pinned	pinned	0.000	F= 178 K= 0.48 Ka= 0.50	F= 184 K= 0.50 Ka= 0.50	F= 190 K= 0.51 Ka= 0.52	F= 203 K= 0.55 Ka= 0.54	F= 220 K= 0.59 Ka= 0.60	F= 243 K= 0.65 Ka= 0.68	F= 271 K= 0.73 Ka= 0.77	F= 299 K= 0.81 Ka= 0.85	F= 318 K= 0.86 Ka= 0.91	F= 330 K= 0.89 Ka= 0.94	F= 346 K= 0.93 Ka= 0.98
309.76	0.00	0.000	F= 178 K= 0.48 Ka= 0.50	F= 185 K= 0.50 Ka= 0.50	F= 191 K= 0.51 Ka= 0.52	F= 202 K= 0.54 Ka= 0.54	F= 220 K= 0.59 Ka= 0.60	F= 243 K= 0.65 Ka= 0.68	F= 273 K= 0.74 Ka= 0.77	F= 299 K= 0.81 Ka= 0.85	F= 320 K= 0.86 Ka= 0.91	F= 332 K= 0.90 Ka= 0.94	F= 348 K= 0.94 Ka= 0.98
154.88	35.35	0.000	F= 178 K= 0.48 Ka= 0.50	F= 185 K= 0.50 Ka= 0.50	F= 191 K= 0.52 Ka= 0.52	F= 202 K= 0.54 Ka= 0.54	F= 220 K= 0.59 Ka= 0.60	F= 243 K= 0.65 Ka= 0.68	F= 273 K= 0.74 Ka= 0.77	F= 299 K= 0.81 Ka= 0.85	F= 320 K= 0.86 Ka= 0.91	F= 333 K= 0.90 Ka= 0.94	F= 349 K= 0.94 Ka= 0.98
77.44	17.67	0.000	F= 178 K= 0.48 Ka= 0.50	F= 185 K= 0.50 Ka= 0.50	F= 191 K= 0.52 Ka= 0.52	F= 202 K= 0.54 Ka= 0.54	F= 220 K= 0.59 Ka= 0.60	F= 245 K= 0.66 Ka= 0.68	F= 273 K= 0.74 Ka= 0.77	F= 301 K= 0.81 Ka= 0.85	F= 321 K= 0.87 Ka= 0.91	F= 334 K= 0.90 Ka= 0.94	F= 349 K= 0.94 Ka= 0.98
38.72	8.84	0.103	F= 178 K= 0.48 Ka= 0.50	F= 185 K= 0.50 Ka= 0.50	F= 191 K= 0.52 Ka= 0.52	F= 202 K= 0.54 Ka= 0.55	F= 220 K= 0.59 Ka= 0.61	F= 243 K= 0.66 Ka= 0.69	F= 274 K= 0.74 Ka= 0.77	F= 301 K= 0.81 Ka= 0.85	F= 323 K= 0.87 Ka= 0.91	F= 337 K= 0.91 Ka= 0.94	F= 353 K= 0.95 Ka= 0.98
19.36	4.42	0.388	F= 179 K= 0.48 Ka= 0.51	F= 185 K= 0.50 Ka= 0.51	F= 191 K= 0.52 Ka= 0.52	F= 203 K= 0.55 Ka= 0.55	F= 220 K= 0.59 Ka= 0.61	F= 244 K= 0.66 Ka= 0.69	F= 275 K= 0.74 Ka= 0.78	F= 303 K= 0.82 Ka= 0.86	F= 325 K= 0.88 Ka= 0.92	F= 341 K= 0.92 Ka= 0.95	F= 356 K= 0.96 Ka= 0.99
9.68	2.21	0.598	F= 179 K= 0.48 Ka= 0.51	F= 185 K= 0.50 Ka= 0.51	F= 191 K= 0.52 Ka= 0.53	F= 203 K= 0.55 Ka= 0.56	F= 221 K= 0.60 Ka= 0.62	F= 246 K= 0.66 Ka= 0.70	F= 276 K= 0.75 Ka= 0.78	F= 306 K= 0.83 Ka= 0.86	F= 329 K= 0.89 Ka= 0.92	F= 345 K= 0.93 Ka= 0.95	F= 361 K= 0.97 Ka= 0.99
4.84	1.10	0.747	F= 179 K= 0.48 Ka= 0.51	F= 185 K= 0.50 Ka= 0.51	F= 190 K= 0.51 Ka= 0.53	F= 203 K= 0.55 Ka= 0.56	F= 221 K= 0.60 Ka= 0.62	F= 245 K= 0.66 Ka= 0.70	F= 278 K= 0.75 Ka= 0.78	F= 308 K= 0.83 Ka= 0.87	F= 333 K= 0.90 Ka= 0.93	F= 348 K= 0.94 Ka= 0.95	F= 364 K= 0.98 Ka= 1.00
2.42	0.55	0.848	F= 179 K= 0.48 Ka= 0.52	F= 185 K= 0.50 Ka= 0.52	F= 190 K= 0.51 Ka= 0.53	F= 203 K= 0.55 Ka= 0.56	F= 220 K= 0.59 Ka= 0.62	F= 247 K= 0.67 Ka= 0.70	F= 278 K= 0.75 Ka= 0.79	F= 311 K= 0.84 Ka= 0.87	F= 336 K= 0.91 Ka= 0.93	F= 351 K= 0.95 Ka= 0.96	F= 367 K= 0.99 Ka= 1.00
1.21	0.28	0.915	F= 179 K= 0.48 Ka= 0.52	F= 185 K= 0.50 Ka= 0.52	F= 190 K= 0.51 Ka= 0.53	F= 203 K= 0.55 Ka= 0.56	F= 220 K= 0.59 Ka= 0.62	F= 247 K= 0.67 Ka= 0.70	F= 279 K= 0.75 Ka= 0.79	F= 311 K= 0.84 Ka= 0.87	F= 336 K= 0.91 Ka= 0.93	F= 352 K= 0.95 Ka= 0.96	F= 370 K= 1.00 Ka= 1.00
rigid	rigid	1.000	F= 179 K= 0.48 Ka= 0.52	F= 185 K= 0.50 Ka= 0.52	F= 190 K= 0.51 Ka= 0.54	F= 203 K= 0.55 Ka= 0.56	F= 220 K= 0.59 Ka= 0.62	F= 247 K= 0.67 Ka= 0.70	F= 279 K= 0.75 Ka= 0.79	F= 313 K= 0.85 Ka= 0.87	F= 339 K= 0.92 Ka= 0.93	F= 355 K= 0.96 Ka= 0.96	F= 371 K= 1.00 Ka= 1.00

Table 8. Plastic load capacities F and rigidity factors K and K_a for frame C. Values of Φ_α, Φ_β and α_α, β_α have been calculated by analytical model described further in this paper.

FRAME C

Base ϕ_β (mrad)	Beam-Column Φ_β (rad)	ϕ_α (mrad) / Φ_α (rad) / β_α(1)	pinned / pinned / 0.000	512.00 / 93.79 / 0.000	256.00 / 46.90 / 0.036	128.00 / 23.45 / 0.090	64.00 / 11.72 / 0.213	32.00 / 5.86 / 0.378	16.00 / 2.93 / 0.558	8.00 / 1.47 / 0.726	4.00 / 0.73 / 0.854	2.00 / 0.37 / 0.915	rigid / rigid / 1.000
pinned	pinned	0.000	F= 336 K= 0.53 Ka= 0.50	F= 343 K= 0.54 Ka= 0.50	F= 352 K= 0.56 Ka= 0.52	F= 364 K= 0.58 Ka= 0.54	F= 399 K= 0.63 Ka= 0.60	F= 443 K= 0.70 Ka= 0.68	F= 503 K= 0.80 Ka= 0.77	F= 566 K= 0.90 Ka= 0.85	F= 605 K= 0.96 Ka= 0.91	F= 603 K= 0.96 Ka= 0.94	F= 598 K= 0.95 Ka= 0.98
512.00	0.00	0.000	F= 336 K= 0.53 Ka= 0.50	F= 344 K= 0.55 Ka= 0.50	F= 351 K= 0.56 Ka= 0.52	F= 366 K= 0.58 Ka= 0.54	F= 400 K= 0.64 Ka= 0.60	F= 444 K= 0.70 Ka= 0.68	F= 502 K= 0.80 Ka= 0.77	F= 566 K= 0.90 Ka= 0.85	F= 605 K= 0.96 Ka= 0.91	F= 605 K= 0.96 Ka= 0.94	F= 604 K= 0.96 Ka= 0.98
256.00	62.53	0.000	F= 336 K= 0.53 Ka= 0.50	F= 344 K= 0.55 Ka= 0.50	F= 351 K= 0.56 Ka= 0.52	F= 366 K= 0.58 Ka= 0.54	F= 400 K= 0.64 Ka= 0.60	F= 444 K= 0.70 Ka= 0.68	F= 502 K= 0.80 Ka= 0.77	F= 566 K= 0.90 Ka= 0.85	F= 607 K= 0.96 Ka= 0.91	F= 607 K= 0.96 Ka= 0.94	F= 603 K= 0.96 Ka= 0.98
128.00	31.26	0.000	F= 336 K= 0.53 Ka= 0.50	F= 344 K= 0.55 Ka= 0.50	F= 352 K= 0.56 Ka= 0.52	F= 366 K= 0.58 Ka= 0.54	F= 400 K= 0.64 Ka= 0.60	F= 444 K= 0.70 Ka= 0.68	F= 504 K= 0.80 Ka= 0.77	F= 566 K= 0.90 Ka= 0.85	F= 607 K= 0.96 Ka= 0.91	F= 607 K= 0.96 Ka= 0.94	F= 605 K= 0.96 Ka= 0.98
64.00	15.63	0.000	F= 336 K= 0.53 Ka= 0.50	F= 344 K= 0.55 Ka= 0.50	F= 352 K= 0.56 Ka= 0.52	F= 366 K= 0.58 Ka= 0.54	F= 400 K= 0.64 Ka= 0.60	F= 444 K= 0.70 Ka= 0.68	F= 504 K= 0.80 Ka= 0.77	F= 568 K= 0.90 Ka= 0.85	F= 607 K= 0.96 Ka= 0.91	F= 607 K= 0.96 Ka= 0.94	F= 605 K= 0.96 Ka= 0.98
32.00	7.82	0.160	F= 336 K= 0.53 Ka= 0.50	F= 344 K= 0.55 Ka= 0.50	F= 352 K= 0.56 Ka= 0.52	F= 372 K= 0.59 Ka= 0.55	F= 400 K= 0.64 Ka= 0.61	F= 444 K= 0.70 Ka= 0.69	F= 504 K= 0.80 Ka= 0.77	F= 568 K= 0.90 Ka= 0.85	F= 608 K= 0.96 Ka= 0.91	F= 608 K= 0.97 Ka= 0.94	F= 607 K= 0.96 Ka= 0.98
16.00	3.91	0.431	F= 336 K= 0.53 Ka= 0.51	F= 344 K= 0.55 Ka= 0.51	F= 352 K= 0.56 Ka= 0.53	F= 372 K= 0.59 Ka= 0.55	F= 400 K= 0.63 Ka= 0.61	F= 443 K= 0.70 Ka= 0.69	F= 504 K= 0.80 Ka= 0.78	F= 571 K= 0.91 Ka= 0.86	F= 609 K= 0.97 Ka= 0.92	F= 620 K= 0.98 Ka= 0.95	F= 626 K= 0.99 Ka= 0.99
8.00	1.95	0.629	F= 336 K= 0.53 Ka= 0.51	F= 344 K= 0.55 Ka= 0.51	F= 352 K= 0.56 Ka= 0.53	F= 372 K= 0.59 Ka= 0.55	F= 400 K= 0.63 Ka= 0.61	F= 445 K= 0.71 Ka= 0.69	F= 507 K= 0.80 Ka= 0.78	F= 574 K= 0.91 Ka= 0.86	F= 613 K= 0.97 Ka= 0.92	F= 622 K= 0.99 Ka= 0.95	F= 628 K= 1.00 Ka= 0.99
4.00	0.98	0.768	F= 336 K= 0.53 Ka= 0.51	F= 344 K= 0.55 Ka= 0.51	F= 352 K= 0.56 Ka= 0.53	F= 371 K= 0.59 Ka= 0.56	F= 400 K= 0.64 Ka= 0.62	F= 445 K= 0.71 Ka= 0.70	F= 508 K= 0.81 Ka= 0.78	F= 577 K= 0.92 Ka= 0.86	F= 616 K= 0.98 Ka= 0.93	F= 626 K= 0.99 Ka= 0.95	F= 630 K= 1.00 Ka= 1.00
2.00	0.49	0.862	F= 336 K= 0.53 Ka= 0.52	F= 344 K= 0.55 Ka= 0.52	F= 352 K= 0.56 Ka= 0.53	F= 371 K= 0.59 Ka= 0.56	F= 400 K= 0.64 Ka= 0.62	F= 445 K= 0.71 Ka= 0.70	F= 508 K= 0.81 Ka= 0.78	F= 577 K= 0.92 Ka= 0.87	F= 616 K= 0.98 Ka= 0.93	F= 628 K= 1.00 Ka= 0.96	F= 630 K= 1.00 Ka= 1.00
rigid	rigid	1.000	F= 336 K= 0.53 Ka= 0.52	F= 345 K= 0.55 Ka= 0.52	F= 351 K= 0.56 Ka= 0.54	F= 371 K= 0.59 Ka= 0.56	F= 401 K= 0.64 Ka= 0.62	F= 445 K= 0.71 Ka= 0.70	F= 511 K= 0.81 Ka= 0.79	F= 582 K= 0.92 Ka= 0.87	F= 620 K= 0.98 Ka= 0.93	F= 630 K= 1.00 Ka= 0.96	F= 630 K= 1.00 Ka= 1.00

Table 9. Plastic load capacities F and rigidity factors K and K_a for frame D. Values of Φ_α, Φ_β and α_α, β_α have been calculated by analytical model described further in this paper.

FRAME D

Base ϕ_β (mrad)	Beam-Column Φ_β (rad)	ϕ_α (mrad) / Φ_α (rad) / α_a(1)	pinned / pinned / 0.000	538.36 / 98.62 / 0.000	269.18 / 49.31 / 0.035	134.59 / 24.65 / 0.083	67.29 / 12.33 / 0.202	33.65 / 6.16 / 0.365	16.82 / 3.08 / 0.545	8.41 / 1.54 / 0.715	4.21 / 0.77 / 0.847	2.10 / 0.39 / 0.914	rigid / rigid / 1.000
pinned	pinned	0.000	F= 336 K= 0.66 Ka= 0.62	F= 339 K= 0.66 Ka= 0.62	F= 345 K= 0.67 Ka= 0.63	F= 352 K= 0.69 Ka= 0.65	F= 364 K= 0.71 Ka= 0.70	F= 383 K= 0.75 Ka= 0.76	F= 423 K= 0.83 Ka= 0.82	F= 452 K= 0.88 Ka= 0.88	F= 474 K= 0.93 Ka= 0.93	F= 489 K= 0.96 Ka= 0.95	F= 495 K= 0.97 Ka= 0.99
108.05	0.00	0.000	F= 336 K= 0.66 Ka= 0.62	F= 340 K= 0.67 Ka= 0.62	F= 345 K= 0.67 Ka= 0.63	F= 352 K= 0.69 Ka= 0.65	F= 372 K= 0.73 Ka= 0.70	F= 395 K= 0.77 Ka= 0.76	F= 424 K= 0.83 Ka= 0.82	F= 454 K= 0.89 Ka= 0.88	F= 477 K= 0.93 Ka= 0.93	F= 489 K= 0.96 Ka= 0.95	F= 503 K= 0.98 Ka= 0.99
54.03	12.33	0.000	F= 336 K= 0.66 Ka= 0.62	F= 340 K= 0.67 Ka= 0.62	F= 345 K= 0.67 Ka= 0.63	F= 352 K= 0.69 Ka= 0.65	F= 372 K= 0.73 Ka= 0.70	F= 395 K= 0.77 Ka= 0.76	F= 424 K= 0.83 Ka= 0.82	F= 454 K= 0.89 Ka= 0.88	F= 479 K= 0.94 Ka= 0.93	F= 491 K= 0.96 Ka= 0.95	F= 504 K= 0.99 Ka= 0.99
27.01	6.17	0.262	F= 336 K= 0.66 Ka= 0.63	F= 340 K= 0.67 Ka= 0.63	F= 345 K= 0.67 Ka= 0.64	F= 352 K= 0.69 Ka= 0.66	F= 372 K= 0.73 Ka= 0.70	F= 395 K= 0.77 Ka= 0.76	F= 426 K= 0.83 Ka= 0.82	F= 457 K= 0.89 Ka= 0.89	F= 482 K= 0.94 Ka= 0.93	F= 494 K= 0.97 Ka= 0.96	F= 508 K= 0.99 Ka= 0.99
13.51	3.08	0.506	F= 336 K= 0.66 Ka= 0.63	F= 340 K= 0.67 Ka= 0.63	F= 345 K= 0.67 Ka= 0.64	F= 352 K= 0.69 Ka= 0.66	F= 372 K= 0.73 Ka= 0.70	F= 397 K= 0.78 Ka= 0.76	F= 426 K= 0.83 Ka= 0.83	F= 459 K= 0.90 Ka= 0.89	F= 485 K= 0.95 Ka= 0.94	F= 498 K= 0.97 Ka= 0.96	F= 509 K= 1.00 Ka= 0.99
6.75	1.54	0.682	F= 336 K= 0.66 Ka= 0.63	F= 340 K= 0.67 Ka= 0.63	F= 345 K= 0.67 Ka= 0.64	F= 352 K= 0.69 Ka= 0.66	F= 372 K= 0.73 Ka= 0.71	F= 397 K= 0.78 Ka= 0.76	F= 429 K= 0.84 Ka= 0.83	F= 462 K= 0.90 Ka= 0.89	F= 488 K= 0.95 Ka= 0.94	F= 502 K= 0.98 Ka= 0.96	F= 511 K= 1.00 Ka= 1.00
3.38	0.77	0.804	F= 336 K= 0.66 Ka= 0.63	F= 340 K= 0.67 Ka= 0.63	F= 345 K= 0.67 Ka= 0.65	F= 352 K= 0.69 Ka= 0.66	F= 372 K= 0.73 Ka= 0.71	F= 398 K= 0.78 Ka= 0.77	F= 429 K= 0.84 Ka= 0.83	F= 464 K= 0.91 Ka= 0.89	F= 492 K= 0.96 Ka= 0.94	F= 505 K= 0.99 Ka= 0.97	F= 511 K= 1.00 Ka= 1.00
1.69	0.39	0.886	F= 336 K= 0.66 Ka= 0.63	F= 340 K= 0.67 Ka= 0.63	F= 345 K= 0.67 Ka= 0.65	F= 354 K= 0.69 Ka= 0.66	F= 372 K= 0.73 Ka= 0.71	F= 398 K= 0.78 Ka= 0.77	F= 431 K= 0.84 Ka= 0.83	F= 465 K= 0.91 Ka= 0.89	F= 493 K= 0.96 Ka= 0.94	F= 507 K= 0.99 Ka= 0.97	F= 511 K= 1.00 Ka= 1.00
0.84	0.19	0.940	F= 336 K= 0.66 Ka= 0.64	F= 340 K= 0.67 Ka= 0.64	F= 345 K= 0.67 Ka= 0.65	F= 354 K= 0.69 Ka= 0.67	F= 372 K= 0.73 Ka= 0.71	F= 398 K= 0.78 Ka= 0.77	F= 431 K= 0.84 Ka= 0.83	F= 467 K= 0.91 Ka= 0.90	F= 494 K= 0.97 Ka= 0.94	F= 507 K= 0.99 Ka= 0.97	F= 511 K= 1.00 Ka= 1.00
0.42	0.10	0.982	F= 336 K= 0.66 Ka= 0.64	F= 340 K= 0.67 Ka= 0.64	F= 345 K= 0.67 Ka= 0.65	F= 354 K= 0.69 Ka= 0.67	F= 372 K= 0.73 Ka= 0.71	F= 398 K= 0.78 Ka= 0.77	F= 431 K= 0.84 Ka= 0.83	F= 467 K= 0.91 Ka= 0.90	F= 495 K= 0.97 Ka= 0.94	F= 509 K= 1.00 Ka= 0.97	F= 511 K= 1.00 Ka= 1.00
rigid	rigid	1.000	F= 336 K= 0.66 Ka= 0.64	F= 341 K= 0.67 Ka= 0.64	F= 345 K= 0.67 Ka= 0.65	F= 354 K= 0.69 Ka= 0.67	F= 372 K= 0.73 Ka= 0.71	F= 398 K= 0.78 Ka= 0.77	F= 431 K= 0.84 Ka= 0.83	F= 467 K= 0.91 Ka= 0.90	F= 495 K= 0.97 Ka= 0.94	F= 509 K= 1.06 Ka= 0.97	F= 511 K= 1.00 Ka= 1.00

In Tables 6 to 9:

- a index $_a$ stands for analytically calculated value, i.e. from the proposed design model,
- F is the plastic load capacity calculated by the FEM analysis
- K is the frame rigidity factor calculated from FEM results as F divided by F_{rr},
- K_a is the frame rigidity factor calculated from proposed analytical design method described further in this paper.
- Φ_α, Φ_β are the modified plastic rotations calculated from proposed analytical design method described further in this paper.
- α_a, β_a are the connection rigidity coefficients calculated from proposed analytical design method described further in this paper.

FRAME RIGIDITY FACTOR K - GENERAL DESCRIPTION

Based on the calculated results for different plastic rotations and different frame geometries (see Tables 6 to 9) the model for calculation of semi-rigid frame plastic load capacity has been derived. The proposed model enables designers to calculate the plastic load capacity of frame with various plastic rotations without a need of conducting plastic FEM analyses of semi-rigid frame. To find the load capacity of semi-rigid frame, the capacity of the rigid frame have to be calculated and multiplied by the frame rigidity factor K_a. For validity of the proposed analytical model the sufficient rotational capacity for all connections is required.

The use of frame rigidity factor method consists of three steps:
1) Calculation of the plastic load capacity for a rigid frame $F_{r,r}$.
2) Calculation of the frame rigidity factor K_a from the proposed analytical model.
3) The plastic load capacity of the semi-rigid frame $F_{\phi\alpha i,\phi\beta i}$ equals to the plastic load capacity of the rigid frame $F_{r,r}$ multiplied by the frame rigidity factor K_a.

Further described research is a comprehensive work carried out by FEM program to derive the relationship between plastic connection rotations and plastic load capacity of a general frame. The frame plastic load capacity has been calculated for various plastic rotations and the analytical model has been derived to fit the best the calculated values.

The values of K for frame C with various plastic rotations ϕ_α and ϕ_β summarised in Table 8 are graphically presented in Figure 4. Note that the axes ϕ_β and ϕ_α are in an exponential scale.

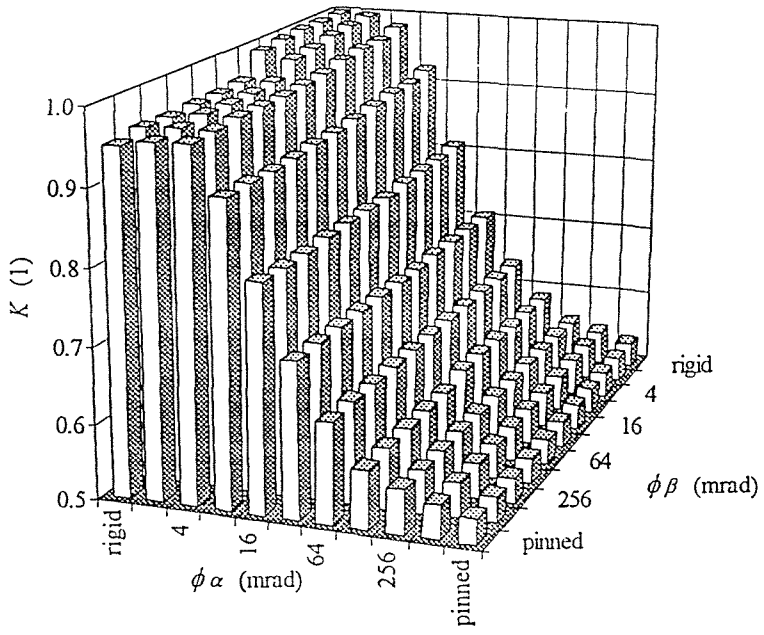

Figure 4. Values of frame rigidity factor K for frame C from table 8.

It can be seen, that for infinite changes of beam-column and base plastic rotations ϕ_α and ϕ_β the frame rigidity factor K creates a surface in three dimensional space with axes K, ϕ_α and ϕ_β. This surface has been plotted in Figure 5.

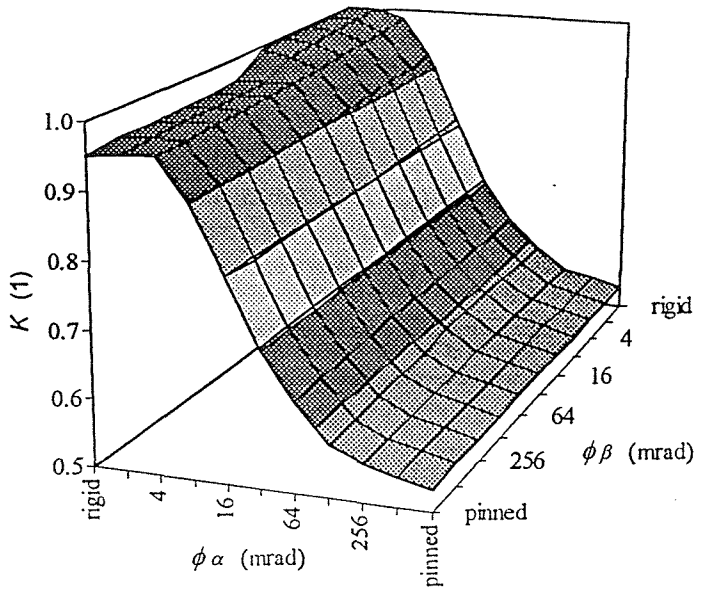

Figure 5. Surface created by the values of frame rigidity factor K for infinite changes of plastic rotations ϕ_β and ϕ_α. Frame C.

The equations for calculation of frame rigidity factor K_a described hereafter have been derived to fit the best the calculated values from FEM analyses (Tables 6 to 9). This is in other words to analytically describe the surface in Figure 5. The proposed model has been derived to take into account different frame sections, material properties and load conditions providing the ratio of vertical to horizontal load equals 10.

In general, the frame rigidity factor K_a is a function of the plastic rotations ϕ_α, ϕ_β, member length L, second moment of area I, member plastic moment M_{pl} and the modulus of elasticity E.

$$K_a = f\left(\phi_\alpha, \phi_\beta, L_b, L_c, I_{y,b}, I_{y,c}, M_{pl,b}, M_{pl,c}, E\right) \tag{1}$$

In the proposed model the frame rigidity factor K is has been defined as a function of the connection rigidity coefficients α and β. Values of α and β has been defined to be in between zero and one.

$$K_a = f(\alpha, \beta) \tag{2}$$

The values of K_a calculated as a function of α and β from proposed frame rigidity factor method are plotted in Figure 6 for frame C.

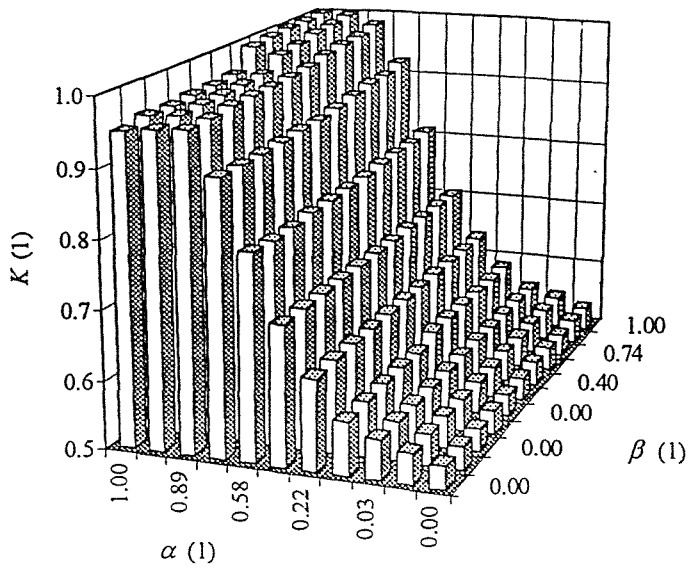

Figure 6. Frame rigidity factor K_a calculated from the connection rigidity coefficients α and β. Frame C.

The connection rigidity coefficients α and β are functions of modified plastic rotations Φ_α and Φ_β respectively.

$$\alpha = f(\Phi_\alpha) \tag{3}$$

$$\beta = f(\Phi_\beta) \tag{4}$$

The modified plastic rotations Φ_α and Φ_β represent the influence of $\phi_\alpha, \phi_\beta, L_b, L_c, I_{y,b}, I_{y,c}, M_{pl,b}, M_{pl,c}$ and E on the frame behaviour.

$$\Phi_\alpha = f(\phi_\alpha, L_b, I_{y,b}, M_{pl,b}, E, r_{z,b}) \tag{5}$$

$$\Phi_\beta = f(\phi_\beta, L_c, I_{y,c}, M_{pl,c}, E, r_{z,c}) \tag{6}$$

Where:

α	is the rigidity coefficient of beam-column connection,
β	is the rigidity coefficient of base connection,
$M_{pl,b}$	is the plastic moment of beam element,
$M_{pl,c}$	is the plastic moment of column element,
$I_{y,b}$	is the second moment of area of beam element,
$I_{y,c}$	is the second moment of area of column element,
L_b	is the length of beam element,
L_c	is the length of column element,
E	is the modulus of elasticity,
$r_{z,b}$	is the radius of gyration of beam element,
$r_{z,c}$	is the radius of gyration of column element,

$F_{p,P}$, $F_{\bar{\phi}\alpha i,\bar{\phi}\beta i}$ see Table 5.

5. FRAME RIGIDITY FACTOR K_a - CALCULATION

A) First the formulas for calculation of modified plastic rotations Φ_α and Φ_β have been proposed. The formulas have been derived according to the theory of plasticity and by numerically calculated influence of connection parameters on the plastic frame capacity. Proposed formulas (7) and (8) describe the influence of element length L, member section characteristics E, I_y, plastic moment of the member section M_{pl} and modulus of elasticity E on the modified plastic rotation Φ_α. and Φ_β.

$$\Phi_\alpha = \frac{\phi_\alpha \cdot E \cdot I_{y,b}}{L_b \cdot M_{pl,b} \cdot r_{z,b}} \tag{7}$$

$$\Phi_\beta = \frac{\phi_\beta \cdot E \cdot I_{y,c}}{L_c \cdot M_{pl,c} \cdot r_{z,c}} \tag{8}$$

When Φ_β is constant, change of the frame rigidity factor K depends only on Φ_α. The relationship between K and Φ_α when Φ_β is constant is shown on Figure 7.

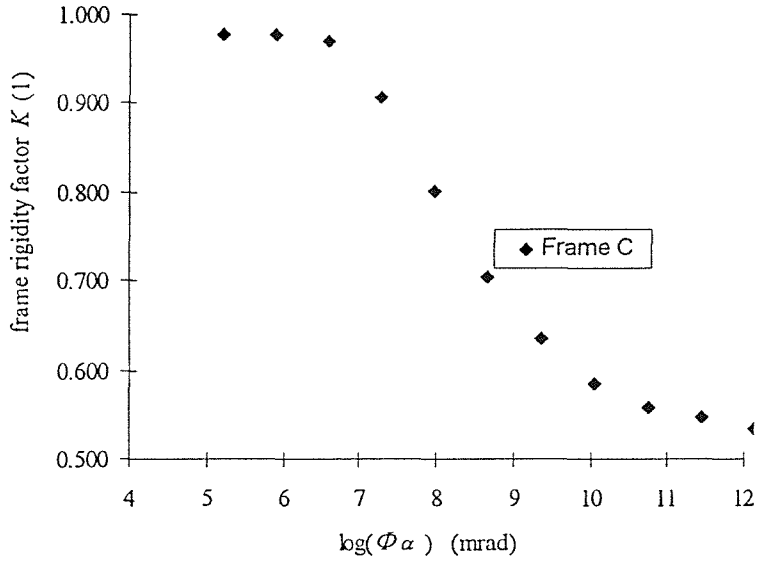

Figure 7. The relationship between modified plastic rotation Φ_α and frame rigidity factor K

B) Second, the calculation of beam-column connection rigidity coefficient α_a and base connection rigidity coefficient β_a has been proposed. The α_a represents the influence of beam-column connection rigidity on the frame rigidity factor K. This influence can be derived from Tables 6 to 9 for the cases with constant plastic rotations of the base connections. The coefficient β_a has been derived similarly to the coefficient α_a. The coefficient α_a is defined to be zero for pinned beam-column connection and one for rigid beam-column connection. The exact value of α_a and β_a can be calculated from Tables 6 to 9 by the following two equations:

$$\alpha = \frac{K(\Phi_\alpha) - K(\Phi_{\alpha,p})}{K(\Phi_{\alpha,r}) - K(\Phi_{\alpha,p})} \tag{9}$$

$$\beta = \frac{K(\Phi_\beta) - K(\Phi_{\beta,p})}{K(\Phi_{\beta,r}) - K(\Phi_{\beta,p})} \tag{10}$$

The analytical formulas for calculating α and β has been proposed in (11), (12), (13) and (14) to fit the best the values of α and β from FEM analyses. The relationship between Φ_α (Φ_β) and α (β) can be numerically expressed as a logarithmic polygon of the third grade:

$$\boxed{\alpha_a = a + b \cdot \ln(\Phi_\alpha) + c \cdot \ln^2(\Phi_\alpha) + d \cdot \ln^3(\Phi_\alpha)} \tag{11}$$

$$\boxed{\beta_a = a + b \cdot \ln(\Phi_\beta) + c \cdot \ln^2(\Phi_\beta) + d \cdot \ln^3(\Phi_\beta)} \tag{12}$$

Formula above is valid for: $\Phi_\alpha \in (0.3;50)$ (13)

and for $\Phi_\beta \in (0.1;12)$ (14)

Above stated limits were obtained from FEM analyses. Outside described interval the connection is considered as rigid or pinned and the connection rigidity coefficient α and β is equal to one or zero respectively:

for beam-column connection: if $\Phi_\alpha > 50$ then $\alpha_a = 0$ pinned connection (15)

if $\Phi_\alpha < 0.3$ then $\alpha_a = 1$ rigid connection (16)

for base connection: if $\Phi_\beta > 12$ then $\beta_a = 0$ pinned connection (17)

if $\Phi_\beta < 0.1$ then $\beta_a = 1$ rigid connection (18)

The constants *a*, *b*, *c* and *d* used for calculation of α were derived to minimise the error between FEM results (Tables 6 to 9) and proposed analytical model results. The values are listed in Table 10.

Table 10. Constants a, b, c, d for the calculation of α_a and β_a.
Constant k for calculation of the rigidity factor K_a.

	α_a	β_a
a	0.803	0.764
b	-0.182	-0.167
c	-0.057	-0.048
d	0.014	-0.007
k	0.963	

The relationship between α_a and frame rigidity factor both calculated from FEM analyses *K* (Table 6 to 9) and from proposed analytical model K_a (19) is shown on Figure 8.

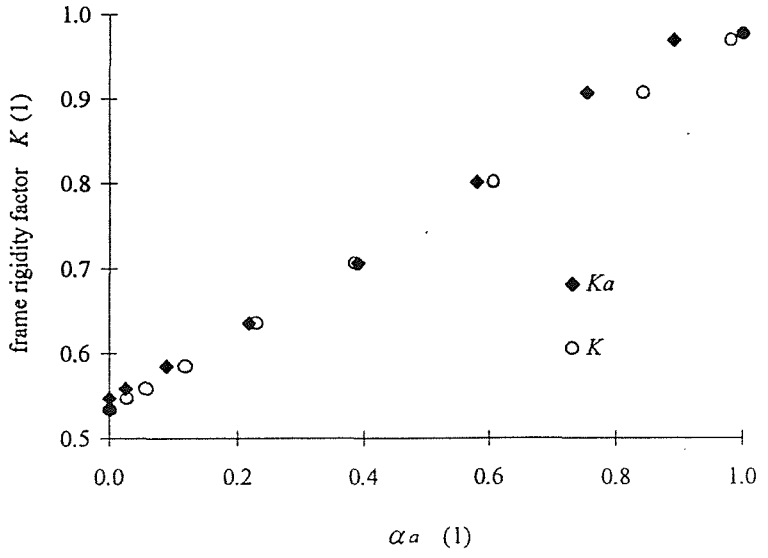

Figure 8. The relationship between rigidity coefficient α, frame rigidity factors K and K_a.

4) The calculation of frame rigidity factor K_a.

$$K_a = K_{a\,pp} + \left(1 - K_{a\,pp}\right) \cdot \left[k \cdot \alpha_a + (1-k) \cdot \beta_a\right] \tag{19}$$

$K_{a\,pp}$ has been derived based on assumption of collapse in the beam element (see Figure 9).

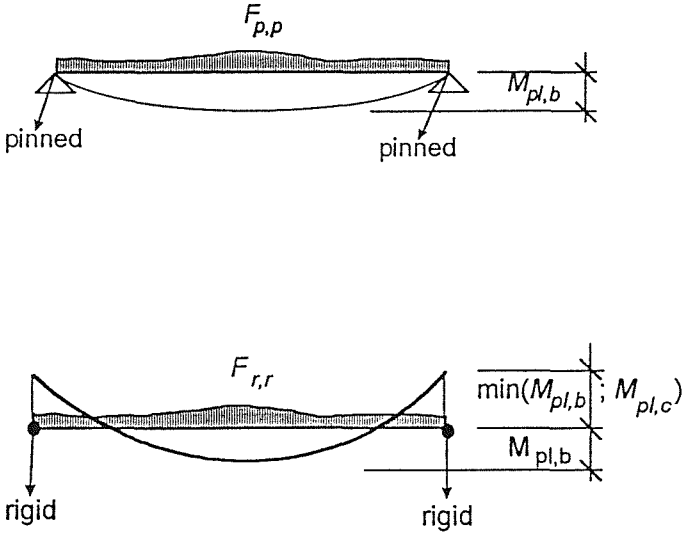

Figure 9. The limit moment distribution of generally loaded beam with pinned and rigid connections.

Neglecting the influence of axial and shear forces, the following equation can be written:

$$\frac{K_{a\,pp}}{K_{rr}} = \frac{M_{pl,b}}{M_{pl,b} + \min\left(M_{pl,b}, M_{pl,c}\right)} \tag{20}$$

Where:

k_1 is derived to fit the best the FEM calculated values (Tables 6 to 9),

$K_{a\,pp}$ is the frame rigidity factor for frame with all connections pinned,

$K_{r,r} = 1$ is the frame rigidity factor for frame with all connections rigid.

resulting K_{pp}:

$$K_{a\,pp} = \frac{M_{pl,b}}{M_{pl,b} + \min\left(M_{pl,b}, M_{pl,c}\right)} \tag{21}$$

COMPARISON OF THE ANALYTICAL MODEL WITH FEM RESULTS

The difference between plastic load capacity calculated by FEM and by the proposed analytical model is smaller than 7 % for all 484 calculated semi-rigid frames. The average error between semi-rigid and rigid frame load capacity calculated by FEM and by use of frame rigidity factor method is 3%. For connections with satisfactory rotational capacity the proposed analytical model can be used with high accuracy.

PARAMETRIC STUDY

The influence of connection rigidity (expressed by plastic rotations ϕ_α and ϕ_β at M_{pl}) on the frame rigidity factor K_a calculated by proposed frame rigidity factor method can be seen in following three Figures. All the graphs are plotted for the frame C (see Table 3). The horizontal axes are in the logarithmic scale. In Figure 10 the relationship between ϕ_β and K_a can be seen for different plastic rotations of beam-column connections ϕ_α.

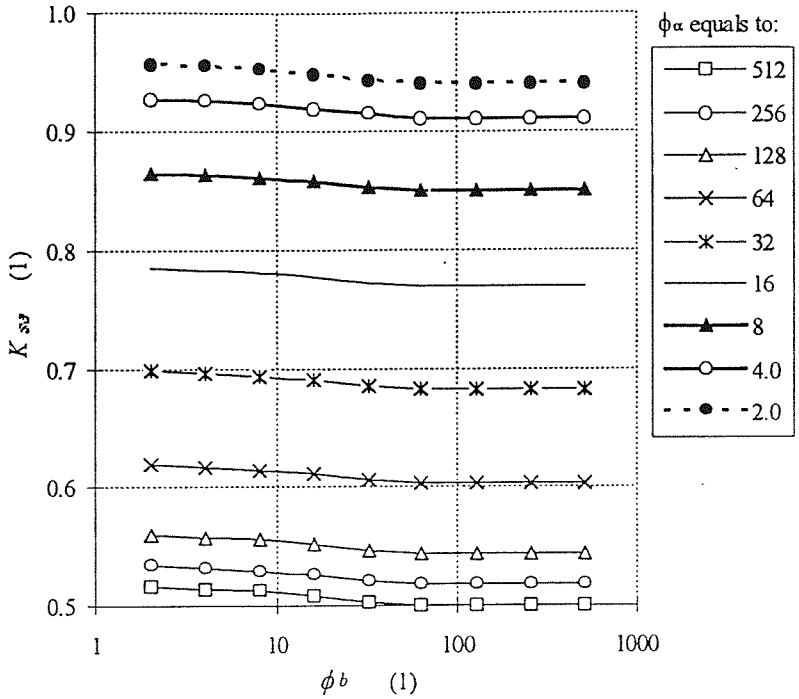

Figure 10. Influence of ϕ_β on frame rigidity factor K_a for constant ϕ_α

In Figure 11 the relationship between and K_a can be seen for different plastic rotations of column base connections ϕ_β.

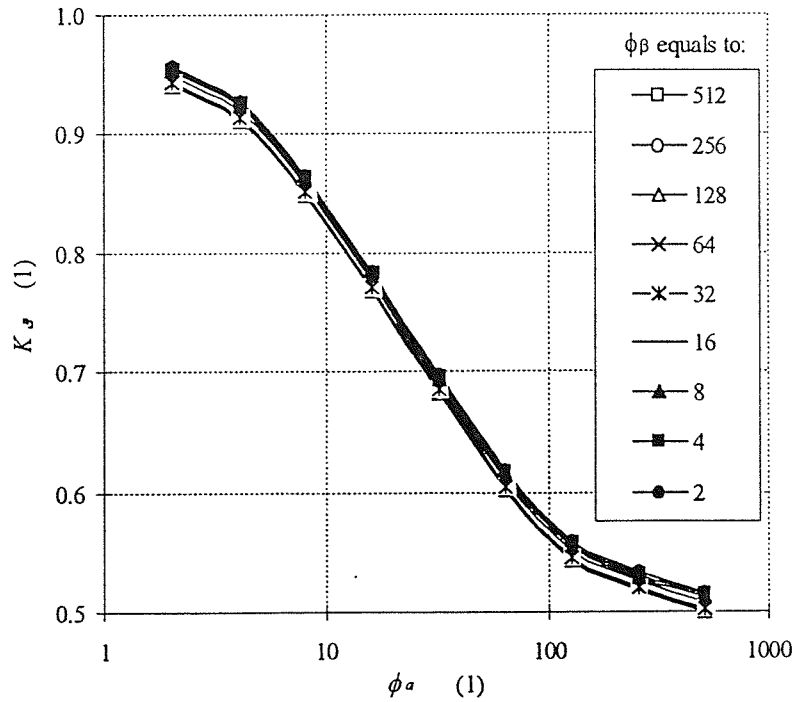

Figure 11. Influence of ϕ_α on frame rigidity factor K_a for constant ϕ_β

In Figure 12 the relationship between ϕ_α and ϕ_β on K_a can be seen for the case when not plotted connections are rigid.

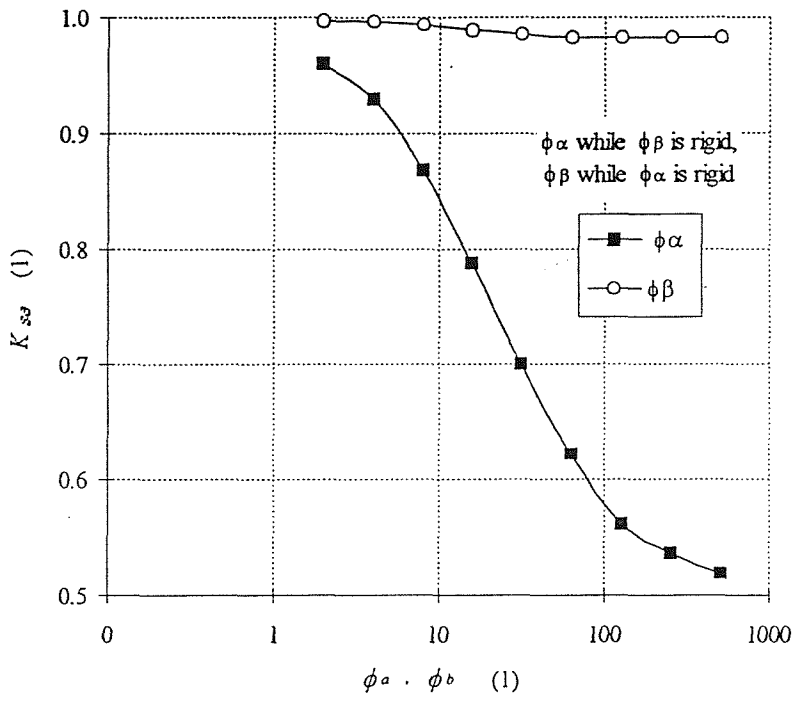

Figure 12. Influence of ϕ_α and ϕ_β on frame rigidity factor K_a.

CONCLUSIONS

The use of plastic analysis for semi-rigid frames reduce the safe assumptions taken for the load capacity design of the frame structures. The proposed analytical model for plastic load capacity calculation significantly simplify the calculation and unable to study the frame behaviour under changing parameters including connection rigidities and geometry. The analytical model for calculation of plastic load capacity was derived from a large database of FEM results published in this paper.

The mathematical expression for semi-rigid frame plastic load capacity calculation (equation xxxxx.) reveals clearly the influence of different parameters on the frame behaviour. In particular the following three facts can be concluded:

- The difference between frame rigidity factors $K_{rr} = 1$ and K_{pp} (equation xxxxx.) indicates the difference of plastic load capacity between rigid and pinned frame. This difference can reach up to 50%, depending on the ratio of second moments of area for beam and column.

- The plastic load capacity of semi-rigid frame is influenced with base rigidity by only 5 % and with the column-beam connection rigidity by 95 %. This influence is expressed by the coefficient k_1 (in the equation xxxxxx)

Appendix F

Frame Analysis with Semi-Rigid Connections
Rigidity Factor Method
Part II Sway Mode

Pertold J, Xiao R Y
Department of Civil & Environmental Engineering
University of Southampton
Southampton, UK

ABSTRACT

In this paper the frame rigidity factor method for sway frames was researched. The idea to introduce frame rigidity factor K defined as a ratio between plastic load capacity of semi-rigid and rigid frame was introduced in Part I of this paper.

The plastic load capacity was calculated for 363 one storey one bay sway frames with various connection rigidities. Based on the results from FEM analyses the analytical model was proposed. Analytical model describes how to calculate the frame rigidity factor K from frame geometry, connection rigidities and from plastic load capacity of the frame with rigid connections.

The derived analytical model reveals the fact, that column base connection influence the frame capacity by 45 % and the beam-column connection influence the frame capacity by 55 %. In contrast to non-sway frame, the influence of base connection rigidity in the case of sway mode is very significant.

The results yielded from analytical model and from FEM analyses differ by less than 11%.

INTRODUCTION

In the past the connections have been simplified as perfectly pinned or perfectly rigid. The Eurocode no.3[1] introduces the criteria for classification of connections as pinned, semi-rigid and rigid, as it is shown on Figure 1, Part I of this paper. In recent years the rigidity of beam-column and column base connections was studied[2-6]. The frames with semi-rigid connections were tested as well[7,8].
When the real connection rigidity is taken into account, the frame design becomes more complicated. In commercial FEM packages there are no elements with in-built connection rigidity and the plastic analysis is time consuming. To overcome these disadvantages and to research in details the influence of connection rigidities, frame rigidity factor method have been proposed. Particularly for sway frames it is very useful to be able to estimate the influence of connections rigidities on the overall frame behaviour so that the designer can choose the connection which is most effective for particular frame.

In this research 363 semi-rigid frames were analysed by FEM program ANSYS 5.3. Based on the numerical simulation results the design model was proposed. The design model is valid for sway frames of different geometries and connection rigidities.

NUMERICAL SIMULATION BY USE OF FEM PROGRAMME

The elements, material properties and loads that were used in numerical model are the same as in Tables 1 to 3, Part I of this Paper.

The geometry of the sway frame modelled is shown in Figure 2. Three different frame models were prepared, each one with different profile of the beam and column section. These models were labelled A, B and C and are summarised in Tables 1, 2 and 3, Part I of this Paper.

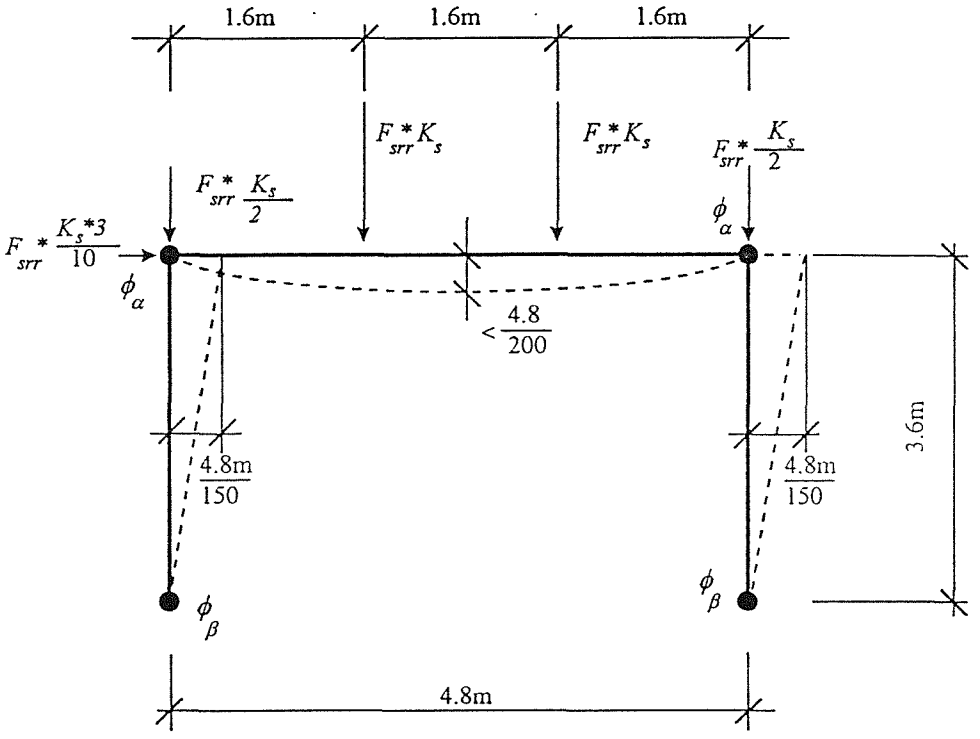

Figure 1. Geometry of FEM model of the sway semi-rigid frame.

Where:

ϕ_α is the plastic rotation at M_{pl} for beam-column connection,

ϕ_β is the plastic rotation at M_{pl} for column base connection,

K_s is the frame rigidity factor,

$F_{r,r}$ is the plastic load capacity of frame with rigid beam-column and base connections at serviceability or ultimate limit state.

FEM RESULTS

The frame plastic load capacity values F_s were calculated by FEM analysis for serviceability and limit states (see Figure 1). The resulting values are summarised in Tables 1 to 3 for geometry models A, B and C. The Tables 1 to 3 contain as well the values of α_s, β_s, Φ_α, Φ_β, K_s and K_{sa} that were calculated by the analytical model proposed further in this paper. If we look carefully at the Tables, from the values of K_s we can see the influence of particular connection rigidity on the overall frame behaviour. Taking into account the K_s values for different geometry, the general design model was derived so it would fit the values from FEM analysis. From the proposed model the frame rigidity factor was calculated and written into the tables labelled as K_{sa}.

Plastic load capacity of the frame with various plastic rotations was labelled in accordance with the Table 1. F_{ij} is defined as the plastic load of the frame. The sub-note i stands for the beam-to-column connections and j stands for the column bases. The sub-note s stands for values for sway frame mode, The sub-note a stands for values calculated by proposed analytical model.

Table 1. Plastic load capacity F_{ij} for the semi-rigid frame

Base connection rigidity \ Beam-Column connection rigidity	pinned $\Phi\alpha$ >30	semirigid $\Phi\alpha$	rigid $\Phi\alpha$ <0.3
pinned $\Phi\beta$ >300	$F_{s\,pp}$	$F_{s\,\Phi\alpha,\,p}$	$F_{s\,rp}$
semirigid $\Phi\beta$	$F_{s\,p,\,\Phi\beta}$	$F_{s\,\Phi\alpha,\,\Phi\beta}$	$F_{s\,r,\,\Phi\beta}$
rigid $\Phi\beta$ <0.75	$F_{s\,pr}$	$F_{s\,\Phi\alpha,\,r}$	$F_{s\,rr}$

Where:

Φ_α is the modified plastic rotation of beam-column connection,

Φ_β is the modified plastic rotation of base connection.

Table 2. Plastic load capacities F_s and rigidity factors K_s and K_{sa} for frame A. Values of Φ_α, Φ_β and α_s, β_s have been calculated by analytical model described further in this paper.

FRAME A

Base / Beam-Column	$\phi\alpha$ (mrad)	pinned	313.67	156.83	78.42	39.21	19.60	9.80	4.90	2.45	1.23	rigid
$\phi\beta$	$\Phi\alpha$ (rad)	pinned	53.53	26.76	13.38	6.69	3.35	1.67	0.84	0.42	0.21	rigid
(mrad)	(rad)	β_s \ α_s(1)	0.000	0.114	0.172	0.291	0.448	0.621	0.785	0.918	0.995	1.000	1.000
pinned	pinned	0.000	F_s= 0 K_s= 0.00 K_{sa}= 0.00	F_s= 10 K_s= 0.02 K_{sa}= 0.06	F_s= 32 K_s= 0.06 K_{sa}= 0.09	F_s= 60 K_s= 0.11 K_{sa}= 0.16	F_s= 100 K_s= 0.18 K_{sa}= 0.25	F_s= 152 K_s= 0.27 K_{sa}= 0.34	F_s= 205 K_s= 0.36 K_{sa}= 0.43	F_s= 246 K_s= 0.43 K_{sa}= 0.50	F_s= 274 K_s= 0.48 K_{sa}= 0.55	F_s= 290 K_s= 0.51 K_{sa}= 0.55	F_s= 309 K_s= 0.54 K_{sa}= 0.55
2150.87	489.40	0.000	F_s= 5 K_s= 0.01 K_{sa}= 0.00	F_s= 20 K_s= 0.04 K_{sa}= 0.06	F_s= 32 K_s= 0.06 K_{sa}= 0.09	F_s= 64 K_s= 0.11 K_{sa}= 0.16	F_s= 105 K_s= 0.18 K_{sa}= 0.38	F_s= 156 K_s= 0.27 K_{sa}= 0.34	F_s= 209 K_s= 0.37 K_{sa}= 0.43	F_s= 250 K_s= 0.44 K_{sa}= 0.50	F_s= 278 K_s= 0.49 K_{sa}= 0.55	F_s= 295 K_s= 0.52 K_{sa}= 0.55	F_s= 314 K_s= 0.55 K_{sa}= 0.55
1075.44	244.70	0.000	F_s= 10 K_s= 0.02 K_{sa}= 0.00	F_s= 22 K_s= 0.04 K_{sa}= 0.06	F_s= 39 K_s= 0.07 K_{sa}= 0.09	F_s= 67 K_s= 0.12 K_{sa}= 0.16	F_s= 108 K_s= 0.19 K_{sa}= 0.25	F_s= 161 K_s= 0.28 K_{sa}= 0.34	F_s= 211 K_s= 0.37 K_{sa}= 0.43	F_s= 254 K_s= 0.45 K_{sa}= 0.50	F_s= 283 K_s= 0.50 K_{sa}= 0.55	F_s= 298 K_s= 0.52 K_{sa}= 0.55	F_s= 317 K_s= 0.56 K_{sa}= 0.55
537.72	122.35	0.042	F_s= 10 K_s= 0.02 K_{sa}= 0.02	F_s= 20 K_s= 0.04 K_{sa}= 0.08	F_s= 45 K_s= 0.08 K_{sa}= 0.11	F_s= 72 K_s= 0.13 K_{sa}= 0.18	F_s= 115 K_s= 0.20 K_{sa}= 0.27	F_s= 167 K_s= 0.29 K_{sa}= 0.36	F_s= 220 K_s= 0.39 K_{sa}= 0.45	F_s= 260 K_s= 0.46 K_{sa}= 0.52	F_s= 290 K_s= 0.51 K_{sa}= 0.57	F_s= 310 K_s= 0.54 K_{sa}= 0.57	F_s= 329 K_s= 0.56 K_{sa}= 0.57
268.86	61.18	0.096	F_s= 20 K_s= 0.04 K_{sa}= 0.04	F_s= 39 K_s= 0.07 K_{sa}= 0.11	F_s= 55 K_s= 0.10 K_{sa}= 0.14	F_s= 84 K_s= 0.15 K_{sa}= 0.20	F_s= 127 K_s= 0.22 K_{sa}= 0.29	F_s= 180 K_s= 0.32 K_{sa}= 0.38	F_s= 235 K_s= 0.41 K_{sa}= 0.47	F_s= 279 K_s= 0.49 K_{sa}= 0.55	F_s= 308 K_s= 0.54 K_{sa}= 0.59	F_s= 324 K_s= 0.57 K_{sa}= 0.59	F_s= 343 K_s= 0.60 K_{sa}= 0.59
134.43	30.59	0.232	F_s= 40 K_s= 0.07 K_{sa}= 0.10	F_s= 60 K_s= 0.11 K_{sa}= 0.17	F_s= 77 K_s= 0.14 K_{sa}= 0.20	F_s= 105 K_s= 0.18 K_{sa}= 0.26	F_s= 151 K_s= 0.26 K_{sa}= 0.35	F_s= 207 K_s= 0.36 K_{sa}= 0.45	F_s= 263 K_s= 0.46 K_{sa}= 0.54	F_s= 308 K_s= 0.54 K_{sa}= 0.61	F_s= 339 K_s= 0.60 K_{sa}= 0.65	F_s= 357 K_s= 0.63 K_{sa}= 0.65	F_s= 371 K_s= 0.65 K_{sa}= 0.65
67.21	15.29	0.420	F_s= 75 K_s= 0.13 K_{sa}= 0.19	F_s= 96 K_s= 0.17 K_{sa}= 0.25	F_s= 114 K_s= 0.20 K_{sa}= 0.28	F_s= 146 K_s= 0.26 K_{sa}= 0.35	F_s= 194 K_s= 0.34 K_{sa}= 0.44	F_s= 252 K_s= 0.44 K_{sa}= 0.53	F_s= 314 K_s= 0.55 K_{sa}= 0.62	F_s= 363 K_s= 0.64 K_{sa}= 0.69	F_s= 393 K_s= 0.69 K_{sa}= 0.74	F_s= 408 K_s= 0.72 K_{sa}= 0.74	F_s= 416 K_s= 0.73 K_{sa}= 0.74
33.61	7.65	0.628	F_s= 132 K_s= 0.23 K_{sa}= 0.28	F_s= 155 K_s= 0.27 K_{sa}= 0.35	F_s= 174 K_s= 0.31 K_{sa}= 0.38	F_s= 208 K_s= 0.37 K_{sa}= 0.44	F_s= 261 K_s= 0.46 K_{sa}= 0.53	F_s= 330 K_s= 0.58 K_{sa}= 0.62	F_s= 398 K_s= 0.70 K_{sa}= 0.71	F_s= 445 K_s= 0.78 K_{sa}= 0.79	F_s= 464 K_s= 0.81 K_{sa}= 0.83	F_s= 470 K_s= 0.82 K_{sa}= 0.83	F_s= 469 K_s= 0.82 K_{sa}= 0.83
16.80	3.82	0.825	F_s= 210 K_s= 0.37 K_{sa}= 0.37	F_s= 236 K_s= 0.41 K_{sa}= 0.44	F_s= 258 K_s= 0.45 K_{sa}= 0.47	F_s= 299 K_s= 0.52 K_{sa}= 0.53	F_s= 358 K_s= 0.63 K_{sa}= 0.62	F_s= 427 K_s= 0.75 K_{sa}= 0.71	F_s= 484 K_s= 0.85 K_{sa}= 0.80	F_s= 515 K_s= 0.90 K_{sa}= 0.88	F_s= 518 K_s= 0.91 K_{sa}= 0.92	F_s= 518 K_s= 0.91 K_{sa}= 0.92	F_s= 517 K_s= 0.91 K_{sa}= 0.92
8.40	1.91	0.982	F_s= 297 K_s= 0.52 K_{sa}= 0.44	F_s= 316 K_s= 0.55 K_{sa}= 0.51	F_s= 329 K_s= 0.58 K_{sa}= 0.54	F_s= 353 K_s= 0.62 K_{sa}= 0.60	F_s= 391 K_s= 0.69 K_{sa}= 0.69	F_s= 439 K_s= 0.77 K_{sa}= 0.78	F_s= 491 K_s= 0.86 K_{sa}= 0.87	F_s= 527 K_s= 0.92 K_{sa}= 0.95	F_s= 536 K_s= 0.94 K_{sa}= 0.99	F_s= 540 K_s= 0.95 K_{sa}= 0.99	F_s= 545 K_s= 0.96 K_{sa}= 0.99
rigid	rigid	1.000	F_s= 301 K_s= 0.53 K_{sa}= 0.45	F_s= 317 K_s= 0.56 K_{sa}= 0.51	F_s= 329 K_s= 0.58 K_{sa}= 0.55	F_s= 354 K_s= 0.62 K_{sa}= 0.61	F_s= 393 K_s= 0.69 K_{sa}= 0.70	F_s= 446 K_s= 0.78 K_{sa}= 0.79	F_s= 502 K_s= 0.88 K_{sa}= 0.88	F_s= 543 K_s= 0.95 K_{sa}= 0.95	F_s= 559 K_s= 0.98 K_{sa}= 1.00	F_s= 563 K_s= 0.99 K_{sa}= 1.00	F_s= 570 K_s= 1.00 K_{sa}= 1.00

Table 3. Plastic load capacities F_s and rigidity factors K_s and K_{sa} for frame B. Values of Φ_α, Φ_β and α_s, β_s have been calculated by analytical model described further in this paper.

FRAME B

Base / Beam-Column	ϕ_α (mrad	pinned	538.36	269.18	134.59	67.29	33.65	16.82	8.41	4.21	2.10	rigid
ϕ_β	Φ_β / Φ_α (rad)	pinned	92.16	46.08	23.04	11.52	5.76	2.88	1.44	0.72	0.36	rigid
(mrad)	(rad)	α_s(1) / β_s(1)	0.000	0.000	0.120	0.193	0.322	0.485	0.658	0.817	0.940	1.000	1.000
pinned	pinned	0.000	F_s= 0 K_s= 0.00 K_{sa}= 0.00	F_s= 6 K_s= 0.02 K_{sa}= 0.00	F_s= 13 K_s= 0.04 K_{sa}= 0.07	F_s= 24 K_s= 0.07 K_{sa}= 0.11	F_s= 42 K_s= 0.12 K_{sa}= 0.18	F_s= 69 K_s= 0.19 K_{sa}= 0.27	F_s= 97 K_s= 0.27 K_{sa}= 0.36	F_s= 124 K_s= 0.35 K_{sa}= 0.45	F_s= 144 K_s= 0.41 K_{sa}= 0.52	F_s= 155 K_s= 0.44 K_{sa}= 0.55	F_s= 176 K_s= 0.48 K_{sa}= 0.55
1239.04	282.80	0.000	F_s= 2 K_s= 0.01 K_{sa}= 0.00	F_s= 9 K_s= 0.03 K_{sa}= 0.00	F_s= 15 K_s= 0.04 K_{sa}= 0.07	F_s= 27 K_s= 0.08 K_{sa}= 0.11	F_s= 45 K_s= 0.13 K_{sa}= 0.28	F_s= 72 K_s= 0.20 K_{sa}= 0.27	F_s= 102 K_s= 0.29 K_{sa}= 0.36	F_s= 128 K_s= 0.36 K_{sa}= 0.45	F_s= 148 K_s= 0.42 K_{sa}= 0.52	F_s= 161 K_s= 0.45 K_{sa}= 0.55	F_s= 175 K_s= 0.49 K_{sa}= 0.55
619.52	141.40	0.044	F_s= 5 K_s= 0.01 K_{sa}= 0.02	F_s= 12 K_s= 0.03 K_{sa}= 0.02	F_s= 19 K_s= 0.05 K_{sa}= 0.09	F_s= 30 K_s= 0.08 K_{sa}= 0.13	F_s= 50 K_s= 0.14 K_{sa}= 0.20	F_s= 75 K_s= 0.21 K_{sa}= 0.29	F_s= 105 K_s= 0.30 K_{sa}= 0.38	F_s= 133 K_s= 0.37 K_{sa}= 0.47	F_s= 153 K_s= 0.43 K_{sa}= 0.54	F_s= 166 K_s= 0.47 K_{sa}= 0.57	F_s= 179 K_s= 0.51 K_{sa}= 0.57
309.76	70.70	0.077	F_s= 9 K_s= 0.03 K_{sa}= 0.03	F_s= 17 K_s= 0.05 K_{sa}= 0.03	F_s= 25 K_s= 0.07 K_{sa}= 0.10	F_s= 37 K_s= 0.10 K_{sa}= 0.14	F_s= 57 K_s= 0.16 K_{sa}= 0.21	F_s= 84 K_s= 0.24 K_{sa}= 0.30	F_s= 114 K_s= 0.32 K_{sa}= 0.40	F_s= 143 K_s= 0.40 K_{sa}= 0.48	F_s= 161 K_s= 0.45 K_{sa}= 0.55	F_s= 176 K_s= 0.50 K_{sa}= 0.58	F_s= 189 K_s= 0.53 K_{sa}= 0.58
154.88	35.35	0.199	F_s= 22 K_s= 0.06 K_{sa}= 0.09	F_s= 31 K_s= 0.09 K_{sa}= 0.09	F_s= 37 K_s= 0.10 K_{sa}= 0.16	F_s= 50 K_s= 0.14 K_{sa}= 0.20	F_s= 70 K_s= 0.20 K_{sa}= 0.27	F_s= 98 K_s= 0.28 K_{sa}= 0.36	F_s= 130 K_s= 0.37 K_{sa}= 0.45	F_s= 158 K_s= 0.45 K_{sa}= 0.54	F_s= 180 K_s= 0.51 K_{sa}= 0.61	F_s= 193 K_s= 0.54 K_{sa}= 0.64	F_s= 207 K_s= 0.58 K_{sa}= 0.64
77.44	17.67	0.378	F_s= 42 K_s= 0.12 K_{sa}= 0.17	F_s= 50 K_s= 0.14 K_{sa}= 0.17	F_s= 57 K_s= 0.16 K_{sa}= 0.24	F_s= 70 K_s= 0.20 K_{sa}= 0.28	F_s= 93 K_s= 0.26 K_{sa}= 0.35	F_s= 123 K_s= 0.35 K_{sa}= 0.44	F_s= 157 K_s= 0.44 K_{sa}= 0.53	F_s= 189 K_s= 0.53 K_{sa}= 0.62	F_s= 212 K_s= 0.60 K_{sa}= 0.69	F_s= 226 K_s= 0.64 K_{sa}= 0.72	F_s= 237 K_s= 0.67 K_{sa}= 0.72
38.72	8.84	0.584	F_s= 74 K_s= 0.21 K_{sa}= 0.26	F_s= 82 K_s= 0.23 K_{sa}= 0.26	F_s= 91 K_s= 0.26 K_{sa}= 0.33	F_s= 106 K_s= 0.30 K_{sa}= 0.37	F_s= 130 K_s= 0.37 K_{sa}= 0.44	F_s= 164 K_s= 0.46 K_{sa}= 0.53	F_s= 203 K_s= 0.57 K_{sa}= 0.62	F_s= 237 K_s= 0.67 K_{sa}= 0.71	F_s= 262 K_s= 0.74 K_{sa}= 0.78	F_s= 273 K_s= 0.77 K_{sa}= 0.81	F_s= 281 K_s= 0.79 K_{sa}= 0.81
19.36	4.42	0.786	F_s= 118 K_s= 0.33 K_{sa}= 0.35	F_s= 128 K_s= 0.36 K_{sa}= 0.35	F_s= 138 K_s= 0.39 K_{sa}= 0.42	F_s= 153 K_s= 0.43 K_{sa}= 0.46	F_s= 181 K_s= 0.51 K_{sa}= 0.53	F_s= 219 K_s= 0.62 K_{sa}= 0.62	F_s= 263 K_s= 0.74 K_{sa}= 0.72	F_s= 299 K_s= 0.84 K_{sa}= 0.80	F_s= 317 K_s= 0.89 K_{sa}= 0.87	F_s= 320 K_s= 0.90 K_{sa}= 0.90	F_s= 321 K_s= 0.90 K_{sa}= 0.90
9.68	2.21	0.954	F_s= 166 K_s= 0.47 K_{sa}= 0.43	F_s= 178 K_s= 0.50 K_{sa}= 0.43	F_s= 188 K_s= 0.53 K_{sa}= 0.50	F_s= 202 K_s= 0.57 K_{sa}= 0.54	F_s= 219 K_s= 0.62 K_{sa}= 0.61	F_s= 244 K_s= 0.69 K_{sa}= 0.70	F_s= 275 K_s= 0.78 K_{sa}= 0.79	F_s= 304 K_s= 0.86 K_{sa}= 0.88	F_s= 324 K_s= 0.91 K_{sa}= 0.95	F_s= 332 K_s= 0.94 K_{sa}= 0.98	F_s= 337 K_s= 0.95 K_{sa}= 0.98
4.84	1.10	1.000	F_s= 178 K_s= 0.50 K_{sa}= 0.45	F_s= 185 K_s= 0.52 K_{sa}= 0.45	F_s= 191 K_s= 0.54 K_{sa}= 0.52	F_s= 201 K_s= 0.57 K_{sa}= 0.56	F_s= 220 K_s= 0.62 K_{sa}= 0.63	F_s= 245 K_s= 0.69 K_{sa}= 0.72	F_s= 276 K_s= 0.78 K_{sa}= 0.81	F_s= 308 K_s= 0.87 K_{sa}= 0.90	F_s= 329 K_s= 0.93 K_{sa}= 0.97	F_s= 337 K_s= 0.95 K_{sa}= 1.00	F_s= 345 K_s= 0.97 K_{sa}= 1.00
rigid	rigid	1.000	F_s= 178 K_s= 0.50 K_{sa}= 0.45	F_s= 186 K_s= 0.52 K_{sa}= 0.45	F_s= 192 K_s= 0.54 K_{sa}= 0.52	F_s= 203 K_s= 0.57 K_{sa}= 0.56	F_s= 220 K_s= 0.62 K_{sa}= 0.63	F_s= 248 K_s= 0.70 K_{sa}= 0.72	F_s= 279 K_s= 0.79 K_{sa}= 0.81	F_s= 311 K_s= 0.88 K_{sa}= 0.90	F_s= 335 K_s= 0.94 K_{sa}= 0.97	F_s= 346 K_s= 0.98 K_{sa}= 1.00	F_s= 355 K_s= 1.00 K_{sa}= 1.00

Table 4. Plastic load capacities F_s and rigidity factors K_s and K_{sa} for frame C. Values of Φ_α, Φ_β and α_s, β_s have been calculated by analytical model described further in this paper.

FRAME C

Base / Beam-Column	ϕ_α (mrad)	pinned	512.00	256.00	128.00	64.00	32.00	16.00	8.00	4.00	2.00	rigid
ϕ_β	Φ_β / Φ_α (rad)	pinned	93.79	46.90	23.45	11.72	5.86	2.93	1.47	0.73	0.37	rigid
(mrad)	(rad) / β =(1)	0.000	0.000	0.120	0.190	0.318	0.481	0.653	0.813	0.937	1.000	1.000
pinned	pinned	0.000	Fs= 0 Ks= 0.00 Ksa= 0.00	Fs= 12 Ks= 0.02 Ksa= 0.00	Fs= 24 Ks= 0.04 Ksa= 0.07	Fs= 45 Ks= 0.07 Ksa= 0.10	Fs= 82 Ks= 0.13 Ksa= 0.17	Fs= 140 Ks= 0.22 Ksa= 0.26	Fs= 220 Ks= 0.35 Ksa= 0.36	Fs= 301 Ks= 0.48 Ksa= 0.45	Fs= 368 Ks= 0.59 Ksa= 0.51	Fs= 399 Ks= 0.64 Ksa= 0.55	Fs= 395 Ks= 0.63 Ksa= 0.55
2048.00	500.22	0.000	Fs= 5 Ks= 0.01 Ksa= 0.00	Fs= 15 Ks= 0.02 Ksa= 0.00	Fs= 27 Ks= 0.04 Ksa= 0.07	Fs= 47 Ks= 0.08 Ksa= 0.10	Fs= 85 Ks= 0.14 Ksa= 0.29	Fs= 144 Ks= 0.23 Ksa= 0.26	Fs= 222 Ks= 0.36 Ksa= 0.36	Fs= 306 Ks= 0.49 Ksa= 0.45	Fs= 372 Ks= 0.60 Ksa= 0.51	Fs= 401 Ks= 0.64 Ksa= 0.55	Fs= 413 Ks= 0.66 Ksa= 0.55
1024.00	250.11	0.000	Fs= 8 Ks= 0.01 Ksa= 0.00	Fs= 17 Ks= 0.03 Ksa= 0.00	Fs= 30 Ks= 0.05 Ksa= 0.07	Fs= 52 Ks= 0.08 Ksa= 0.10	Fs= 89 Ks= 0.14 Ksa= 0.17	Fs= 149 Ks= 0.24 Ksa= 0.26	Fs= 226 Ks= 0.36 Ksa= 0.36	Fs= 309 Ks= 0.50 Ksa= 0.45	Fs= 376 Ks= 0.60 Ksa= 0.51	Fs= 404 Ks= 0.65 Ksa= 0.55	Fs= 415 Ks= 0.66 Ksa= 0.55
512.00	125.05	0.042	Fs= 11 Ks= 0.02 Ksa= 0.02	Fs= 20 Ks= 0.03 Ksa= 0.02	Fs= 35 Ks= 0.06 Ksa= 0.08	Fs= 57 Ks= 0.09 Ksa= 0.12	Fs= 95 Ks= 0.15 Ksa= 0.19	Fs= 156 Ks= 0.25 Ksa= 0.28	Fs= 235 Ks= 0.38 Ksa= 0.38	Fs= 319 Ks= 0.51 Ksa= 0.47	Fs= 385 Ks= 0.62 Ksa= 0.53	Fs= 412 Ks= 0.66 Ksa= 0.57	Fs= 421 Ks= 0.67 Ksa= 0.57
256.00	62.53	0.093	Fs= 25 Ks= 0.04 Ksa= 0.04	Fs= 35 Ks= 0.06 Ksa= 0.04	Fs= 47 Ks= 0.08 Ksa= 0.11	Fs= 70 Ks= 0.11 Ksa= 0.15	Fs= 109 Ks= 0.17 Ksa= 0.22	Fs= 170 Ks= 0.27 Ksa= 0.31	Fs= 251 Ks= 0.40 Ksa= 0.40	Fs= 335 Ks= 0.54 Ksa= 0.49	Fs= 399 Ks= 0.64 Ksa= 0.56	Fs= 423 Ks= 0.68 Ksa= 0.59	Fs= 429 Ks= 0.69 Ksa= 0.59
128.00	31.26	0.227	Fs= 47 Ks= 0.08 Ksa= 0.10	Fs= 60 Ks= 0.10 Ksa= 0.10	Fs= 72 Ks= 0.12 Ksa= 0.17	Fs= 95 Ks= 0.15 Ksa= 0.21	Fs= 135 Ks= 0.22 Ksa= 0.28	Fs= 198 Ks= 0.32 Ksa= 0.37	Fs= 280 Ks= 0.45 Ksa= 0.46	Fs= 368 Ks= 0.59 Ksa= 0.55	Fs= 427 Ks= 0.68 Ksa= 0.62	Fs= 439 Ks= 0.70 Ksa= 0.65	Fs= 446 Ks= 0.72 Ksa= 0.65
64.00	15.63	0.413	Fs= 88 Ks= 0.14 Ksa= 0.19	Fs= 102 Ks= 0.16 Ksa= 0.19	Fs= 114 Ks= 0.18 Ksa= 0.25	Fs= 139 Ks= 0.22 Ksa= 0.29	Fs= 180 Ks= 0.29 Ksa= 0.36	Fs= 246 Ks= 0.39 Ksa= 0.45	Fs= 333 Ks= 0.53 Ksa= 0.55	Fs= 423 Ks= 0.68 Ksa= 0.63	Fs= 464 Ks= 0.74 Ksa= 0.70	Fs= 471 Ks= 0.75 Ksa= 0.74	Fs= 476 Ks= 0.76 Ksa= 0.74
32.00	7.82	0.621	Fs= 161 Ks= 0.26 Ksa= 0.28	Fs= 174 Ks= 0.28 Ksa= 0.28	Fs= 189 Ks= 0.30 Ksa= 0.35	Fs= 215 Ks= 0.34 Ksa= 0.38	Fs= 261 Ks= 0.42 Ksa= 0.45	Fs= 333 Ks= 0.53 Ksa= 0.54	Fs= 421 Ks= 0.67 Ksa= 0.64	Fs= 494 Ks= 0.79 Ksa= 0.73	Fs= 510 Ks= 0.82 Ksa= 0.79	Fs= 514 Ks= 0.82 Ksa= 0.83	Fs= 515 Ks= 0.82 Ksa= 0.83
16.00	3.91	0.820	Fs= 268 Ks= 0.43 Ksa= 0.37	Fs= 284 Ks= 0.45 Ksa= 0.37	Fs= 299 Ks= 0.48 Ksa= 0.44	Fs= 328 Ks= 0.52 Ksa= 0.47	Fs= 378 Ks= 0.60 Ksa= 0.54	Fs= 439 Ks= 0.70 Ksa= 0.63	Fs= 498 Ks= 0.80 Ksa= 0.73	Fs= 546 Ks= 0.87 Ksa= 0.82	Fs= 548 Ks= 0.88 Ksa= 0.88	Fs= 556 Ks= 0.89 Ksa= 0.92	Fs= 557 Ks= 0.89 Ksa= 0.92
8.00	1.95	0.978	Fs= 341 Ks= 0.55 Ksa= 0.44	Fs= 349 Ks= 0.56 Ksa= 0.44	Fs= 355 Ks= 0.57 Ksa= 0.51	Fs= 368 Ks= 0.59 Ksa= 0.55	Fs= 402 Ks= 0.64 Ksa= 0.62	Fs= 444 Ks= 0.71 Ksa= 0.71	Fs= 504 Ks= 0.81 Ksa= 0.80	Fs= 560 Ks= 0.90 Ksa= 0.89	Fs= 580 Ks= 0.93 Ksa= 0.96	Fs= 589 Ks= 0.94 Ksa= 0.99	Fs= 598 Ks= 0.96 Ksa= 0.99
rigid	rigid	1.000	Fs= 341 Ks= 0.55 Ksa= 0.45	Fs= 348 Ks= 0.56 Ksa= 0.45	Fs= 356 Ks= 0.57 Ksa= 0.52	Fs= 369 Ks= 0.59 Ksa= 0.56	Fs= 405 Ks= 0.65 Ksa= 0.63	Fs= 450 Ks= 0.72 Ksa= 0.72	Fs= 515 Ks= 0.82 Ksa= 0.81	Fs= 580 Ks= 0.93 Ksa= 0.90	Fs= 607 Ks= 0.97 Ksa= 0.97	Fs= 617 Ks= 0.99 Ksa= 1.00	Fs= 624 Ks= 1.00 Ksa= 1.00

In Tables 2 to 4:

F_s is the plastic load capacity of sway frame calculated by the FEM analysis

K_s is the sway frame rigidity factor calculated from FEM results as F_s divided by $F_{s.rr}$,

K_{sa} is the sway frame rigidity factor calculated by proposed analytical model for sway frames (described further in this paper).

Φ_α, Φ_β are the modified plastic rotations calculated from proposed analytical design method (described further in this paper).

α_{sa}, β_{sa} are the connection rigidity coefficients calculated from proposed analytical design method described further in this paper.

SWAY FRAME RIGIDITY FACTOR K_S - GENERAL DESCRIPTION

The analytical model for sway frame was derived and can be used in similar way like the model for non-sway frame described in Part I of this Paper. The difference from non-sway mode is the high influence of base rigidity on the frame behaviour.

The values of K_s for frame A with various plastic rotations ϕ_α and ϕ_β from Table 2 are graphically presented in Figure 2. Note that the axes ϕ_β and ϕ_α are in an exponential scale.

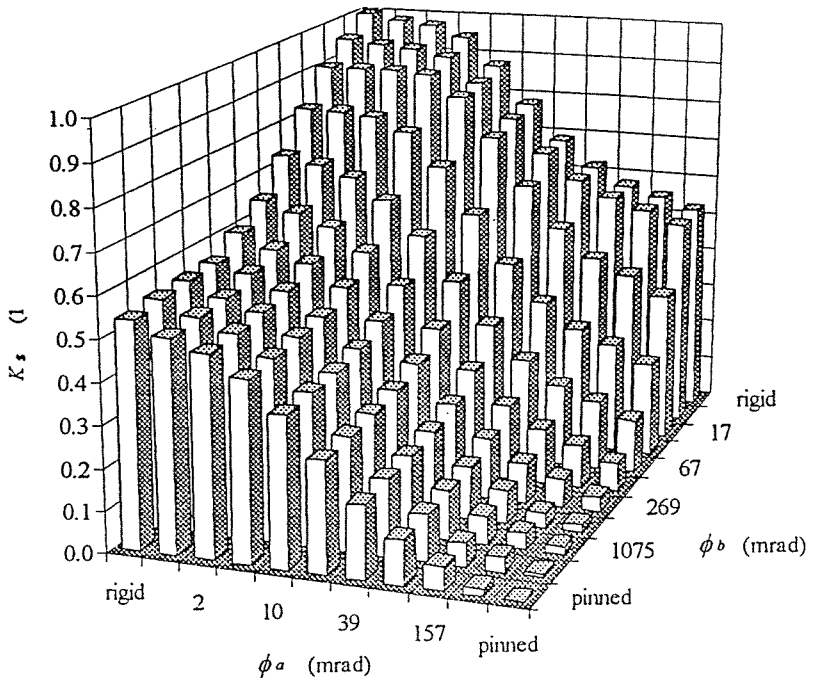

Figure 2. Values of frame rigidity factor K_s for frame A from table 8.

It can be seen, that for the infinite changes of beam-column and base plastic rotations ϕ_α and ϕ_β the frame rigidity factor K_s creates a surface in three dimensional space with axes K_s, ϕ_α and ϕ_β. This surface has been plotted in Figure 3.

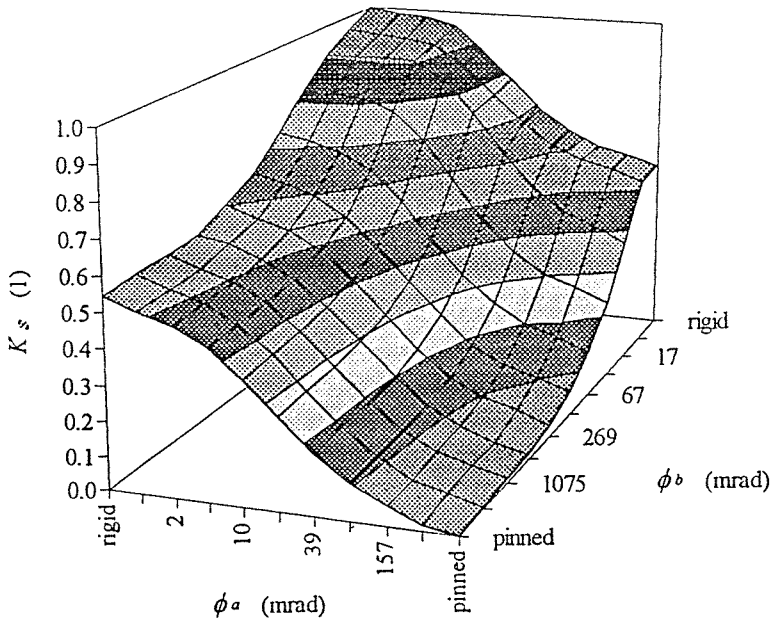

Figure 3. Surface created by the values of frame rigidity factor K_s for infinite

changes of plastic rotations ϕ_β and ϕ_α. Frame A.

The equations for calculation of frame rigidity factor K_{sa} have been derived to fit the best the calculated values from FEM analyses (Tables 2 to 4). This is in other words to analytically describe the surface in Figure 3. The proposed model has been derived to take into account different frame sections, material properties and load conditions providing the ratio of vertical to horizontal load equals 10 and the beam and column have the same sections.

The values of K_{sa} calculated as a function of α_s, and β_s from proposed frame rigidity factor method are plotted in Figure 4 for frame A.

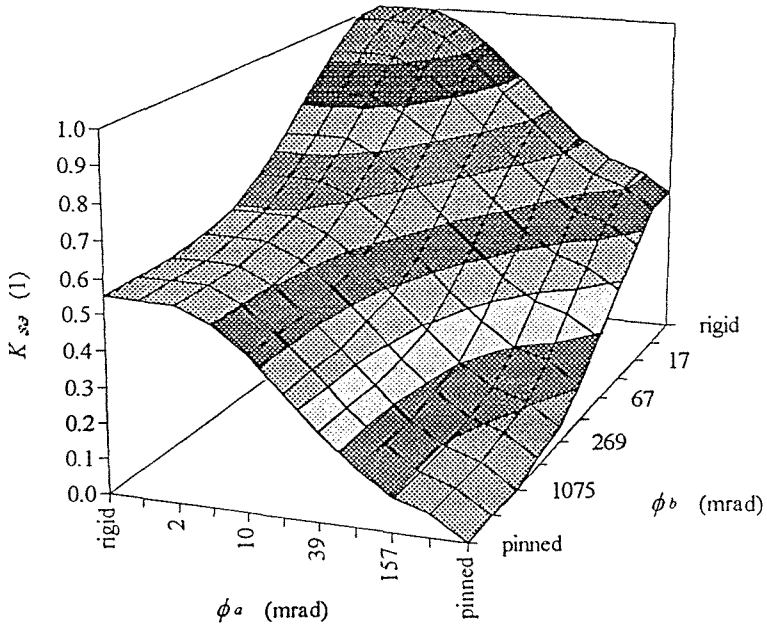

Figure 4. Frame rigidity factor K_{as} calculated from the proposed analytical model. Frame A.

5. SWAY FRAME RIGIDITY FACTOR K_{sa} - CALCULATION

The modified plastic rotations Φ_α and Φ_β can be calculated for sway frame in the same way like for the non sway frame. See equations (7) and (8) from Part I of this Paper.

The rigidity coefficients α_s and β_s for beam-column and column base connections respectively are defined to be zero for pinned connections and one for rigid connections. The relationship between α_s (β_s) and Φ can be calculated directly from Tables 2 to 4 by the following equations:

$$\alpha_s = \frac{K_s(\Phi_\alpha) - K_s(\Phi_{\alpha,p})}{K_s(\Phi_{\alpha,r}) - K_s(\Phi_{\alpha,p})} \tag{1}$$

$$\beta_s = \frac{K_s(\Phi_\beta) - K_s(\Phi_{\beta,p})}{K_s(\Phi_{\beta,r}) - K_s(\Phi_{\beta,p})} \tag{2}$$

The equation for α_{sa} and β_{sa} has been derived to fit the best the numerically calculated values of α_s and β_s from (1) and (2):

$$\alpha_{sa} = a_{s\alpha} + b_{s\alpha} \cdot \ln(\Phi_\alpha) + c_{s\alpha} \cdot \ln^2(\Phi_\alpha) + d_{s\alpha} \cdot \ln^3(\Phi_\alpha) \quad (3)$$

$$\beta_{sa} = a_{s\beta} + b_{s\beta} \cdot \ln(\Phi_\beta) + c_{s\beta} \cdot \ln^2(\Phi_\beta) + d_{s\beta} \cdot \ln^3(\Phi_\beta) \quad (4)$$

Formula above is valid for: $\Phi_\alpha \in (0.4;80)$ (5)

and for $\Phi_\beta \in (1.9;125)$ (6)

Above stated limits for connection rigidity were obtained from FEM analyses. Outside described interval the connection is considered as rigid or pinned and the connection rigidity coefficient α_{sa} and β_{sa} is equal to one or zero respectively:

for beam-column connection: if $\Phi_\alpha > 80$ then $\alpha_{sa} = 0$ pinned connection (7)

if $\Phi_\alpha < 0.4$ then $\alpha_{sa} = 1$ rigid connection (8)

for base connection: if $\Phi_\beta > 125$ then $\beta_{sa} = 0$ pinned connection (9)

if $\Phi_\beta < 1.9$ then $\beta_{sa} = 1$ rigid connection (10)

The values constants a_s, b_s, c_s and d_s are listed in Table 10.

Table 10. Constants a_s, b_s, c_s and d_s for the calculation of α_{sa} and β_{sa}. Constant k_s for calculation of the rigidity factor K_{sa}.

	α_{sa}	β_{sa}
a_s	0.888	1.065
b_s	-0.177	-0.066
c_s	-0.051	-0.104
d_s	0.012	0.015
k_s	0.549	

4) The calculation of frame rigidity factor K_{sa}.

$$K_{sa} = k_{sa} \cdot \alpha_{sa} + (1 - k_{sa}) \cdot \beta_{sa} \quad (11)$$

The plastic sway frame resistance can be than calculated as:

$$F_{sa} = K_{sa} F_{sr,r} \quad (12)$$

Where:

α_{sa}, β_{sa} are the rigidity coefficients of beam-column and base connection respectively calculated from analytical model,

a_s, b_s, c_s, d_s, k_s are the constants used to calculate α_{sa}, β_{sa},
K_s is the frame rigidity coefficient calculated by FEM analysis,
K_{sa} is the frame rigidity coefficient calculated by analytical model,
F_{sa} is the plastic load capacity of the semi-rigid sway frame,

COMPARISON OF THE ANALYTICAL MODEL WITH FEM RESULTS

The difference between plastic load capacity calculated by FEM and by the proposed analytical model is smaller than 11 % of the rigid frame capacity for all 484 calculated semi-rigid frames. The average error between semi-rigid and rigid frame load capacity calculated by FEM and by use of frame rigidity factor method is 3%. For connections with satisfactory rotational capacity the proposed analytical model can be used with a high accuracy.

PARAMETRIC STUDY

The influence of connection rigidity (expressed by plastic rotations ϕ_α and ϕ_β at M_{pl}) on the frame rigidity factor K_{sa} calculated by proposed frame rigidity factor method can be seen in following three Figures. All the graphs are plotted for the frame A (see Table 1, Part I Paper). The horizontal axes are in the logarithmic scale. In Figure 5 the relationship between ϕ_β and K_{sa} can be seen for different plastic rotations of beam-column connections ϕ_α.

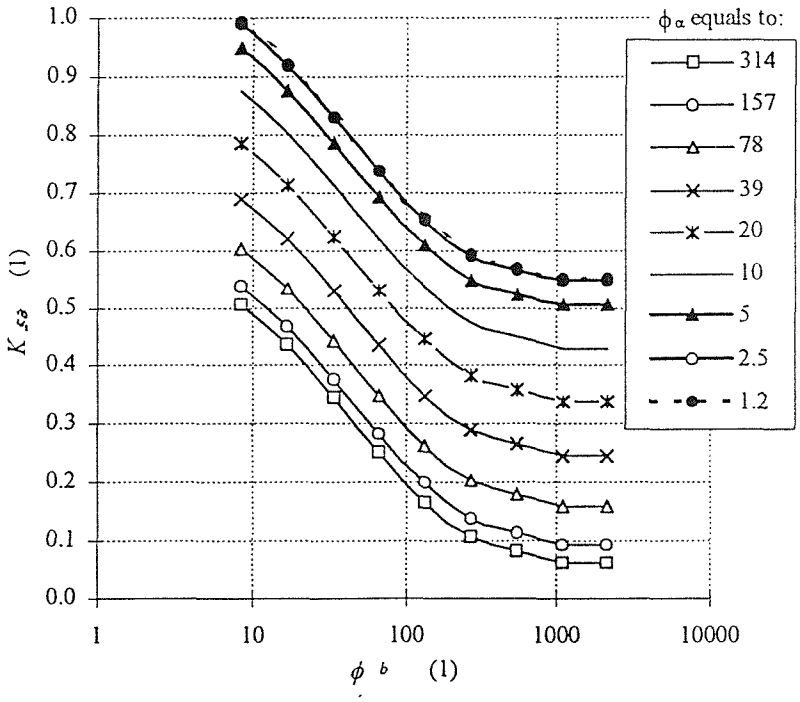

Figure 5. Influence of ϕ_β on frame rigidity factor K_a for constant ϕ_α

In Figure 6 the relationship between and K_{sa} can be seen for different plastic rotations of column base connections ϕ_β.

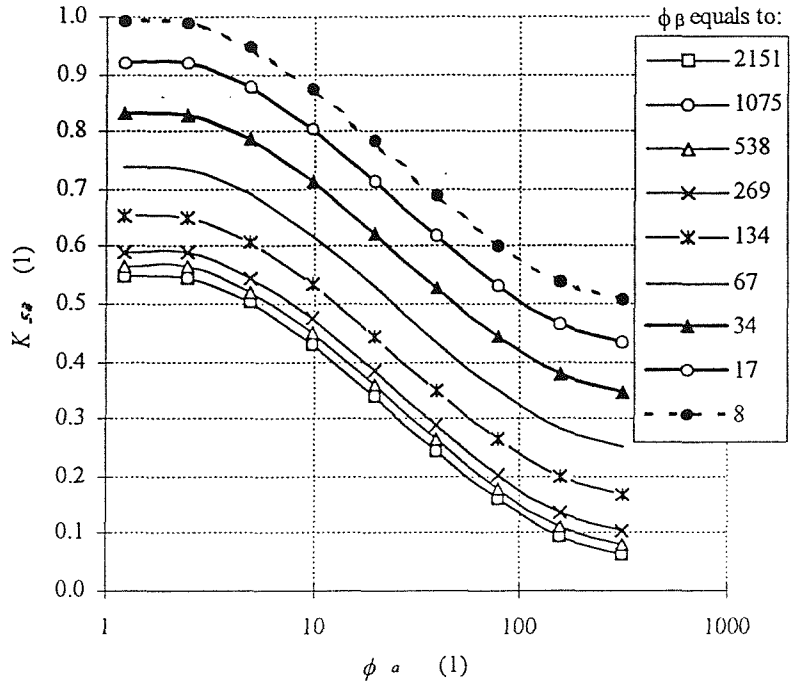

Figure 6. Influence of ϕ_α on frame rigidity factor K_a for constant ϕ_β

In Figure 7 the relationship between ϕ_α and ϕ_β on K_{sa} can be seen for the case when not plotted connections are rigid.

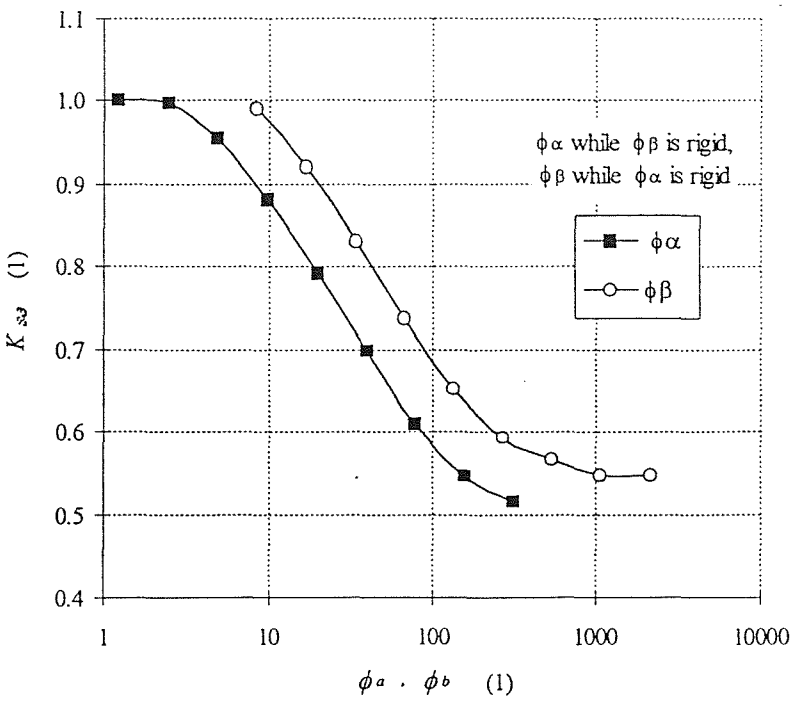

Figure 7. Influence of ϕ_α and ϕ_β on the frame rigidity factor K_{sa}

CONCLUSIONS

The Analytical model for design of semi-rigid sway frames has been proposed in this paper. The frame rigidity factor calculation has been derived from database of numerical results. From the proposed equation (11) it can be seen that column base connection rigidity influence the frame capacity by 45% and beam-column connection rigidity by 55%. The limits of connection rigidity have been set to define the rigid and pinned connections (7) to (10).

Proposed frame rigidity method is a fast and simple method to design frames in plastic region. It can be as well used to study the influence of various types of connections on the frame response.

The analytical model for calculation of plastic load capacity was derived from a large database of FEM results published in this paper.

The frame load capacity depends on $\phi_\alpha, \phi_\beta, L_b, L_c, I_{y,b}, I_{y,c}, M_{pl,b}, M_{pl,c}, E$ as it was described above in details.

Results of this research could lead to a reduction of the cost for steel frame fabrication.

ACKNOWLEDGEMENT

The authors are grateful to the support from the Royal Society for Dr J Pertold for his post-doctoral research on column bases and steel frame at the Department of Civil & Environmental Engineering, University of Southampton.